DSS. ETH NO. 24764

Application of a spatially Explicit Biophysical Crop Model to Assess Drought Impacts on Crop Yield and Crop-Drought Vulnerability in Sub-Saharan Africa

A thesis submitted to attain the degree of

DOCTOR OF SCIENCES of ETH ZURICH
(Dr. sc. ETH Zurich)

presented by

BAHAREH KAMALI
M.Eng. in Water Resource Engineering, Amirkabir University of Technology

born on 16.09.1984

Citizen of Iran

accepted on the recommendation of

Prof. Dr. Bernhard Wehrli, ETH Zurich, examiner
Prof. Dr. Hong Yang, Eawag, co-examiner
Prof. Karim C. Abbaspour, Eawag, co-examiner
Prof. Dr. Stefan Siebert, Bonn, co-examiner

2018

To MY PARENTS AND TO MY LOVE

Contents

Summary **1**

Zusammenfassung **3**

Chapter 1 Introduction **5**

1.1. Background and motivation 5

1.1.1 Principles of drought vulnerability: definitions and issues relating to the agricultural sector 5

1.1.2 Application of crop models for spatially-explicit drought vulnerability assessment 8

1.1.3 Crop drought vulnerability in the context of socio-economic conditions conferring adaptation 9

1.2. Objectives of the research 9

1.3. Research outline and contents of dissertation 10

1.4. Reference 11

Chapter 2 Uncertainty-based auto-calibration for crop yield – the EPIC$^+$ procedure for a case study in Sub-Saharan Africa **16**

Abstract 17

2.1. Introduction 17

2.2. Methodology 19

2.2.1. Site description 19

2.2.2. Programs EPIC and SUFI-2 19

2.2.3. EPIC$^+$ architecture 20

2.2.4. EPIC$^+$ setup for SSA countries 22

2.2.4.1. Input data for EPIC$^+$ 22

2.2.5. Efficiency criteria, sensitivity analysis, and parameterization 24

2.3. Results 26

2.3.1. Country level model performance with default parameters 26

2.3.2. Calibration of planting date (*PD*) (Step 1) 27

2.3.3. Calibration of Operation parameters (Step 2) 29

2.3.4. Calibration of Crop and Model parameters (Step 3) 32

2.4. Discussion and conclusion 37

2.4.1. Country level maize calibration 37

2.4.2. Parameter regionalization in SSA countries 39

2.4.3. The EPIC$^+$ tool for calibration purposes 41

2.4.4. Limitation of study and future perspectives 42

2.5. Reference 42
2.6. Supplementary material 47
2.7. Overview of EPIC+ and its architecture 54
2.7.1. Main window 54
2.7.2. General settings 55
2.7.3. Operation settings 56
2.7.4. Parameterization 58
2.7.5. The SUFI-2 calibration 60
2.7.6. The EPIC+ application for calibration at field scale 62
Chapter 3 Spatial assessment of maize physical drought vulnerability in Sub-Saharan Africa: Linking drought exposure with crop failure 65
Abstract 66
3.1. Introduction 66
3.2. Data and methods 69
3.2.1. Study area 69
3.2.2. Crop model and calibration 69
3.2.3. Model inputs 70
3.2.4. Components of crop drought vulnerability 71
3.2.5. Crop drought vulnerability 73
3.3. Results 74
3.3.1. The performance of EPIC crop simulator 74
3.3.2. Drought exposure indices in SSA 76
3.3.3. The relation between *DEI* and *CFI* 77
3.3.4. Country-level and grid-level crop drought vulnerability in SSA 78
3.4. Discussion 81
3.4.1. The effectiveness of standardized approach for vulnerability assessment 81
3.4.2. The impact of different timescales of DEI_{PCP} and $DEI_{PCP-PET}$ 82
3.4.3. Comparison of maize drought vulnerability in different countries 83
3.5. Conclusion 84
3.6. Reference 84
3.7. Supplementary material 88
Chapter 4 Drought vulnerability assessment of maize in Sub-Saharan Africa: insights from physical and social perspectives 94
Abstract 95
4.1. Introduction 95
4.2. Methodology 96
4.2.1. Simulation and calibration of maize yield using EPIC 96
4.2.2. Conceptualizing crop drought vulnerability 99

4.2.3. Definition of Drought Exposure Index (*DEI*) 99
4.2.4. Definitions of the physical and social Crop Failure Indices (CFI_{phy} and CFI_{soc}) 100
4.2.5. Drought vulnerability definition based on incorporating *DEI* and *CFI* 101
4.3. Results 102
4.3.1. Calibration performance of EPIC 102
4.3.2. Spatiotemporal pattern of *DEI* and CFI_{phy} 104
4.3.3. Physical and social crop drought vulnerability 106
4.4. Discussion and conclusion 108
4.4.1. The effectiveness of proposed methodology for quantifying $CDVI_{soc}$ and $CDVI_{phy}$ 108
4.4.2. Implications of $CDVI_{phy}$ and $CDVI_{soc}$ for SSA countries 109
4.5. Conclusion and limitation 110
4.6. Reference 110
Chapter 5 A quantitative analysis of socio-economic determinants conferring crop drought vulnerability in Sub-Saharan Africa 118
Abstract 119
5.1. Introduction 119
5.2. Methodology 121
5.2.1. Site description 121
5.2.2. Quantifying drought exposure index 122
5.2.3. Definition of Crop Drought Vulnerability Index (*CDVI*) 122
5.2.4. Selecting socio-economic variables relating to *CDVI* 123
5.2.5. Linking *CDVI* and socio-economic variables using regression models 126
5.3. Results 126
5.3.1. Temporal and spatial patterns of *CDVI* 126
5.3.2. Socio-economic factors influencing *CDVI* 129
5.3.3. Relations between time-invariant socio-economic variables and *CDVI* 132
5.3.4. Assessing relations between time-variant socio-economic variables and *CDVI* 132
5.4. Discussion 134
5.4.1. Changes in crop drought vulnerability 134
5.4.2. Major factors influencing drought vulnerability 135
5.4.3. Comparison of models explaining the relationship between *CDVI* and socio-economic variables 137
5.4.4. Limitation and conclusion of the study 137
5.5. Reference 138
5.6. Supplementary material 141
Chapter 6 General conclusions and outlook 145
6.1. General conclusion 145
6.2. Limitations 147

6.3. Outlook 148
6.4. Reference 149
Acknowledgement 151
Curriculum Vita 153

Summary

Drought is a slow-onset phenomenon with devastating effects on many aspects of human livelihood. Drought events around the world have had significant impacts on agricultural production. Sub-Saharan Africa (SSA) is at the core of this threat because rainfed subsistence farming dominates the food production and where socio-economic infrastructure are often inadequately prepared to cope with disasters. The recurrence of droughts in the past decades has triggered many famines in SSA and is projected to increase as a consequence of climate change. There is therefore a need to develop a research framework, which quantifies the crop drought vulnerability and identifies influencing physical and socio-economic factors. This study applies a biophysical crop model to map out hotspots of maize drought vulnerability across SSA and investigates the physical and socio-economic drivers. The derived knowledge from linking vulnerability to socio-economic factors support strategies to mitigate the negative impacts of drought on agricultural production

To achieve the goal of the project, we first developed a user-friendly software to couple EPIC (Environmental Policy Integrated Climate) crop model to the SUFI-2 auto-calibration procedure (Sequential Uncertainty Fitting Procedure). The developed model (EPIC^{+}) increases the reliability of simulated crop yield in replicating historic yield. It also greatly speeds up the calibration process with quantification of parameter ranges and prediction uncertainty. We calibrated three sets of parameters referred to as Planting Date, Operation (e.g., fertilizer application, planting density), and Model parameters (e.g., Harvest index, biomass-energy ratio, water stress harvest index) in three steps to avoid parameter interaction. The model performance is significantly improved with these three sets of calibration. We also found that the simulation results for the countries with less socio-political volatility improved most by calibration. For countries where agricultural production had increasing or decreasing trends, we suggested improving the calibration results by applying linear de-trending transformations.

The calibrated EPIC^{+} was then applied to develop a physical Crop Drought Vulnerability Index (*CDVI*) through linking the Drought Exposure Index (*DEI*) with the Crop Failure Index (*CFI*). Two different *DEI*s; DEI_{PCP} and $DEI_{PCP\text{-}PET}$ were calculated. DEI_{PCP} was derived from the cumulative distribution functions fitted to precipitation, and $DEI_{PCP\text{-}PET}$ was obtained from cumulative distribution functions fitted to the difference between precipitation and potential evapotranspiration. In addition, these indices were calculated for different time scales (i.e., X = 1, 3, 6, 9 and 12 months). Similarly, *CFI* was calculated by fitting a cumulative distribution function to maize yield simulated in EPIC^{+}. Using a power function, curves were fitted to establish *CFI* and *DEI* relations. The highest correlation

between *CFI* and $DEI_{PCP\text{-}PET}$ in Central Africa was found at 1 month time scale, while in other parts of SSA, *CFI* was strongly correlated to $DEI_{PCP\text{-}PET}$ at 3 and 6 month time scales. The final results highlighted that Southern African countries and some regions of Sahelian strip are highly vulnerable to drought due to experiencing more water stress, whereas vulnerability in Central African countries pertains to temperature stresses.

In the next step, we quantified the physical and social *CDVI*. We applied a probabilistic framework combining DEI_p (calculated in the previous step) with a physical or social Crop Failure Index (*CFI*). Maize yields, simulated with EPIC$^+$, were used to build physical *CFI*, whereas the residuals of simulated and FAO recorded yields were used to construct social *CFI*. The construction of social *CDVI* is based on the idea that in some countries/areas, a mild drought can lead to a severe level of vulnerability due to the lack of social-economic capacity to adapt the drought impact, whereas in some other cases, a relatively severe drought may only cause a mild impact on yield because of the higher level of social adaptive capacity. The results showed that Southern and partially Central Africa are more vulnerable to physical drought as compared to other regions. Central and Western Africa, however, are socially highly vulnerable.

In the last step, we examined the extents to which socio-economic factors are influencing crop vulnerability to drought. Social *CDVI*, calculated based on the residual of simulated and FAO recorded yields, were related to potential socio-economic variables using the regression techniques. The key variables which have significantly influenced social *CDVI* were identified. The results showed that the level of fertilizer use strongly influences vulnerability. In general, countries with higher fertilizer application, human development index, and better infrastructure are more resilient to drought, thus have lower vulnerability. The role of government effectiveness was less apparent due to the generally low level and static status of this variable across the SSA countries over time.

In conclusion, the proposed methodologies provided a generic and comprehensive framework for quantifying different degrees of vulnerabilities and can be applied to different regions and scales. The comparison of physical *CDVI* and social *CDVI* revealed that societal factors cause higher level of vulnerability than physical variables in most SSA countries. Therefore, quantification of both vulnerabilities helps to better characterize droughts and identify regions where more investments for drought preparedness are required. Improving adaptations to drought through appropriate policies have become more important amid the expected intensification of drought in terms of frequency and severity in the future.

Zusammenfassung

Dürren zeichnen sich durch einen schleichenden Beginn und verheerende Auswirkungen auf den Menschen und seine Umwelt aus. In verschiedenen Regionen der Welt hatten Dürren bereits grosse Beeinträchtigungen der landwirtschaftlichen Produktion zur Folge. Eine der gefährdetsten Regionen befindet sich in Afrika südlich der Sahara (ASS), wo Selbstversorgung ohne anthropogene Bewässerung weit verbreitet ist und wo die sozioökonomische Infrastruktur besonders verwundbar ist in Bezug auf Naturkatastrophen. Dürren verursachten viele Hungersnöte in ASS während den vergangenen Jahrzehnten und bedingt durch die Klimaänderung werden diese zunehmen. Der Einfluss von Dürren auf die landwirtschaftliche Produktion, inklusive der zugrundeliegenden sozioökonomischen Faktoren bedarf deshalb weiterer Froschung. In der vorliegenden Arbeit wird ein bio-physikalisches Erntemodell angewendet, um besonders dürreanfällige Maisanbaugebiete in ASS zu identifizieren und die physikalischen und sozioökonomischen Einflussfaktoren zu untersuchen. Das so erarbeitete Wissen kann verwendet werden, um die Auswirkungen von Dürren auf die landwirtschaftliche Produktion zu minimieren.

Um diese Ziele zu erreichen, entwickelten wir eine benutzerfreundliche Anwendung, die das Erntemodell EPIC (Environmental Policy Integrated Climate) mit dem Kalibrierungsalgorithmus SUFI-2 (Sequential Uncertainty Fitting Procedure) koppelt. Diese Software (im Folgenden EPIC$^+$ genannt) produziert verlässlichere Vorhersagen von beobachteten vergangenen Ernten. EPIC$^+$ beschleunigt den Kalibrierungsprozess, die Bestimmung der Parameterunsicherheit sowie der Unsicherheiten der Vorhersagen. Die Parameter wurden in folgende drei Gruppen unterteilt: Zeitpunkt der Saat, Anbau (z.B. Düngung, Saatdichte) und Modellparameter (z.B. Ernteindex, Biomasse-Energie-Verhältnis, Wasser-StressErnte Index). Die Kalibrierung erfolgte gruppenweise nacheinander, um Parameterinteraktionen zu vermeiden. Die Kalibrierung hat sich mit diesem dreistufigen Verfahren als wesentlich effizienter herausgestellt. Vor allem in Ländern mit kleiner sozio-politischer Volatilität führte die Kalibrierung zu besseren Modellergebnissen. Im Falle von Ländern mit zu- oder abnehmender landwirtschaftlicher Produktion hat sich die Bereinigung von linearen Trends bewährt, um die Kalibrierung zu vereinfachen.

Das kalibrierte EPIC$^+$-Modell wurde anschliessend verwendet um einen physikalischen Indikator für die Anfälligkeit auf Dürren (Crop Drought Vulnerability Index, *CDVI*) zu entwickeln, indem der Indikator für die Exposition in Bezug auf Dürren (Drought Exposure Index, *DEI*) mit demjenigen für die Anfälligkeit der Ernte (Crop Failure Index, *CFI*) verknüpft wurde. Es wurde zwischen zwei verschiedenen Expositionsindizes unterschieden: DEI_P wurde von der kumulativen Niederschlagsverteilung abgeleitet und DEI_R von der kumulativen Differenz zwischen Niederschlag

und Evapotranspiration. Zudem wurden diese Indizes für verschiedene Zeitskalen berechnet (d.h. X= 1, 3, 6, 9 und 12 Monate). *CFI* wurde aus der kumulativen Maisernte (EPIC^{+}) geschätzt. Die Beziehung zwischen *CFI* und *DEI* wurde durch Potenzfunktionen beschrieben. Die höchste Korrelation zwischen *CFI* und DEI_{R-1} fanden wir in Zentralafrika, wohingegen in andern Regionen in ASS der *CFI* stark mit DEI_{P-3} und DEI_{P-6} korreliert war. Am anfälligsten auf Dürren scheinen gemäss unseren Resultaten einige Südafrikanische Länder zu sein, sowie die westliche Sahelzone und Teile von Ostafrika. Der *CDVI* war eher tief in Zentralafrika, bedingt durch relativ viel Niederschlag und dem seltenen Auftreten von Dürrestress.

Im nächsten Schritt haben wir den physikalischen und sozialen *CDVI* quantifiziert. Dazu haben wir ein probabilistisches Modell eingesetzt, das den *DEI* mit einem physikalischen oder sozialen *CFI* (Crop Failure Index) verbindet. Die Maisernten (simuliert durch EPIC^{+}) wurden verwendet für den physikalischen *CFI*, wohingegen die Differenz zwischen simulierten und durch die FAO erfassten Ernten verwendet wurden um den sozialen *CFI* zu berechnen. Die Berechnung des sozialen *CDVI* basiert auf der Tatsache, dass es grosse Unterschiede in der sozialen Anpassungsfähigkeit und somit in der Anfälligkeit auf Dürre geben kann. Die Resultate zeigen, dass Gebiete in Süden und speziell im Zentrum Afrikas anfällig für physikalische Dürren sind. Soziale Faktoren spielen hauptsächlich in Zentral- und Westafrika eine Rolle für die Verwundbarkeit in Bezug auf Dürren.

Im letzten Schritt haben wir untersucht inwiefern sich sozioökonomische Faktoren auf die Anfälligkeit auf Dürre auswirken. Die Beziehung zwischen sozialem *CDVI* und potenziellen sozioökonomischen Einflussfaktoren wurde durch Regressionsanalyse untersucht. Als stärkster Einflussfaktor wurde der Einsatz von Düngemitteln identifiziert. Generell zeigten sich Länder mit höherem Düngemitteleinsatz, höherem Entwicklungsstandard und besser ausgebauter Infrastruktur weniger anfällig für Auswirkungen von Dürren. Der Einfluss der Effizienz der Behörden war nicht offensichtlich, wahrscheinlich bedingt durch das allgemein tiefe Niveau und die kleine Varianz dieses Faktors in den untersuchten Ländern über die Zeit.

Zusammenfassend stellen die hier entwickelten Methoden ein generelles und umfangreiches Instrument zur Quantifizierung verschiedener Grade der Anfälligkeit auf Dürren dar, die in verschiedenen Regionen und auf verschiedene Zeitskalen anwendbar sind. Der Vergleich des physikalischen und sozialen *CDVI* zeigten, dass in den meisten Ländern südlich der Sahara gesellschaftliche Faktoren mehr zur Anfälligkeit auf Dürre beitragen als physikalische Faktoren. Deshalb ist es wichtig, beide Gruppen von Faktoren miteinzubeziehen für ein verbessertes Verständnis von Dürren und für die Identifizierung von Regionen, in denen zusätzliche Investitionen für die Vorbereitung auf Dürren getroffen werden müssen. Durch die erwartete Zunahme der Stärke und Häufigkeit von Dürren wird es immer wichtiger, geeignete Massnahmen zu entwickeln, um deren Auswirkungen zu reduzieren.

Chapter 1

Introduction

1.1. Background and motivation

1.1.1 Principles of drought vulnerability: definitions and issues relating to the agricultural sector

Over the last two decades, worldwide concerns has been growing regarding the increase in the frequency and severity of droughts and their significant consequences on human and natural systems (Thornton et al., 2014). Drought and water stress affect plant growth and put agricultural systems under a heavy strain (Boyer et al., 2013). On the other hand, more than 25% of the current global population of 7 billion lives with food insecurity (Wheeler and Von Braun, 2013). The food demand will continue to increase as an additional 2.5 billion people will live by 2050 (Lipper et al., 2014). Faced with the concurrent challenge of increasing drought and food demand, there is an urgent need for developing effective polices that mitigate the impact of droughts and improve the resilience of society to drought.

The threat of food insecurity is more prominent in the less developed countries, such as those in Sub-Saharan Africa (SSA), where the livelihood of people heavily depends on agriculture. SSA has been and is still one of the regions of the world with low agricultural productivity due to a variety of factors ranging from nutrient depleted soils to lack of investment in infrastructure and adverse climate change (Folberth et al., 2014; Gaiser et al., 2010; Webber et al., 2014). On this sub-continent, drought is a part of natural climatic variability varying from lack of rain in one season to prolonged drought periods of up to several years. The weak adaptation capacity has made most of the SSA countries' crop production vulnerable to drought (Challinor et al., 2007).

The crop drought vulnerability assessment is one of the most important schemes for the development of drought management plans. It provides the base to identify the root causes of drought impacts from physical and social aspects. However, vulnerability is a multidimensional and complex context (Sivakumar et al., 2014), and varies enormously across geography, income levels, livelihood types, and governance arrangements (O'Brien et al., 2004). Therefore, a broad diversity of drought vulnerability assessments has been conducted at different scales from national (Naumann et al., 2014; Simelton et al., 2009) to state, district, or farm levels (Antwi-Agyei et al., 2012; Keshavarz et al., 2014; Murthy et al., 2015; Shahid and Behrawan, 2008). Commonly used approaches in drought vulnerability assessment include modeling (Challinor et al., 2010; Fraser et al., 2013), fuzzy system (Cheng and Tao, 2010; Sun et al., 2014), or curve assessment (Guo et al., 2016; Wang et al., 2013).

A number of definitions have been proposed for vulnerability. The most widely used definition is from the IPCC (Intergovernmental Panel on Climate Change) Third Assessment Report which defines vulnerability as "a function of the character, magnitude, and rate of climate variation to which a system is exposed, its sensitivity, and its adaptive capacity" (IPCC, 2001). Therefore, vulnerability generally is described with three components, exposure, sensitivity, and adaptive capacity. "Exposure" is the likelihood of an occurring event. "Sensitivity" defines how a particular system will respond to a particular event. "Adaptive Capacity" is a measure of how a particular society withstands the impacts of drought.

Following the IPCC's definition of vulnerability, Allen Consulting Group (2005) illustrated 'vulnerability' diagrammatically (Figure 1.1) and explained that "exposure to a climate event combined with sensitivity to that event may be interpreted as potential harm. Furthermore, that potential impact might be exaggerated or compensated by adaptive capacity". In the context of drought, "Drought Exposure (*DEI*)" is representative of frequency, magnitude, and duration of drought. "Sensitivity", also referred to as "Crop Failure (*CFI*)", is crop's response to drought. "Adaptive Capacity (*AC*)" is representative of a variety of intrinsic or extrinsic factors exacerbating or mitigating drought vulnerability.

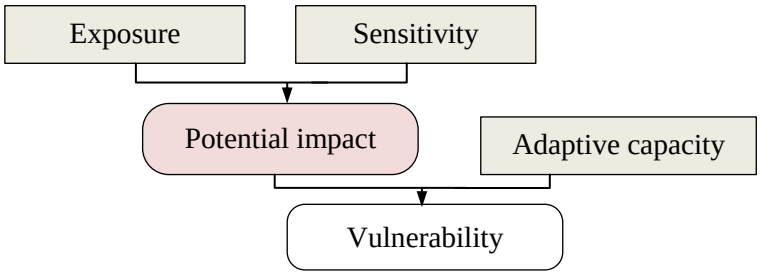

Figure 1.1. Conceptual and diagrammatic model of vulnerability first proposed by Schroter et al. (2004) and later modified by Allen Consulting Group (2005)

Many studies attempt to conceptualize vulnerability. Most of them have been established on the three components, *DEI*, *CFI*, and *AC*. However, a variety of approaches have been followed in the literature to aggregate these components to build the Drought Vulnerability Index (*DVI*). Table 1.1 summarizes some of the most implemented methods to aggregate *DEI*, *CFI*, and *AC* found in the literature. As shown in Table 1.1, methods 1-7 generally combined components of vulnerability linearly. Despite their simplicity, the main drawback of the linear aggregation is that the final *DVI* can vary within any range from 0 to ∞. This makes vulnerability classification and its spatial comparison across regions difficult. Method 8 attempts to assign various weights to each component. However, it also does not follow a standardized procedure for aggregation. The curve assessment method attempts to relate the components using different linear and nonlinear functions such as power or exponential

equations. However, the existing studies that implemented this approach did not look at details of the severity of vulnerability after curve fitting.

Table 1.1. Review of the construction of drought vulnerability built with the three components *DEI*, *CFI*, and *AC*

Aggregation method	Study	Region
1) $DVI = DEI + CFI - AC$	Antwi-Agyei et al. (2012) Murthy et al. (2015) De Stefano et al. (2015) Liu et al. (2013) Damm (2009) Gbetibouo and Hassan (2005) Gbetibouo and Ringler (2009) Epule et al. (2017)	Ghana India Europe Mongolia in China Germany South Africa South Africa Uganda
2) $DVI = \frac{DEI+CFI}{AC}$	Assimacopoulos et al. (2014) Fontaine and Steinemann (2009) Zarafshani et al. (2016)	Europe Washington DC or state? Iran
3) $DVI = \frac{DEI+CFI+(1-AC)}{3}$	Lindoso et al. (2014)	Brazilian farming
4) $DVI = CFI + AC$	Wu et al. (2013)	Yellow river in China
5) $DVI = \frac{CFI}{DEI}$	Simelton et al. (2009) Simelton et al. (2012) Fraser et al. (2013) Huai (2016)	China Global Global Australia
6) $DVI = f(\frac{DEI \times CFI}{ACI})$	Bryan et al. (2015)	Australia
7) $DVI = DEI + CFI + AC$	Wu et al. (2011)	China
8) Composite indicator: Assigning weights to different components. Aggregation methods varied in different studies.	Shahid and Behrawan (2008) Zarafshani et al. (2012) Gbetibouo et al. (2010) Naumann et al. (2014) Brooks et al. (2005) Keshavarz et al. (2017) Wirehn et al. (2015)	Bangladesh Iran farms South Africa Africa Africa Iran Sweden
9) Curve assessment: The relationship between components is explained by fitting curves such as exponential, polynomial, or power functions	Naumann et al. (2015) Wang et al. (2013) Guo et al. (2016) Jia et al. (2012)	Europe China Global China

Another important issue is that the variables used to calculate *DEI*, *CFI*, and *AC* vary significantly from one study to the other. For example, Simelton et al. (2009) used precipitation to define *DEI* in the agricultural vulnerability assessment in China. Later, the group used soil water as the proxy variable to measure drought exposure at global scale (Simelton et al., 2012). A recent study by Naumann et al. (2015) at the European scale applied different drought indices namely, Standardized Precipitation

Index (*SPI*), Standardized Precipitation Evapotranspiration Index (*SPEI*), and Reconnaissance Drought Index (*RDI*). Similarly, the variables used to formulate *CFI* varied in different studies. For example, Wang et al. (2011) used potential and actual yields, while Shahid and Behrawan (2008) employed crop land area as a measure of production.

The above brief review shows that vulnerability assessment should be improved in terms of standardizing its procedure to reflect its multidimensional characteristics. To address the challenge of crop drought vulnerability, it is important to develop an integrated approach in which the components of vulnerability are defined on a consistent and comparable basis with a reasonable spatial resolution. Such studies are still lacking in the literature and especially for SSA.

1.1.2 Application of crop models for spatially-explicit drought vulnerability assessment

The dynamic process-based crop models can be used as a tool for a better understanding of interactions of food production, risk to drought, and their vulnerability. They mimic plant physiology and crop response to weather and climate using a set of equations. These models link various processes such as crop growth, water-soil interactions, photosynthesis and carbon assimilation, nitrogen, phosphorous-carbon cycles, and agricultural management. An appropriate crop model should be responsive to the key climate variables and be able to model main crops, cropping systems and management strategies.

So far, a number of crop simulation models with different levels of complexity have been developed. Among others, the Environmental Policy Integrated Climate (EPIC) model (Williams et al., 1989), the Agricultural Production Systems sIMulator (APSIM) (Holzworth et al., 2015), the Decision Support System for Agrotechnology Transfer (DSSAT) (Jones and Sanyang, 2008), or the Lund-Potsdam-Jena managed Land model (LPJmL) (Sitch et al., 2003) have been used to evaluate the impact of climate anomaly on crop production in different regions (Folberth et al., 2013; Liu et al., 2016; Muller, 2013).

All crop models were initially developed for field scale studies. Over the last two decades and with increase in high resolution climate data, efforts have been made to extend their application to larger scales (Ewert et al., 2011; Liu and Yang, 2010) by dividing large areas into a number of subareas or girds. Many research groups have developed grid-based crop models to simulate crop productivity at different spatial extents. There is a general push towards increasing spatial resolutions (Liu et al., 2009) in assessing impacts of climate change (Rosenzweig et al., 2013), and extreme weather events, such as drought (Schauberger et al., 2017). These models have a considerable level of complexity. However, to be used for different purposes such as drought risk assessments, they need to be calibrated and evaluated in the regions they are applied (Ewert et al., 2015). Generally, a crop model should be complex enough to capture the response of the crop to the environment, yet, the parameters of crop models should be estimated at a reasonable scale (Challinor et al., 2007).

A large body of studies attempted to increase the reliability of crop modeling by increasing spatial resolution (Folberth et al., 2012), adjusting model parameters (Balkovic et al., 2013; Xiong et al., 2016), or model structures (Muller et al., 2017). However, an important lack in implementation of crop models at large scale is to increase their reliability in terms of replicating historic yield for a long period of time. The first constraint to such work is the lack of detailed crop-specific input data to the model. A second drawback is a lack of access to tools which can speed up the model simulation, because crop calibration at large scale is an expensive procedure in terms of time and computation. Therefore, further improvements are needed to develop a calibration procedure that can speed up the calibration and increase the reliability of simulated yields.

1.1.3 Crop drought vulnerability in the context of socio-economic conditions conferring adaptation

An important aspect requiring further investigation in the context of vulnerability is to understand why in some regions, small droughts can cause serious harvest loss (high *CFI*), whereas in some other regions, large droughts do not have such major effects on crop yields. The first case is representative of "sensitive" regions or high vulnerability, whereas the latter is a case of "resilient" with low vulnerability. In order to understand the possible reasons resulting in any of these two contrasting situations, biophysical as well as socio-economic factors should be taken into account in agricultural vulnerability assessment. Despite many studies on vulnerability assessment, little attention has been paid to quantify biophysical and socio-economic vulnerability separately and to measure the differences between them.

Apart from quantification of two aspects, many studies attempted to identify factors that influence adaptive capacity (Naumann et al., 2014; Stefano et al., 2015; Zarafshani et al., 2012). Such identification plays key role in defining strategies for mitigating the drought effects and vulnerability. This is important as countries that are extremely drought vulnerable also experience pressures such as population growth, poor infrastructure, resource depletion, weak governance, and poverty. Strategies that lessen pressures on resources, advance sustainable development, and enhance adaptive capacity can at the same time reduce the vulnerability to climate stresses. Therefore, understanding the relation between these factors and vulnerability is a prerequisite for targeting interventions to reduce the adverse impacts of drought.

1.2. Objectives of the research

The overall objective of this study is to assess drought vulnerability in SSA by developing and applying a spatially-explicit crop model. Maize is taken as a case study because it is the staple food in most of the countries in SSA. The specific tasks are (Figure 1.2):

Task 1: To develop a grid-based SSA scale crop model linked with an uncertainty based calibration tool in an interface called EPIC$^+$ for the purpose of replicating historic maize yields (1980-2012); model parameters are estimated and the uncertainties associated with parameter identification are evaluated.

Task 2: To apply the developed EPIC$^+$ model for quantifying maize physical drought vulnerability at grid level using the interaction of *DEI* and *CFI* in a probability-based framework and map maize physical drought vulnerability.

Task 3: To develop a framework that distinguishes physical crop drought vulnerability from socio-economic vulnerabilities across SSA countries and identify the gaps between the two.

Task 4: To link the crop drought vulnerability index (*CDVI*) to socio-economic determinants and identify factors important for mitigating crop drought vulnerability.

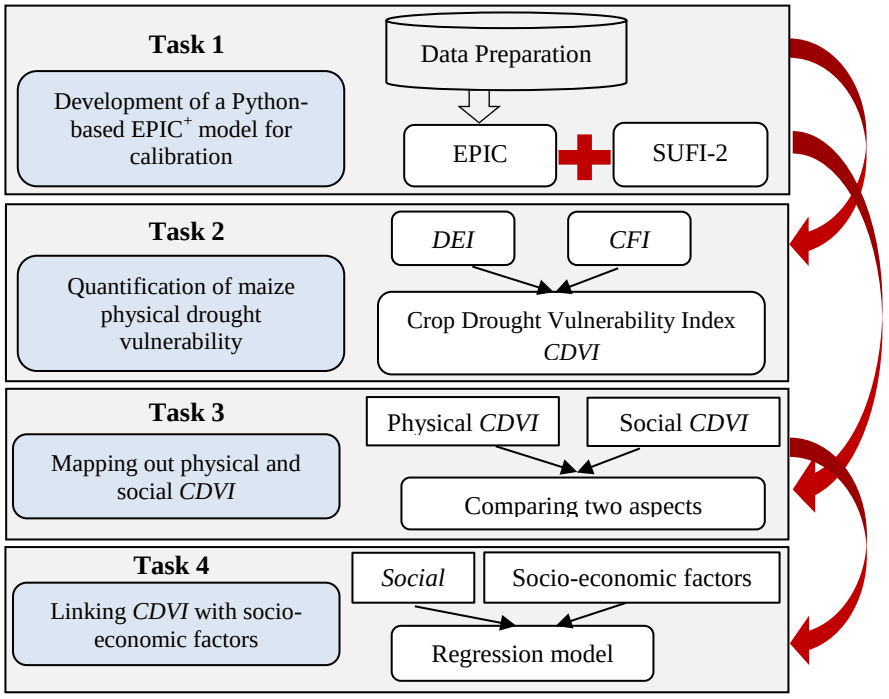

Figure 1.2. Research framework explaining connections of different tasks

1.3. Research outline and contents of dissertation

The dissertation consists of four research chapters (Chapters 2–5) and a general conclusion chapter (Chapter 6).

Chapter 2 introduces the EPIC$^+$ model which is an extended version of EPIC model linked with the Sequential Uncertainty Fitting algorithm for calibration. EPIC was applied to calibrate three sets of parameters referred to as planting date, agricultural operation parameters and model parameters in three steps to avoid parameter interactions. Using the FAO reported yields, crop and model parameters are separately determined for each country.

Chapter 3 quantifies maize biophysical drought vulnerability using the outputs obtained from the calibrated EPIC^{+} model. The developed crop drought vulnerability index links *DEI* to *CFI* in a power function. *DEI* and *CFI* were calculated based on cumulative distribution probability of precipitation and simulated maize yield. Vulnerability was then classified into five classes depending on the shapes of power function.

Chapter 4 uses the simulated crop yield and observed yields as a base to distinguish physical vulnerability from socio-economic vulnerability. The methodology measures the scope of each aspects and determines the hotspots of vulnerability on the two dimensions.

Chapter 5 presents the results on regression analysis which links crop drought vulnerability index to socio-economic factors from economic, human, resource, infrastructure and governance categories. The most influential factors are identified and their implications for vulnerability mitigation are discussed.

Chapter 6 draws the conclusions of the entire study regarding modeling, vulnerability and influential factors. The limitations of the study are discussed and three outlooks are recommended highlighting the importance for future study.

1.4. Reference

Allen Consulting Group (2005). Climate Change, Risk and Vulnerability: Promoting an efficient adaptation response in Australia.

Antwi-Agyei, P., Fraser, E. D. G., Dougill, A. J., Stringer, L. C., and Simelton, E. (2012). Mapping the vulnerability of crop production to drought in Ghana using rainfall, yield and socioeconomic data. *Applied Geography* **32**, 324-334.

Assimacopoulos, D., Kampragou, E., Andreu, J., Bifulco, C., de Carli, A., Lucia De Stefano, Dias, S., Gudmundsson, L., Haro-Monteagudo, D., Musolino, D., Paredes-Arquiola, J., Rego, F., Irmi Seidl, Abel Solera, Julia Urquijo, Henny van Lanen, and Wolters, W. (2014). FUTURE DROUGHT IMPACT AND VULNERABILITY -CASE STUDY SCALE.

Balkovic, J., van der Velde, M., Schmid, E., Skalsky, R., Khabarov, N., Obersteiner, M., Sturmer, B., and Xiong, W. (2013). Pan-European crop modelling with EPIC: Implementation, up-scaling and regional crop yield validation. *Agricultural Systems* **120**, 61-75.

Boyer, J., Byrne, P., Cassman, K., Cooper, M., Delmer, D., Greene, T., Gruis, F., Habben, J., Hausmann, N., and Kenny, N. (2013). The US drought of 2012 in perspective: A call to action. *Global Food Security* **2**, 139-143.

Brooks, N., Adger, W. N., and Kelly, P. M. (2005). The determinants of vulnerability and adaptive capacity at the national level and the implications for adaptation. *Global Environmental Change-Human and Policy Dimensions* **15**, 151-163.

Bryan, B. A., Huai, J., Connor, J., Gao, L., King, D., Kandulu, J., and Zhao, G. (2015). What actually confers adaptive capacity? Insights from agro-climatic vulnerability of Australian wheat. *Plos One* **10**.

Challinor, A., Wheeler, T., Garforth, C., Craufurd, P., and Kassam, A. (2007). Assessing the vulnerability of food crop systems in Africa to climate change. *Climatic Change* **83**, 381-399.

Challinor, A. J., Simelton, E. S., Fraser, E. D. G., Hemming, D., and Collins, M. (2010). Increased crop failure due to climate change: Assessing adaptation options using models and socio-economic data for wheat in China. *Environmental Research Letters* **5**.

Cheng, J., and Tao, J. P. (2010). Fuzzy Comprehensive Evaluation of Drought Vulnerability Based on the Analytic Hierarchy Process-An Empirical Study from Xiaogan City in Hubei Province. *International Conference on Agricultural Risk and Food Security 2010* **1**, 126-135.

Damm, M. (2009). Mapping Social-Ecological Vulnerability to Flooding-A sub-national approach for Germany, Bonn, Rheinischen Friedrich-Wilhelms-Universität.

De Stefano, L., González Tánago, I., Ballesteros, M., Urquijo, J., Blauhut, V., H. Stagge, J., and Stahl, K. (2015). METHODOLOGICAL APPROACH CONSIDERING DIFFERENT FACTORS INFLUENCING VULNERABILITY – PAN-EUROPEAN SCALE. Universidad Complutense de Madrid (UCM), Albert-Ludwigs-Universität Freiburg, Germany (ALU-FR), Universitetet i Oslo, Norway (UiO)

Epule, T. E., Ford, J. D., and Lwasa, S. (2017). Projections of maize yield vulnerability to droughts and adaptation options in Uganda. *Land Use Policy* **65**, 154-163.

Ewert, F., Rotter, R. P., Bindi, M., Webber, H., Trnka, M., Kersebaum, K. C., Olesen, J. E., van Ittersum, M. K., Janssen, S., Rivington, M., Semenov, M. A., Wallach, D., Porter, J. R., Stewart, D., Verhagen, J., Gaiser, T., Palosuo, T., Tao, F., Nendel, C., Roggero, P. P., Bartosova, L., and Asseng, S. (2015). Crop modelling for integrated assessment of risk to food production from climate change. *Environmental Modelling & Software* **72**, 287-303.

Ewert, F., van Ittersum, M. K., Heckelei, T., Therond, O., Bezlepkina, I., and Andersen, E. (2011). Scale changes and model linking methods for integrated assessment of agri-environmental systems. *Agriculture Ecosystems & Environment* **142**, 6-17.

Folberth, C., Gaiser, T., Abbaspour, K. C., Schulin, R., and Yang, H. (2012). Regionalization of a large-scale crop growth model for Sub-Saharan Africa: Model setup, evaluation, and estimation of maize yields. *Agriculture Ecosystems & Environment* **151**, 21-33.

Folberth, C., Yang, H., Gaiser, T., Abbaspour, K. C., and Schulin, R. (2013). Modeling maize yield responses to improvement in nutrient, water and cultivar inputs in Sub-Saharan Africa. *Agricultural Systems* **119**, 22-34.

Folberth, C., Yang, H., Gaiser, T., Liu, J. G., Wang, X. Y., Williams, J., and Schulin, R. (2014). Effects of ecological and conventional agricultural intensification practices on maize yields in Sub-Saharan Africa under potential climate change. *Environmental Research Letters* **9**, 1-12.

Fontaine, M. M., and Steinemann, A. C. (2009). Assessing vulnerability to natural hazards: Impact-based method and application to drought in Washington state. *Natural Hazards Review* **10**, 11-18.

Fraser, E. D. G., Simelton, E., Termansen, M., Gosling, S. N., and South, A. (2013). "Vulnerability hotspots": Integrating socio-economic and hydrological models to identify where cereal production may decline in the future due to climate change induced drought. *Agricultural and Forest Meteorology* **170**, 195-205.

Gaiser, T., de Barros, I., Sereke, F., and Lange, F. M. (2010). Validation and reliability of the EPIC model to simulate maize production in small-holder farming systems in tropical sub-humid West Africa and semi-arid Brazil. *Agriculture Ecosystems & Environment* **135**, 318-327.

Gbetibouo, G. A., and Hassan, R. M. (2005). Measuring the economic impact of climate change on major South African field crops: a Ricardian approach. *Global and Planetary Change* **47**, 143-152.

Gbetibouo, G. A., and Ringler, C. (2009). Mapping South African farming sector vulnerability to climate change and variability: A Subnational assessment. Environment and Production Technology Division, The International Food Policy Research Institute (IFPRI).

Gbetibouo, G. A., Ringler, C., and Hassan, R. (2010). Vulnerability of the South African farming sector to climate change and variability: An indicator approach. *Natural Resources Forum* **34**, 175-187.

Guo, H., Zhang, X., Lian, F., Gao, Y., Lin, D., and Wang, J. a. (2016). Drought risk assessment based on vulnerability surfaces: a case study of maize. *Sustainability* **8**.

Holzworth, D. P., Snow, V., Janssen, S., Athanasiadis, I. N., Donatelli, M., Hoogenboom, G., White, J. W., and Thorburn, P. (2015). Agricultural production systems modelling and software: Current status and future prospects. *Environmental Modelling & Software* **72**, 276-286.

Huai, J. J. (2016). Integration and typologies of vulnerability to climate change: A case study from Australian wheat sheep zones. *Scientific Reports* **6**.

IPCC (2001). Climate change 2001: Impacts, adaptation, and vulnerability.

Jia, H. C., Wang, J. A., Cao, C. X., Pan, D. H., and Shi, P. J. (2012). Maize drought disaster risk assessment of China based on EPIC model. *International Journal of Digital Earth* **5**, 488-515.

Jones, M. P., and Sanyang, S. (2008). Multiple pressures of soaring food prices and food security in Africa. *Current Science* **95**, 1317-1319.

Keshavarz, M., Karami, E., and Zibaei, M. (2014). Adaptation of Iranian farmers to climate variability and change. *Regional Environmental Change* **14**, 1163-1174.

Keshavarz, M., Maleksaeidi, H., and Karami, E. (2017). Livelihood vulnerability to drought: A case of rural Iran. *International Journal of Disaster Risk Reduction* **21**, 223-230.

Lindoso, D. P., Rocha, J. D., Debortoli, N., Parente, I. I., Eiro, F., Bursztyn, M., and Rodrigues, S. (2014). Integrated assessment of smallholder farming's vulnerability to drought in the Brazilian Semi-arid: a case study in Ceara. *Climatic Change* **127**, 93-105.

Lipper, L., Thornton, P., Campbell, B. M., Baedeker, T., Braimoh, A., Bwalya, M., Caron, P., Cattaneo, A., Garrity, D., Henry, K., Hottle, R., Jackson, L., Jarvis, A., Kossam, F., Mann, W., McCarthy, N., Meybeck, A., Neufeldt, H., Remington, T., Sen, P. T., Sessa, R., Shula, R., Tibu, A., and Torquebiau, E. F. (2014). Climate-smart agriculture for food security. *Nature Climate Change* **4**, 1068-1072.

Liu, J. G., and Yang, H. (2010). Spatially explicit assessment of global consumptive water uses in cropland: Green and blue water. *Journal of Hydrology* **384**, 187-197.

Liu, J. G., Zehnder, A. J. B., and Yang, H. (2009). Global consumptive water use for crop production: The importance of green water and virtual water. *Water Resources Research* **45**.

Liu, W., Yang, H., Folberth, C., Wang, X., Luo, Q., and Schulin, R. (2016). Global investigation of impacts of PET methods on simulating crop-water relations for maize. *Agricultural and Forest Meteorology* **221**, 164–175.

Liu, X. Q., Wang, Y. L., Peng, J., Braimoh, A. K., and Yin, H. (2013). Assessing vulnerability to drought based on exposure, sensitivity and adaptive capacity: A case study in middle Inner Mongolia of China. *Chinese Geographical Science* **23**, 13-25.

Muller, C. (2013). African Lessons on Climate Change Risks for Agriculture. *Annual Review of Nutrition, Vol 33* **33**, 395-411.

Muller, C., Elliott, J., Chryssanthacopoulos, J., Arneth, A., Balkovic, J., Ciais, P., Deryng, D., Folberth, C., Glotter, M., Hoek, S., Iizumi, T., Izaurralde, R. C., Jones, C., Khabarov, N., Lawrence, P., Liu, W. F., Olin, S., Pugh, T. A. M., Ray, D. K., Reddy, A., Rosenzweig, C., Ruane, A. C., Sakurai, G., Schmid, E., Skalsky, R., Song, C. X., Wang, X. H., de Wit, A., and Yang, H. (2017). Global gridded crop model evaluation: benchmarking, skills, deficiencies and implications. *Geoscientific Model Development* **10**, 1403-1422.

Murthy, C. S., Yadav, M., Ahamed, J. M., Laxman, B., Prawasi, R., Sai, M. V. R. S., and Hooda, R. S. (2015). A study on agricultural drought vulnerability at disaggregated level in a highly irrigated and intensely cropped state of India. *Environmental Monitoring and Assessment* **187**.

Naumann, G., Barbosa, P., Garrote, L., Iglesias, A., and Vogt, J. (2014). Exploring drought vulnerability in Africa: An indicator based analysis to be used in early warning systems. *Hydrology and Earth System Sciences* **18**, 1591-1604.

Naumann, G., Spinoni, J., Vogt, J. V., and Barbosa, P. (2015). Assessment of drought damages and their uncertainties in Europe. *Environmental Research Letters* **10**, 1748-9326.

O'Brien, K., Leichenko, R., Kelkar, U., Venema, H., Aandahl, G., Tompkins, H., Javed, A., Bhadwal, S., Barg, S., Nygaard, L., and West, J. (2004). Mapping vulnerability to multiple stressors: climate change and globalization in India. *Global Environmental Change-Human and Policy Dimensions* **14**, 303-313.

Rosenzweig, C., Jones, J. W., Hatfield, J. L., Ruane, A. C., Boote, K. J., Thorburn, P., Antle, J. M., Nelson, G. C., Porter, C., Janssen, S., Asseng, S., Basso, B., Ewert, F., Wallach, D., Baigorria, G., and Winter, J. M. (2013). The Agricultural Model Intercomparison and Improvement Project (AgMIP): Protocols and pilot studies. *Agricultural and Forest Meteorology* **170**, 166-182.

Schauberger, B., Archontoulis, S., Arneth, A., Balkovic, J., Ciais, P., Deryng, D., Elliott, J., Folberth, C., Khabarov, N., Muller, C., Pugh, T. A. M., Rolinski, S., Schaphoff, S., Schmid, E., Wang, X. H., Schlenker, W., and Frieler, K. (2017). Consistent negative response of US crops to high temperatures in observations and crop models. *Nature Communications* **8**.

Schroter, D., Metzger, M. J., Cramer, W., and Leemans, R. (2004). Vulnerability assessment-analysing the human-environment system in the face of global environmental change. *In* "the ESS Bulletin", Vol. 2.

Shahid, S., and Behrawan, H. (2008). Drought risk assessment in the western part of Bangladesh. *Natural Hazards* **46**, 391-413.

Simelton, E., Fraser, E. D. G., Termansen, M., Benton, T. G., Gosling, S. N., South, A., Arnell, N. W., Challinor, A. J., Dougill, A. J., and Forster, P. M. (2012). The socioeconomics of food crop production and climate change vulnerability: A global scale quantitative analysis of how grain crops are sensitive to drought. *Food Security* **4**, 163-179.

Simelton, E., Fraser, E. D. G., Termansen, M., Forster, P. M., and Dougill, A. J. (2009). Typologies of crop-drought vulnerability: an empirical analysis of the socio-economic factors that influence the sensitivity and resilience to drought of three major food crops in China (1961-2001). *Environmental Science & Policy* **12**, 438-452.

Sitch, S., Smith, B., Prentice, I. C., Arneth, A., Bondeau, A., Cramer, W., Kaplan, J., Levis, S., Lucht, W., and Sykes, M. T. (2003). Evaluation of ecosystem dynamics, plant geography and terrestrial carbon cycling in the LPJ dynamic global vegetation model. *Global Change Biology* **9**, 161-185.

Sivakumar, M. V. K., Wilhite, D. A., Pulwarty, R. S., and Stefanski, R. (2014). The High-Level Meeting on National Drought Policy. *Bulletin of the American Meteorological Society* **95**, 85-88.

Stefano, L. D., Tánago, I. G., Mario Ballesteros, Julia Urquijo, Veit Blauhut, James H. Stagge, and Stahl, K. (2015). Methodological approach considering different factors influencing vulnerability- Pan-Europran scale. DROUGHT-R&SPI: Fostering European Drought Research and Science-Policy Interfacing project.

Sun, Z. Y., Zhang, J. Q., Zhang, Q., Hu, Y., Yan, D. H., and Wang, C. Y. (2014). Integrated risk zoning of drought and waterlogging disasters based on fuzzy comprehensive evaluation in Anhui Province, China. *Natural Hazards* **71**, 1639-1657.

Thornton, P. K., Ericksen, P. J., Herrero, M., and Challinor, A. J. (2014). Climate variability and vulnerability to climate change: a review. *Global change biology* **20**, 3313-3328.

Wang, D. B., Hejazi, M., Cai, X. M., and Valocchi, A. J. (2011). Climate change impact on meteorological, agricultural, and hydrological drought in central Illinois. *Water Resources Research* **47**, 1-13.

Wang, Z. Q., He, F., Fang, W. H., and Liao, Y. F. (2013). Assessment of physical vulnerability to agricultural drought in China. *Natural Hazards* **67**, 645-657.

Webber, H., Gaiser, T., and Ewert, F. (2014). What role can crop models play in supporting climate change adaptation decisions to enhance food security in Sub-Saharan Africa? *Agricultural Systems* **127**, 161-177.

Wheeler, T., and Von Braun, J. (2013). Climate change impacts on global food security. *Science* **341**, 508-513.

Williams, J. R., Jones, C. A., Kiniry, J. R., and D.A., S. (1989). The EPIC crop growth model. *Transaction of the ASAE*, 497-454.

Wirehn, L., Danielsson, A., and Neset, T. S. S. (2015). Assessment of composite index methods for agricultural vulnerability to climate change. *Journal of Environmental Management* **156**, 70-80.

Wu, D., Yan, D. H., Yang, G. Y., Wang, X. G., Xiao, W. H., and Zhang, H. T. (2013). Assessment on agricultural drought vulnerability in the Yellow River basin based on a fuzzy clustering iterative model. *Natural Hazards* **67**, 919-936.

Wu, J. J., He, B., Lu, A. F., Zhou, L., Liu, M., and Zhao, L. (2011). Quantitative assessment and spatial characteristics analysis of agricultural drought vulnerability in China. *Natural Hazards* **56**, 785-801.

Xiong, W., Rastislav, S., Cheryl H., P., Juraj, B., James, W. J., and Di , Y. (2016). Calibration-induced uncertainty of the EPIC model to estimate climate change impact on global maize yield. *Journal of Advances in Modeling Earth Systems* **8**, 1358–1375.

Zarafshani, K., Sharafi, L., Azadi, H., Hosseininia, G., De Maeyer, P., and Witlox, F. (2012). Drought vulnerability assessment: The case of wheat farmers in Western Iran. *Global and Planetary Change* **98-99**, 122-130.

Zarafshani, K., Sharafi, L., Azadi, H., and Van Passel, S. (2016). Vulnerability assessment models to drought: toward a conceptual framework. *Sustainability* **8**, 1-16.

Chapter 2

Uncertainty-based auto-calibration for crop yield – the EPIC^{+} procedure for a case study in Sub-Saharan Africa

Based on

Uncertainty-based auto-calibration for crop yield – the EPIC^{+} procedure for a case study in Sub-Saharan Africa

European Journal of Agronomy, 93: 57-72 (2018)

Authors

Bahareh Kamali[1, 2], Karim C. Abbaspour[1], Anthony Lehmann[3], Bernhard Wehrli[2], Hong Yang[1,4]

[1] *Eawag, Swiss Federal Institute of Aquatic Science and Technology, Duebendorf, Switzerland*

[2] *Institute of Biogeochemistry and Pollutant Dynamics, ETH Zurich, Switzerland*

[3] *EnviroSPACE, Forel institute for Environmental Sciences, University of Geneva, Geneva, Switzerland*

[4] *Department of Environmental Sciences, University of Basel, Switzerland*

Abstract

Process-based crop models are increasingly used to assess the effects of different agricultural management practices on crop yield. However, calibration of historic crop yield is a challenging and time-consuming task due to data limitation and lack of adaptive auto-calibration tools compatible with the model to be calibrated on different spatial and temporal scales. In this study, we linked the general auto-calibration procedure SUFI-2 (Sequential Uncertainty Fitting Procedure) to the crop model EPIC (Environmental Policy Integrated Climate) to calibrate maize yield in Sub-Saharan African (SSA) countries. This resulted in the creation of a user-friendly software, EPIC$^+$, for crop model calibration at spatial levels of grid to continent. EPIC$^+$ greatly speeds up the calibration process with quantification of parameter ranges and prediction uncertainty. In the SSA application, we calibrated three sets of parameters referred to as Planting Date (*PD*), Operation (e.g., fertilizer application, planting density), and Model parameters (e.g., harvest index, biomass-energy ratio, water stress harvest index, SCS curve number) in three steps to avoid parameter interaction and identifiability problems. In the first step, by adjusting *PD* parameters, the simulated yield results improved in Western and Central African countries. In the next step, Operation parameters were calibrated for individual countries resulting in a better model performance by more than 40% in many countries. In the third step, Model parameters were calibrated with significant improvements in all countries by an average of 50%. We also found that countries with less socio-political volatility benefited most from the calibration. For countries where agricultural production had trends, we suggest improving the calibration results by applying linear de-trending transformations, which we will explore in more detail in a subsequent study.

2.1. Introduction

Process-based crop models are increasingly used to assess the impact of land use and climate change, management, and adaptation strategies in relation to agricultural production. They advance our understanding of crop behavior in macro-environment and assessment of potential crop production in different agricultural systems. Currently, different crop models are used widely. These include the EPIC (Environmental Policy Integrated Climate) model (Williams et al., 1989), DSSAT (Decision Support System for Agrotechnology Transfer) (Jones et al., 2003), APSIM (Agricultural Production Systems sIMulator) (Holzworth et al., 2014), ALMANAC (Agricultural Land Management Alternative with Numerical Assessment Criteria) (Kiniry et al., 2013), CROPSYST (Cropping Systems Simulation Model) (Stockle et al., 2003), and WOFOST (WOrld FOod STudies) (Van Ittersum et al., 2002), etc. These models have been implemented for a wide variety of applications from assessing the impact of climate change or increased carbon dioxide concentration in the atmosphere (Oliver et al., 2009; Stockle, 1992) to environmental pollution (Manevski et al., 2016).

Early crop models were developed based on field studies and were driven by input data and parameters that had physical interpretations and represented various crop characteristics (Xiong et al.,

2014). Their applications were later extended to regional, national, continental, or global levels. There is a growing literature on the application of crop models (Angulo et al., 2013a; Folberth et al., 2012a; Liu et al., 2007; Tao et al., 2009) to project future crop yields based on scenarios of climate change (Challinor et al., 2009; Lobell et al., 2011; Niu et al., 2009), management practices (Liu and Yang, 2010; Saseendran et al., 2004; Vanuytrecht et al., 2014), and carbon sequestration (Causarano et al., 2008; Doraiswamy et al., 2007). A starting point for application of crop models is to investigate if they adequately represent the reality and are able to replicate data from historic periods (Bryan et al., 2009; Webber et al., 2014) by calibration and validation of the model under certain ranges of uncertainties. This is of essence, as the knowledge gained from the historic analysis can validate the predictive correctness of the future crop simulation, enhance its reliability for assessing climate change impacts, and facilitate societal preparedness to deal with climate impacts (Challinor et al., 2009).

In the literature, automatic calibration of crop models is mostly tested on farms or small regions (Causarano et al., 2008; Sumathy et al., 2017), or on different crop varieties and parameters in each model (Ahmed et al., 2016; Sexton et al., 2016; Zhao et al., 2014). A few calibration programs such as SPOTPY (SPOTting Model Parameters Using a Ready-Made Python Package) (Houska et al., 2015) and PEST (Parameter Estimation) (Doherty, 2001) are available for use with different models. However, a major problem with implementing these algorithms is the lack of compatibility with the input/output format of crop model. Therefore, calibration of large areas is mostly performed manually by trial and error (Balkovic et al., 2013). Other common practices include:

1) applying default parameters or using universally recommended values without accounting for the spatial variability of parameters (Balkovic et al., 2013; Folberth et al., 2012a);
2) temporally aggregating observed yield and adjusting parameters based on deviation from long-term averages without considering temporal yield fluctuations (Liu et al., 2016; Xiong et al., 2016);
3) spatially aggregating yields of large area and neglecting spatial variations of yields or parameters (Angulo et al., 2013a; Chun et al., 2016).

However, efforts to regionalize parameters and take into account temporal fluctuation of yield have often failed due to lack of data availability, knowledge of parameters, and efficient calibration models. Spatially detailed calibration of crop models on large areas is generally impractical by using manual approaches. The method used should enable implementation of different approaches to tune parameters within reasonable time and on multiple locations simultaneously.

The goal of this study is to develop an auto-calibration procedure that fills the above needs and use it to simulate maize yield in SSA. To achieve this, we coupled the EPIC crop model with the calibration algorithm SUFI-2 (Sequential Uncertainty Fitting Procedure) (Abbaspour et al., 2004; Abbaspour et al., 2007) using a graphical user interface (GUI) written in Python (hereafter EPIC$^+$). The user-friendly coupled program is referred to as EPIC$^+$ and is freely available upon request. EPIC$^+$ can be used to: 1) calibrate yield on different temporal and spatial scales using different criteria for

evaluating model performance, 2) identify spatial variability of parameters, and 3) speed up the calibration process. In this work, we obtained spatially distributed parameters for each country in SSA.

2.2. Methodology

2.2.1. Site description

SSA is home to over one billion people. Average annual precipitation across SSA is 795 mm yr^{-1}, with diverse distribution ranging from 100 mm yr^{-1} in the Sahelian Strip to over 2,000 mm yr^{-1} in the Gulf of Guinea (Ward et al., 2016). The region contains very large dryland areas. Small landholders depend on agriculture as their primary livelihood source. Agricultural development in SSA is facing considerable challenges (Ward et al., 2016). Population increases and climate change have exacerbated the risk of hunger (Iglesias et al., 2011). Maize is the most widely grown crop and is a staple food in SSA, accounting for nearly 20% of the total calorie intake (Folberth et al., 2014). It is mostly cultivated under rainfed conditions with <3% of the area irrigated (Portmann et al., 2010). From the 1990s to the 2010s average maize yields in SSA have increased from around 1.4 to 1.8 t ha^{-1}, and from 2.5 to 4.5 t ha^{-1} in South Africa, but are still at the very bottom of globally reported maize yields (FAO, 2012).

2.2.2. Programs EPIC and SUFI-2

EPIC is designed to simulate crop-related processes at a specific site and operates on daily time step. The model offers different options to calculate potential evapotranspiration and agricultural operations and has been successfully applied to a wide range of agricultural studies under different climatic conditions, and different crops and management schemes (Balkovic et al., 2013; Folberth et al., 2014; Gassman et al., 2005). Further information on EPIC crop-related processes is given in Williams et al. (1989). We extended the application of EPIC from one to multiple sites using a GUI written in Python. This extension is done through dividing a country into a number of grids depending on the spatial resolution (e.g. 1^{o}, 0.5^{o}, 0.25^{o} or smaller) defined by the user and then treating each grid as a site. This flexibility allows the user to apply $EPIC^{+}$ at field or continental scales. For example, 0.5^{o} might be valid for applying EPIC at the continental scale, but is very coarse in field scale studies. Similarly, obtaining data at field scale for an entire continent is not feasible because of the large number of grids. In $EPIC^{+}$, each country can also be split into a number of sub-regions and yields aggregated for that sub-region.

SUFI-2 is used to calibrate different agro-hydrologic projects. It is already coupled to the Soil and Water Assessment Tool (SWAT) to calibrate components such as hydrology (Abbaspour et al., 2015; Azari et al., 2016; Me et al., 2015), crop yield (Azimi et al., 2013; Faramarzi et al., 2010; Vaghefi et al., 2015), and sediment transport (Lemann et al., 2016; Monteiro et al., 2016). SUFI-2 is an iterative

procedure that accounts for parameter uncertainty from all sources (e.g., inputs, parameters, and model structure). Uncertainties are expressed through distributions assigned to parameters, which are described by a multivariate uniform distribution in a parameter hypercube. Latin hypercube is used to sample the parameters. The output uncertainty is quantified as the 95% prediction uncertainty band (95PPU) calculated at the 2.5% and 97.5% levels of the cumulative distribution function of the output variables (Abbaspour et al., 2007). Two indices quantify the goodness of model calibration and uncertainty level. These are *P-factor* and *R-factor* (Abbaspour, 2015). *P-factor* is the fraction of measured data bracketed by the 95PPU band and varies from 0 to 1, where 1 indicates 100% bracketing of the measured data within model prediction uncertainty. *R-factor*, on the other hand, is the ratio of the average width of the 95PPU band to the standard deviation of the measured variable. The SUFI-2 algorithm tries to achieve a high *P-factor* while keeping the *R-factor* as small as possible.

2.2.3. EPIC$^+$ architecture

The architecture of EPIC$^+$ consists of four modules (Figure 2.1). The modules of "General settings" and "Operation settings" deal with the extension of EPIC from field to a desired level, and the modules of "Parameterization" and "SUFI-2 calibration" are for setting up calibration algorithm. The four modules together appear in a user-friendly workspace. The function of each module is briefly described as follows:

i) In the "General settings" module, inputs of physiographic information of all desired grids within the selected region are defined. These include elevation, slope, rainfed harvested area, irrigated harvested area, as well as climate, soil, and sub region codes in ASCII format. EPIC files required for simulation are defined and the printing formats are provided.

ii) In the "Operation settings" module, the agricultural operations from planting to harvest (such as tillage, planting, fertilization, and irrigation), the dates of each operations, and their relevant parameters are defined. Two options are available for defining agricultural operations (OPS1 and OPS2). OPS1 is used to calibrate planting date (*PD*). Using OPS1, *PD* for each grid can vary in a given range (e.g. between earliest and latest *PD*). OPS2 is used when the *PD* is fixed for each grid and when other parameters such as potential heat units (*PHU*) and fertilizer application rates need to be calibrated.

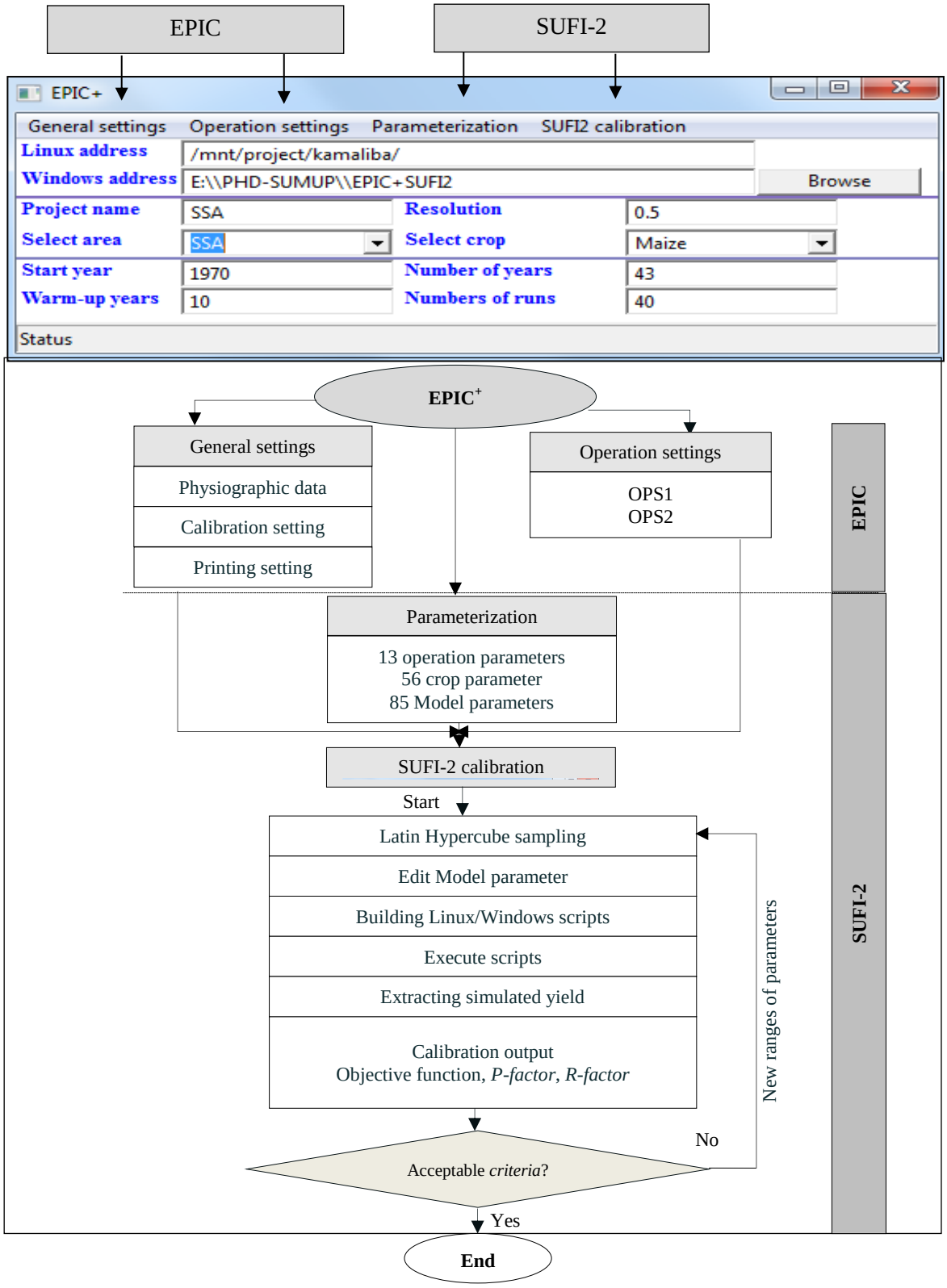

Figure 2.1. Schematic representation of the main window of EPIC^{+} and flow of the four modules.

iii) In the "Parameterization" module, there are three categories of parameters: Operation (13 parameters), Crop (56 parameters), and Model (85 parameters) parameters. The 13 Operation parameters, such as *PHU*, are stored in the TEMP.OPS file, the 56 Crop parameters, such as Harvest

Index (*HI*) are included in the CROPCOM.DAT file, and the 85 Model parameters, such as water stress-harvest index, are documented in the file PARM0810.DAT of EPIC.

iv) In the "SUFI-2 calibration" module, parameters and their ranges are chosen for calibration. The sampled values, using a Latin hypercube scheme, are stored in corresponding EPIC files (e.g. TEMP.OPS, CROPCOM.DAT, and PARM0810.DAT). Python scripts are built for Windows and Linux operating systems to run EPIC on each grid cell. The Linux script is optimized to speed up the process of simulation and is more relevant for larger scale applications. After simulations, the desired output variable (e.g. yield) is extracted from EPIC output files and aggregated to a user-defined level (here national level) using the weighted areal averages based on rainfed (A_{RF}) and irrigated (A_{IR}) cultivated areas as shown in Eq 2.1 (Folberth et al., 2012b; Liu et al., 2007):

$$Y_{sim} = \frac{\sum_{i=1}^{n} Y_{RF,i} \times A_{RF,i} + Y_{IR,i} \times A_{IR,i}}{\sum_{i=1}^{n} (A_{RF,i} + A_{IR,i})} \quad (2.1)$$

where $Y_{RF,i}$ *and* $Y_{IR,i}$ are, respectively, rainfed and irrigated yields obtained from the model for grid *i* in t ha^{-1}.

In the next step, SUFI-2 parameters, *P-factor*, and *R-factor* are calculated using a choice of 11 different objective functions (Abbaspour, 2015). Upon acceptable values of *P-factor* and *R-factor*, the parameter ranges are considered as the calibrated parameter ranges of the study area (Figure 2.1). Otherwise, another iteration is performed using a set of new parameter ranges calculated based on the best parameter sets of the current iteration and the 95PPU band (Abbaspour et al., 2007).

2.2.4. EPIC^{+} setup for SSA countries

2.2.4.1. Input data for EPIC^{+}

EPIC^{+} was applied to simulate maize yield in SSA countries at a spatial resolution of 0.5^{o} aggregated to a national scale. All data required were prepared at this resolution and are summarized in Table 2.1. The site-specific input data include longitude, latitude, slope, and elevation (DEM). Soil database included parameters such as organic carbon content [%], pH, cation exchange capacity [mol kg^{-1}], sand [%], silt [%], bulk density [t m^{-3}], soil layer depth [m], and electrical conductivity [mmho cm^{-1}]. Agricultural operations such as tillage, fertilizer application, planting and harvest dates were set chronologically in the model based on fixed dates obtained for each operation. Planting and harvest dates were obtained from the sources summarized in Table 2.1. Fertilizers application (nitrogen (N), phosphorus (P), and potassium (K)) and tillage were, respectively, done 15 and 10 days before planting (Wang et al., 2005).

The total number of heat units required for a plant to reach maturity (*PHU*) was calculated for each grid based on the maximum and minimum temperatures, *PD*, and length of growing seasons (Sacks et al., 2010). The heat unit (*HU*) accumulation for a given day is calculated as:

$$HU = T_{avg} - T_{base} \qquad if \;\; T_{avg} > T_{base} \tag{2.2}$$

where T_{avg} is the average daily temperature (^oC) and T_{base} is the plant's base temperature for growth (8 ^{o}C for maize). The total number of heat units required for a plant to reach maturity (in m days) is calculated as:

$$PHU = \sum_{d=1}^{m} HU_d \tag{2.3}$$

We calibrated our model for the period 1970-2012, considering the first 10 years as equilibrating period for soil moisture and nitrogen initial conditions. The reported results are thus for the period of 1980-2012. The annual maize yields reported by FAO for different countries (FAO, 2012) were used as observed yield values (Y_{obs}). As far as we know, the FAO reported data are the only publically available source for maize yield time series in SSA.

Table 2.1. Summary of input data and their sources used for simulating maize in SSA. All data were transformed into 0.5^{o}x0.5^o resolution

Input data	Description	Resolution	Year	Source
DEM, Slope	Digital elevation model GTOPO30	1 km (5″x5″)	Edition 2004	U.S. Geological Survey (2004)
A_{RF}	Rainfed cultivated area	10 km (5′x5′)	2000	MIRCA2000[1] version 1.1 Portmann et al. (2010)
Climate	Daily maximum and minimum temperature, precipitation, solar radiation, relative humidity, wind speed, CO_2 concentration	50 km (0.5^{o}x0.5^o)	1970-2012	WFDEI[2] meteorological forcing data Weedon et al. (2011)
Soil	Soil map and database	10 km (5′x5′)	2006	ISRIC-WISE[3] Batjes (2006)
Planting and harvesting dates	Based on temperature linked to crop calendar	50 km (0.5^{o}x0.5^o)	1990s to early 2000s	SAGE[4] Sacks et al. (2010)
Fertilizer	Fertilizer use (N, P, K)	National	2002	FertiStat (FAO, 2007)

[1] Monthly Irrigated and Rainfed Crop Areas
[2] WATCH-Forcing-Data-ERA-Interim
[3] International Soil Reference and Information Centre-World Inventory of Soil Emission Potentials
[4] Center for Sustainability and the Global Environment

2.2.5. Efficiency criteria, sensitivity analysis, and parameterization

As model efficiency criteria, we used coefficient of determination, R^2, and standardized root mean square error (*RSR*) (Singh et al., 2005). The two functions consider different charactrisitics of the yield series. R^2 describes the level of linearity between the two signals and varies between 0 and 1, with 1 being the best value. *RSR* is a measure of the difference between the observed and simulated yields. It varies between 0 and ∞, where 0 is the best value. *RSR* was used as the objective function, *Q*, expressed as:

$$Q = RSR = \frac{RMSE}{STDEV_{obs}} = \frac{\sqrt{\sum_{t=1}^{Y}(Y_{obs,t} - Y_{sim,t})^2}}{\sqrt{\sum_{t=1}^{Y}(Y_{obs,t} - \bar{Y}_{obs})^2}} \quad (2.4)$$

where $Y_{obs,t}$ and $Y_{sim,t}$ are observed and simulated yields, respectively. Parameter sensitivities were determined by calculating a multiple regression system where the parameters are regressed against the objective functions as:

$$Q = \alpha + \sum_{i=1}^{m} \beta_i b_i \quad (2.5)$$

Where α is he constant of regression and β_i is the coefficient of parameter b_i. A *t-test* is used to identify the relative significance of each parameter. The sensitivities given above are estimates of the average changes in the objective function resulting from changes in each parameter, while all other parameters are changing. This gives relative sensitivities based on linear approximations and, hence, only provides partial information about the sensitivity of the objective function to model parameters. In this analysis, the larger, in absolute value, the value of *t*-stat, and the smaller the *p*-value, the more sensitive is the parameter.

To minimize parameter interaction and consequently identifiability problems, in Step 1 we ran 50 simulations with planting dates alone and then fixed the parameters to their best values (i.e., the values that produced the smallest objective function) for each grid within a country (Table 2.2). The SAGE planting dates used in this study were the results of compilation from six sources and contain three variables: earliest time for planting date, latest time for planting date, and mean planting date. As highlighted by Sacks et al. (2010), the SAGE approach has several limitations such as: 1) the variables being estimated are at the country or relatively large scales; and 2) the observation data used to estimate planting dates are mostly for the period of 1990s and early 2000s. Therefore, it does not capture changes in other time spans. To partially overcome this limitation for the period of our study (1980-2012), we let the *PD*s vary within the earliest and the latest dates proposed by SAGE for different countries using grid-based parameterization feature we embedded in EPIC$^+$.

Table 2.2. Default parameters and initial parameter ranges (uncertainties) used in Steps 1 to 3 of the proposed calibration procedure.

		Parameters	Description	Default values	Initial ranges
Step 1	Planting date	*PD*	Planting date	Gridded data	AC[3] [earliest date, latest date]
Step 2	Operation parameters	*PHU*	Potential heat unit [^{0}C]	*[1]	RC[4][-0.45, 0.45]
		Pdensity	Planting density [Plant m^{-2}]	5	RC [-0.45, 0.45]
		N-app	Maximum annual nitrogen application [kg.ha^{-1}]	*[2]	RC [-0.45, 0.45]
		K-app	Potassium application rate [kg ha^{-1}]	6	RC [-0.45, 0.45]
		BFT0	Nitrogen fertilizer trigger [-]	0.85	RC [-0.45, 0.45]
		P-app	Phosphorus application rate [kg ha^{-1}]	*[2]	RC [-0.45, 0.45]
Step 3	Crop parameters	*WA*	Biomass-energy ratio [kg ha^{-1} MJ^{-1} m^2]	40	AC [30, 40]
		HI	Harvest index [-]	0.4	AC [0.35,0.55]
		TOPC	Optimal temperature for plant growth [^{0}C]	25	AC [22, 40]
		TBSC	Minimum temperature for plant growth [^{0}C]	8	AC [7, 9]
		WSYF	Lower limit of harvest index [-]	0.01	AC [0.01, 0.03]
		WCY	Fraction of water in crop [-]	0.15	AC [0.12, 0.18]
	Model parameters	*PARM*(03)	Water stress harvest index [-] (sets fraction of growing season when water stress starts to reduce *HI*)	0.50	AC [0.48, 0.52]
		PARM(42)	SCS curve number index [-] (regulates the effect of potential evapotranspiration in driving the SCS curve number retention parameter)	1.2	AC [1.25, 1.35]

[1] The default values are calculated based on Eqs.2&3 for each grid
[2] The default values are obtained from FertiStat database (FAO, 2007) for each grid
[3] AC indicates an absolute change where the initial parameter value in replaced by another value
[4] RC indicates a relative change where initial parameters are multiplied by (1+ a given value)

In Step 2, we calibrated six Operation parameters, which were suggested by Niu et al. (2009) and Wang et al. (2012) to be the most sensitive parameters (Table 2.2), and again fixed them to their best values. We calibrated fertilizer rates because the available data represented values for the years around 2002. As we did not have the temporal variability of fertilization application rate, we allowed a relative change of ±45% and calibrate it for different countries.

In Step 3, we calibrated six Crop and two Model parameters (Table 2.2), which are highlighted in the literature as the most sensitive parameters for crop yield (Gaiser et al., 2010; Wang et al., 2005; Wang et al., 2012). These parameters are identified separately for each country and are the same for all grids within a country. A range of variability is defined for each parameter (Table 2.2), where the maximum and minimum bounds were obtained from values reported in the literature (Table S2.1 in Supplementary material).

2.3. Results

2.3.1. Country level model performance with default parameters

Country-level annual simulations with default parameters showed poor results in most countries (Figure 2.2). However, depending on the country, the goodness of fit varied considerably. For instance, the model overestimated maize yields in Angola, Benin, and Ghana, but underestimated in Mauritania, Namibia, or Tanzania. It is also noted that long-term averages (1980-2012) in countries like Burkina Faso and Nigeria showed remarkable agreement as overestimation in some periods were offset by underestimation in other periods (Figure 2.2). In these countries, the difference between the long-term averages of simulated and observed yields were nearly 0 (Figure S2.1). Hence, obtaining good fits based on average long-term data does not necessarily mean we have a good model of crop yield. We therefore conclude that the default parameters did not have a fine enough spatial resolution to be applicable to the entire SSA countries.

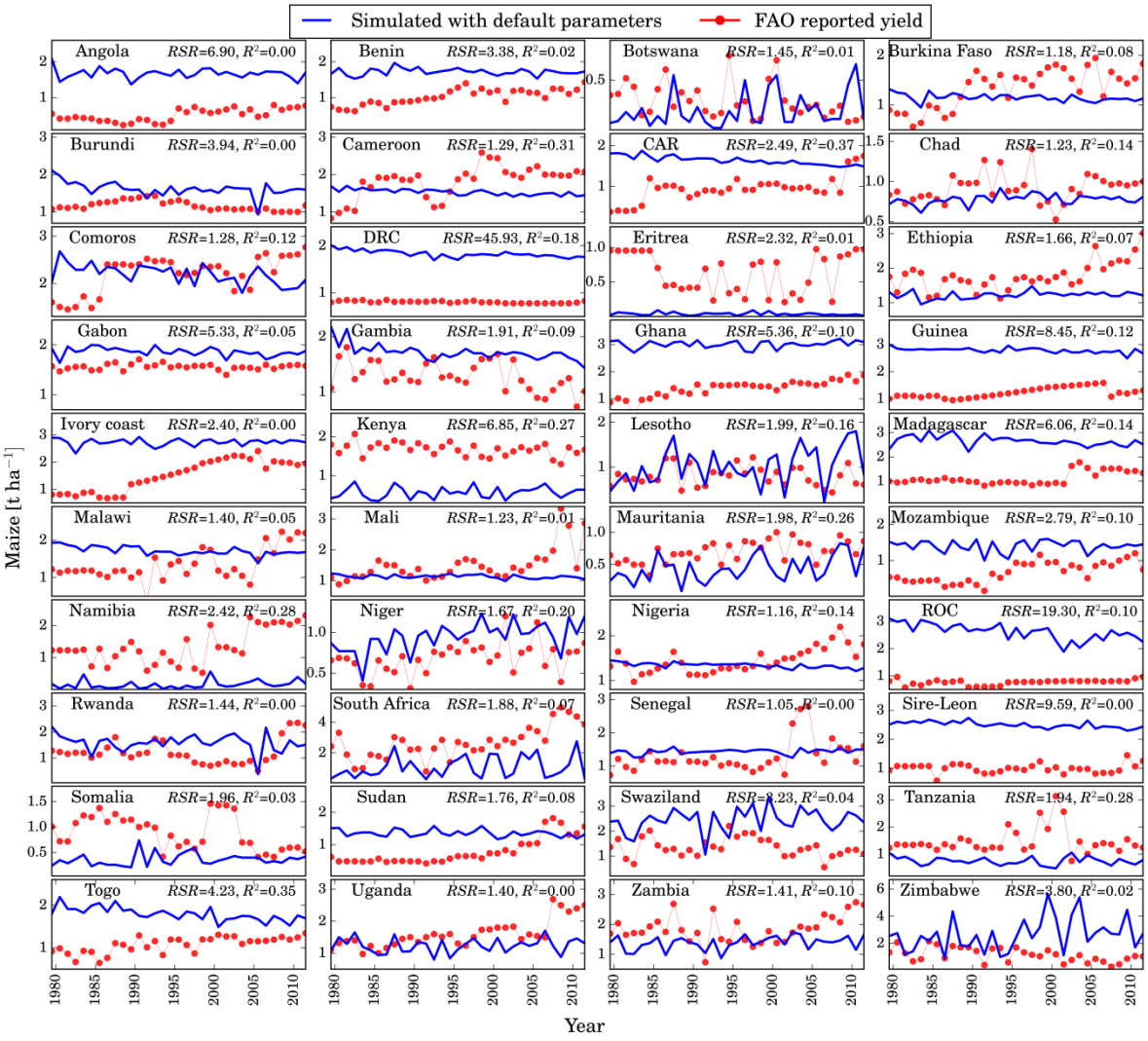

Figure 2.2. Annual simulated crop yields based on default parameters (non-calibrated model) compared with FAO reported yields during 1980-2012.

In general, the default model underestimated maize yield in the Horn of Africa, Southern Africa, and parts of Western Africa (Figure S2.1), whereas it overestimated it in Central Africa and other parts of Eastern and Western Africa. The *RSR* for 13 countries ranged from 3 to 38, whereas 27 countries had *RSR*s between 1.05 and 3. The R^2 values were larger than 0.2 only in 8 countries: Cameroon, Central African Republic (CAR), Kenya, Mauritania, Namibia, Niger, Togo, and Tanzania (Figure 2.2). As highlighted by Kenya and CAR, a good R^2 does not mean a satisfactory simulation, as a model can systematically over or under predict the measured data. Overall, the long-term average maize yield corresponded poorly with FAO reported yields over SSA (R^2=0.02 and *RSR*=1.89) (Figure 2.3a) indicating the necessity for calibration.

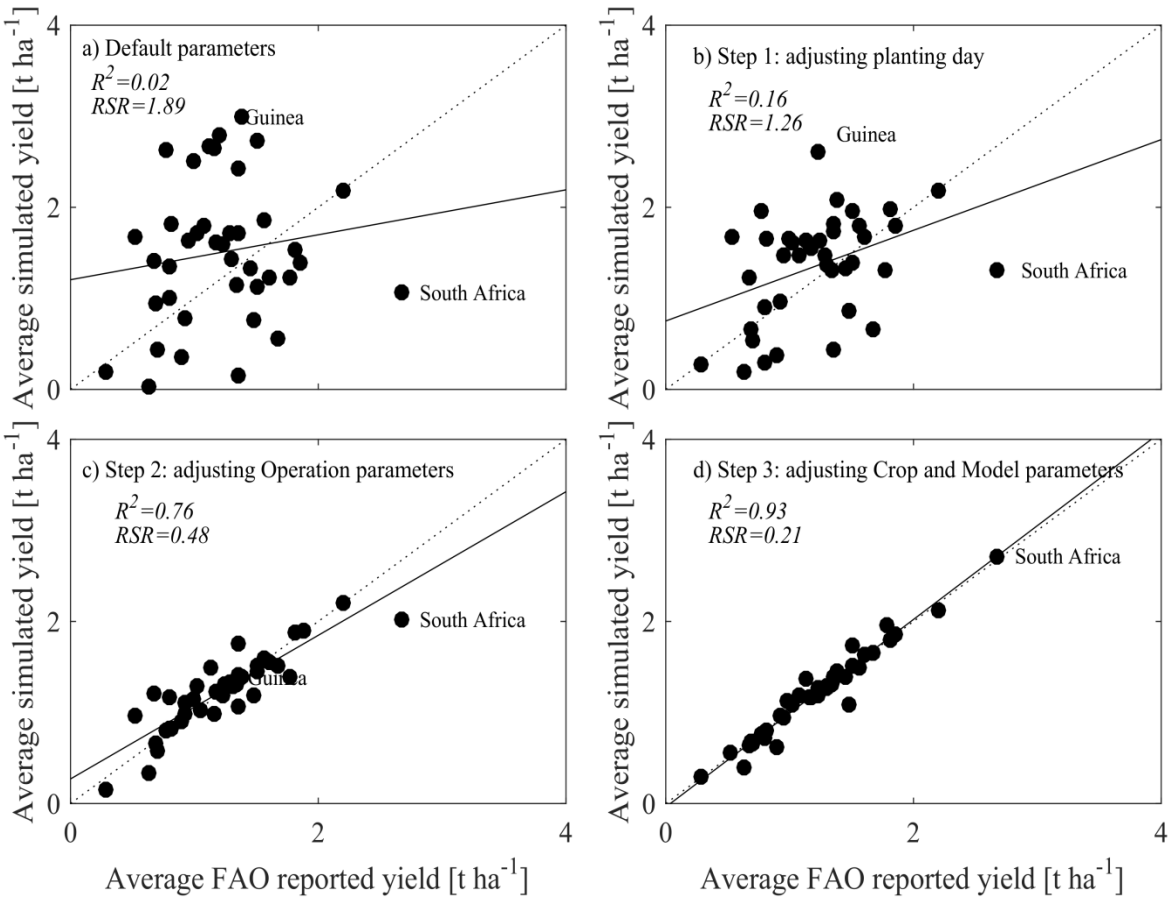

Figure 2.3. Comparison of the long-term average maize yield reported by FAO and simulated yields over SSA countries under four situations: a) EPIC default parameters, b) after adjusting planting data, c) after adjusting Operation parameters, and d) final calibration of Crop and Model parameters.

2.3.2. Calibration of planting date (*PD*) (Step 1)

In the first step of calibration, we adjusted the grid-based *PD*. This led to a reduction of biases between the long-term average simulated and observed yields as the R^2 of country-based long-term average yield increased from 0.02 to 0.16 and *RSR* improved from 1.89 to 1.26 (Figure 2.3b). However, the improvement in the simulated yields was not equally shared by all countries. Substantial

variations were seen in terms of *RSR* improvement over SSA (Figure 2.4a). While some countries like Madagascar, Zimbabwe and Sire-Leon improved by more than 50%, others like Uganda, Malawi, and Angola hardly showed any significant improvement (Figure 2.4a).

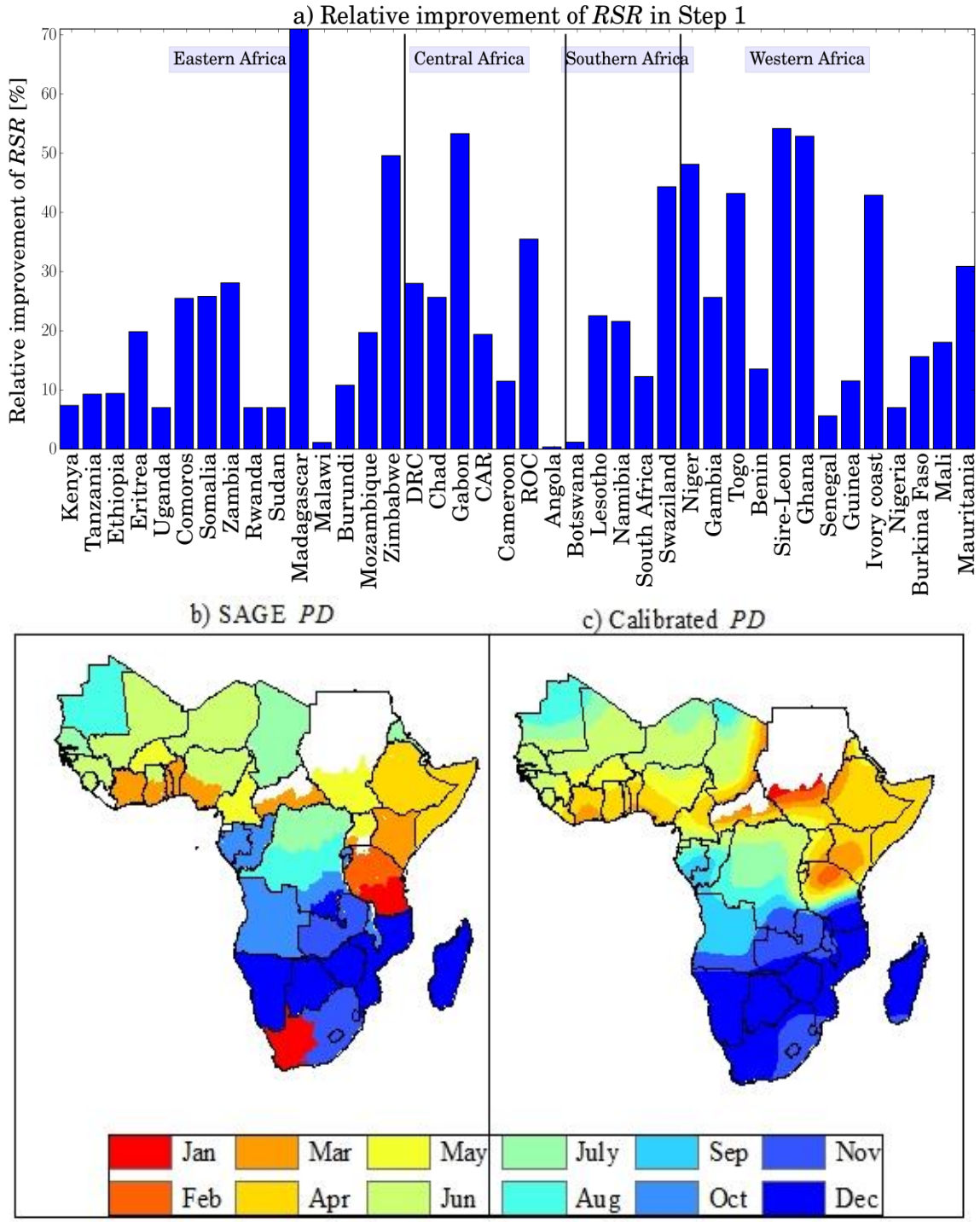

Figure 2.4. a) The relative improvement in *RSR* [%] achieved owing to implementing Step 1 in each country; b) spatial variation of *PD* based on SAGE data, c) Spatial variation of *PD* obtained after applying Step 1.

The time series country-based yields (Figure S2.2 in Supplementary material) showed significant improvements in R^2 for some countries such as Chad, Mauritania, and Niger, where the values increased from 0.14, 0.26, and 0.20 to, respectively, 0.22, 0.31, and 0.29 as a result of *PD* adjustment. In these countries, *RSRs* were around 1 or less, indicating closer agreements.

The spatial distribution of *PD* based on the SAGE data does not show significant variation within a country in most cases (Figure 2.4b). The adjusted values obtained in Step 1 of calibration (Figure 2.4c) showed higher spatial variation. On the average, Western and Central Africa benefited most from *PD* adjustment in terms of *RSR* values (Figure 2.4a). At the same time these regions showed the highest country-based variations in *PD* (Figure 2.4c), which may indicate a resolution problem in the SAGE data.

2.3.3. Calibration of Operation parameters (Step 2)

In this step, the six Operation parameters were allowed a relative change of within ±45%. Calibration of the six Operation parameters led to a further improvement in the simulated maize yields as the long-term average yields improved from R^2 of 0.16 in Step 1 to 0.76 in Step 2 (Figure 2.3c). A further decrease was also seen in the *RSR* values from 1.26 to 0.48 (Figure 2.3c). The country-based decreases in the *RSR* values showed that more than 50% improvement were made in Kenya and Burundi from Eastern Africa; Democratic Republic of Congo (DRC), Republic of Congo (ROC), and Angola from Central Africa; Namibia and South Africa from Southern Africa; and Benin, Sire Leon, and Guinea from Western Africa (Figure 2.5a). After the two steps of calibration, countries the least improved were Botswana, Ethiopia, and Tanzania, which are mostly in East Africa. The time series yield data (Figure S2.3) indicated $R^2>0.25$ accompanied by $RSR<1.5$ in seven countries: Kenya, Chad, Lesotho, Mauritania, Namibia, Niger, and Tanzania.

The final calibrated parameters differed widely from country to country (Figure 2.5b-g) with larger values in countries such as Kenya, DRC, ROC, and Angola. In these countries, a significant mismatch was noted between observed and simulated yields in Step 1 (Table 2.3). The calculated *PHU* values were underestimated for mostly Central and Eastern Africa (except Horn Africa) countries, while overestimated for Southern and Western Africa (Figure 2.5b).

The default *Pdensity* was on the average underestimated for Eastern and Southern Africa and overestimated for Central and West Africa (Figure 2.5c). The default *N-app* values were overestimated for most Eastern SSA, while *K-app* was overestimated for Southern and most Eastern Africa and underestimated for Central and Western Africa (Figure 2.5d, e). The default *BFT0* and *P-app* were overestimated for some countries and underestimated for others with no specific pattern (Figure 2.5d, e).

The result of a sensitivity analysis at this point indicated that *PHU* and *Pdensity* were the most sensitive parameters in all countries (*p-values*=0, *t-stats*$>>t_{critial}$) with *N-app* being the third most

sensitive parameter (Table S2.2). *K-app* was not sensitive over the entire region, but it was locally sensitive for some countries. *BFT0* and *P-app* were the least sensitive parameters for maize in SSA.

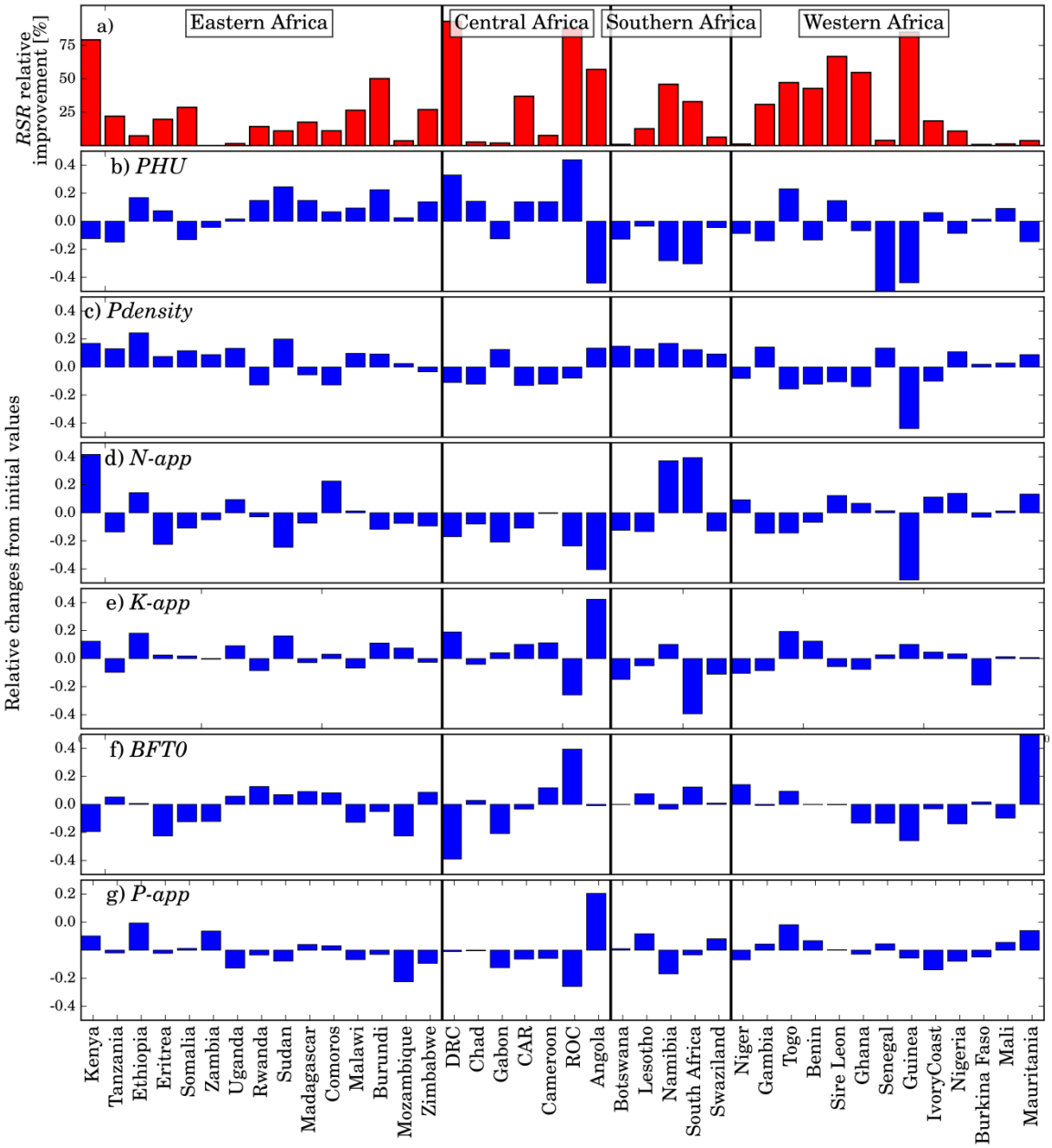

Figure 2.5. a) The relative improvement in the *RSR* values after implementation of Step 2; the y-axis indicates the percentage of improvement as compared to Step 1. b-g) The best relative changes from their initial values in Operation parameters obtained after implementation of Step 2.

Table 2.3. The final country level values of Operation parameters obtained from SUFI-2 algorithm in Step 2.

	Country	*PHU*[*]	*N-app*	*P-app*	*K-app*	*Pdensity*	*BFT0*
		[^oC]	[$Kg\ ha^{-1}$]	[$Kg\ ha^{-1}$]	[$Kg\ ha^{-1}$]	[$Plant\ m^{-2}$]	[-]
Eastern Africa	Kenya	2088	35.41	9.4	5.6	5.84	0.75
	Tanzania	1662	6.9	5.9	5.4	5.65	0.89
	Ethiopia	2004	16.01	9.9	5.1	6.22	0.82
	Eritrea	1937	5.43	4.5	6.1	5.38	0.94
	Somalia	1852	4.5	5.1	6.1	5.58	0.75
	Zambia	2363	25.7	6.8	6.0	5.44	0.75
	Uganda	2306	13.2	5.2	6.5	5.67	0.90
	Rwanda	2583	4.9	3.9	5.5	4.36	0.95
	Sudan	2276	9.8	5.7	6.0	6.00	0.75
	Madagascar	2251	14.9	5.2	5.8	4.72	0.93
	Comoros	2014	6.1	4.9	6.2	4.36	0.92
	Malawi	2236	17.2	4.7	5.6	5.49	0.75
	Burundi	2277	4.4	4.9	6.7	5.47	0.81
	Mozambique	2791	6.5	5.6	5.3	5.13	0.86
	Zimbabwe	2805	48.15	4.55	5.8	4.83	0.92
Central Africa	DRC	2107	8.3	5.5	6.9	4.45	0.89
	Chad	1456	12.0	5.0	5.8	4.39	0.87
	Gabon	1438	7.9	5.7	6.5	5.63	0.75
	CAR	1620	8.9	4.7	6.6	4.34	0.82
	Cameroon	2108	8.9	4.7	6.7	4.39	0.95
	ROC	2066	12.9	5.2	5.3	4.61	0.83
	Angola	2539	14.5	5.3	5.5	5.68	0.74
Southern Africa	Botswana	1881	26.3	15.2	5.1	5.74	0.85
	Lesotho	2445	21.8	16.8	5.7	5.65	0.91
	Namibia	1914	37.2	4.4	5.5	5.84	0.83
	South Africa	1796	66.6	13.5	5.4	5.62	0.89
	Swaziland	2004	6.1	5.4	5.3	5.47	0.86
Western Africa	Niger	1767	5.5	2.8	5.4	4.60	0.95
	Gambia	1670	4.3	3.1	5.5	5.71	0.84
	Togo	1670	2.6	2.9	6.0	4.22	0.95
	Benin	1733	7.4	3.2	6.7	4.39	0.85
	Sire Leon	2278	5.6	3.0	5.7	4.48	0.85
	Ghana	1846	23.5	2.9	5.5	4.30	0.75
	Senegal	1690	12.2	3.1	6.2	5.68	0.75
	Guinea	2166	5.21	2.6	6.7	4.81	0.81
	IvoryCoast	2210	13.3	2.6	6.3	4.50	0.82
	Nigeria	1551	6.8	2.8	6.2	5.54	0.75
	Burkina Faso	1690	9.7	2.6	6.6	5.10	0.92
	Mali	2007	10.1	3.2	6.1	5.14	0.77
	Mauritania	1518	15.8	3.4	6.0	5.44	0.95

* The mentioned *PHU*s are the average of grids within each country.

2.3.4. Calibration of Crop and Model parameters (Step 3)

In the last step of calibration, six Crop and two Model parameters (Table 2.2) were adjusted. The best value of the objective function was reached in 6 iterations of 50 simulations each. A major amendment was made to the parameters in this step, where R^2 for long-term average yield increased to 0.93 (from 0.76 in Step 2) and *RSR* decreased to 0.21 (from 0.48 in Step 2) (Figure 2.3d). The 95PPU uncertainty bands bracketed a large number of observed data for the period of 1980-2012. As indicated by the *P-factors* (Figure 2.6), in all countries more than 30% of observed data was bracketed by the simulated 95PPU band. The low *P-factors* in countries such as Madagascar, Togo, and Burundi were mainly due to presence of trend in the yield (due to factors like technology and variety change), which was not accounted by models. In majority of the countries *P-factors* were >50% and *R-factor* were <2. In some countries, such as Guinea, the *R-factor* was larger indicating larger uncertainty in maize yield prediction. Higher *R-factors* were also noticed in the countries with trends in yield, where EPIC$^+$ attempted to increase *P-factors* at the expense of larger *R-factors*.

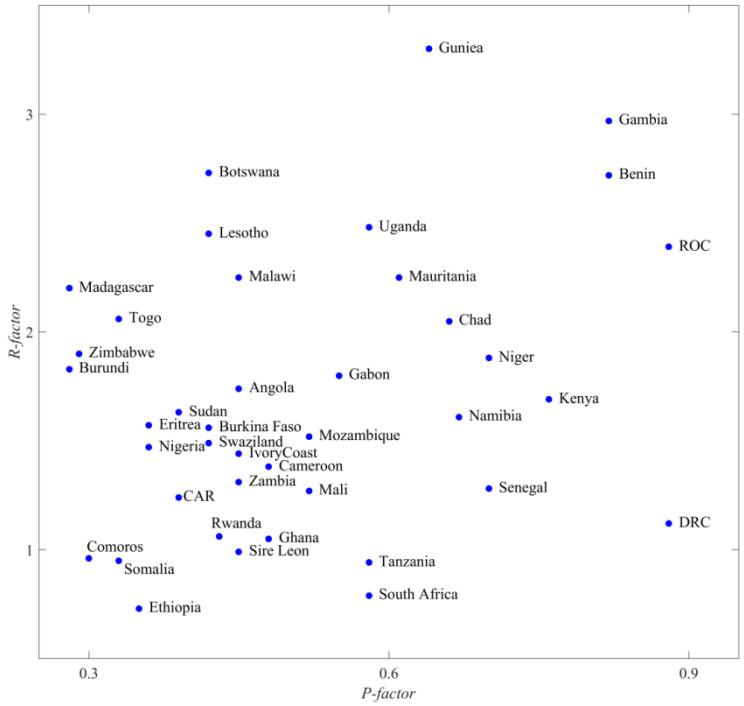

Figure 2.6. *P-factor* versus *R-factor*. *P-factor* is the percentage of observed data bracketed by the 95PPU. *R-factor* is the width of the 95PPU band representing predictive uncertainty.

At this step, the results for many countries showed significant improvement as illustrated in Figure 2.7, where the 95PPU is also shown. The *RSRs* decreased to values around 1 or less in all countries. The most significant changes occurred in Uganda, and Gambia, where the R^2 increased from 0.08, and 0.06 (in Step 2) to 0.4, and 0.33, respectively, followed by Ethiopia, Swaziland, Zambia, and

Sudan where the R^2 improved from 0.01, 0.04, 0.11, and 0.04 to 0.20, 0.22, 0.27, and 0.17, respectively. Overall, 16 countries showed R^2 above 0.20.

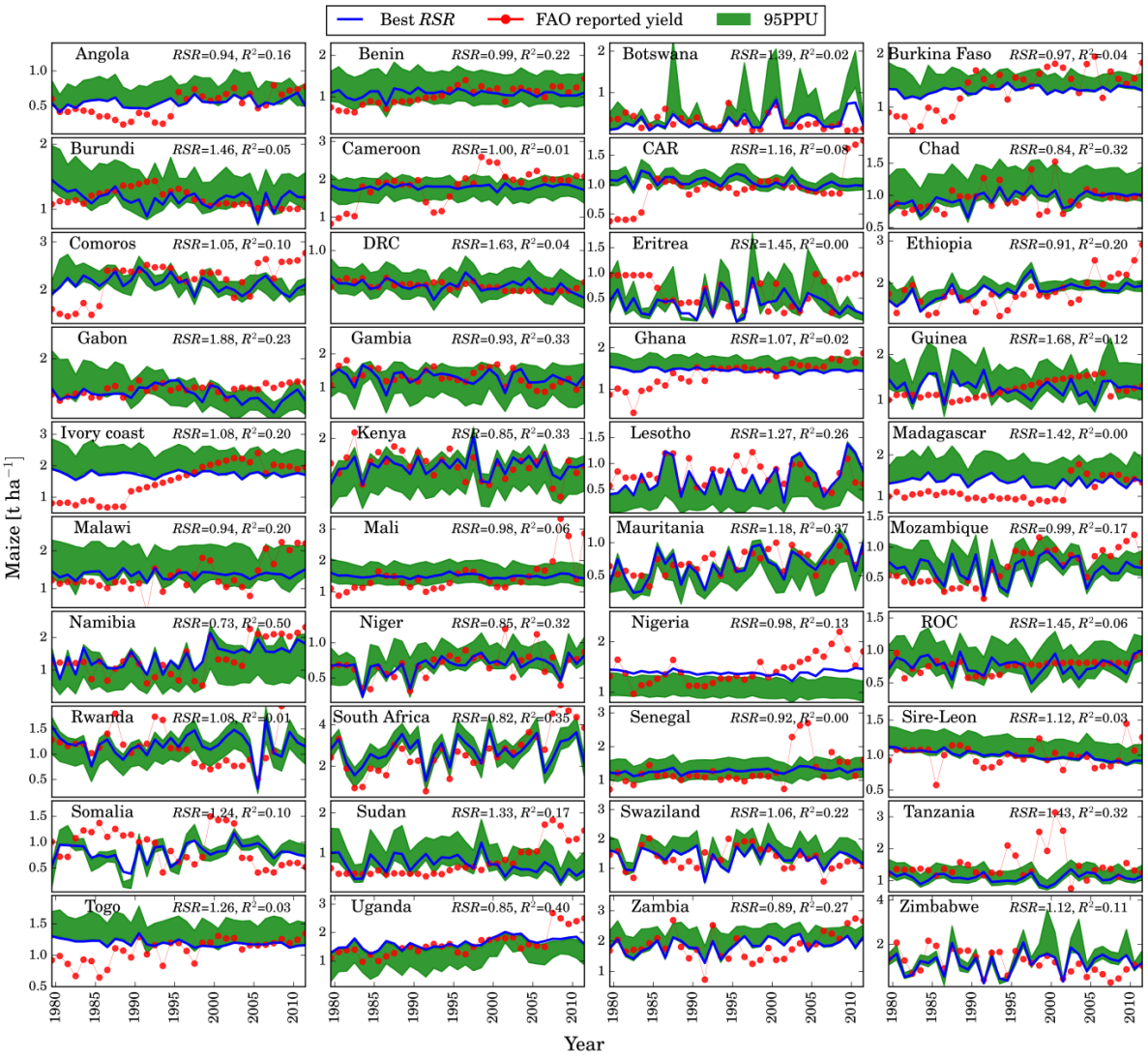

Figure 2.7. Comparison of the FAO reported (red line) and simulated maize yields expressed as 95PPU prediction uncertainty band (green bound) and best simulation obtained from *RSR* criteria (blue line) in 40 countries in SSA during 1980-2012.

The final calibrated Crop parameter ranges showed large variability in different countries (Tables 2.4&2.5) (Figures S2.4&S2.5). *WA* ranged between 30 and 43 kg ha^{-1} MJ^{-1} m^2. The ranges were higher in Madagascar, Somalia, Malawi and Burundi in Eastern Africa, and CAR in Central Africa, whereas they were lower in Comoros, Gabon, Cameroon, Benin, and Mauritania. The lower bound within the later countries were 30 kg ha^{-1} MJ^{-1} m^2.

Table 2.4. The final ranges of Crop parameters in Step 3. The values inside brackets indicate the best parameters.

	Countries	*WA*	*HI*	*TOPC*	*TBSC*	*WSYF*	*WCY*
		[kg $ha^{-1}MJ^{-1}m^2$]	[-]	[^{0}C]	[^{0}C]	[-]	[-]
Eastern Africa	Kenya	34-39(37)	0.40-0.48(0.46)	24-29(27)	7.5-8.3(7.8)	0.02-0.035 (0.03)	0.16-0.19(0.17)
	Tanzania	35-39(36)	0.42-0.52 (0.50)	28-34(34)	7-9 (7.1)	0.01-0.03(0.03)	0.13-0.17(0.16)
	Ethiopia	31-38(38)	0.33-0.44 (0.35)	20-27(26)	8-9.5(9.3)	0.005-0.02(.006)	0.12-0.18(0.16)
	Eritrea	33-40(39)	0.48-0.56 (0.52)	26-35(28)	5.7-7.3(7.3)	0.022-0.04(0.03)	0.11-0.17(0.16)
	Somalia	35-42(40)	0.39-0.49 (0.40)	20-26(24)	7-9(7.3)	0.05-0.07 (0.06)	0.1-0.15 (0.12)
	Zambia	30-38(33)	0.44-0.52(0.44)	26-35(33)	8.1-9(8.9)	0.02-0.03 (0.03)	0.15-0.18(0.18)
	Uganda	33-38(38)	0.40-0.49(0.48)	30-35(31)	8.4-9.4 (8.6)	0.014-0.04(0.02)	0.12-0.18(0.16)
	Rwanda	30-36(31)	0.30-0.41(0.31)	28-32(30)	6.9-7.8(7.1)	0.024-0.04(.035)	0.13-0.17(0.15)
	Sudan	33-38(36)	0.38-0.44(0.39)	20-26(20)	8-9 (8.05)	0.05-0.06(0.055)	0.15-0.18(0.17)
	Madagascar	36-41(39)	0.32-0.38(0.36)	21-27(26)	8.5-9.5 (8.7)	0.024-0.04 (0.02)	0.12-0.16(0.13)
	Comoros	30-35(34)	0.30-0.38(0.33)	20-28(24)	8.3-9.6(8.5)	0.03-0.045(0.04)	0.13-0.16(0.14)
	Malawi	36-42(40)	0.37-0.45(0.38)	20-26(25)	8.8-10(10)	0.01-0.02(0.018)	0.11-0.14(0.13)
	Burundi	37-41(39)	0.30-0.37(0.31)	20-28(27)	7-8.5(7.7)	0.02-0.03(0.03)	0.11-0.15(0.14)
	Mozambique	33-40(37)	0.35-0.45 (0.35)	22-30(28)	7-9(8.3)	0.01-0.03(0.03)	0.13-0.15(0.14)
	Zimbabwe	30-37(36)	0.32-0.44(0.34)	27-35(35)	6-8(7.9)	0.02-0.03(0.02)	0.15-0.18(0.16)
Central Africa	DRC	33-38(35)	0.31-0.40(0.35)	26-32(27)	7.6-8.5(8.1)	0.03-0.05 (0.03)	0.11-0.13(0.12)
	Chad	30-40 (38)	0.35-0.53(0.39)	22-34(28)	7-9(8.9)	0.01-0.03(0.02)	0.15-0.18(0.16)
	Gabon	34-38(36)	0.33-0.38(0.35)	32-35(33)	7.6-8.8(8.5)	0.005-0.03(0.01)	0.12-0.18(0.15)
	CAR	39-43(39)	0.30-0.36(0.30)	20-25(25)	7.5-9(7.6)	0.02-0.03(0.03)	0.13-0.18(0.15)
	Cameroon	30-34 (31)	0.36-0.45(0.41)	30-35(33)	8.3-9.4(8.5)	0.03-0.04(0.03)	0.11-0.16(0.12)
	ROC	34-39(37)	0.34-0.42(0.36)	21-28(25)	8.2-9(8.9)	0.02-0.04(0.02)	0.14-0.17(0.16)
	Angola	36-39(37)	0.32-0.39(0.35)	23-28(25)	7.7-8.3(8.0)	0.01-0.03(0.03)	0.12-0.16(0.14)
Southern Africa	Botswana	30-40(38)	0.35-0.50(0.38)	22-33(24)	7-9(8.9)	0.01-0.03(0.02)	0.12-0.18(0.14)
	Lesotho	31-37(32)	0.35-0.47 (0.36)	27-35(27)	6.2-8(7)	0.005-0.02(0.02)	0.14-0.18(0.14)
	Namibia	36-40(39)	0.40-0.47 (0.43)	24-28(26)	7.1-8(7.6)	0.028-0.04(0.03)	0.10-0.16(0.15)
	South Africa	36-39(37)	0.42-0.50 (0.45)	28-33(30)	7.1-8(7.6)	0.035-0.04(0.04)	0.10-0.15(0.13)
	Swaziland	32-39(33)	0.40-0.48 (0.44)	31-35(33)	8-9(8.6)	0.02-0.03(0.02)	0.12-0.18(0.13)
Western Africa	Niger	30-40(30)	0.35-0.53 (0.40)	22-33(32)	7-9(8.0)	0.01-0.03(0.024)	0.15-0.18(0.17)
	Gambia	32-37(33)	0.30-0.35 (0.33)	20-29(28)	7-8.8(7.6)	0.03-0.05(0.04)	0.15-0.18(0.16)
	Togo	33-39(35)	0.30-0.40 (0.33)	20-34(33)	6.9-8.3(7)	0.01-0.02(0.011)	0.11-0.14(0.14)
	Benin	30-36(32)	0.33-0.45 (0.32)	22-33(26)	6.5-8.2(8)	0.02-0.03(0.021)	0.11-0.16(0.13)
	Sire Leon	31-37(36)	0.31-0.37(0.35)	31-35(32)	7.5-8.7(8.4)	0.01-0.02(0.019)	0.15-0.18(0.17)
	Ghana	30-34(33)	0.30-0.35(0.32)	30-35(31)	7.5-9(8.7)	0.01-0.02(0.019)	0.15-0.18(0.16)
	Senegal	33-39(36)	0.30-0.46 (0.32)	22-34(29)	7.5-8.5(8)	0.0 1-0.02(0.018)	0.12-0.14(0.13)
	Guinea	35-40(35)	0.31-0.40(0.34)	21-30(26)	8-9(8.7)	0.04-0.06 (0.06)	0.12-0.16(0.15)
	Ivory Coast	30-40(35)	0.36-0.50(0.41)	22-35(26)	7-9(8.7)	0.01-0.03 (0.02)	0.14-0.16(0.15)
	Nigeria	35-39(37)	0.30-0.40(0.37)	26-34(31)	7-9.5(9.1)	0.02-0.03(0.03)	0.12-0.18(0.15)
	Burkina Faso	31-40(31)	0.40-0.48(0.41)	21-33(22)	7.8-10(8.9)	0.02-0.04(0.02)	0.13-0.16(0.13)
	Mali	31-39(33)	0.35-0.55(0.45)	22-35(34)	7-9(8)	0.01-0.03(0.03)	0.15-0.18(0.17)
	Mauritania	32-35(34)	0.48-0.53(0.51)	24-34(26)	7.6-9(8.8)	0.04-0.08(0.05)	0.15-0.18(0.16)

Table 2.5. The final ranges of Model parameters *PARM*(03) and *PARM*(42). Values inside rackets indicate the best parameter values.

	Countries	*PARM*(03)	*PARM*(42)
		[-]	[-]
Eastern Africa	Kenya	0.44-0.48(0.45)	1.18-1.29(1.25)
	Tanzania	0.48-0.52 (0.49)	1.25-1.33(1.32)
	Ethiopia	0.43-0.49 (0.44)	1.20-1.30(1.23)
	Eritrea	0.49-0.51 (0.51)	1.27-1.33(1.31)
	Somalia	0.30-0.35 (0.31)	1.27-1.34(1.27)
	Zambia	0.47-0.50 (0.48)	1.31-1.36 (1.35)
	Uganda	0.52-0.55 (0.52)	1.35-1.46 (1.45)
	Rwanda	0.46-0.49 (0.49)	1.31-1.37 (1.35)
	Sudan	0.42-0.48 (0.42)	1.20-1.30(1.30)
	Madagascar	0.47-0.49 (0.48)	1.30-1.40(1.39)
	Comoros	0.47-0.52 (0.50)	1.20-1.30(1.28)
	Malawi	0.47-0.49 (0.48)	1.34-1.4 (1.39)
	Burundi	0.43-0.46 (0.44)	1.25-1.34 (1.28)
	Mozambique	0.48-0.52 (0.49)	1.28-1.33 (1.29)
	Zimbabwe	0.49-0.51 (0.51)	1.23-1.31 (1.24)
Central Africa	DRC	0.48-0.54 (0.51)	1.17-1.26(1.18)
	Chad	0.48-0.52 (0.49)	1.25-1.35 (1.29)
	Gabon	0.44-0.51 (0.49)	1.25-1.33 (1.34)
	CAR	0.45-0.48 (0.47)	1.25-1.32 (1.32)
	Cameroon	0.48-0.50 (0.50)	1.25-1.30 (1.25)
	ROC	0.51-0.55 (0.53)	1.24-1.31 (1.27)
	Angola	0.47-0.50 (0.49)	1.29-1.39(1.34)
Southern Africa	Botswana	0.48-0.52 (0.51)	1.25-1.35(1.26)
	Lesotho	0.49-0.52 (0.49)	1.20-1.30(1.27)
	Namibia	0.48-0.51 (0.50)	1.25-1.32(1.29)
	South Africa	0.49-0.51 (0.50)	1.22-1.31(1.26)
	Swaziland	0.50-0.52 (0.51)	1.19-1.27(1.25)
Western Africa	Niger	0.48-0.52 (0.50)	125-1.35(1.31)
	Gambia	0.45-0.51 (0.46)	1.23-1.26(1.24)
	Togo	0.48-0.51(0.49)	1.23-1.31(1.24)
	Benin	0.47-0.50 (0.50)	1.22-1.31(1.24)
	Sire Leon	0.49-0.51 (0.51)	1.30-1.34(1.33)
	Ghana	0.45-0.50 (0.48)	1.23-1.33(1.25)
	Senegal	0.49-0.51 (0.51)	1.28-1.33(1.25)
	Guinea	0.44-0.50 (0.47)	1.25-1.31(1.26)
	Ivory Coast	0.48-0.52 (0.51)	1.25-1.35(1.34)
	Nigeria	0.50-0.52 (0.5)	1.22-1.28 (1.23)
	BurkinaFaso	0.43-0.48 (0.47)	1.25-1.38 (1.36)
	Mali	0.48-0.52 (0.52)	1.25-1.34 (1.29)
	Mauritania	0.49-0.52 (0.50)	1.23-1.31 (1.28)

For *HI*, overall higher ranges (>0.4) were obtained in the Horn of Africa, Southern Africa, Mali and Mauritania where the yields were underestimated. In Central Africa and some Western African countries, the ranges were below 0.35. *TOPC* showed higher variability in Eastern and Central Africa compared to Southern and Western Africa where the ranges were between 22 and 35 ^{o}C. More variability of *TBSC* was noticed in Eastern Africa. Similar variations were observed for *WSYF*, *WCY* (Table 2.4) (Figure S2.4) and *PARM*(*03*) and *PARM*(*42*) (Table 2.5) (Figure S2.5). The relatively large parameter ranges in Tables 2.4 and 2.5 indicate the inadequacy in the concept of the "best" solution and the need to express the uncertainty in the calibration results.

After the final step of calibration, 15 countries remained with $R^2 < 0.1$. A probable reason could be large errors in reported yield, or disruption of agricultural activities due to wars and social unrests. We hypothesized that simple manipulation of reported observed data by linear de-trending techniques would help to improve the calibration results. This idea was tested for 18 countries (Figure 2.8). We found that the calibrated R^2 improved significantly in 6 countries including Angola, Botswana, Burkina Faso, Burundi, Comoros, and Madagascar with values above 0.2 (Figure 2.8). There was not a significant increase in R^2 of other countries. The *RSR* values decreased in a few countries such as Botswana, Burkina Faso, Madagascar, Somalia, Sudan, and Togo. The *RSR* values for some countries like Guinea and Ivory coast remained rather high. The reason is related to linear trends in yield in these countries. De-trending resulted in almost constant yield for all years.

Overall, the results show that linear de-trending is not promising for all countries and trend removal requires testing the performance of different techniques and evaluating their performances. Testing other methods was beyond the scope of this paper. The simple linear technique in this study was mostly helpful to improve the *P-factor* and the *R-factor* (Figure S2.6).

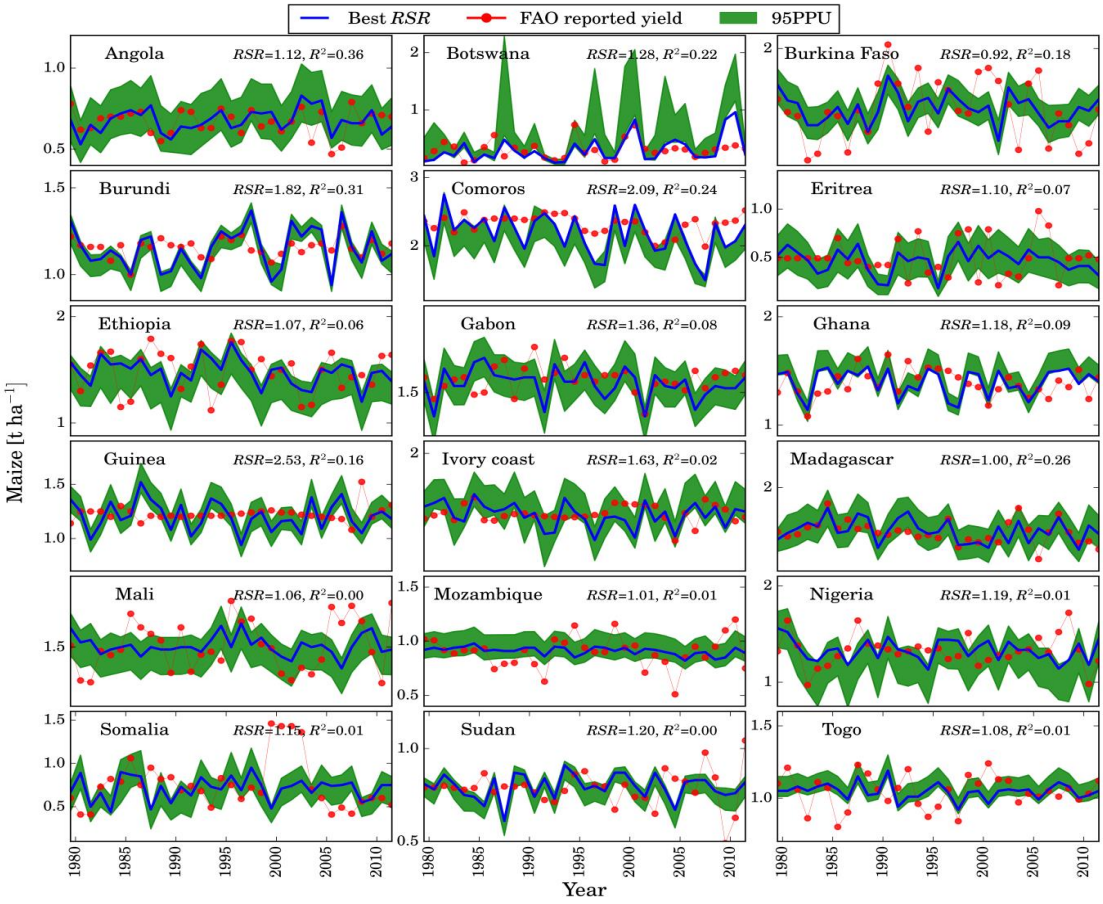

Figure 2.8. Comparison of the FAO reported (red line with dots) and simulated maize yields expressed as 95PPU prediction uncertainty band (green bound) and the best simulation (blue line) in 18 countries that linear de-trending was applied.

2.4. Discussion and conclusion

2.4.1. Country level maize calibration

In the last decades, SSA has been the focus of attention in many studies due to the low productivity, existing potential for improvement, as well as a high vulnerability to climate change (Conceicao et al., 2016; Webber et al., 2014). However, poor data status affects the ability of decision makers to make the right management decisions to increase the crop yield (Beguy, 2016). Therefore, there is a need to advance crop modeling to generate reliable output by improving their performance through calibration and uncertainty analysis, understanding the inter-annual yield variability, and identifying model parameters on various spatial scales. In this work, we achieved these objectives by creating EPIC^{+} to calibrate a maize model for individual SSA countries. We also identified the important parameters at the national level.

We did not find much literatures to compare our results, as we considered a long time-span of multiple decades. Folberth et al. (2012a) obtained R^2 values of 0.25 for the entire SSA countries for the year 2000. Liu et al. (2007) provided results on the country level with much high R^2 values of (0.8-0.9)

for wheat, however, the results were also only for the year 2000. Jones and Thornton (2003) simulated maize in Africa using DSSAT (Decision Support System for Agro-technology Transfer) and obtained a poor agreement with R^2 of 0.03 mainly due to the lack of crop-specific land use at the time of the study. Through calibrating each country individually, we obtained a higher R^2 of 0.92 for the entire SSA. Although our results are not directly comparable to the other studies, we found that EPIC$^+$ was capable of estimating reasonable biophysical plant growth parameters for maize, which can be used as a base for testing further adaptation strategies in SSA.

After three steps of calibration, we obtained satisfactorily performances at the country level for most countries. In some countries such as South Africa, Kenya, and Tanzania where the quality of input data are higher, we obtained more satisfactory results as indicated by lower *RSR* and higher R^2 values. *RSRs* for all countries were between 0.8 and 2 and the final R^2 values for 44% of the countries were >0.2. Although the *RSR* values were within acceptable ranges for maize yield, R^2 remained quite low for a few countries. We attributed these discrepancies to probable errors in the reported yield data and the social volatility and wars in these countries in the past 30 years.

The reported annual yield trends in different countries show different patterns. Grassini et al. (2013) described six statistical models describing time series trends in historic crop yield and found yield stagnation in e.g., DRC, Eritrea, and Ghana or Linear-upper plateau pattern in e.g., Ivory Coast, Burundi, and Madagascar. Ben-Ari and Makowski (2014) also found high inter-annual maize variability especially in Southern Africa and decomposed variables into three informative components. In this paper, we tested the effect of manipulation of past yield by trend analysis on the calibration results for several countries in SSA. Although we only used a simple linear trend, we found quite promising results for some countries. However, our initial test in 18 countries showed that linear de-trending is not effective for all cases and testing other de-trending methods are necessary. In a subsequent publication, we will explore in more details the effect of different de-trending techniques on calibration for countries affected by different societal conflicts.

The developed EPIC$^+$ can be applied for calibration of crop yields at different scales (field, region, country). The present study mainly considers SSA at the country level. The major limitation for calibration of crop models at smaller scales (e.g., sub-national and field) is the lack of observed yield data. This restricts determination of crop parameters at local level. Besides, even at the country level, the quality of the FAO data is questionable specially in under-developed countries (Lee et al., 2013). Adjusting the Crop and EPIC parameters at the sub-national scales increases their reliability, as these parameters are usually defined based on experimental data. Such detailed parameter estimation is only feasible for small-scale studies and is too ambitious for the entire SSA. In this study, we could only estimate the parameters and their uncertainties at the country level, as the only available time series yield data existed at this level. To the best of our knowledge, this has not been done before for SSA. To demonstrate the capability of EPIC$^+$ in estimating parameters at the field level, we tested the model

at six fields in Burkina Faso where observed maize yields were available during 2002-2007. Comparing simulated and observed yields shows promising results at the field scales where the *P-factor* and the *R-factor* values indicated a better performance of calibration at the field scale.

2.4.2. Parameter regionalization in SSA countries

The initial parameters used in this study came from different sources at different resolutions. After calibration, we identified parameters with better spatial definitions. Folberth et al. (2012a) and Therond et al. (2011) pointed out that next to plant growth parameters, a reliable estimation of planting date is important for a more accurate simulation of crop growth. On the large scales, *PD* contains large uncertainties stemming from poor spatial resolutions to the data source. In this study, after calibrating *PD*, there was a significant improvement in the simulation results, and we obtained a better identification of the spatial resolution for planting date for different regions in SSA. Using the available *PD* adjustment function in EPIC^{+}, we considered planting date as a calibration parameter and adjusted it between the earliest and the latest planting dates. This feature could be used to determine the best possible dates to achieve the highest yields according to climate conditions.

Calibration of Operation parameters also made a significant improvement in the results indicating the existence of large uncertainties in the default parameters we had used. In fairness to the fertilizer data used in this study, the FertiSat data was collected over a short time period of 1998 to 2004. However, because of a lack of more data, we used it for the entire period of this study. We assessed the impact of adjusting the Operation parameters such as fertilizer application and *PHU* by applying the relative change option in EPIC^{+}. In some countries with significant mismatch between observed and simulated yields in Step 1 (e.g. Kenya, DRC, or ROC), the adjusted values were higher. More detailed analysis on parameters uncertainty and spatial aggregation methods required more detailed data about agricultural activities at the field level which were not available at the scale of our study.

The parameter *Pdensity* was identified as one of the most sensitive parameters. Finding the optimum *Pdensity* has been the focus of attention in many studies (Deng et al., 2012; Overman and Scholtz, 2011). Folberth et al. (2012a) suggested a *Pdensity* value of between 2 and 6 plant m^{-2}, and used a value of 4 plant m^{-2} for the entire Africa. Tatsumi (2016) applied higher ranges from 5.6 to 9.0 plant m^{-2} and used ensemble mean of 7.9 plant m^{-2} for USA, which reflects the high productivity in USA compared to SSA. We parameterized *Pdensity* on the country level and found values ranging between 4.2 to 6.2 plant m^{-2}.

The calibration of Crop and Model parameters made a substantial improvement in the simulation results. The adjusted *HI* for most countries ranged between 0.30-0.55 with most countries below 0.44. This is smaller than the 0.55 suggested by Kiniry et al. (1995), or the range of 0.45-0.60 suggested by Wang et al. (2005) in Wisconsin regions, and 0.5 of Balkovic et al. (2013) for Europe. However, our value for SSA corresponds well with the smaller values of 0.35 reported by Folberth et al. (2012a), and 0.4 reported by Gaiser et al. (2010). Variations in *HI* within a crop are mainly attributed to differences

in crop management (Yang and Zhang, 2010) and therefore is low in SSA compared to global average. Jensen et al. (2003) suggested *HI* range of 0.22-0.34 for Tanzania based on their analysis of maize yield prior to 2000, which is smaller than our range of 0.42-0.52. The major reason for this discrepancy is due to a significant increase in maize yield after 2000, which leads to a higher *HI* for Tanzania. Yunusa and Gworgwor (1991) suggested *HI* of 0.10-0.32 for Nigeria, which is also smaller than our suggested ranges of 0.26-0.40 as the country has seen a significant increase in maize yield since the last decade.

The parameter *WA* measures dry biomass, including roots, produced per unit of intercepted photosynthetically active radiation under non-stressed condition. EPIC suggests a default value of 40 kg ha^{-1} MJ^{-1} m^2 for maize (Sharpley and Williams, 1990). Kiniry et al. (1995) applied the same value in northern Great Plains regions, and Balkovic et al. (2013) used it for the whole Europe. Wang et al. (2005), suggested a range of 30-45 kg ha^{-1} MJ^{-1} m^2, which is wider than the final ranges we obtained for each country. Bulatewicz et al. (2009) suggested 47 kg $ha^{-1}MJ^{-1}m^2$ for Sheridon region in Kansas, which is higher than the maximum upper bound in our study (43 kg $ha^{-1}MJ^{-1}m^2$ in CAR) mainly due to irrigation. *WA* in EPIC is assumed to be only based on data with no stress. The 35 and 35.4 kg ha^{-1} MJ^{-1} m^2 values reported by Causarano et al. (2008) for Iowa and Causarano et al. (2007) at Alabama, respectively, are close to our best values obtained for countries such as Guinea, South Africa, Sire Leon, and smaller than most Eastern African countries.

The *TOPC* and *TBSC* are the next two important parameters. Temperature is a key factor affecting the rate of crop growth. Crop responses to temperature differ among crop varieties and throughout their life cycle (Hatfield and Prueger, 2015). At any given stage of development, it is possible to define the "minimum temperature" below which a plant will not grow, "suboptimal temperatures" where a further increase in temperature will result in increased growth, and "optimal temperatures" when growth is at its maximum. However, the growth phases are not defined explicitly in EPIC. Therefore, these two parameters are more representative of the entire plant growth stages and should be adjusted by calibration. Our final adjusted *TOPC* for some Central and Eastern Africa countries were between 19-25 ^oC and higher in other countries. Balkovic et al. (2013) applied a fixed value of 22.5 ^oC, and Bulatewicz et al. (2009) estimated 27.2 ^oC. The adjusted *TBSC* varied between 7.5-9 ^oC in SSA. Bulatewicz et al. (2009) considered an initial range of 5-15 ^oC and a final value of 8.2 ^oC while a value of 8 ^oC was suggested by Kiniry et al. (1995).

Folberth et al. (2012a) and Gaiser et al. (2010) applied a value of 0.01 for *WSYF* for the entire Africa. The final adjusted ranges we found varied significantly from one country to the other within the range 0.005 to 0.06. For *PARM*(03) and *PARM*(42), Wang et al. (2005) suggested ranges between (0.3-0.7) and (0.5-2), respectively. For all these parameters, we narrowed down these ranges and defined an optimized range for each specific country.

Overall, the process of crop model calibration at large scale contains different levels of uncertainty such as heterogeneity in agricultural operations and their relevant parameters, the size and

discretization of the study area, the uncertainty of input data, the parameterization strategies, and the methods of aggregation. As many factors may significantly influence the model performance and representative parameters, implementing different calibration strategies and using expert information to assess the parameters are highly recommended to avoid distortion of final values. In this study, we compared the important parameters with previous works at SSA and other places across USA.

2.4.3. The EPIC$^+$ tool for calibration purposes

EPIC$^+$ is a promising tool with a user friendly GUI for calibration of the EPIC model. The program has several advantages:

- use of variable spatial scales (grid, country, regional or continent) and time scale (years to decade);
- ease of implementing different strategies for agricultural operations based on a flexible crop calendar in each grid; the ability to fit all EPIC parameters;
- possibility to run parallel EPIC$^+$ under the Linux environment, which substantially speeds up the calibration process;
- the compatibility in format with the optimization algorithms in the SWAT-CUP program, which allows for expansion of EPIC$^+$ to include other optimization techniques such as Particle Swarm Optimization (PSO).

There is also potential for future investigation of other uncertainty analysis techniques such as Bayesian approaches, which are based on the theorem of the conditional probability. This approach may provide a more comprehensive information on the relative uncertainty of parameters and their impacts on capturing regional variability in crop yield (Angulo et al., 2013b). Such levels of flexibility in structure gives opportunities to test different strategies for increasing the reliability of input data as well as improving the model performance.

The EPIC$^+$ structure is designed to fulfill the five criteria of broadness, modularity, independency, scalability, and accessibility identified by Houska et al. (2015) for a package development. Holzworth et al. (2015) emphasized on the speed as well. As the design of EPIC$^+$ structure is consistent with the SWAT-CUP program, other calibration techniques such as PSO, Generalized Likelihood Uncertainty Estimation, Markov Chain Monte Carlo can be easily embedded. Therefore, EPIC$^+$ is considered as a broad package, which is applicable to any scale. The model has several modules for the parameter adjustment, objective function selection, and output saving. The SUFI-2 algorithm in EPIC$^+$ is directly obtained from SWAT-CUP, which can be independently applied to calibration of many other models. EPIC$^+$ execution is accessible in Windows and Linux environment. Future studies can also explore the impact of downscaling model inputs such as fertilizer rate on calibration performance. Therefore, in

the presence of high-resolution data, the procedure remains valid and EPIC$^+$ can be applied to increase the accuracy of estimated parameters.

2.4.4. Limitation of study and future perspectives

A major limitation of this study is the lack of detailed observed data, especially observed yields on regional scales. This was a constraining factor in exploring model performance at sub-country and regional levels. Global soil datasets were used without calibration of their parameters. Literatures shows that EPIC is sensitive to aluminum tolerance index (*ALT*) and critical aeration factors (*CAF*), and field capacity (Gaiser et al., 2010; Wang et al., 2012). So, the effect of soil parameter uncertainty on crop yield calibrations requires further investigation. In addition, sensitivity analysis is not included in EPIC$^+$. We will include and yield trend analysis in the further development of EPIC$^+$.

2.5. Reference

Abbaspour, K. C. (2015). SWAT-CUP; SWAT calibration and uncertainty programs - A user manual.

Abbaspour, K. C., Johnson, C. A., and van Genuchten, M. T. (2004). Estimating uncertain flow and transport parameters using a sequential uncertainty fitting procedure. *Vadose Zone Journal* **3**, 1340-1352.

Abbaspour, K. C., Rouholahnejad, E., Vaghefi, S., Srinivasan, R., Yang, H., and Klove, B. (2015). A continental-scale hydrology and water quality model for Europe: Calibration and uncertainty of a high-resolution large-scale SWAT model. *Journal of Hydrology* **524**, 733-752.

Abbaspour, K. C., Yang, J., Maximov, I., Siber, R., Bogner, K., Mieleitner, J., Zobrist, J., and Srinivasan, R. (2007). Modelling hydrology and water quality in the pre-ailpine/alpine Thur watershed using SWAT. *Journal of Hydrology* **333**, 413-430.

Ahmed, M., Akram, M. N., Asim, M., Aslam, M., Hassan, F. U., Higgins, S., Stockle, C. O., and Hoogenboom, G. (2016). Calibration and validation of APSIM-Wheat and CERES-Wheat for spring wheat under rainfed conditions: Models evaluation and application. *Computers and Electronics in Agriculture* **123**, 384-401.

Angulo, C., Roetter, R., Trnka, M., Pirttioja, N., Gaiser, T., Hlavinka, P., and Ewert, F. (2013a). Characteristic 'fingerprints' of crop model responses data at different spatial resolutions to weather input. *European Journal of Agronomy* **49**, 104-114.

Angulo, C., Rotter, R., Lock, R., Enders, A., Fronzek, S., and Ewert, F. (2013b). Implication of crop model calibration strategies for assessing regional impacts of climate change in Europe. *Agricultural and Forest Meteorology* **170**, 32-46.

Azari, M., Moradi, H. R., Saghafian, B., and Faramarzi, M. (2016). Climate change impacts on streamflow and sediment yield in the North of Iran. *Hydrological Sciences Journal-Journal Des Sciences Hydrologiques* **61**, 123-133.

Azimi, M., Heshmati, G. A., Farahpour, M., Faramarzi, M., and Abbaspour, K. C. (2013). Modeling the impact of rangeland management on forage production of sagebrush species in arid and semi-arid regions of Iran. *Ecological Modelling* **250**, 1-14.

Balkovic, J., van der Velde, M., Schmid, E., Skalsky, R., Khabarov, N., Obersteiner, M., Sturmer, B., and Xiong, W. (2013). Pan-European crop modelling with EPIC: Implementation, up-scaling and regional crop yield validation. *Agricultural Systems* **120**, 61-75.

Batjes, N. H. (2006). ISRIC-WISE derived soil properties on a 5 by 5 arc-minutes global grid. ISRIC - World Soil Information, Wageningen, Netherlands.

Beguy, D. (2016). Poor data affects Africa's ability to make the right policy decisions. *In* "Time Live".

Ben-Ari, T., and Makowski, D. (2014). Decomposing global crop yield variability. *Environmental Research Letters* **9**.

Bryan, E., Deressa, T. T., Gbetibouo, G. A., and Ringler, C. (2009). Adaptation to climate change in Ethiopia and South Africa: options and constraints. *Environmental Science & Policy* **12**, 413-426.

Bulatewicz, T., Jin, W., Staggenborg, S., Lauwo, S., Miller, M., Das, S., Andresen, D., Peterson, J., Steward, D. R., and Welch, S. M. (2009). Calibration of a crop model to irrigated water use using a genetic algorithm. *Hydrology and Earth System Sciences* **13**, 1467-1483.

Causarano, H. J., Doraiswarny, P. C., McCarty, G. W., Hatfield, J. L., Milak, S., and Stern, A. J. (2008). EPIC modeling of soil organic carbon sequestration in croplands of Iowa. *Journal of Environmental Quality* **37**, 1345-1353.

Causarano, H. J., Shaw, J. N., Franzluebbers, A. J., Reeves, D. W., Raper, R. L., Balkcom, K. S., Norfleet, M. L., and Izaurralde, R. C. (2007). Simulating field-scale soil organic carbon dynamics using EPIC. *Soil Science Society of America Journal* **71**, 1174-1185.

Challinor, A. J., Ewert, F., Arnold, S., Simelton, E., and Fraser, E. (2009). Crops and climate change: progress, trends, and challenges in simulating impacts and informing adaptation. *Journal of Experimental Botany* **60**, 2775-2789.

Chun, J. A., Li, S., Wang, Q. G., Lee, W. S., Lee, E. J., Horstmann, N., Park, H., Veasna, T., Vanndy, L., Pros, K., and Vang, S. (2016). Assessing rice productivity and adaptation strategies for Southeast Asia under climate change through multi-scale crop modeling. *Agricultural Systems* **143**, 14-21.

Conceicao, P., Levine, S., Lipton, M., and Warren-Rodriguez, A. (2016). Toward a food secure future: Ensuring food security for sustainable human development in Sub-Saharan Africa. *Food Policy* **60**, 1-9.

Deng, J. M., Ran, J. Z., Wang, Z. Q., Fan, Z. X., Wang, G. X., Ji, M. F., Liu, J., Wang, Y., Liu, J. Q., and Brown, J. H. (2012). Models and tests of optimal density and maximal yield for crop plants. *Proceedings of the National Academy of Sciences of the United States of America* **109**, 15823-15828.

Doherty, J. (2001). PEST-ASP Users' manual Brisbane, Australia.

Doraiswamy, P. C., McCarty, G. W., Hunt, E. R., Yost, R. S., Doumbia, M., and Franzluebbers, A. J. (2007). Modeling soil carbon sequestration in agricultural lands of Mali. *Agricultural Systems* **94**, 63-74.

FAO (2007). FertiSTAT - Fertilizer Use Statistics. Food and Agricultural Organization of the UN, Rome, http://www.fao.org/ag/agl/fertistat/index_en.htm.

FAO (2012). FAOSTAT Statistical Database. Rome: Food and Agricultural Organization of the UN.

Faramarzi, M., Yang, H., Schulin, R., and Abbaspour, K. C. (2010). Modeling wheat yield and crop water productivity in Iran: Implications of agricultural water management for wheat production. *Agricultural Water Management* **97**, 1861-1875.

Folberth, C., Gaiser, T., Abbaspour, K. C., Schulin, R., and Yang, H. (2012a). Regionalization of a large-scale crop growth model for Sub-Saharan Africa: Model setup, evaluation, and estimation of maize yields. *Agriculture Ecosystems & Environment* **151**, 21-33.

Folberth, C., Yang, H., Gaiser, T., Liu, J. G., Wang, X. Y., Williams, J., and Schulin, R. (2014). Effects of ecological and conventional agricultural intensification practices on maize yields in Sub-Saharan Africa under potential climate change. *Environmental Research Letters* **9**, 1-12.

Folberth, C., Yang, H., Wang, X. Y., and Abbaspour, K. C. (2012b). Impact of input data resolution and extent of harvested areas on crop yield estimates in large-scale agricultural modeling for maize in the USA. *Ecological Modelling* **235**, 8-18.

Gaiser, T., de Barros, I., Sereke, F., and Lange, F. M. (2010). Validation and reliability of the EPIC model to simulate maize production in small-holder farming systems in tropical sub-humid West Africa and semi-arid Brazil. *Agriculture Ecosystems & Environment* **135**, 318-327.

Gassman, P. W., Williams, J. R., Benson, V. W., Izaurralde, R. C., Hauck, L. M., Jones, C. A., Atwood, J. D., Kiniry, J., and Flowers, J. D. (2005). Historical development and applications of the EPIC and APEX models. *Working Paper 05-WP 397.*

Grassini, P., Eskridge, K. M., and Cassman, K. G. (2013). Distinguishing between yield advances and yield plateaus in historical crop production trends. *Nature Communications* **4**.

Hatfield, J. L., and Prueger, J. H. (2015). Temperature extremes: Effect on plant growth and development. *Weather and Climate Extremes* **10**, 4-10.

Holzworth, D. P., Huth, N. I., Devoil, P. G., Zurcher, E. J., Herrmann, N. I., McLean, G., Chenu, K., van Oosterom, E. J., Snow, V., Murphy, C., Moore, A. D., Brown, H., Whish, J. P. M., Verrall, S., Fainges, J., Bell, L. W., Peake, A. S., Poulton, P. L., Hochman, Z., Thorburn, P. J., Gaydon, D. S., Dalgliesh, N. P., Rodriguez, D., Cox, H., Chapman, S., Doherty, A., Teixeira, E., Sharp, J., Cichota, R., Vogeler, I., Li, F. Y., Wang, E. L., Hammer, G. L., Robertson, M. J., Dimes, J. P., Whitbread, A. M., Hunt, J., van Rees, H., McClelland, T., Carberry, P. S., Hargreaves, J. N. G., MacLeod, N., McDonald, C., Harsdorf, J., Wedgwood, S., and Keating, B. A. (2014). APSIM - Evolution towards a new generation of agricultural systems simulation. *Environmental Modelling & Software* **62**, 327-350.

Holzworth, D. P., Snow, V., Janssen, S., Athanasiadis, I. N., Donatelli, M., Hoogenboom, G., White, J. W., and Thorburn, P. (2015). Agricultural production systems modelling and software: Current status and future prospects. *Environmental Modelling & Software* **72**, 276-286.

Houska, T., Kraft, P., Chamorro-Chavez, A., and Breuer, L. (2015). SPOTting Model Parameters Using a Ready-Made Python Package. *Plos One* **10**.

Iglesias, A., Quiroga, S., and Diz, A. (2011). Looking into the future of agriculture in a changing climate. *European Review of Agricultural Economics* **38**, 427-447.

Jensen, J. R., Bernhard, R. H., Hansen, S., McDonagh, J., Moberg, J. P., Nielsen, N. E., and Nordbo, E. (2003). Productivity in maize based cropping systems under various soil-water-nutrient management strategies in a semi-arid, alfisol environment in East Africa. *Agricultural Water Management* **59**, 217-237.

Jones, J. W., Hoogenboom, G., Porter, C. H., Boote, K. J., Batchelor, W. D., Hunt, L. A., Wilkens, P. W., Singh, U., Gijsman, A. J., and Ritchie, J. T. (2003). The DSSAT cropping system model. *European Journal of Agronomy* **18**, 235-265.

Jones, P. G., and Thornton, P. K. (2003). The potential impacts of climate change on maize production in Africa and LatinAmerica in 2055. *Global Environmental Change-Human and Policy Dimensions* **13**, 51-59.

Kiniry, J. R., Anderson, L. C., Johnson, M. V. V., Behrman, K. D., Brakie, M., Burner, D., Cordsiemon, R. L., Fay, P. A., Fritschi, F. B., Houx, J. H., Hawkes, C., Juenger, T., Kaiser, J., Keitt, T. H., Lloyd-Reilley, J., Maher, S., Raper, R., Scott, A., Shadow, A., West, C., Wu, Y., and Zibilske, L. (2013). Perennial biomass grasses and the Mason-Dixon line: Comparative productivity across latitudes in the Southern Great plains. *Bioenergy Research* **6**, 276-291.

Kiniry, J. R., Major, D. J., Izaurralde, R. C., Williams, J. R., Gassman, P. W., Morrison, M., Bergentine, R., and Zentner, R. P. (1995). Epic model parameters for cereal, oilseed, and forage crops in the Northern great-plains region. *Canadian Journal of Plant Science* **75**, 679-688.

Lee, C. M., Chandler, C., Lazarus, M., and X. Johnson, F. (2013). Assessing the climate impacts of cookstove projects: issues in emissions accounting. *Challenges in Sustainability* **1**, 53-71.

Lemann, T., Zeleke, G., Amsler, C., Giovanoli, L., Suter, H., and Roth, V. (2016). Modelling the effect of soil and water conservation on discharge and sediment yield in the upper Blue Nile basin, Ethiopia. *Applied Geography* **73**, 89-101.

Liu, J. G., Williams, J. R., Zehnder, A. J. B., and Yang, H. (2007). GEPIC - Modelling wheat yield and crop water productivity with high resolution on a global scale. *Agricultural Systems* **94**, 478-493.

Liu, J. G., and Yang, H. (2010). Spatially explicit assessment of global consumptive water uses in cropland: Green and blue water. *Journal of Hydrology* **384**, 187-197.

Liu, W., Yang, H., Folberth, C., Wang, X., Luo, Q., and Schulin, R. (2016). Global investigation of impacts of PET methods on simulating crop-water relations for maize. *Agricultural and Forest Meteorology* **221**, 164–175.

Lobell, D. B., Schlenker, W., and Costa-Roberts, J. (2011). Climate trends and global crop production since 1980. *Science* **333**, 616-620.

Manevski, K., Borgesen, C. D., Li, X. X., Andersen, M. N., Zhang, X. Y., Abrahamsen, P., Hu, C. S., and Hansen, S. (2016). Optimising crop production and nitrate leaching in China: Measured and simulated effects of straw incorporation and nitrogen fertilisation. *European Journal of Agronomy* **80**, 32-44.

Me, W., Abell, J. M., and Hamilton, D. P. (2015). Effects of hydrologic conditions on SWAT model performance and parameter sensitivity for a small, mixed land use catchment in New Zealand. *Hydrology and Earth System Sciences* **19**, 4127-4147.

Monteiro, J. A. F., Kamali, B., Srinivasan, R., Abbaspour, K. C., and Gücker, B. (2016). Modelling the effect of riparian vegetation restoration on sediment transport in a human-impacted Brazilian catchment. *Ecohydrology*.

Niu, X. Z., Easterling, W., Hays, C. J., Jacobs, A., and Mearns, L. (2009). Reliability and input-data induced uncertainty of the EPIC model to estimate climate change impact on sorghum yields in the US Great Plains. *Agriculture Ecosystems & Environment* **129**, 268-276.

Oliver, R. J., Finch, J. W., and Taylor, G. (2009). Second generation bioenergy crops and climate change: a review of the effects of elevated atmospheric CO2 and drought on water use and the implications for yield. *Global Change Biology Bioenergy* **1**, 97-114.

Overman, A. R., and Scholtz, R. V. (2011). Model of yield response of corn to plant population and absorption of solar energy. *Plos One* **6**.

Portmann, F. T., Siebert, S., and Doll, P. (2010). MIRCA2000-Global monthly irrigated and rainfed crop areas around the year 2000: A new high-resolution data set for agricultural and hydrological modeling. *Global Biogeochemical Cycles* **24**, 1-24.

Sacks, W. J., Deryng, D., Foley, J. A., and Ramankutty, N. (2010). Crop planting dates: An analysis of global patterns. *Global Ecology and Biogeography* **19**, 607-620.

Saseendran, S. A., Nielsen, D. C., Ma, L., Ahuja, L. R., and Halvorson, A. D. (2004). Modeling nitrogen management effects on winter wheat production using RZWQM and CERES-wheat. *Agronomy Journal* **96**, 615-630.

Sexton, J., Everingham, Y., and Inman-Bamber, G. (2016). A theoretical and real world evaluation of two Bayesian techniques for the calibration of variety parameters in a sugarcane crop model. *Environmental Modelling & Software* **83**, 126-142.

Sharpley, A. N., and Williams, J. R. (1990). EPIC erosion/productivity impact calculator: model documentation. United States Department of Agriculture, 1-235.

Singh, J., Knapp, H. V., Arnold, J. G., and Demissie, M. (2005). Hydrological modeling of the iroquois river watershed using HSPF and SWAT. *Journal of the American Water Resources Association* **41**, 343-360.

Stockle, C. O. (1992). Canopy photosynthesis and transpiration estimates using radiation interception models with different levels of detail. *Ecological Modelling* **60**, 31-44.

Stockle, C. O., Donatelli, M., and Nelson, R. (2003). CropSyst, a cropping systems simulation model. *European Journal of Agronomy* **18**, 289-307.

Sumathy, S., Kyle R., D.-M., and Collin Craige (2017). Field-scale calibration of crop-yield parameters in the Soil and Water Assessment Tool *Agricultural Water Management* **180**, 61-69.

Tao, F. L., Zhang, Z., Liu, J. Y., and Yokozawa, M. (2009). Modelling the impacts of weather and climate variability on crop productivity over a large area: A new super-ensemble-based probabilistic projection. *Agricultural and Forest Meteorology* **149**, 1266-1278.

Tatsumi, K. (2016). Effects of automatic multi-objective optimization of crop models on corn yield reproducibility in the USA. *Ecological Modelling* **322**, 124-137.

Therond, O., Hengsdijk, H., Casellas, E., Wallach, D., Adam, M., Belhouchette, H., Oomen, R., Russell, G., Ewert, F., Bergez, J. E., Janssen, S., Wery, J., and Van Ittersum, M. K. (2011). Using a cropping system model at regional scale: Low-data approaches for crop management information and model calibration. *Agriculture Ecosystems & Environment* **142**, 85-94.

U.S. Geological Survey (2004). Global Digital Elevation Model (GTOPO30). (ESRI, ed.), Redlands, California, USA.

Vaghefi, S. A., Mousavi, S. J., Abbaspour, K. C., Srinivasan, R., and Arnold, J. R. (2015). Integration of hydrologic and water allocation models in basin-scale water resources management considering crop pattern and climate change: Karkheh River Basin in Iran. *Regional Environmental Change* **15**, 475-484.

Van Ittersum, M. K., Leffelaar, P. A., Van Keulen, H., Kropff, M. J., Bastiaans, L., and Goudriaan, J. (2002). Developments in modelling crop growth, cropping systems and production systems in the Wageningen School. *Netherlands Journal of Agricultural Science* **50**, 239-247.

Vanuytrecht, E., Raes, D., Steduto, P., Hsiao, T. C., Heng, L. K., Vila, M. G., Moreno, P. M., and Moreno, P. M. (2014). AquaCrop: FAO's crop water productivity and yield response model. *Environmental Modelling & Software* **62**, 351-360.

Wang, X., He, X., Williams, J. R., Izaurralde, R. C., and Atwood, J. D. (2005). Sensitivity and uncertainty analyses of crop yields and soil organic carbon simulated with EPIC. *Transaction of the ASAE* **48**, 1041-1054.

Wang, X., Williams, J. R., Gassman, P. W., Baffaut, C., Izaurralde, R. C., Jeong, J., and Kiniry, J. R. (2012). EPIC and APEX: model use, calibration, and validation. *Transaction of the ASABE* **55**, 1447-1462.

Ward, C. S., Torquebiau, R., and Xie, H. (2016). improved agricultural water management for Africa's Washington, D.C. .

Webber, H., Gaiser, T., and Ewert, F. (2014). What role can crop models play in supporting climate change adaptation decisions to enhance food security in Sub-Saharan Africa? *Agricultural Systems* **127**, 161-177.

Weedon, G. P., Gomes, S., Viterbo, P., Shuttleworth, W. J., Blyth, E., Osterle, H., Adam, J. C., Bellouin, N., Boucher, O., and Best, M. (2011). Creation of the WATCH forcing data and its use to assess global and regional reference crop evaporation over land during the twentieth century. *Journal of Hydrometeorology* **12**, 823-848.

Williams, J. R., Jones, C. A., Kiniry, J. R., and D.A., S. (1989). The EPIC crop growth model. *Transaction of the ASAE*, 497-454.

Xiong, W., Balkovic, J., van der Velde, M., Zhang, X. S., Izaurralde, R. C., Skalsky, R., Lin, E., Mueller, N., and Obersteiner, M. (2014). A calibration procedure to improve global rice yield simulations with EPIC. *Ecological Modelling* **273**, 128-139.

Xiong, W., Rastislav, S., Cheryl H., P., Juraj, B., James, W. J., and Di , Y. (2016). Calibration-induced uncertainty of the EPIC model to estimate climate change impact on global maize yield. *Journal of Advances in Modeling Earth Systems* **8**, 1358–1375.

Yang, J. C., and Zhang, J. H. (2010). Crop management techniques to enhance harvest index in rice. *Journal of Experimental Botany* **61**, 3177-3189.

Yunusa, I. A. M., and Gworgwor, N. A. (1991). Growth and yield of maize genotypes during dry seasons in Northern Nigeria. *Experimental Agriculture* **27**, 397-405.

Zhao, G., Bryan, B. A., and Song, X. D. (2014). Sensitivity and uncertainty analysis of the APSIM-wheat model: Interactions between cultivar, environmental, and management parameters. *Ecological Modelling* **279**, 1-11.

2.6. Supplementary material

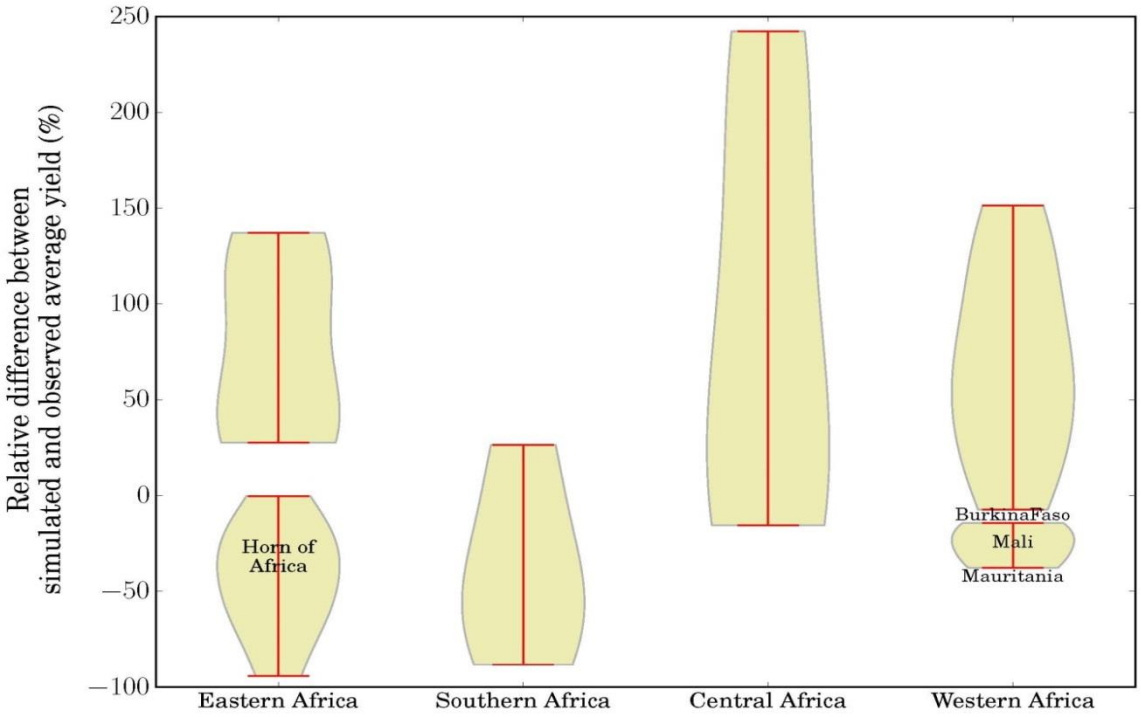

Figure S2.1. Distribution of the difference between FAO-reported and simulated long-term average yields in four SSA regions. Simulated yield is based on average default parameters. Difference is converted to the percentage change related to the FAO-reported average yield.

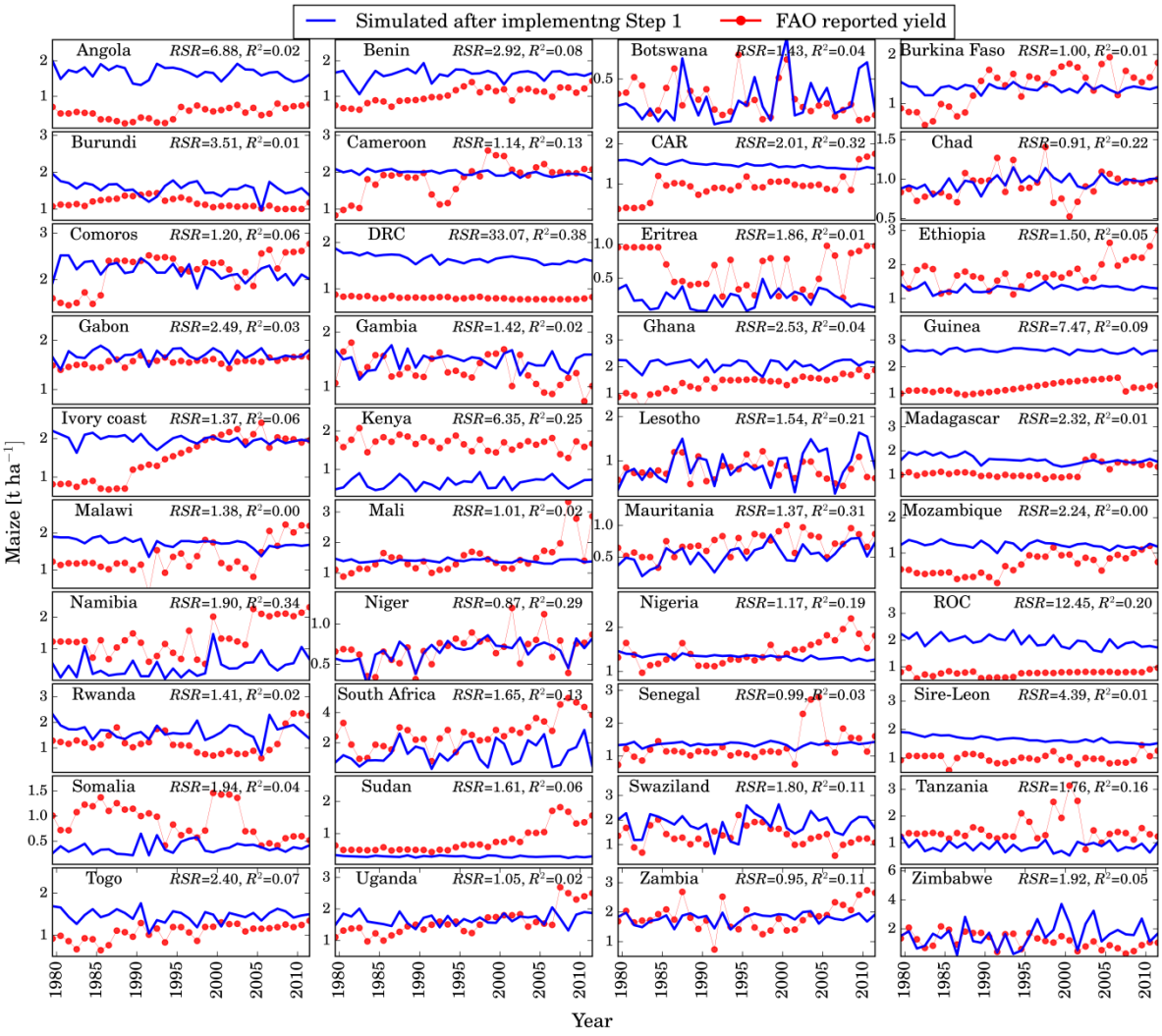

Figure S2.2. Annual simulated crop yields after Step 1 compared with the FAO-reported yields characterized by two efficiency criteria (*RSR* and R^2) at country level during 1980-2012.

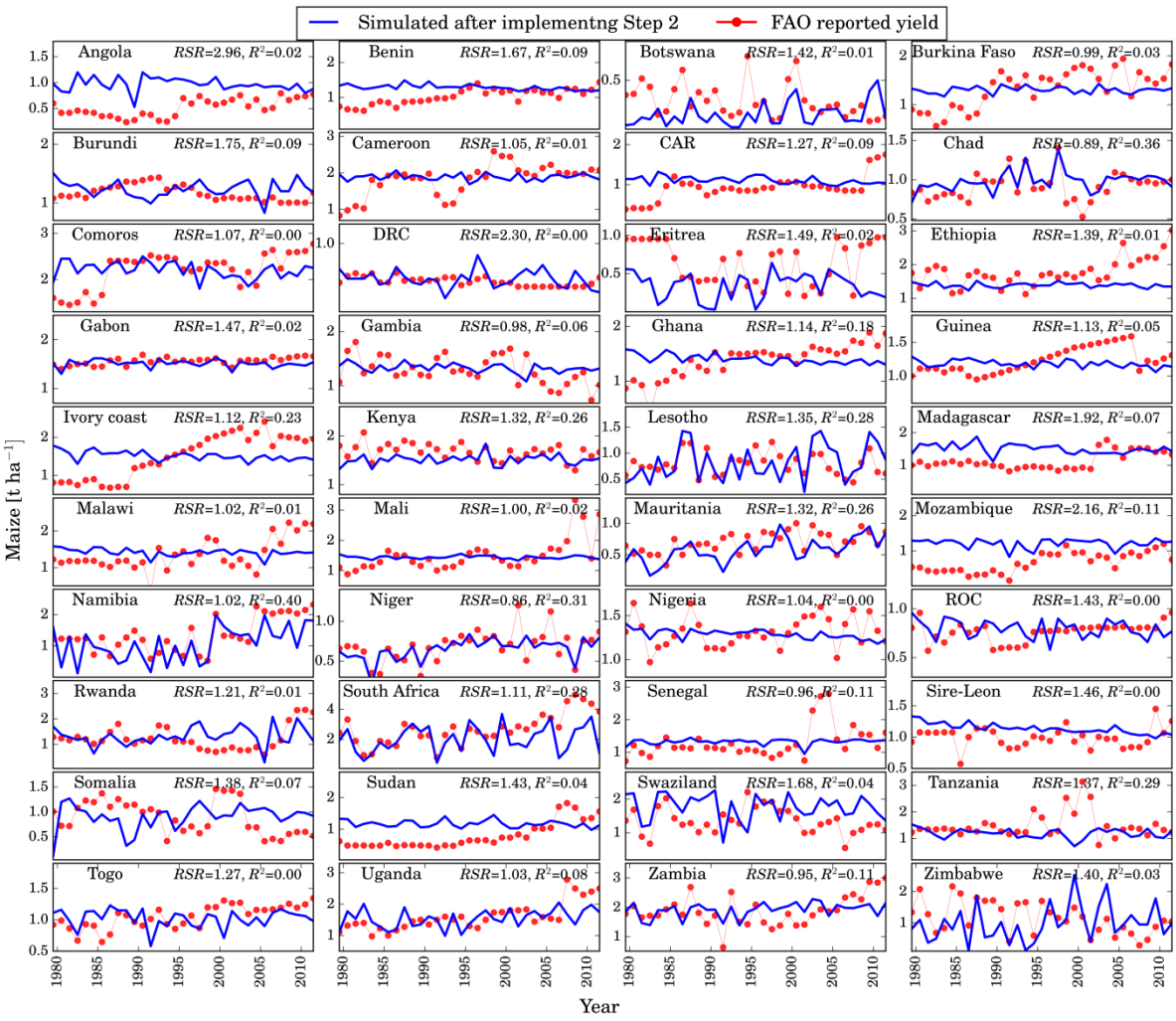

Figure S2.3. Annual simulated crop yields after Step 2 compared with the FAO-reported yields characterized by two efficiency criteria (*RSR* and R^2) at country level during 1980-2012.

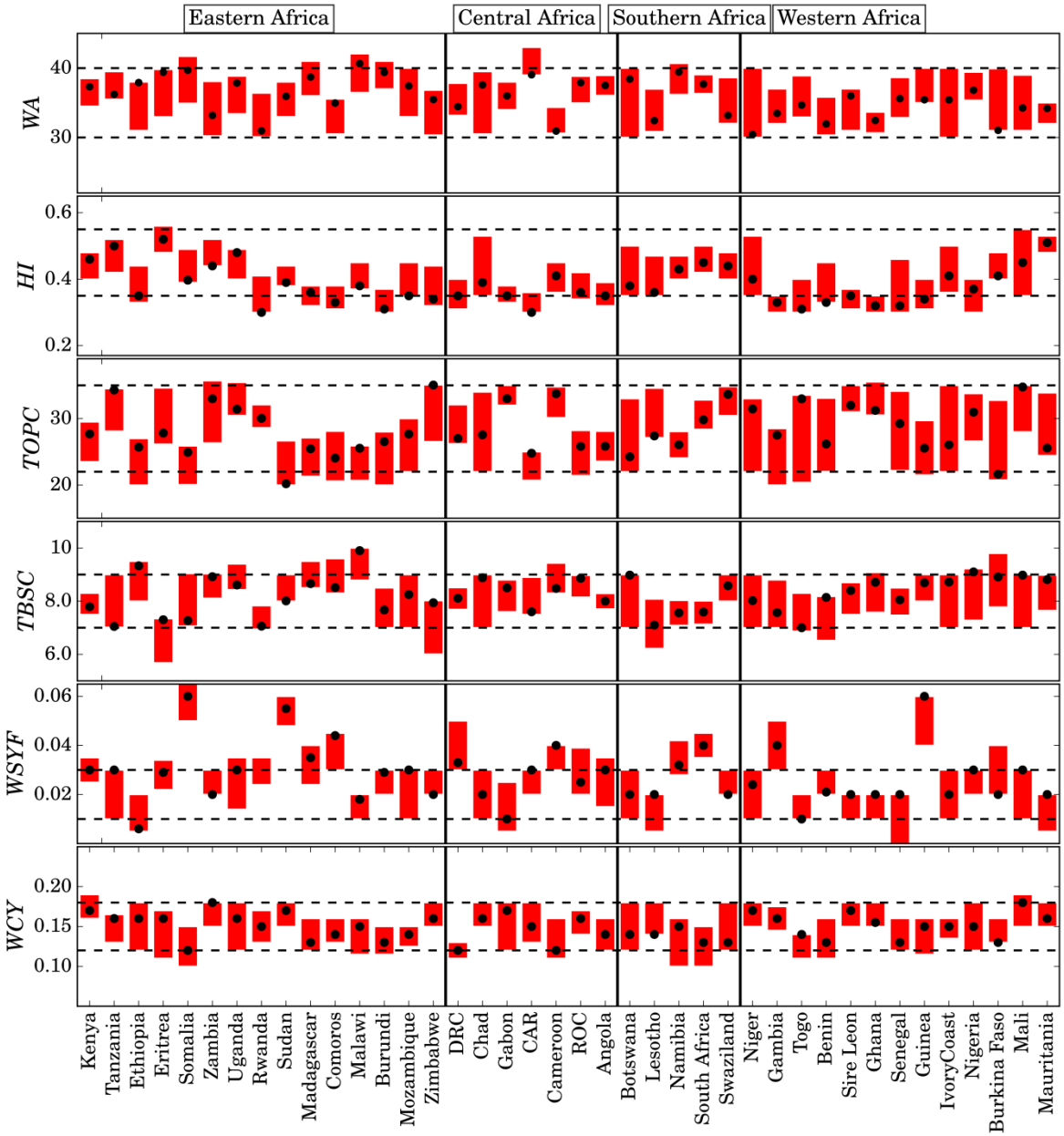

Figure S2.4. The final ranges of Crop parameters (red bar) obtained from the SUFI2 algorithm after Step 3 at country level. The horizontal black dashed lines indicate the initial ranges considered in the calibration, the black circles show the best solution based on *RSR*.

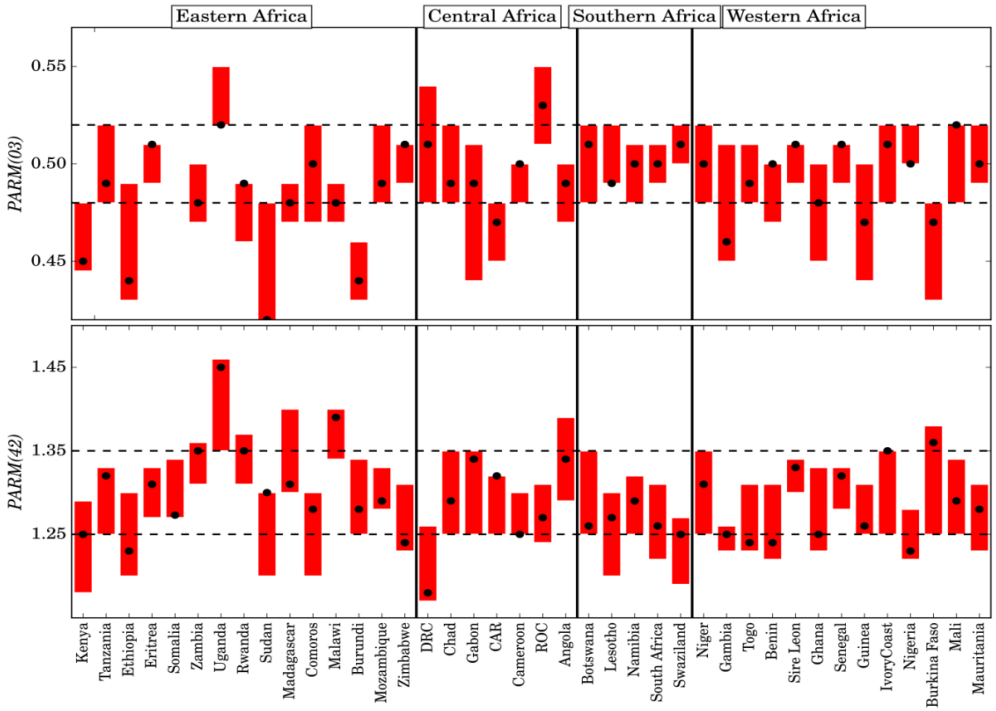

Figure S2.5. The final ranges of Model parameters (red bar) obtained from the SUFI2 algorithm after Step 3 at country level. The horizontal black dashed lines indicate the initial ranges considered in the calibration, the black circles show the best solution based on *RSR* criteria.

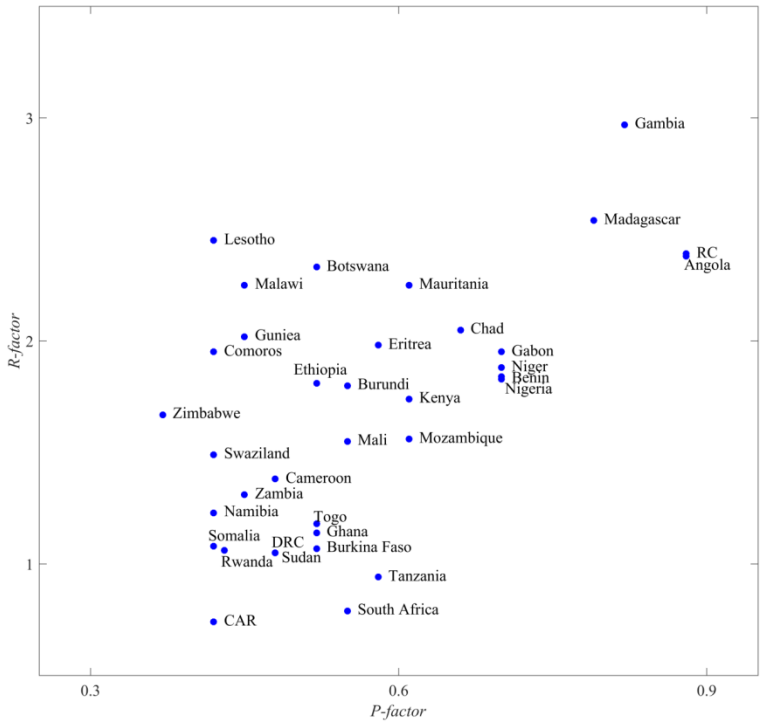

Figure S2.6. *P-factor* versus *R-factor* after implementing linear de-trending. *P-factor* is the percentage of observed data bracketed by the 95PPU. *R-factor* is the width of the 95PPU band representing predictive uncertainty.

Table S2.1. The initial ranges of the Crop and EPIC parameters which were calibrated in Step 3 of the proposed methodlogy and the maximum allowable ranges for each parameter obtained from the literature.

		Parameters	Initial ranges	Maximum allowable ranges	Reference
Step 3	Crop parameters	*WA*	AC [30, 40]	30-45	(Wang et al., 2005)
		HI	AC [0.35,0.55]	0.30-0.60	(Folberth et al., 2012a; Jensen et al., 2003; Wang et al., 2005)
		TOPC	AC [22, 35]	20-35	(Bulatewicz et al., 2009)
		TBSC	AC [7, 9]	5-10	(Folberth et al., 2012b)
		WSYF	AC [0.01, 0.03]	0.01-0.3	(Folberth et al., 2012b)
		WCY	AC [0.12, 0.18]	0.12-0.18	±45% from initial value of 0.45
	Model parameters	*PARM*(03)	AC [0.48, 0.52]	0.3-0.7	(Wang et al., 2005)
		PARM(42)	AC [1.25, 1.35]	0.5-2	(Wang et al., 2005)

WCY: based on personal communication with model developer

Table S2.2**.** *p-values* (*t-stats*), and R^2 obtained from multiple linear regression sensitivity analysis of Operation parameters. Parameters were allowed to change between (-0.45,0.45) from default values, highlighted boxes show most sensitive parameters.

		PHU	*Pdensity*	*N-app*	*K-app*	*BFT0*	*P-app*	R^2
Eastern Africa	Kenya	0.0(144)	0.0(-17.7)	0.25(1.2)	0.65(-0.4)	0.08(1.8)	0.32(-1.0)	0.79
	Tanzania	0.0(506)	0.0(141.3)	0.19(1.3)	0.81(-0.2)	0.67(-0.4)	0.57(-0.6)	1.00
	Ethiopia	0.0(47.5)	0.0(41.4)	0.78(0.3)	0.29(-1.1)	0.69(-0.4)	0.73(0.3)	0.95
	Eritrea	0.0(290)	0.0(23.8)	0.50(-0.7)	0.45(-0.8)	0.07(1.8)	0.83(0.2)	0.87
	Somalia	0.0(211)	0.0(4.12)	0.0 (-8.4)	0.42(-0.6)	0.36(-0.9)	0.98(0.1)	0.69
	Zambia	0.0(182)	0.0(5.9)	0.27(-0.1)	0.11(-3.1)	0.01(0.1)	0.89(-0.8)	0.93
	Uganda	0.0(24.1)	0.0(24.3)	0.74(0.3)	0.02(2.3)	0.2(-1.3)	0.96(-0.0)	0.87
	Rwanda	0.0(27.1)	0.0(4.9)	0.0(4.1)	0.0(8.5)	0.24(1.2)	0.91(-0.1)	0.80
	Sudan	0.0(299)	0.0(-34.1)	0.0(3.1)	0.37(0.9)	0.69(-0.4)	0.0(3.4)	0.70
	Madagascar	0.0(102)	0.0(-17.6)	0.12(-1.6)	0.03(2.2)	0.47(-0.7)	0.44(-0.8)	0.62
	Comoros	0.0(41.7)	0.0(14.3)	0.0(3.3)	0.44(-0.8)	0.79(0.3)	0.92(-0.1)	0.82
	Malawi	0.0(781)	0.0(-21.6)	0.73(-1.1)	0.12(1.6)	0.41(-2.7)	0.44(-0.1)	0.87
	Burundi	0.0(14)	0.0(-13.6)	0.14 (1.5)	0.8(0.3)	0.05(-2.0)	0.35(-0.9)	0.98
	Mozambique	0.0(120)	0.0(23.9)	0.0(-10.2)	0.0(-13.5)	0.68(-0.4)	0.1(-1.7)	0.89
	Zimbabwe	0.0(72.8)	0.0(-9.6)	0.28(1.2)	0.09(0.3)	0.54(-0.3)	0.95(0.04)	0.94
Central Africa	DRC	0.0(66.4)	0.0(-20.1)	0.06(1.9)	0.03(2.3)	0.88(-0.2)	0.79(0.3)	0.62
	Chad	0.0(86.1)	0.0(22.3)	0.01(-1.1)	0.52(-0.8)	0.74(0.9)	0.77(-0.2)	0.38
	Gabon	0.0(297.2)	0.0(24.4)	0.97(11.5)	0.0(3.5)	0.90(-0.3)	0.4(0.6)	0.33
	CAR	0.0(169.3)	0.0(-6.0)	0.31(2.7)	0.6(-0.6)	0.90(0.3)	0.8(-0.3)	0.96
	Cameroon	0.0(175.8)	0.0(-25.2)	0.01(6.4)	0.33(2.4)	0.12(0.6)	0.03(0.7)	0.89
	ROC	0.0(197.4)	0.0(-46.3)	0.0(1.0)	0.03(0.6)	0.87(0.1)	0.67(-0.3)	0.74
Southern Africa	Angola	0.0(227.4)	0.0(-22.8)	0.0(2.1)	0.21(-3.3)	0.46(0.4)	0.22(0.1)	0.99
	Botswana	0.0(1001)	0.0(-14.2)	0.04(-6.8)	0.0(2.2)	0.7(0.2)	0.89(0.4)	0.85
	Lesotho	0.0(117.6)	0.0(-35.9)	0.0(0.3)	0.27(-1.6)	0.53(0.8)	0.89(0.8)	0.38
	Namibia	0.0(169.1)	0.0(-6.0)	0.0(2.7)	0.0(-0.7)	0.68(0.3)	0.1(-0.3)	0.89
	South Africa	0.0(155.3)	0.0(-26.6)	0.25(2.7)	0.75(-0.9)	0.78(-1.6)	0.97(-2.2)	0.5
	Swaziland	0.0(120.4)	0.0(23.9)	0.0(-10.2)	0.15(-13)	0.08(-0.4)	0.66(-1.7)	0.85
Western Africa	Niger	0.0(305)	0.02(98.9)	0.01(-3.9)	0.56(1.3)	0.07(-0.7)	0.53(-1.3)	0.17
	Gambia	0.0(1385)	0.0(39.3)	0.0(3.3)	0.72(-0.8)	0.69(0.4)	0.87(0.9)	0.31
	Togo	0.0(423)	0.0(6.8)	0.19 (4.8)	0.81(1.7)	0.67(0.8)	0.57(-0.6)	1.00
	Benin	0.0(347)	0.0(22.3)	0.0(3.0)	0.1(-1.5)	0.4(-1.8)	0.56(-0.4)	0.45
	Sire Leon	0.0(274)	0.0(34.8)	0.74(16.6)	0.02(-1.8)	0.2(0.1)	0.96(1.1)	0.87
	Ghana	0.0(1705)	0.0(5.6)	0.0(4.4)	0.07(1.1)	0.91(-0.6)	0.3(0.1)	0.95
	Senegal	0.0(648)	0.0(-6.1)	0.06(-3.1)	0.03(-0.4)	0.88(-0.4)	0.79(0.2)	0.82
	Guinea	0.0(519)	0.0(-21.6)	0.0(8.2)	0.0(-0.3)	0.24(0.8)	0.91(-1.5)	0.55
	IvoryCoast	0.0(3835)	0.0(-26.4)	0.0(2.4)	0.37(2.5)	0.69(0.9)	0.0(-0.9)	0.93
	Nigeria	0.0(135)	0.02(68.9)	0.0(3.1)	0.43(1.5)	0.59(0.9)	0.01(-0.5)	0.94
	Burkina Faso	0.0(670)	0.0(2.43)	0.25(-2.7)	0.65 (0.6)	0.08(1.8)	0.32(-0.6)	0.79
	Mali	0.0(881)	0.0(-14.9)	0.0(0.2)	0.75(0.3)	0.42(-0.7)	0.13(0.6)	0.85
	Nigeria	0.0(243)	0.0(-4.9)	0.02(-3.1)	0.02(1.5)	0.36(0.8)	0.351.1)	0.89
	Mauritania	0.0 (74.7)	0.0(-35.9)	0.0(-1.1)	0.13(1.7)	0.43(-0.6)	0.27(-0.1)	0.27

2.7. Overview of EPIC$^+$ and its architecture

EPIC$^+$ is the first version of EPIC with calibration capabilities. The purpose of developing EPIC$^+$ is to extend its application from grid to region, country, and beyond. The base data required for simulation under 0.5^0 resolution are also included in the package. Three software packages have been used to develop EPIC$^+$:

1) The EPIC executable files and FORTRAN source codes for Windows platform can be obtained from: http://epicapex.tamu.edu/model-executables/. The codes are compiled in both Windows and Linux. Both executable files are available in EPIC$^+$.
2) The SUFI2 uncertainty algorithm is used in the SWAT-CUP 5.1 package. This software is freely available from: http://www.neprashtechnology.ca/
3) All scripts for setting up the EPIC$^+$ interface were coded in Python 3.4. Enthought Canopy freely downloadable from: https://store.enthought.com/downloads/#default. The wxPython Wrapper used for programming graphical user interfaces (GUI) of EPIC$^+$ can be freely downloaded from: http://www.wxpython.org/download.php

The EPIC$^+$ interface consists of one main window with four modules: "General settings", "Operation settings", "Parameterization" and "SUFI2 calibration" (Figure S2.7). The first two modules allow extending the application of EPIC from the field scale to a larger region. The last two allow parameterization and calibration with uncertainty quantification using SUFI-2. An explanation of each module is given below.

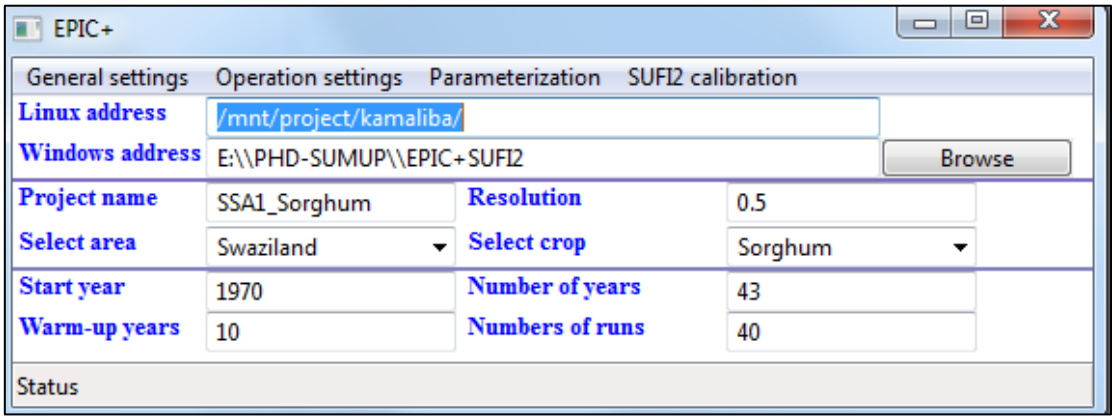

Figure S2.7. The EPIC$^+$ main window

2.7.1. Main window

In this window, the user specifies the general information required to build a project. These include "project address", "project name", "study area", "resolution of grids", "crops to be simulated", "start and end of simulations", "warm up years", and the "total number of runs in each calibration" (Figure S2.7).

2.7.2. General settings

Three windows exist in this module: “Physiographic layer”, “Calibration settings”, and “Print settings” (Figure S2.8).

- In the “Physiographic layer”, the location of physiographic information is specified and includes: dem, slope, climate files, and soil files for each grid, and regional division if calibration is applied on a scale smaller than a country. The “RF harvested area”, and “IR harvested area” files are also defined, where RF stands for rainfed and IR stands for irrigated.

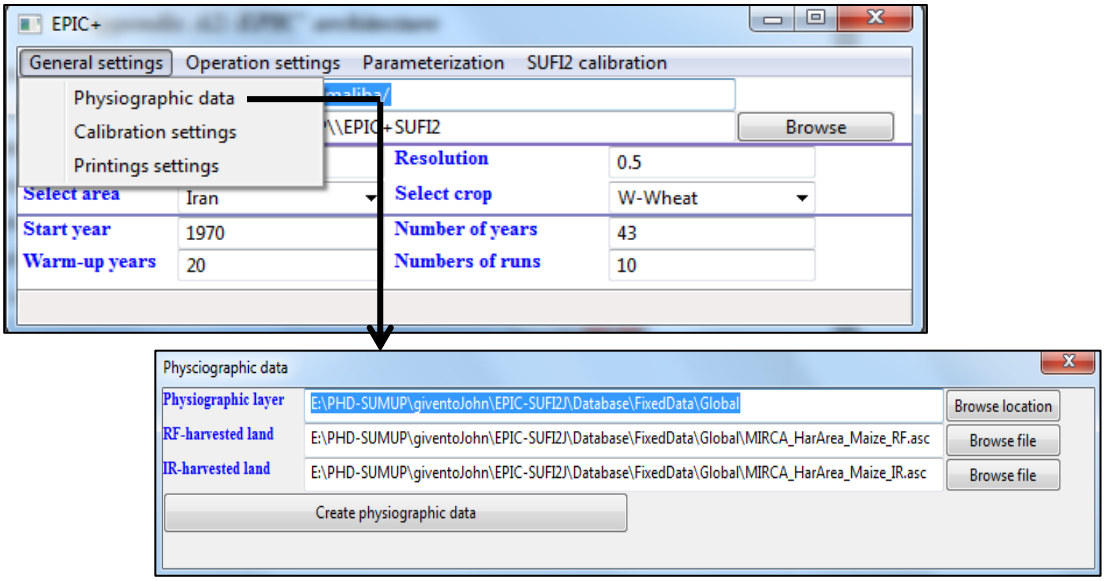

Figure S2.8. The “Physiographic data” window

- In the “Calibration settings”, the user defines the number of runs for calibration, and the location of EPIC original files (Figure S2.9).

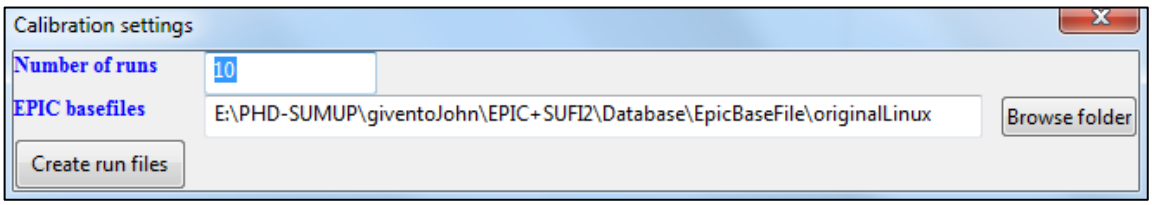

Figure S2.9. The “Calibration settings” window

- In the “Print settings”, the user defines the program outputs based on the desired variables (Figure S2.10).

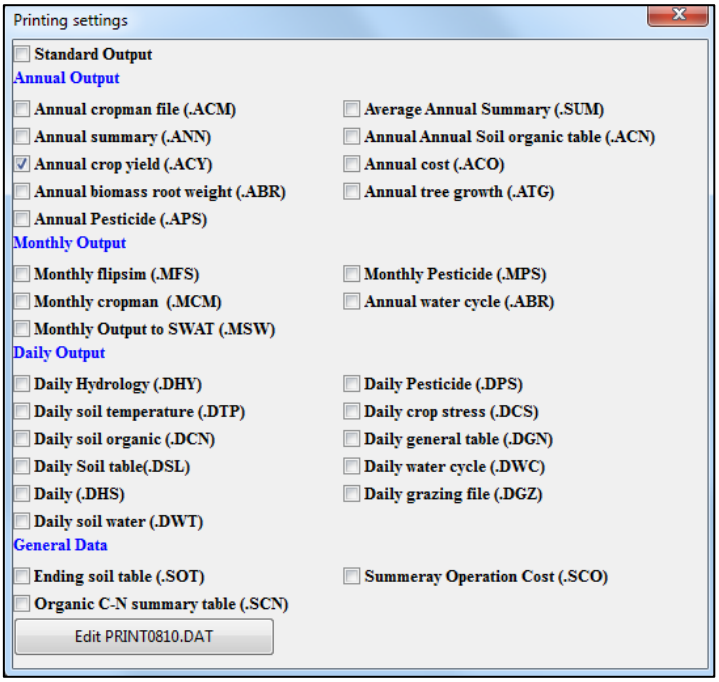

Figure S2.10. The "Print settings" window

2.7.3. Operation settings

This module has two windows: "OPS1" and "OPS2" (Figure S2.11). In each window, the agricultural operations are defined differently depending on the objective and data of the user. Both windows are applicable in rainfed, irrigation, rainfed-irrigation systems. In "OPS1", planting dates are fixed and provided to the program. In "OPS2" the user allows adjustment of planting date between earliest and latest time in each grid, i.e. planting date is considered as a calibrating parameter.

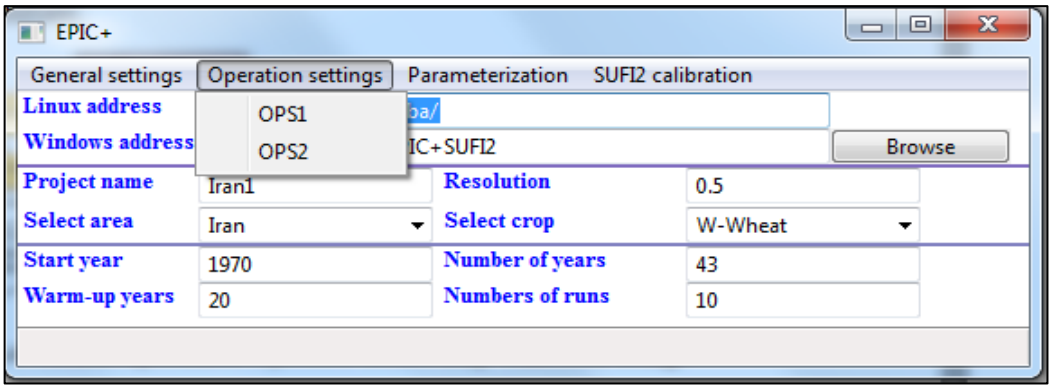

Figure S2.11. "Operation settings" with its two embedded windows

In both windows, Potential Heat Unit (*PHU*), fertilizer application rate (N, P, K), and irrigation application rate can be defined as a fixed value for all grids or different values for each grid. When the values are different for each grid, a .txt file with three columns: longitude, latitude, and value of the variable is defined. Different operations from planting to harvesting are as follows:

- *Planting*: Two options are available “plant in row” and “plant with drill”. This operation needs Planting density and *PHU* as input (Figure S2.12). In the “OPS1” window, the file indicates earliest and latest day of planting. In the “OPS2” window (Figure S2.13), only the day of planting is defined.
- *Tillage*: It is possible to apply tillage operations in one crop calendar. The time of operation should be defined for each grid.
- *Pesticide*. This operation needs time of operation and pesticide rate as input.
- *Irrigation*: This operation needs time of operation and irrigation rate as input.
- *Fertilizer:* N, P, K or others can be selected. Each one needs time of operation and Fertilization rate as input.
- *Harvest*: Two options are available “harvest with kill” and “harvest once”. They can be defined for specific grains and forages. The time of operation is also required
- *Kill crop*: This operation also requires the time of operation as input.

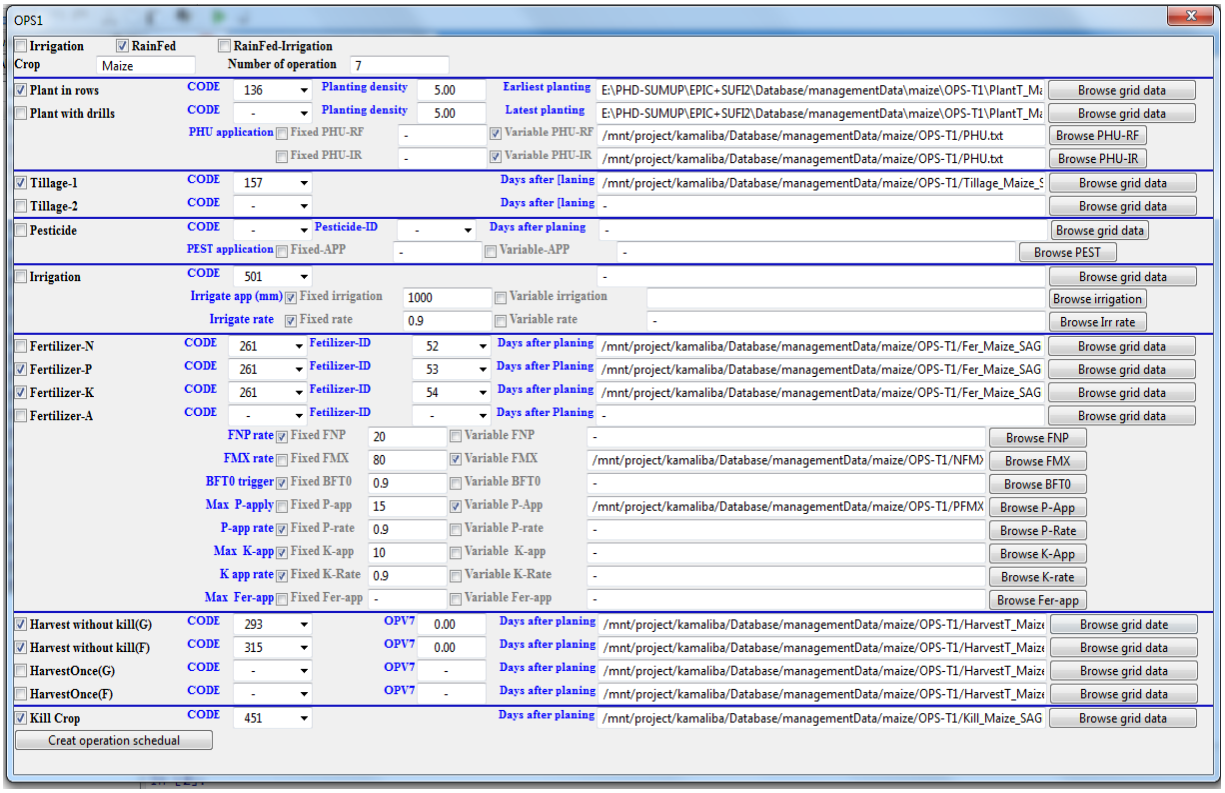

Figure S2.12. The “OPS1” window and its fields

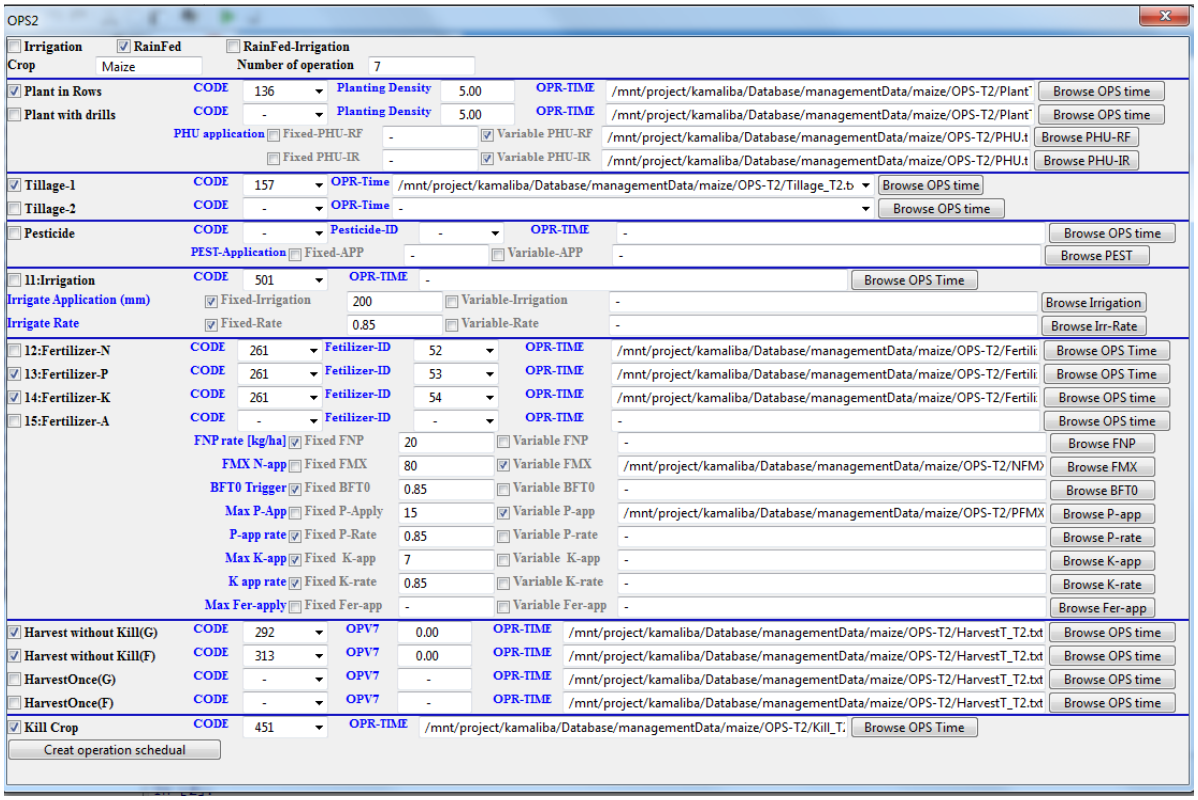

Figure S2.13. Schematic representation of the "OPS2" window

2.7.4. Parameterization

The "Parameterization" module is for selecting parameters to be calibrated and their minimum and maximum values. This is available only in "OPS2" operation. The parameters are classified into three sets and chosen from three different windows. These are "Operation.OPS2", "CROPCOM.OPS2" and "PARM0810.OPS2" (Figure S2.14).

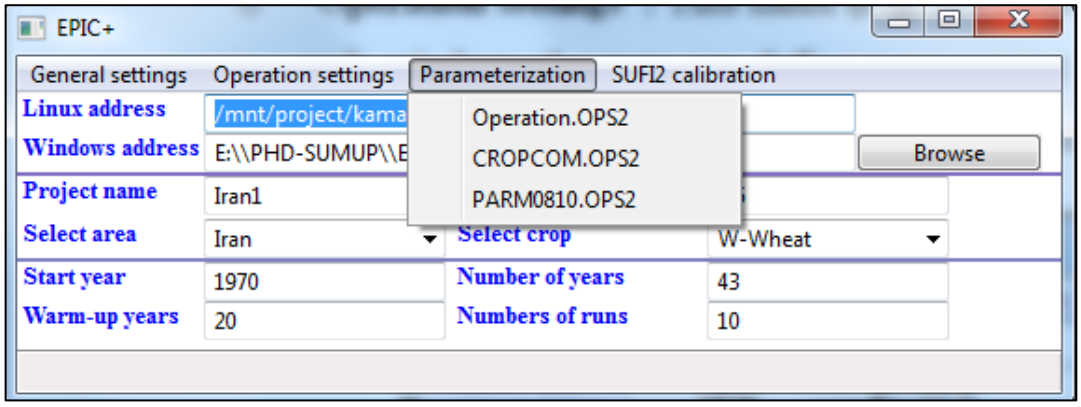

Figure S2.14. "Parameterization" with its three embedded windows

- In "Operation.OPS2", total number of parameters, and the number of parameters from each of three classes are defined (Figure S2.15). The parameter of the "Operation" class are related to agricultural operations like fertilizer application rate, irrigation rate, or planting density.

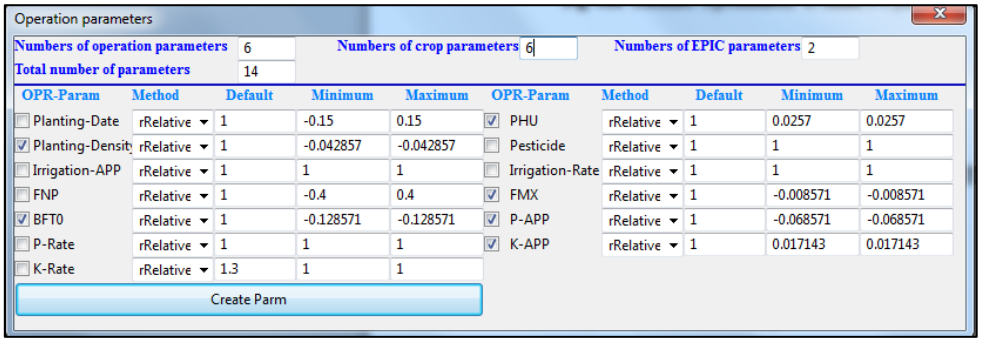

Figure S2.15. The "Operation.OPS2" window for parameterization of Operation parameters

- In "CROPCOM.OPS", the user edits parameters stored in the CROPCOM.DAT file of the original EPIC model (Figure S2.16). They are referred to as "Model parameters". .

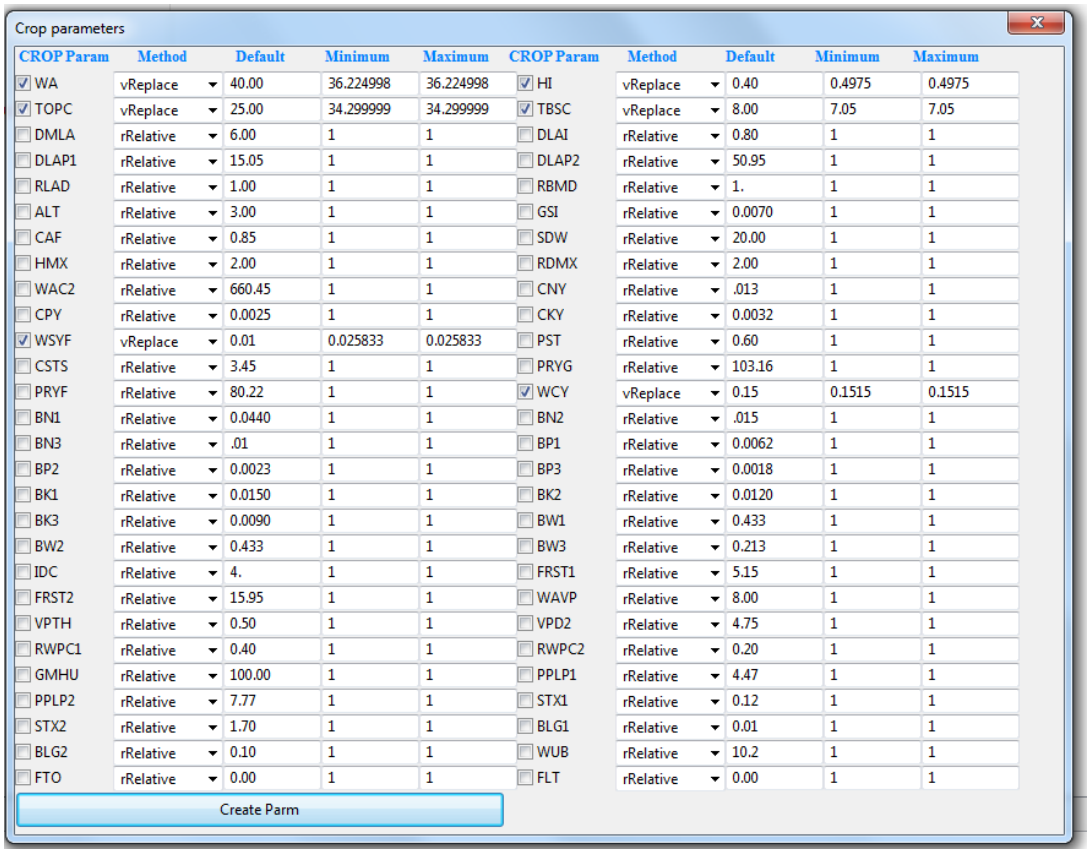

Figure S2.16. The "CROPCOM.OPS2" window for parameterization of "Crop parameters"

- In the "PARM0810.OPS2" window (Figure S2.17), the user edits parameters defined in the PARM0810.DAT file of the original EPIC model. They are referred to as "Model parameters".

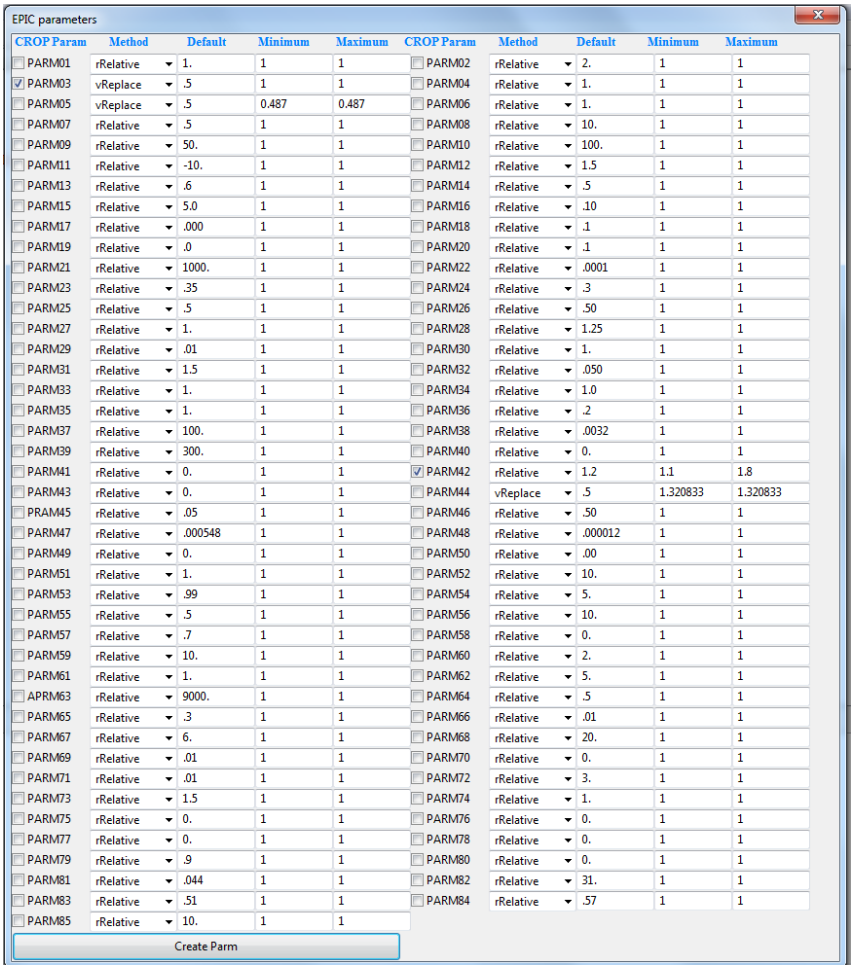

Figure S2.17.Tthe "PARM0810.OPS2" window for parameterization of Model parameters

2.7.5. The SUFI-2 calibration

The "SUFI2 calibration" window, executes the SUFI-2 algorithm step by step (Abbaspour et al., 2007, 2015). The different steps include: parameter sampling and editing, EPIC execution, output extraction from EPIC output files, and calibration output results (plots, 95PPU, parameter ranges, values of objective functions). All these processes are implemented in three windows which are embedded in the SUFI2 calibration module: "SUFI2.pre", one of "SUFI2.RUN"s, "SUFI2.POST" (Figure S2.18).

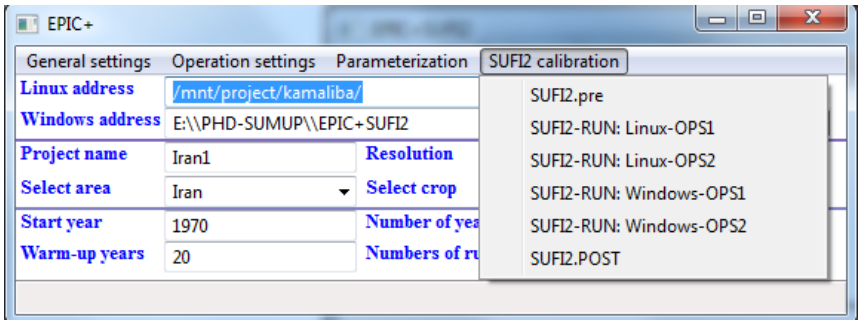

Figure S2.18. "SUFI-2 calibration" with its six operation windows

- In "SUFI2.pre", parameters are sampled using the Latin Hypercube sampling method and their values are stored in relevant files (Figure S2.19). The "Operation parameters" are edited using the OperationFile-EDIT (OPS2) tab. The "Crop parameters" are edited with the CROPCOM-EDIT (OPS2) tab, and the "Model parameters" are edited via PARM0810-EDIT (OPS2).

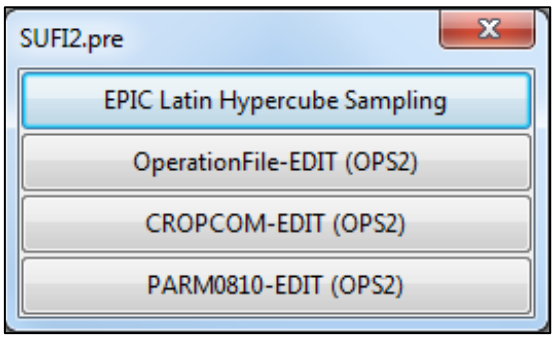

Figure S2.19. The "SUFI2.pre" window and its four tabs

- The "*SUFI2.RUN*" window is for running EPIC. Depending on the selected operation methods (Figure S2.19) and the operating systems, the user opens one of the four windows . Regardless of which is selected, project address, climate data address, soil data address, and management operation database address are specified (Figure S2.20). The scripts are then created and EPIC is executed for each script.

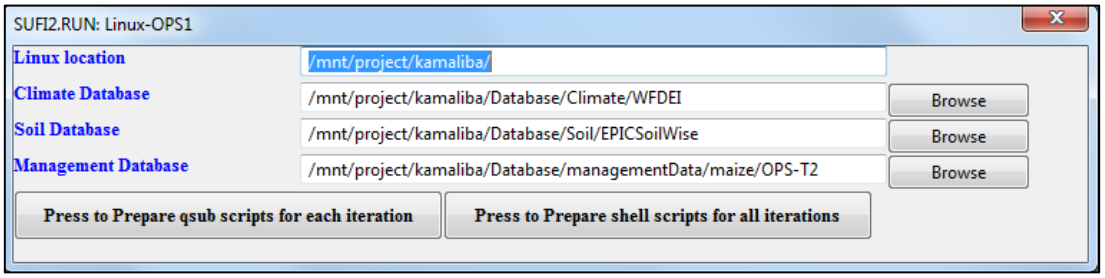

Figure S2.20. schematic representation of the "SUFI2.RUN" window

- In "SUFI2.POST" window, The user defines the objective function, the threshold, and address to observed yield data file (Figure S2.21). The user can then compare observed and simulated values with a choice of 11 different objective functions and calculate the 95 percent prediction uncertainty (95PPU) graph.

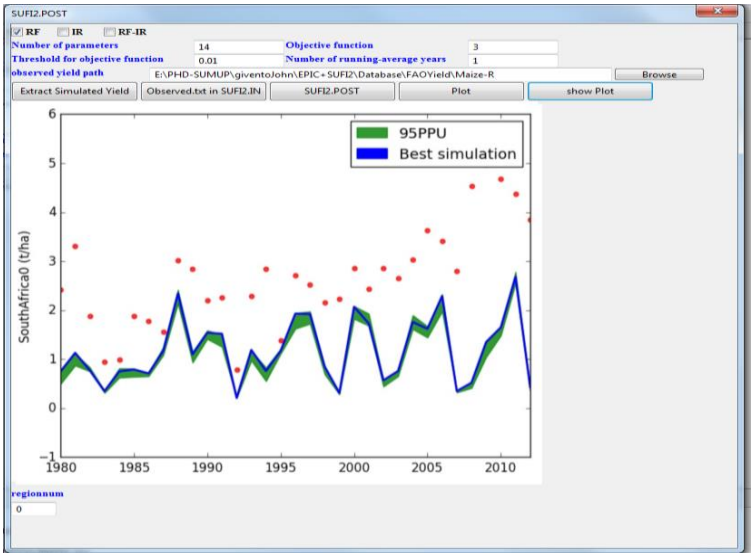

Figure S2.21. Schematic representation of the "SUFI2.POST" window

EPIC$^+$ produces different outputs stored in different .txt files in SUFI.OUT folder of project:

- The values of different criteria in each country, *p-factor* and *r-factor*
- the best simulated yield
- best parameters
- new parameter ranges

Based on the criteria, *p-factor, and r-factor* values, the users decides whether to do another simulation or not. If these criteria are not satisfied , the new parameters are used as the initial ranges for the next iteration (Figure S2.7)

2.7.6. The EPIC$^+$ application for calibration at field scale

The EPIC$^+$ tool can be applied to any scales from field to country or continent. The required settings for field scale application is made in the "Physiographic data" Window (Figure S2.8). In the default EPIC$^+$, all grids within a country are considered as one region. However, the user can treat a grid or a number of grids as one region by changing the physiographic layer. In other words, each country can be split into a number of regions. It is also possible to execute EPIC$^+$ for those regions that observed yield data is available and exclude others from further assessment. We tested this feature of EPIC$^+$ on six fields in Burkina Faso (Field1-Field6) where observed maize yields were available during 2002-2007 (Figure S2.22).

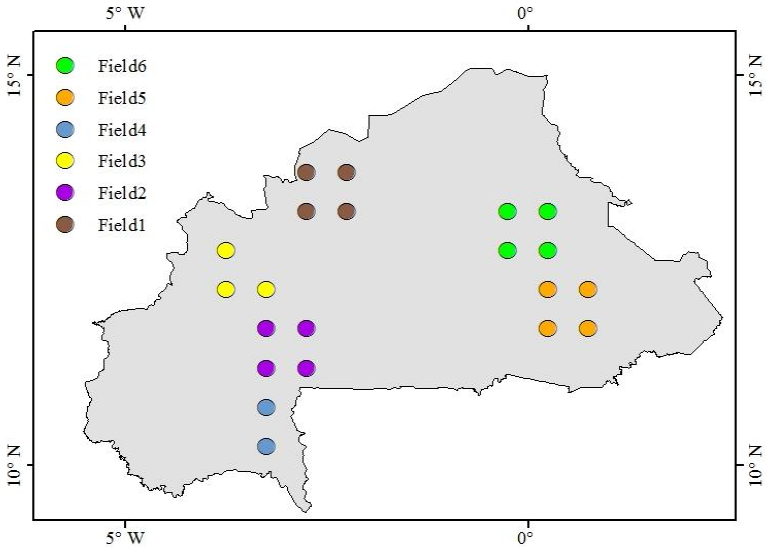

Figure S2.22. The location of six fields in Burkina Faso (Field1-Field6) where maize yield are available during 2002-2007

Comparing simulated and observed yields shows promising results at the field scale. The *RSR* values are below 1.5 in all six fields (Figure S2.23). The 95PPU uncertainty bands bracketed most observed data indicating high performance of field scale calibration. The *P-factor* values at the field level are larger than 0.5 and the *R-factor* values vary between 1.31 and 1.62, which are satisfactory.

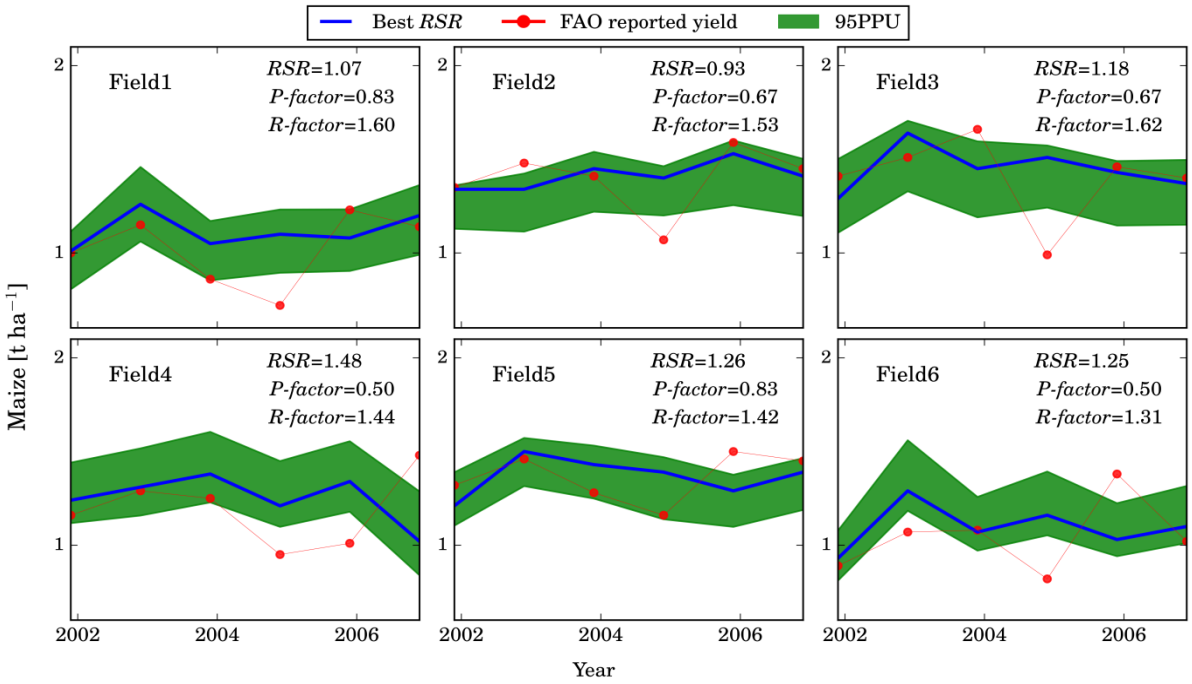

Figure S2.23. Comparison of the FAO reported and simulated maize yields expressed as 95PPU prediction uncertainty band (green bound) and the best simulation (blue line) in six fields in Burkina Faso during 2002-2007.

Chapter 3

Spatial assessment of maize physical drought vulnerability in Sub-Saharan Africa: Linking drought exposure with crop failure

Based on

Spatial assessment of maize physical drought vulnerability in Sub-Saharan Africa: Linking drought exposure with crop failure

Environmental Research Letters, in revision

Authors

Bahareh Kamali[1,2], Karim C. Abbaspour[1], Anthony Lehmann[3], Bernhard Wehrli[2], Hong Yang[1,4]

[1] *Eawag, Swiss Federal Institute of Aquatic Science and Technology, Dübendorf, Switzerland*

[2] *Institute of Biogeochemistry and Pollutant Dynamics, ETH Zurich, Switzerland*

[3] *EnviroSPACE, Forel institute for Environmental Sciences, University of Geneva, Geneva, Switzerland*

[4] *Department of Environmental Sciences, University of Basel, Switzerland*

Abstract

Crop yields exhibit known responses to droughts. However, quantifying crop drought vulnerability is often not straightforward, because components of vulnerability are not defined in a standardized and spatially comparable quantity in most cases and it must be defined on a fine spatial resolution. This study aims to develop a physical crop drought vulnerability index through linking the Drought Exposure Index (*DEI*) with the Crop Sensitivity Index (*CSI*) in Sub-Saharan Africa. Two different *DEI*s were compared. One was derived from the cumulative distribution functions fitted to precipitation and the other from the difference between precipitation and potential evapotranspiration. *DEI*s were calculated for one, three, six, nine, and twelve-month time scales. Similarly, *CSI* was calculated by fitting a cumulative distribution function to maize yield simulated using the Environmental Policy Integrated Climate (EPIC) model. Using a power function, curves were fitted to *CSI* and *DEI* relations resulting in different shapes explaining the severity of vulnerability. The results indicated that in Central Africa the highest correlation was found between *CSI* and *DEI* obtained from the difference between precipitation and potential evapotranspiration in one-month time scale, while this was not the case for other parts of Africa, where *CSI* was strongly correlated to precipitation based *DEI* in three and six-month time scales. Our findings show that Southern African countries and some regions of Sahelian strip are highly vulnerable to drought due to experiencing more water stress, whereas vulnerability in Central African countries pertains to temperature stresses. The proposed methodology provides complementary information on quantifying different degrees of vulnerabilities and the underlying reasons. The methodology can be applied to different regions and spatial scales.

3.1. Introduction

Climate variability and mean temperatures are expected to increase across many regions of the world due to climate change (Rezaei et al., 2015). The agricultural sector exhibits known responses to climate anomalies, and this has huge impacts on food security. SSA as a home to one billion people (World Bank, 2016) is also at the core of this threat. The recurrence of droughts in the past decades has triggered many famines, resulting in the deaths of millions of people and food insecurity across the continent. In SSA, an estimated 41% of the population live on drought-prone lands (Svendsen, 2009). Rainfall variability has a large impact on food production of most countries and livelihoods of the people in the continent due to dependance of continent on rainfed agriculture (Hellmuth et al., 2007). The expected adverse impacts of climate change on crop production adds further risk to the future food security of the region (Liu et al., 2008; Muller, 2011; Roudier et al., 2011; Schlenker and Lobell, 2010). Factors such as slow progress in drought risk management, increased population, and degradation of land and environment have aggravated the situation (Masih et al., 2014). The IPCC's assessments of climate change impacts also suggest declining grain yield to be a likely future scenario. Therefore, understanding drought vulnerability is an important step to finding feasible solutions for mitigating drought impacts, overcoming food insecurity, and associated drought risks.

According to the IPCC's fourth assessment report, vulnerability is defined as the interaction between three constituent components: exposure, sensitivity, and adaptive capacity (Parry et al., 2007). O'Brien et al. (2004) defined exposure as the degree of climate stress on a particular unit of analysis such as magnitude or frequency. It may be represented as either long-term changes in climate conditions, or by changes in climate variability, including the magnitude and frequency of extreme events. Sensitivity is described as the degree of influence of a variable on a system (in this paper, crop yield) when it is stimulated by climatic factors (Parry et al., 2007). Adaptive capacity has been defined as the capacity of a system to adjust to climate change effects to reduce the potential damages or to take advantage of associated opportunities. Vulnerability of a system, hence, entails both physical and socioeconomic aspects. Physical vulnerability refers to the properties of physical structures. It determines their potential damage when the system is exposed to disaster. Factors such as constructing infrastructure or irrigation systems can be used as adaptation strategies of a society to mitigate the impact of exposure. Providing a physical drought vulnerability index resulting only from intrinsic and, in particular, climatic variables would be very useful for water resources managers and policy makers to develop adaptation strategies to alleviate risks of crop failure in areas of high physical vulnerability. Therefore, the central focus of the present study is to assess the physical drought vulnerability.

Several methods are available for quantifying drought vulnerability. A large group of studies have assessed crop drought vulnerability which refers to the extent to which a drought of a given magnitude has an impact on agricultural production. Simelton et al. (2009) defined drought vulnerability through relating meteorological droughts to crop harvest loss to identify regions that are resilient or vulnerable to rainfall variation in China. Wu et al. (2004) established a relationship between the indicators of moisture supply and agricultural production through linking weekly-based Standardized Precipitation Index (*SPI*) (McKee et al., 1993) and Crop Specific Drought Index with the ratio of actual to potential yield. Fraser et al. (2013); Huai (2016); Simelton (2011), and Simelton et al. (2012) have applied a similar approach to determine physical vulnerability of crop production in other regions. These studies have the major limitation of using a simple ratio-based definition that does not allow comparison of vulnerabilities over different areas due to the lack of a standardized scale. As the ratios can vary over a large scale (or range) (0 to ∞), comparing drought vulnerability in different regions becomes very difficult. In addition, when the components of vulnerability (e.g. drought exposure or crop sensitivity) are calculated with different standards, their values vary within different ranges. Therefore, it is not possible to compare their severity of one component with the other with one base. In other words, a certain value for drought exposure or crop sensitivity might be representative of different severities under different standards. Overall, the current studies of drought vulnerability assessment suffer from the lack of standardized procedure for defining their components.

Another approach to define crop drought vulnerability is by curve fitting to find a relationship between drought intensity and yield loss variables. Wang et al. (2013) used physical vulnerability curves to define a relationship between drought intensity and yield loss. Jia et al. (2012); Naumann et

al. (2015), and Guo et al. (2016) have also provided physical drought vulnerability maps by fitting assessment curves through drought intensity and yield loss variables. Drought intensities were obtained from *SPI* and Standardized Precipitation Evapotranspiration Index (*SPEI*) (Vicente-Serrano et al., 2010). The drawback of studies based on fitting curve approaches is that the severity of vulnerability is not clearly explained according to the shape of the fitted curves. In other words, there is a lack of clarity on differentiating between different degrees of severity at different spatial and geographical locations.

Despite extensive studies on agricultural vulnerability assessment, most analyses have been performed at the country level (Brooks et al., 2005; Naumann et al., 2014; Naumann et al., 2015; Shahid and Behrawan, 2008), This is because crop databases are usually available at country level, which do not provide information on finer spatial coverage (Thornton et al., 2009). Regional crop yield data have been sparsely collected and are available for a limited period. SSA is a case where crop data is incomplete and in most cases of poor quality; hence the available data cannot explain the sub-national heterogeneity. Crop drought vulnerability assessment studies in SSA are mostly done at country level. The sub-national studies of SSA are limited to specific regions, and are not applied at Pan-SSA level. The application of a crop model helps to obtain data at fine spatial resolution. Therefore, and for a better understanding of drought-failure relations on large scales, process-based physical crop models need to be used to obtain information on finer resolutions. Apart from providing spatial heterogeneity, crop models provide complementary concepts on identifying different stresses that a crop may experience during its growth periods. Linking a fine resolution conceptual crop model with vulnerability concepts has been less researched specially at continental scale such as SSA.

In recent years, input data (e.g. climate or soil data) required for crop models are usually available at grid level with different resolutions. Several studies have attempted to select the optimal grid cell resolution (Mearns et al., 2002; Orrego et al., 2014). de Wit et al. (2005), for example, concluded that the grid size of 50×50 km is an appropriate geospatial resolution. To address the above mentioned gaps, we quantify the physical vulnerability of maize to drought for SSA by simulating maize yield at 0.5° resolution using the calibrated EPIC crop model. Maize was selected because it is a staple food crop covering about 20% of the calorie intake and 13% of the total cultivated land in SSA (FAO, 2010). We specifically aim to address the following questions:

1) How can grid level components of vulnerability (drought exposure and crop failure) be framed using a normalized metrics across SSA? And how should they be aggregated to better characterize the severity of crop drought vulnerability?

2) What time scale of drought exposure indices does exert the strongest sensitivity on crop yield?

3) Where are the vulnerability hotspots in SSA at sub-national level? and what are the underlying factors making one region physically more vulnerable to drought?

We demonstrate the utility of our approach in vulnerability assessment of maize in SSA by providing a vulnerability map and discuss the implications of our method for future researches and practices.

3.2. Data and methods

3.2.1. Study area

SSA is home to 1 billion people (World Bank, 2016) and is frequently struck by droughts. Rainfall variability has a large impact on food production of most countries and livelihoods of the people in the continent (Hellmuth et al., 2007). In SSA, an estimated 41% of the population (ca. 260 million) live on drought-prone lands (Svendsen, 2009). The recurrence of droughts in the past decades has triggered many famines, resulting in the deaths of millions of people and food insecurity across the sub-continent. The expected adverse impacts of climate change on crop production in SSA adds further risk to the future food security of the region (Liu et al., 2008; Muller, 2011; Roudier et al., 2011; Schlenker and Lobell, 2010).

3.2.2. Crop model and calibration

Maize yield was simulated using an extended version of EPIC (EPIC^{+}, Kamali et al. (2018a)). EPIC is a field-scale crop model designed to simulate the different processes of farming systems as well as their interactions using data such as weather, soil, land use, and crop management parameters (Williams et al., 1989). EPIC operates on a daily time step and can simulate crop growth under various climate and environment conditions, as well as complex management schemes. Further information on EPIC crop-related processes is given in Williams et al. (1989). In order to extend the application of EPIC from field to the SSA scale, we divided the study area into 0.5°×0.5° grids and executed EPIC on each grid cell using a framework programmed in Python (Kamali et al., 2018a).

For model calibration, the developed framework was also coupled with the Sequential Uncertainty Fitting (SUFI-2) algorithm (Abbaspour et al., 2007). SUFI-2 was chosen because of its flexibility and efficiency compared with other algorithms (Uniyal et al., 2015; Yang et al., 2008). The algorithm calculates the uncertainty of model prediction and expresses the output as the 95% prediction uncertainty (95PPU), which is obtained through propagating parameter uncertainties. We calibrated the model at national level using recorded FAO yield (Y_{obs}) during 1980–2012 (33 years). The yields were de-trended using a linear de-trending method which appeared to be a suitable approaches in most cases to remove any influence of technology or socio-economic factors (Osborne and Wheeler, 2013). We chose the Standardized Root Mean Square Error (*RSR*) (Singh et al., 2005) as the criterion to compare the performance of country-level simulated yield (Y_{sim}) with Y_{obs} as:

$$RSR = \frac{RMSE}{STDEV_{obs}} = \frac{\sqrt{\sum_{t=1}^{33}(Y_{obs,t} - Y_{sim,t})^2}}{\sqrt{\sum_{t=1}^{33}(Y_{obs,t} - \bar{Y}_{obs})^2}} \quad (3.1)$$

Y_{sim} was obtained from simulating irrigated and rainfed yields in the EPIC model on *n* grids within a country. It was then aggregated to the country level using weighted cultivated areal averages (Kamali et al., 2018a).

Two criteria in SUFI-2, *r-factor* and *p-factor*, judge the goodness-of-fit and the level of uncertainty of the model. The *p-factor* represents the fraction of measured data bracketed by the 95PPU uncertainty band and varies from 0 to 1, where 1 means 100% of the measured data are bracketed by the model simulation (expressed as the 95PPU). Values around 0.5 are usually acceptable for crop simulation (Abbaspour et al., 2015). The *r-factor* is the average width of the 95PPU band divided by the standard deviation of the measured variable, which is a measure of the prediction uncertainty. The ideal value for the *r-factor* is 0, with an acceptable practical value of around 2 for crop yield and is defined as.

$$r-factor = \frac{\frac{1}{33}\sum_{t=1}^{33}(Y_{sim,97.5,t}-Y_{sim,2.5,t})}{\sigma_{obs}} \quad (3.2)$$

where $Y_{sim,97.5}$ and $Y_{sim,2.5}$ are the upper and lower boundaries of 95PPU and σ_{obs} is the standard deviation of Y_{obs}. A larger *p-factor* can be achieved at the expense of a larger *r-factor*. At acceptable values of *r-factor* and *p-factor*, the parameter ranges are taken as the calibrated parameters. More details on the parameters used for calibration are found in Kamali et al. (2018a).

3.2.3. Model inputs

All data required for EPIC simulation were prepared at 0.5^{o} resolution and are summarized in Table 3.1. These include site-specific data (longitude, latitude, slope, elevation), daily climate data (precipitation, solar radiation, maximum and minimum air temperature, relative humidity, and wind speed), and soil information (organic carbon content [%], pH, Cation exchange capacity [cmol kg^{-1}], sand [%], silt [%], bulk density [t m^{-3}], layer depth [m], and electrical conductivity [mmho cm^{-1}]).

Agricultural operations, including tillage, fertilizer, planting, and harvest, require information such as dates of application (Table 3.1), fertilization rate, and potential heat unit. The operations were set chronologically, by applying fertilizers 10 days before planting (Wang et al., 2005) (Table 3.1). The total number of heat units required for a plant to reach maturity was calculated for each grid based on the maximum and minimum temperatures, planting date, and length of growing seasons using the methodology proposed by the Blackland Research Center (2010).

Table 3.1. Summary of the input data and the sources used for simulating maize in SSA. All data were transformed into a 0.5°x0.5° resolution.

Input data	Description	Resolution	Year	Source
DEM, Slope	Digital elevation model GTOPO30	1 km (5″x5″)	Edition 2004	U.S. Geological Survey (2004)
A_{RF}	Rainfed cultivated area	10 km (5′x5′)	2000	MIRCA2000[1]version 1.1 Portmann et al. (2010)
Climate	Daily maximum and minimum temperature, precipitation, solar radiation, relative humidity, wind speed, CO_2 concentration	50 km (0.5^ox0.5^o)	1970-2012	WFDEI[2] meteorological forcing data Weedon et al. (2011)
Soil	Soil map and database	10 km (5′x5′)	2006	ISRIC-WISE[3] Batjes (2006)
Planting & harvesting dates	Based on temperature linked to crop calendar	50 km (0.5^ox0.5^o)	1990s to early 2000s	SAGE[4] Sacks et al. (2010)
Fertilizer	Fertilizer use	National	2002	FertiStat (FAO, 2007)

[1] Monthly Irrigated and Rainfed Crop Areas

[2] WATCH-Forcing-Data-ERA-Interim

[3] International Soil Reference and Information Centre-World Inventory of Soil Emission Potentials

[4] Center for Sustainability and the Global Environment

3.2.4. Components of crop drought vulnerability

The definition of crop drought vulnerability is based on linking the Drought Exposure Index (*DEI*) to the Crop Sensitivity Index (*CSI*). *DEI* measures the degree of stress on the system and *CSI* indicates the response of the system to the respective stress. Two definitions of *DEI* are used and compared. DEI_{PCP} is derived from precipitation (*PCP*) and $DEI_{PCP\text{-}PET}$ is derived from the difference between precipitation and potential evapotranspiration (*PCP-PET*) in a similar procedure as that used for calculating *SPI* and *SPEI*. Potential evapotranspiration is calculated using the Hargreaves method (Hargreaves and Samani, 1985). The *SPI* and *SPEI* are computed by first fitting a probability distribution function to precipitation and (*PCP-PET*), respectively. The associated Cumulative Distribution Functions (*CDF*) are subsequently estimated and transformed to a normal distribution. The *SPI* (or *SPEI*) and its associated CDF_{PCP} (or $CDF_{PCP\text{-}PET}$) are transferable to each other (Figure. 3.1). In this paper, we directly use CDF_{PCP} and $CDF_{PCP\text{-}PET}$ to define *DEIs* as*:*

$$DEI_{PCP} = 1 - CDF_{PCP}$$
$$DEI_{PCP-PET} = 1 - CDF_{PCP-PET} \quad (3.3)$$

The above definitions calculate the exceedance probability of different intensities of drought as described in Table 3.2, which was implemented by Carrão et al. (2016) for drought assessment. The *DEI* ranges from 0 to 1, with 1 indicating the highest exposure to drought. *CDF*s smaller than 0.5 are representative of drought situations, whereas values larger than 0.5 indicate non-drought conditions. Five classifications could be defined between 0 and 1: wet, near normal, mild to moderate drought, severe to extreme drought, and exceptional drought (Svoboda et al., 2002) (Table 3.2). More details on the procedure to calculate *DEI* are explained in Kamali et al. (2018b)

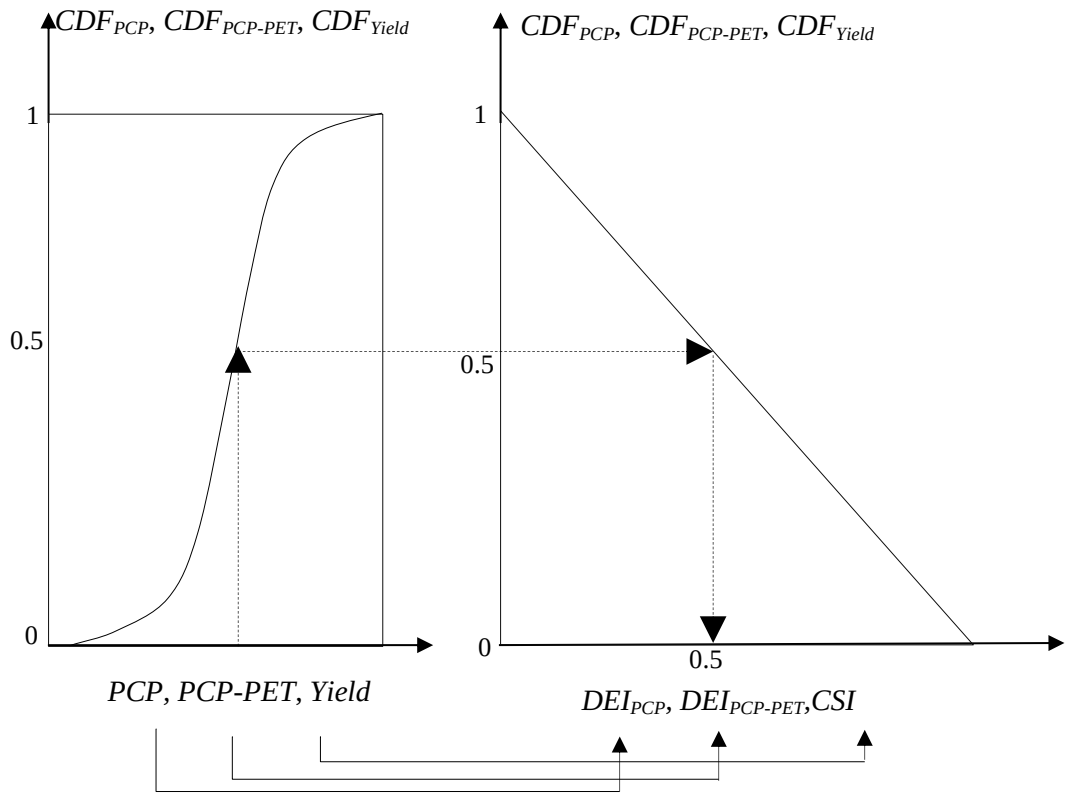

Figure 3.1. Schematic representation of transforming precipitation (*PCP*), the difference between precipitation and potential evapotranspiration (*PCP-PET*), and simulated rainfed yield (*Yield*) into their cumulative distribution functions (CDF_{PCP}, $CDF_{PCP-PET}$, CDF_{Yield}) and then into Drought Exposure Indices (DEI_{PCP}, $DEI_{PCP-PET}$), and Crop Sensitivity Index (*CSI*), respectively.

Table 3.2. Five categories of cumulative distribution functions (CDF_{PCP}, CDF_{R}, CDF_{PCP}, $CDF_{PCP-PET}$, CDF_{Yield}) and equivalent Drought Exposure (*DEI*) and Crop Sensitivity Indices (*CSI*).

Category	CDF_{PCP}, $CDF_{PCP-PET}$, CDF_{Yield}	DEI_{PCP}, $DEI_{PCP-PET}$, CSI
Wet	0.692 to 1.00	0.00 to 0.308
Near normal	0.308 to 0.692	0.308 to 0.692
Mild to moderate	0.115 to 0.308	0.692 to 0.885
Severe to extreme	0.023 to 0.115	0.885 to 0.997
Exceptional	0.00 to 0.0230	0.977 to 1.00

Different probability distribution functions can be fitted to *P* and *R*. Based on the literature, we chose a 2-parameter gamma distribution as the probability distribution function (Bordi et al., 2001; Lloyd-Hughes and Saunders, 2002). A log-logistic distribution was selected for $CDF_{PCP\text{-}PET}$ (Begueria et al., 2014; Vicente-Serrano et al., 2010) where the parameters of distribution were calculated from the unbiased probability weighted method (Begueria et al., 2014). We also tested the suitability of five one, three, six, nine, and twelve-month time scales for *DEI*s. DEI_{PCP} at the *X*-month time scale was obtained from total precipitation over the last *X* months. For example, DEI_{PCP} at three-month time scale and at the end of March accumulates the precipitation of January, February, and March of the year. The same notation is used for $DEI_{PCP\text{-}PET}$. Similarly, a suitable probability distribution function is fitted to the simulated Y_{RF} at the grid level and *CSI* is derived from the associated cumulative distribution function (CDF_{Yield}) as:

$$CSI = 1 - CDF_{Yield} \tag{3.4}$$

3.2.5. Crop drought vulnerability

The concept of vulnerability was adapted from the work done by Simelton et al. (2009). According to their definition, if a drought with high magnitude triggers a low harvest loss, then the region is "resilient", meaning that vulnerability is low. Conversely, if a small drought results in a high crop failure, then the case is "sensitive" and highly vulnerable. Therefore, the level of vulnerability is determined by relating *DEI* to *CSI*. In this paper, we translated this concept into the shape of power function obtained from fitting a curve to *DEI* and *CSI*. The different shapes of fitted curves explain how crop sensitivity increases/decreases in relation to drought exposure. Vulnerability is then defined by a power function relating DEI_{PCP} (or $DEI_{PCP\text{-}PET}$) to *CSI* as:

$$\begin{aligned} CSI &= (DEI_{PCP})^{\beta} \\ CSI &= (DEI_{PCP-PET})^{\beta} \end{aligned} \tag{3.5}$$

The β values were obtained by fitting the above power functions to *DEI*s and *CSI*. The values of β explain the degree of vulnerability and as elaborated in section 2.4, we defined *DEI* and *CSI* with the same base, meaning that a certain value of *CSI* or *DEI* have the same meaning in terms of severity level. This facilitates measuring the degree of vulnerability based on the shape of power function. As shown (Figure 3.2), vulnerability becomes smaller as β increases. In the simplest form, β=1 means that the relationship between *DEI* and *CSI* is linear. From agricultural point of view, this explains cases where a certain degree of *DEI* results in the same severity of *CSI* (medium vulnerability). The power function curves falling above the linear curve (β=*1*) for β>1 representing more vulnerable situation. This means that a certain value of *DEI* causes higher severity of *CSI*. Conversely, β>1 means that occurring droughts lead to lower *CSI*.

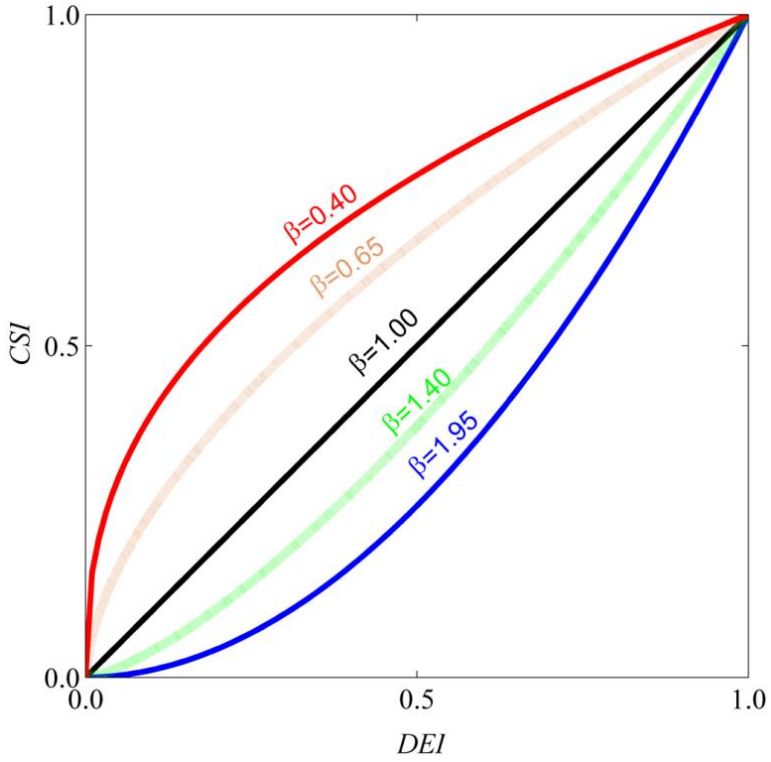

Figure 3.2. Schematic representation of the Crop Drought Vulnerability Index (*CDVI*) based on the different β values.

3.3. Results

3.3.1. The performance of EPIC crop simulator

The *RSR* values for simulated maize before and after calibration (Table 3.3) indicate significant improvement in model performance after calibration. The *RSR* values for all countries except Democratic Republic of the Congo, decreased to around 1 or less. In the latter country, however, *RSR* decreased significantly from 45.9 to 6.27. The main reason for high *RSR* in this country is a reported constant yield of 0.8 t ha^{-1} for the entire 33-year period, which is not realistic. The *p-factor* with values around 0.5 or more in all countries indicates that nearly 50% of observed data are bracketed within the 95PPU band, which are satisfactory values for crop calibration during the time span of 33 years. Their values are smaller than 2.5 and in most countries even smaller than 2, which is acceptable for yield simulations as suggested by Abbaspour et al (2007).

Table 3.3. Country-level results of the EPIC calibration with the SUFI-2 algorithm based on *RSR* before and after calibration, *p-factor* and *r-factor* (Eq. 3.3) criteria. More Details are explained in Kamali et al. (2018a)

	Country	*RSR* Before calibration	*RSR* After calibration	*p-factor*	*r-factor*
Eastern Africa	Burundi	3.94	1.38	0.55	1.80
	Comoros	1.28	1.13	0.42	1.95
	Eritrea	2.32	1.45	0.58	1.98
	Ethiopia	1.66	0.91	0.52	1.81
	Kenya	6.85	0.86	0.61	1.74
	Madagascar	6.06	1.42	0.79	2.54
	Malawi	1.40	0.94	0.45	2.25
	Mozambique	2.79	1.12	0.61	1.56
	Rwanda	1.44	1.08	0.43	1.04
	Somalia	1.96	1.22	0.42	1.08
	Sudan	1.76	1.33	0.48	1.05
	Tanzania	1.94	1.20	0.58	0.94
	Uganda	1.40	0.85	0.58	2.48
	Zambia	1.41	0.89	0.45	1.31
	Zimbabwe	3.80	1.12	0.37	1.67
Central Africa	Angola	6.90	0.99	0.88	2.38
	Cameroon	1.29	1.00	0.48	1.38
	Central African Republic	2.49	1.16	0.49	0.74
	Chad	1.23	0.84	0.66	2.05
	Democratic Republic of the Congo	45.9	6.27	0.48	1.05
	Gabon	5.33	1.35	0.70	1.95
	Republic of Congo	19.3	2.16	0.88	2.39
Southern Africa	Botswana	1.45	1.39	0.52	2.33
	Lesotho	1.99	1.27	0.42	2.45
	Namibia	2.42	1.02	0.42	1.23
	South Africa	1.88	0.92	0.55	0.79
	Swaziland	3.23	1.06	0.42	1.49
Western Africa	Benin	3.38	0.99	0.70	1.83
	Burkina Faso	1.18	0.97	0.52	1.07
	Djibouti	4.87	1.20	0.70	2.73
	Gambia	1.74	0.93	0.82	2.97
	Ghana	5.36	1.07	0.52	1.14
	Guinea	8.45	1.96	0.45	2.02
	Ivory coast	2.40	1.08	0.48	1.44
	Mali	1.23	0.98	0.55	1.55
	Mauritania	1.98	1.18	0.61	2.25
	Niger	1.67	0.85	0.70	1.88
	Nigeria	1.16	0.98	0.70	1.84
	Sierra Leone	9.59	1.09	0.53	2.07
	Senegal	1.05	0.92	0.86	2.44
	Togo	4.23	1.26	0.52	1.18

3.3.2. Drought exposure indices in SSA

The monthly values of DEI_{PCP} and $DEI_{PCP\text{-}PET}$ calculated at the country level for three and twelve-month time scales (Figures S3.1 and S3.2) indicated a number of dry periods with different severities during 1980–2012. DEI_{PCP} and $DEI_{PCP\text{-}PET}$ at three-month time scale showed higher frequencies of dry and wet periods than DEI_{PCP} and $DEI_{PCP\text{-}PET}$ at twelve-month time scale which distinguish between short- and long-term droughts. The spatial comparison of DEI_{PCP} and $DEI_{PCP\text{-}PET}$ at twelve-month time scale shows a general agreement in characterizing drought periods (Figures 3.3 and S3.3). Both indices indicated that SSA countries experienced more severe droughts with longer persistency during 1980–1995 than 1996–2012. The 1982–1985 and 1992–1996 periods were identified as the two most extreme drought periods in many countries. Between 1982 and 1985, all countries in Western and Southern Africa experienced severe to extreme droughts. Eastern Africa was mostly exposed to severe to extreme drought in 1984. During 1992–1996, many Southern and Central African countries were exposed to severe to extreme droughts as identified by both indices.

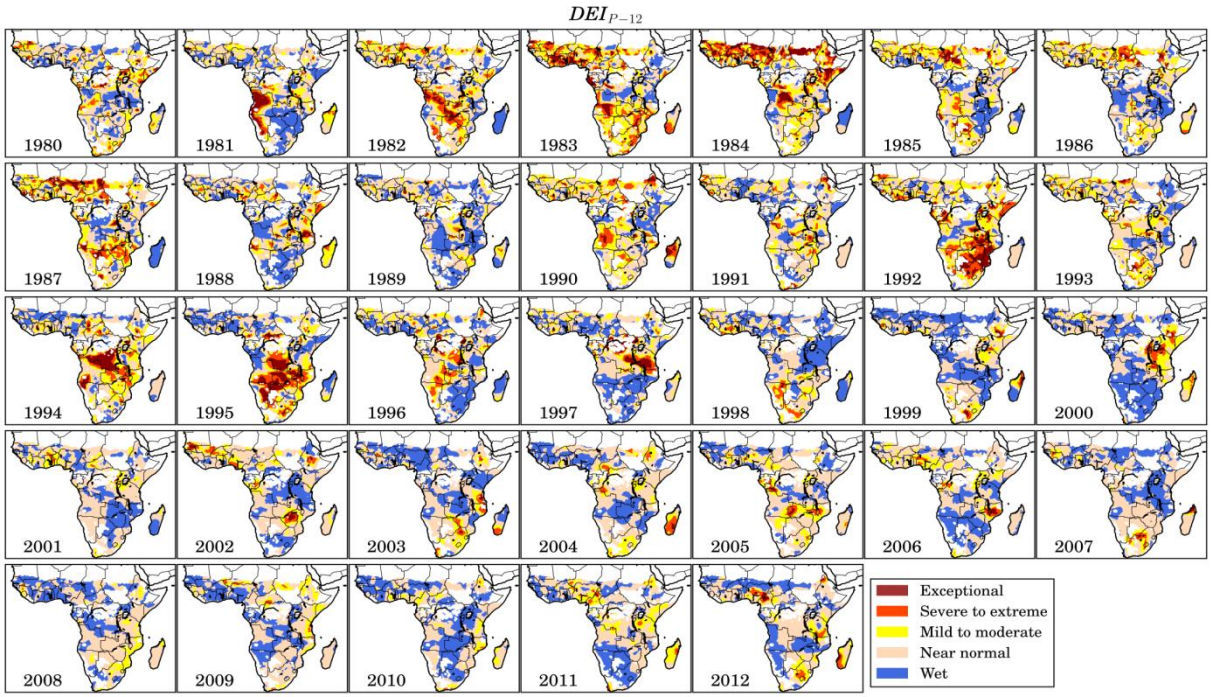

Figure 3.3. The grid level annual spatial distribution of precipitation based Drought Exposure Index ($DEI_{P\text{-}12}$) during 1981–2012

After 1995, both DEI_{PCP} and $DEI_{PCP\text{-}PET}$ at twelve-month time scale showed fewer droughts, but with different severities in the two indices. $DEI_{PCP\text{-}PET}$ at twelve-month time scale indicated more droughts, whereas based on DEI_{PCP} at twelve-month time scale, SSA was in a near normal status. Such differences were more obvious in Central Africa in 2005 and in Western Africa in 2002 and 2009, where only near normal droughts were noticeable based on DEI_{PCP} at twelve-month time scale. The differences between drought events in the two indices arose most likely from changes in temperature

rather than precipitation. The Mann–Kendall test (Figure S3.4) also confirmed significant increases in maximum and minimum temperatures in most SSA countries, except for some regions in Somalia, Ethiopia, Burkina Faso, and Ivory Coast (Figure S3.4). Increasing temperature resulted in more drought events than was discernable only with DEI_{PCP} at twelve-month time scale. The precipitation trend showed insignificant increases in almost all SSA countries, resulting in less drought characterization after 1995.

3.3.3. The relation between *DEI* and *CFI*

To define the most representative timescales, we calculated the grid-level correlation coefficient of *CSI* with DEI_{PCP} (and $DEI_{PCP\text{-}PET}$) in one, three, six, nine, twelve-month time scales (Figure 3.4). A rolling metric was used to calculate each time scale. This means that for example *DEI* of three-month time scale on March 1989 was derived from precipitation summed over January, February, and March of that year. After calculating monthly *DEI*s, the most relevant time span of each year was selected using the planting and maturity dates (growing season) at each grid. Therefore, the average of monthly *DEIs* over growing season resulted in yearly *DEI*. After calculating the correlation coefficient between yearly *DEI*s and *CSI*, from the five time scales, we selected the one with the highest correlation with *CSI*.

For both indices, the correlation coefficient was larger in Southern Africa, Horn of Africa, and Sahelian countries where the values were mostly above 0.5. In these regions, the three and six-month time scales, with values mostly larger than 0.75, had the highest correlation. In Southern Africa, DEI_{PCP} and DEI_{PCP} at three and six-month time scale had higher correlation than $DEI_{PCP\text{-}PET}$ at the same time scale indicating that agriculture was more influenced by precipitation than temperature. The correlation coefficient values in Central African countries were generally low (values were below 0.5), however, higher values were found with $DEI_{PCP\text{-}PET}$. At one and three-month time scale. Overall, DEI_{PCP} and $DEI_{PCP\text{-}PET}$ at twelve-month time scale were least correlated to *CSI* in SSA countries, especially in Central Africa (Figure 3.4). The values were mostly below 0.5 (or even 0.1), indicating that longer time periods were not as representative for agricultural drought vulnerability assessments as shorter timescales.

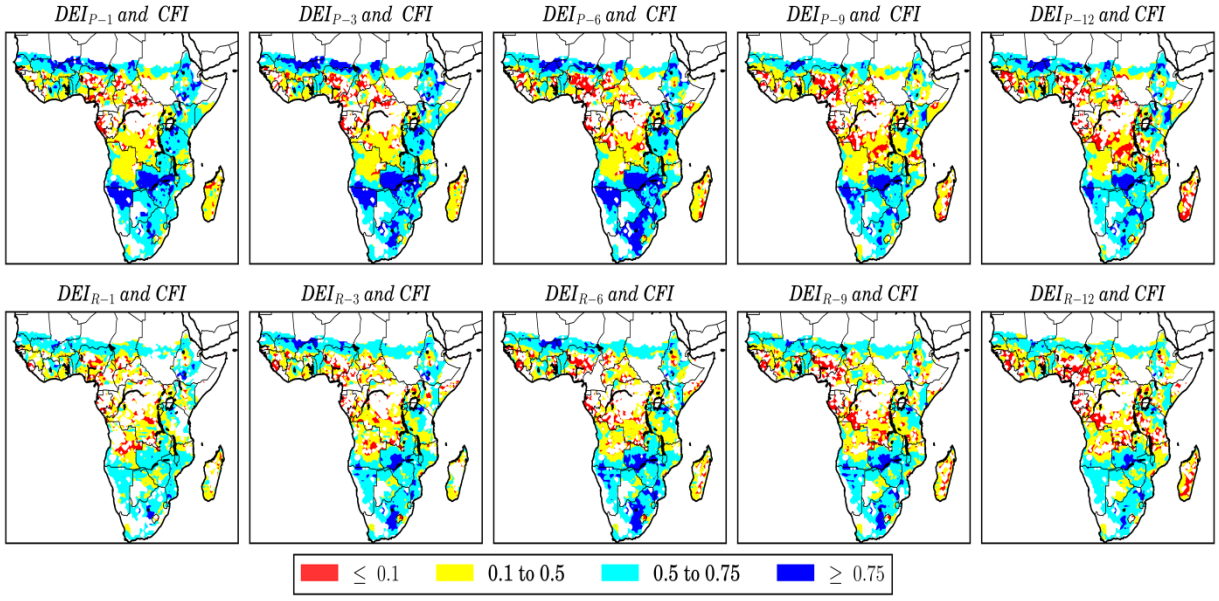

Figure 3.4. The correlation coefficient between precipitation based Drought Exposure Index (DEI_P) and Crop Failure Index (*CFI*) (top row); and the Drought Exposure Index based on the residual of precipitation and potential evapotranspiration (DEI_R) and *CFI* (bottom row) in 1, 3, 6, 9 and 12-month timescales

3.3.4. Country-level and grid-level crop drought vulnerability in SSA

At each grid point and from each time scales of DEI_{PCP} and $DEI_{PCP\text{-}PET}$, we chose the one with the highest correlation with *CSI* for vulnerability analysis. The power function was then fitted to the relation of DEI_{PCP} (or $DEI_{PCP\text{-}PET}$) and *CSI* (Eq. 3.4). For the country analysis, we calculated the average and 95PPU bands for all grids within a country (Figures 3.5 and S3.5). The shape of average fitted curves and the β values varied from one country to another, indicating that each country has a different type of vulnerability curve described in Figure 3.2. Using DEI_{PCP} and based on the β values of smaller than 0.9 (Figure 3.5), countries such as Central African Republic of Congo, Madagascar, Zimbabwe, and Mauritania were identified as high vulnerability countries. The average β for these countries are 0.88, 0.9, 0.85, and 0.88 respectively. The $\beta<1$ value indicate that the average curves lay above the $y=x$ line. This means that a certain intensity of DEI_{PCP} results in a higher intensity of *CSI* (Figure 3.2). In countries such as Kenya, the average β values are larger than 1 representing low vulnerability. In other words, the fitted curve falls below $y=x$, which is associated with lower crop sensitivity during drought.

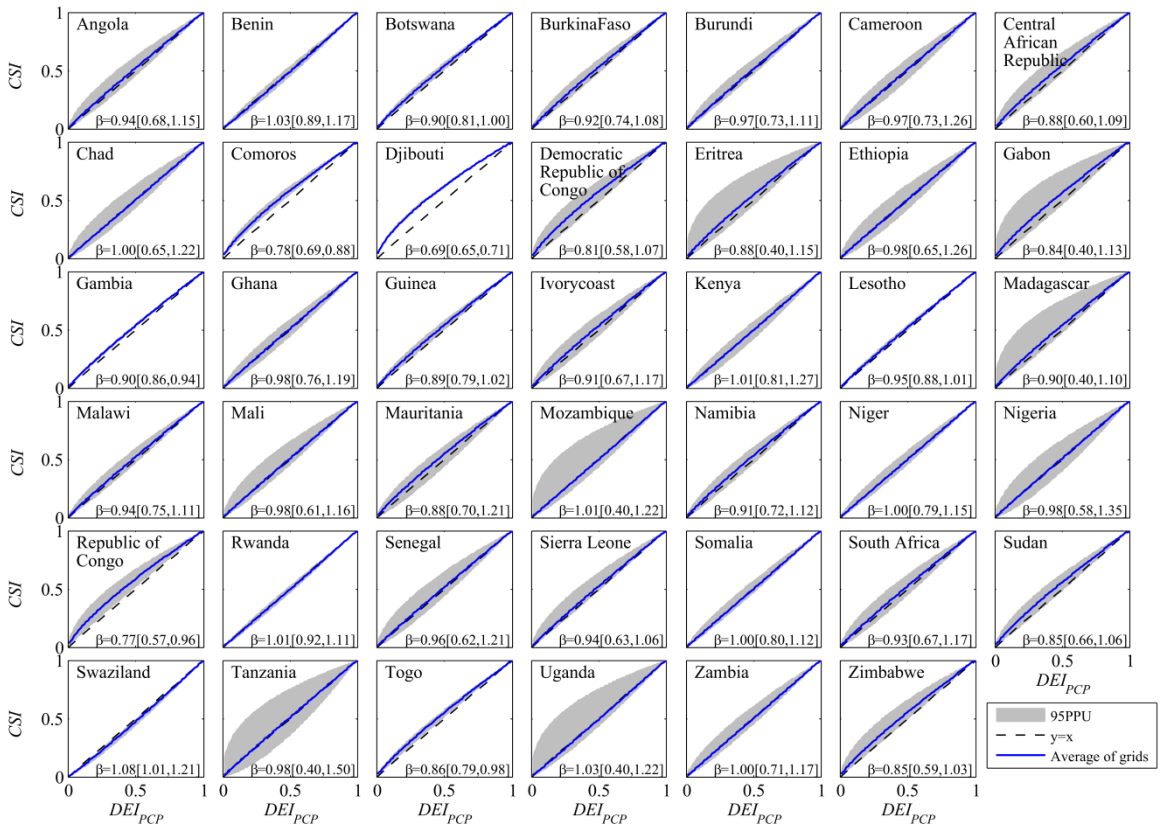

Figure 3.5. Country-level comparison of the interaction between precipitation based Drought Exposure Index (DEI_{PCP}) and the Crop Sensitivity Index (*CSI*) using power curves fitted to each grid within a country. The grey band indicates 95PPU and the blue line is the average curve obtained from all fitted curves to grids of a country. The average, minimum, and maximum values of β are shown as: β= average β [minimum β, maximum β]

We also found that there is a significant difference between the maximum and minimum β values obtained from grids within a country indicating that the degree of vulnerability vary significantly from one region to another (Figures 3.5 and S3.5). For example in Tanzania the β values varies between 0.4 and 1.5. To understand the spatial vulnerability, the spatial distribution of *CDVI*s were mapped out at each grid cell based on β. The maps indicated that most parts of SSA experienced a certain level of vulnerability as the β values are smaller than 1.05 in most regions. The *CDVI* map based on linking DEI_{PCP} to *CSI* shows that Southern Angola, Zimbabwe, and Zambia from Southern Africa, Central Africa countries, and some Sahelian countries such as Sudan and Mauritania with β values smaller than 0.9 are most vulnerable (Figure 3.6).

Comparison of *CDVI* maps based on DEI_{PCP} and $DEI_{PCP\text{-}PET}$ shows that there is general agreement between the most vulnerable countries, however, the *CDVI* map based on $DEI_{PCP\text{-}PET}$ showed slightly higher vulnerability. As expected measuring drought exposure based on a combination of precipitation and temperature variables can better represent vulnerability as both have significant impacts on crop growth.

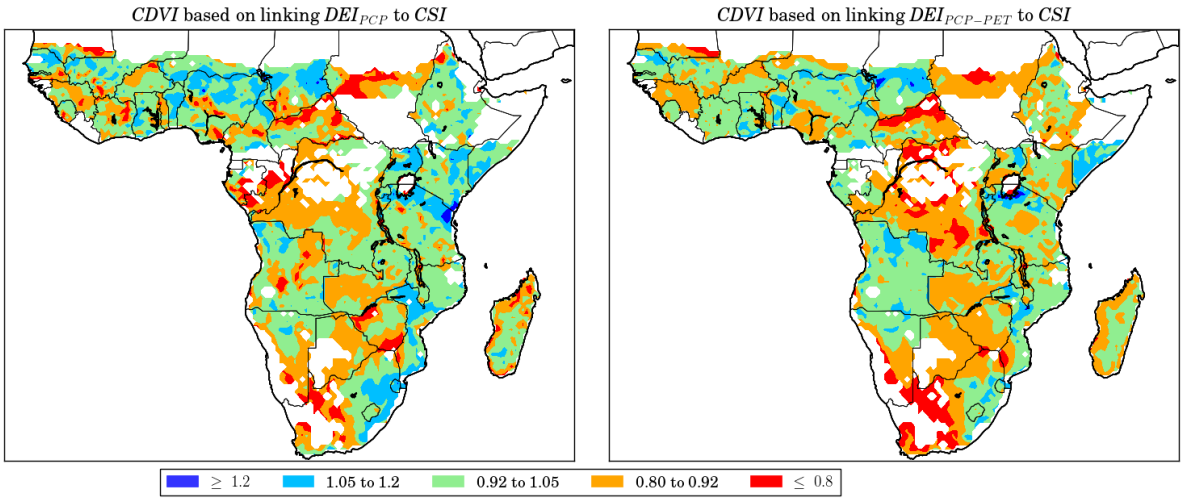

Figure 3.6. Spatial distribution of maize drought vulnerability based on the five types of *CDVI* defined in Figure 3.2

In order to identify the possible factors what makes a region more vulnerable to drought, we calculated the correlation coefficient between simulated yield and three types of stresses (water stress, nitrogen stress, and temperature stress) during its growth period. We explored the influence of these stresses in four stages of crop growths (emergence, heading, anthesis, and maturity) (Figure 3.7). In Southern and Eastern African countries as well as in Sahelian strip countries, water stress was the limiting factors for maize growth. Within these regions, the correlation coefficient between crop yield and water stress was above 0.5. The role of water stress was more apparent during heading and anthesis stages of crop growth. In Central African countries, despite the high amount of rainfall (Figure S3.6), higher vulnerability of maize to drought was observed. As shown, there is significant correlation between maize yield and temperature in these regions. We also noticed that *CDVI* map based on the relation of $DEI_{PCP\text{-}PET}$ and yield showed higher vulnerability. In Western African countries, maize growth is more vulnerable to drought due to experiencing more Nitrogen stress specially during heading and anthesis stages.

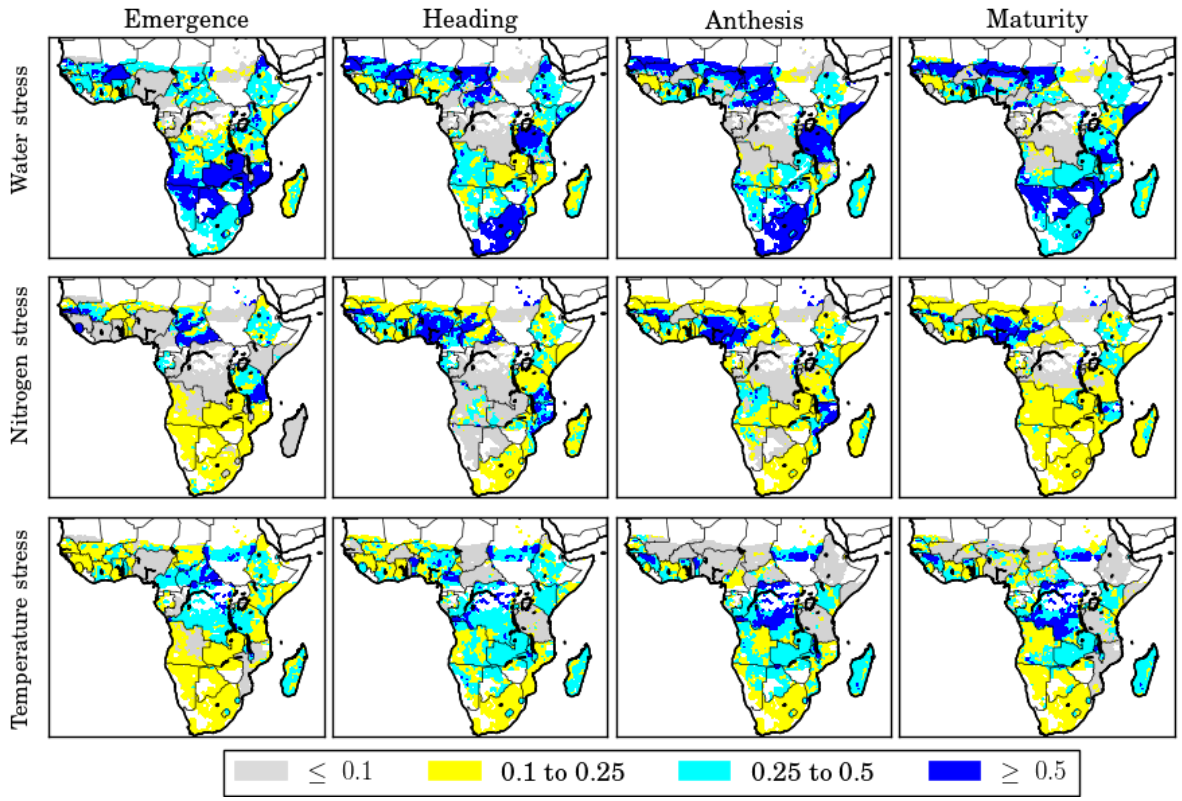

Figure 3.7. Correlation coefficient between simulated maize yield and different stress types (top row: water stress, middle row: Nitrogen stress, and bottom row: temperature stress) at four stages of maize growth i.e. emergence, heading, anthesis, and maturity.

3.4. Discussion

This paper quantifies maize drought vulnerability in SSA by linking probability-based *DEI* (Drought Exposure Index) with *CSI* (Crop Sensitivity Index) using a power function. *CSI* was obtained from the physically based EPIC crop model at the grid level and the fitted curve explaining the interaction of these two components. Our study assesses the impacts of drought conditions on crop yield during growing season. We answer the three questions raised in the introduction in three below sub-sections.

3.4.1. The effectiveness of standardized approach for vulnerability assessment

Concerning the first question, we used the probability-based procedure to define normalized *DEI*s and *CSI*. This approach advances current approaches in several ways. First, the standardized metrics are more robust compared to the ratio-based definitions in current literature (Huai, 2016; Simelton et al., 2009). In addition, the standardized definition facilities their comparison with other most widely used drought indices such as the Palmer Drought Severity Index (*PDSI*) (Palmer, 1965) or drought indices based on joint distribution functions of different variables (e.g. precipitation and soil moisture) found in the study of Hao and AghaKouchak (2014). Finally, defining components of vulnerability with the same base facilitates interpretation of fitted curves obtained from their aggregation in a power function.

Our approach was tested for SSA countries with two drought exposure indices (DEI_{PCP} and $DEI_{PCP-PET}$). The work has built the foundation to be applied in different regions on different spatial scales. It provides a methodological template to compile a larger range of drought exposure indices to capture uncertainties associated with variables that may be incorporated to defined drought exposure. Finally, our proposed approach requires and also has the future potential for including the third dimension of vulnerability i.e. adaptive capacity defined by the IPCC, which we will explore next.

3.4.2. The impact of different timescales of DEI_{PCP} and $DEI_{PCP-PET}$

The drought events identified based on DEI_{PCP} and $DEI_{PCP-PET}$ at twelve-month time scale were consistent with actual droughts in SSA reported in recent literature (Anderson et al., 2012; Masih et al., 2014). For example, both indices highlighted the two extreme drought periods of 1982–1985 and 1992–1996 reported by Masih et al. (2014) or the prolonged drought in Sudan after 2000 reported by Elagib and Elhag (2011). We found some differences in drought periods identified by DEI_{PCP} and $DEI_{PCP-PET}$ at twelve-month time scale. For example, drought events occurring after 2006 in Central Africa and some Eastern African countries such as Somalia and Djibouti (Dutra et al., 2013) were better recognized by $DEI_{PCP-PET}$ than DEI_{PCP}, which showed only mild droughts. $DEI_{PCP-PET}$ is based on both temperature and precipitation, where a combination of climate events (e.g. low precipitation and high temperature) may cause significant impact on a system, as discussed by Mazdiyasni and AghaKouchak (2015). We also found some differences in the drought events calculated at different time scales. Due to these differences and also because of the differences in the DEI_{PCP} and $DEI_{PCP-PET}$ severities (in some countries), their suitability for crop vulnerability assessment should be evaluated in detail. As also mentioned by Masih et al. (2014), the suitability of drought indices should be evaluated according to the sector it influences. In this study, we selected the most appropriate time scale for the agricultural sector based on their correlation with *CSI*.

The correlation coefficient between DEI_{PCP} (and $DEI_{PCP-PET}$) at different time scale with *CSI* showed overall smaller values in Central Africa and some Western African countries such as Nigeria, Ghana, and Cameroon. This is related to high precipitation in these regions exceeding 1000 mm yr^{-1} (Figure S3.6). In some countries such as Gabon, Liberia, and South Nigeria the yearly precipitation is above 2000 mm yr^{-1}. Therefore, crops are less exposed to water stress. In other words, while these regions might be exposed to meteorological drought, the amount of precipitation remains sufficient for crop growth and therefore agricultural drought does not happen. In these region, the correlation of $DEI_{PCP-PET}$ with *CSI* is slightly higher than DEI_{PCP} and *CSI*. This suggests that within these regions both precipitation and temperature should be considered as variable to determine drought exposure. On the other hand, in Southern Africa and Sahelian countries with yearly precipitation below 660 mm y^{-1}, the correlation between DEI_{PCP} (and $DEI_{PCP-PET}$) with *CSI* is larger than 0.8 with higher values for DEI_{PCP} compared to $DEI_{PCP-PET}$ meaning that precipitation is a more limiting factor than temperature for these regions.

Concerning the second question, the comparison of different timescales of DEI_{PCP} showed that the highest correlations of DEI_{PCP} with *CSI* were for three and six-month timescales and mostly in the Southern African and Sahelian countries. This corroborates the studies of Manatsa et al. (2010) and Rouault and Richard (2005). Labudová et al. (2016) also found that the three-month timescale correlated very well with maize yield in the Danubian Lowland and the east Slovakian Lowland. Overall, DEI_{PCP} and $DEI_{PCP\text{-}PET}$ at twelve-month time scale were the least correlated with *CSI* compared to other timescales. This is because the twelve-month time scale is based on the accumulation of precipitation over the last 12 months. Therefore, the weight of single months becomes smaller and less significant. However, water shortage at certain phonological periods may be more important than at other phonological periods. For example, much greater losses could be expected as a result of prolonged water stress during the tasselling and ear formation stages of corn growth (Cakir (2004) than during vegetative growth.

3.4.3. Comparison of maize drought vulnerability in different countries

With the help of a process-based crop model, maize yields were obtained on a 0.5° grid level and vulnerability hotspots were identified with the same resolution, which is a more reasonable resolution for vulnerability assessment for sub-national studies. One advantage of our approach was that the applied crop model was coupled with SUFI-2 calibration technique which increased the reliability of simulated yields. We believe this is important, since our calibration procedure provided the possibility of taking into account the temporal variability for over three decades, which is long enough to cover various weather conditions. The evolution of drought exposure in Figure 3.3 and S3.3 indicates that within this time span all grids experienced extreme wet to dry conditions. It is clear that any calibrated model does not apply to conditions beyond which it was calibrated for, but as EPIC is a physically based model, it should simulate well given a given set of condition if known.

With the aim of EPIC, we added deeper insights on different underlying stresses making maize of one region physically vulnerable. The vulnerability maps (Figure 3.6) showed that Southern Africa and some Sahelian countries were found to be high vulnerable regions due to experiencing more periods of water stress as a result of low precipitation (Figures 3.7 and S3.6). Central Africa were vulnerable due to temperature stress and for this reason we found that drought exposure based on the difference between precipitation and potential evapotranspiration ($DEI_{PCP\text{-}PET}$) showed higher vulnerability compared to DEI_{PCP}. Other studies assessed the impact of temperature on maize growth (Butler and Huybers, 2015; Deryng et al., 2014; Gourdji et al., 2013). Gourdji et al. (2013) for example found that crops ate physiologically sensitive to temperatures in the reproductive stage. Here, we noticed highest correlation to temperature during heading and anthesis. EPIC does not consider crop phenology explicitly, therefore we could not specify separate critical temperature for each growth stage of crop. Future studies can attempt to upgrade model to overcome this limitation.

3.5. Conclusion

The physical drought vulnerability maps on the fine spatial resolution provide the geographical bases for identifying vulnerable hotspots at sub-national scale. Such improved understanding is important for early warning on drought vulnerability. It also enables sub-national, national, and international policy makers to prioritize proactive and reactive agricultural adaptation strategies in response to drought. The approaches developed here can be used to project the vulnerability under future scenarios of climate change and measure the long-term impacts of droughts on food production. It is, however, important to emphasize that propose of mitigating policies for local and regional farmers, managers, and engineers by strategies such as changing the land use to grow more drought resistant crops and varieties, providing adequate water infrastructures or water use to combat water stress will need additional information and studies.

One of the limitations of this study is the lack of detailed input data such as temporal variability of cultivated area at the grid level. In addition, some FAOSTAT yield data are of poor quality in SSA. But, unfortunately, this is the only available source for the moment and is a general problem of any study in the region. However, this limitation does not significantly influence the robustness of the methodology and the general results derived because the vulnerability assessments were based on rainfed maize yield simulated on the grid level using the EPIC crop model which has a unit of t ha^{-1}. The results can be easily validated as more regional data become available.

3.6. Reference

Abbaspour, K. C., Rouholahnejad, E., Vaghefi, S., Srinivasan, R., Yang, H., and Klove, B. (2015). A continental-scale hydrology and water quality model for Europe: Calibration and uncertainty of a high-resolution large-scale SWAT model. *Journal of Hydrology* **524**, 733-752.

Abbaspour, K. C., Yang, J., Maximov, I., Siber, R., Bogner, K., Mieleitner, J., Zobrist, J., and Srinivasan, R. (2007). Modelling hydrology and water quality in the pre-ailpine/alpine Thur watershed using SWAT. *Journal of Hydrology* **333**, 413-430.

Anderson, W. B., Zaitchik, B. F., Hain, C. R., Anderson, M. C., Yilmaz, M. T., Mecikalski, J., and Schultz, L. (2012). Towards an integrated soil moisture drought monitor for East Africa. *Hydrology and Earth System Sciences* **16**, 2893-2913.

Batjes, N. H. (2006). ISRIC-WISE derived soil properties on a 5 by 5 arc-minutes global grid. ISRIC - World Soil Information, Wageningen, Netherlands.

Begueria, S., Vicente-Serrano, S. M., Reig, F., and Latorre, B. (2014). Standardized precipitation evapotranspiration index (SPEI) revisited: parameter fitting, evapotranspiration models, tools, datasets and drought monitoring. *International Journal of Climatology* **34**, 3001-3023.

Blackland Research Center (2010). Potential Heat Unit Program, http://swatmodel.tamu.edu/software/potential-heat-unit-program.

Bordi, I., Frigio, S., Parenti, P., Speranza, A., and Sutera, A. (2001). The analysis of the standardized precipitation index in the mediterranean area: large-scale patterns. *Annali Di Geofisics* **44**, 965-978.

Brooks, N., Adger, W. N., and Kelly, P. M. (2005). The determinants of vulnerability and adaptive capacity at the national level and the implications for adaptation. *Global Environmental Change-Human and Policy Dimensions* **15**, 151-163.

Butler, E. E., and Huybers, P. (2015). Variations in the sensitivity of US maize yield to extreme temperatures by region and growth phase. *Environmental Research Letters* **10**.

Cakir, R. (2004). Effect of water stress at different development stages on vegetative and reproductive growth of corn. *Field Crops Research* **89**, 1-16.

Carrão, H., Naumann, G., and Barbosa, P. (2016). Mapping global patterns of drought risk: An empirical framework based on sub-national estimates of hazard, exposure and vulnerability. *Global environmental Change* **39**, 108-124.

de Wit, A. J. W., Boogaard, H. L., and van Diepen, C. A. (2005). Spatial resolution of precipitation and radiation: The effect on regional crop yield forecasts. *Agricultural and Forest Meteorology* **135**, 156-168.

Deryng, D., Conway, D., Ramankutty, N., Price, J., and Warren, R. (2014). Global crop yield response to extreme heat stress under multiple climate change futures. *Environmental Research Letters* **9**.

Dutra, E., Magnusson, L., Wetterhall, F., Cloke, H. L., Balsamo, G., Boussetta, S., and Pappenberger, F. (2013). The 2010-2011 drought in the Horn of Africa in ECMWF reanalysis and seasonal forecast products. *International Journal of Climatology* **33**, 1720-1729.

Elagib, N. A., and Elhag, M. M. (2011). Major climate indicators of ongoing drought in Sudan. *Journal of Hydrology* **409**, 612-625.

FAO (2007). FertiSTAT - Fertilizer Use Statistics. Food and Agricultural Organization of the UN, Rome, http://www.fao.org/ag/agl/fertistat/index_en.htm.

FAO (2010). FAOSTAT statistical database. Food and Agricultural Organization of the UN, Rome.

Fraser, E. D. G., Simelton, E., Termansen, M., Gosling, S. N., and South, A. (2013). "Vulnerability hotspots": Integrating socio-economic and hydrological models to identify where cereal production may decline in the future due to climate change induced drought. *Agricultural and Forest Meteorology* **170**, 195-205.

Gourdji, S. M., Sibley, A. M., and Lobell, D. B. (2013). Global crop exposure to critical high temperatures in the reproductive period: historical trends and future projections. *Environmental Research Letters* **8**.

Guo, H., Zhang, X., Lian, F., Gao, Y., Lin, D., and Wang, J. a. (2016). Drought risk assessment based on vulnerability surfaces: a case study of maize. *Sustainability* **8**.

Hao, Z. C., and AghaKouchak, A. (2014). A nonparametric multivariate multi-Index drought monitoring framework. *Journal of Hydrometeorology* **15**, 89-101.

Hargreaves, G. H., and Samani, Z. A. (1985). Reference crop evapotranspiration from temperature. *Applied Engineering in Agriculture* **1**, 96-99.

Hellmuth, M. E., Moorhead, A., Thomson, M. C., and Williams, J. (2007). Climate risk management in Africa: learning from practice. International Research Institute for Climate and Society (IRI), , Columbia University, NewYork, USA.

Huai, J. J. (2016). Integration and typologies of vulnerability to climate change: A case study from Australian wheat sheep zones. *Scientific Reports* **6**.

Jia, H. C., Wang, J. A., Cao, C. X., Pan, D. H., and Shi, P. J. (2012). Maize drought disaster risk assessment of China based on EPIC model. *International Journal of Digital Earth* **5**, 488-515.

Kamali, B., Abbaspour, K. C., Lehmann, A., Wehrli, B., and Yang, H. (2018a). Uncertainty-based auto-calibration for crop yield – the EPIC^{+} procedure for a case study in Sub-Saharan Africa. *European Journal of Agronomy* **19**, 57–72.

Kamali, B., Abbaspour, K. C., Wehrli, B., and Yang, H. (2018b). Drought vulnerability assessment of maize in Sub-Saharan Africa: Insights from physical and social perspectives. *Global and Planetary Change*.

Labudová, L., Labuda, M., and Takáč, J. (2016). Comparison of SPI and SPEI applicability for drought impact assessment on crop production in the Danubian Lowland and the East Slovakian Lowland. *Theoretical and Applied Climatology*, 1-16.

Liu, J. G., Fritz, S., van Wesenbeeck, C. F. A., Fuchs, M., You, L. Z., Obersteiner, M., and Yang, H. (2008). A spatially explicit assessment of current and future hotspots of hunger in Sub-Saharan Africa in the context of global change. *Global and Planetary Change* **64**, 222-235.

Lloyd-Hughes, B., and Saunders, M. A. (2002). A drought climatology for Europe. *International Journal of Climatology* **22**, 1571-1592.

Manatsa, D., Mukwada, G., Siziba, E., and Chinyanganya, T. (2010). Analysis of multidimensional aspects of agricultural droughts in Zimbabwe using the Standardized Precipitation Index (SPI). *Theoretical and Applied Climatology* **102**, 287-305.

Masih, I., Maskey, S., Mussa. F. E. F., and P., T. (2014). A review of droughts in the African Continent: a geospatial and long-term perspective. *Hydrology and Earth System Sciences* **18**, 2679-2718.

Mazdiyasni, O., and AghaKouchak, A. (2015). Substantial increase in concurrent droughts and heatwaves in the United States. *Proceedings of the National Academy of Sciences of the United States of America* **112**, 11484-11489.

McKee, T. B., Doesken, N. J., and kleist, J. (1993). The relationship of drought frequency and duration to time scales. *In* "In proceedings of the 8th Conference on Applied Climatology", pp. 179- 184.

Mearns, L. O., Easterling, W., Hays, C., and Marx, D. (2002). Comparison of agricultural impacts of climate change calculated from high and low resolution climate change scenarios: Part I. The uncertainty due to spatial scale (vol 51, pg 131, 2001). *Climatic Change* **52**, 245-245.

Muller, C. (2011). Agriculture: Harvesting from uncertainties. *Nature Climate Change* **1**, 253-254.

Naumann, G., Barbosa, P., Garrote, L., Iglesias, A., and Vogt, J. (2014). Exploring drought vulnerability in Africa: An indicator based analysis to be used in early warning systems. *Hydrology and Earth System Sciences* **18**, 1591-1604.

Naumann, G., Spinoni, J., Vogt, J. V., and Barbosa, P. (2015). Assessment of drought damages and their uncertainties in Europe. *Environmental Research Letters* **10**, 1748-9326.

O'Brien, K., Leichenko, R., Kelkar, U., Venema, H., Aandahl, G., Tompkins, H., Javed, A., Bhadwal, S., Barg, S., Nygaard, L., and West, J. (2004). Mapping vulnerability to multiple stressors: climate change and globalization in India. *Global Environmental Change-Human and Policy Dimensions* **14**, 303-313.

Orrego, R., Avila, A., Meza, F., and Matus, F. (2014). Using a crop simulation model to select the optimal climate grid cell resolution: A study case in Araucan a Region. *Journal of Soil Science and Plant Nutrition* **14**, 407-420.

Osborne, T. M., and Wheeler, T. R. (2013). Evidence for a climate signal in trends of global crop yield variability over the past 50 years. *Environmental Research Letters* **8**.

Palmer, W. C. (1965). Meteorological drought. U.S. Weather Bureau, Washington, D.C.

Parry, M., Canziani, O., Palutikof, J., van der Linden, P., and Hanson, C. (2007). Climate change 2007: impacts, adaptation and vulnerability, Cambridge University Press, Cambridge, UK,, 273–313.

Portmann, F. T., Siebert, S., and Doll, P. (2010). MIRCA2000-Global monthly irrigated and rainfed crop areas around the year 2000: A new high-resolution data set for agricultural and hydrological modeling. *Global Biogeochemical Cycles* **24**, 1-24.

Rezaei, E. E., Webber, H., Gaiser, T., Naab, J., and Ewert, F. (2015). Heat stress in cereals: Mechanisms and modelling. *European Journal of Agronomy* **64**, 98-113.

Rouault, M., and Richard, Y. (2005). Intensity and spatial extent of droughts in southern Africa. *Geophysical Research Letters* **32**, 1-4.

Roudier, P., Sultan, B., Quirion, P., and Berg, A. (2011). The impact of future climate change on West African crop yields: What does the recent literature say? *Global Environmental Change-Human and Policy Dimensions* **21**, 1073-1083.

Sacks, W. J., Deryng, D., Foley, J. A., and Ramankutty, N. (2010). Crop planting dates: An analysis of global patterns. *Global Ecology and Biogeography* **19**, 607-620.

Schlenker, W., and Lobell, D. B. (2010). Robust negative impacts of climate change on African agriculture. *Environmental Research Letters* **5**.

Shahid, S., and Behrawan, H. (2008). Drought risk assessment in the western part of Bangladesh. *Natural Hazards* **46**, 391-413.

Simelton, E. (2011). Food self-sufficiency and natural hazards in China. *Food Security* **3**, 35-52.

Simelton, E., Fraser, E. D. G., Termansen, M., Benton, T. G., Gosling, S. N., South, A., Arnell, N. W., Challinor, A. J., Dougill, A. J., and Forster, P. M. (2012). The socioeconomics of food crop production and climate change vulnerability: A global scale quantitative analysis of how grain crops are sensitive to drought. *Food Security* **4**, 163-179.

Simelton, E., Fraser, E. D. G., Termansen, M., Forster, P. M., and Dougill, A. J. (2009). Typologies of crop-drought vulnerability: an empirical analysis of the socio-economic factors that influence the sensitivity and resilience to drought of three major food crops in China (1961-2001). *Environmental Science & Policy* **12**, 438-452.

Singh, J., Knapp, H. V., Arnold, J. G., and Demissie, M. (2005). Hydrological modeling of the iroquois river watershed using HSPF and SWAT. *Journal of the American Water Resources Association* **41**, 343-360.

Svendsen, M., Ewing, M., Msangi, S., (2009). Measuring irrigation performance in Africa. *IFPRI Discussion Paper,*.

Svoboda, M., LeComte, D., Hayes, M., Heim, R., Gleason, K., Angel, J., Rippey, B., Tinker, R., Palecki, M., Stooksbury, D., Miskus, D., and Stephens, S. (2002). The drought monitor. *Bulletin of the American Meteorological Society* **83**, 1181-1190.

Thornton, P. K., Jones, P. G., Alagarswamy, G., and Andresen, J. (2009). Spatial variation of crop yield response to climate change in East Africa. *Global Environmental Change-Human and Policy Dimensions* **19**, 54-65.

U.S. Geological Survey (2004). Global Digital Elevation Model (GTOPO30). (ESRI, ed.), Redlands, California, USA.

Uniyal, B., Jha, M. K., and Verma, A. K. (2015). Parameter identification and uncertainty analysis for simulating streamflow in a river basin of Eastern India. *Hydrol Process* **29**, 3744-3766.

Vicente-Serrano, S. M., Begueria, S., and Lopez-Moreno, J. I. (2010). A Multiscalar drought index sensitive to global warming: the standardized precipitation evapotranspiration index. *Journal of Climate* **23**, 1696-1718.

Wang, X., He, X., Williams, J. R., Izaurralde, R. C., and Atwood, J. D. (2005). Sensitivity and uncertainty analyses of crop yields and soil organic carbon simulated with EPIC. *Transaction of the ASAE* **48**, 1041-1054.

Wang, Z. Q., He, F., Fang, W. H., and Liao, Y. F. (2013). Assessment of physical vulnerability to agricultural drought in China. *Natural Hazards* **67**, 645-657.

Weedon, G. P., Gomes, S., Viterbo, P., Shuttleworth, W. J., Blyth, E., Osterle, H., Adam, J. C., Bellouin, N., Boucher, O., and Best, M. (2011). Creation of the WATCH forcing data and its use to assess global and regional reference crop evaporation over land during the twentieth century. *Journal of Hydrometeorology* **12**, 823-848.

Williams, J. R., Jones, C. A., Kiniry, J. R., and D.A., S. (1989). The EPIC crop growth model. *Transaction of the ASAE*, 497-454.

World Bank (2016). World Bank Open Data;http: //data.worldbank.org/indicator/SP.POP.TOTL. Washington, DC.

Wu, H., Hubbard, K. G., and Wilhite, D. A. (2004). An agricultural drought risk-assessment model for corn and soybeans. *International Journal of Climatology* **24**, 723-741.

Yang, J., Reichert, P., Abbaspour, K. C., Xia, J., and Yang, H. (2008). Comparing uncertainty analysis techniques for a SWAT application to the Chaohe Basin in China. *Journal of Hydrology* **358**, 1-23.

3.7. Supplementary material

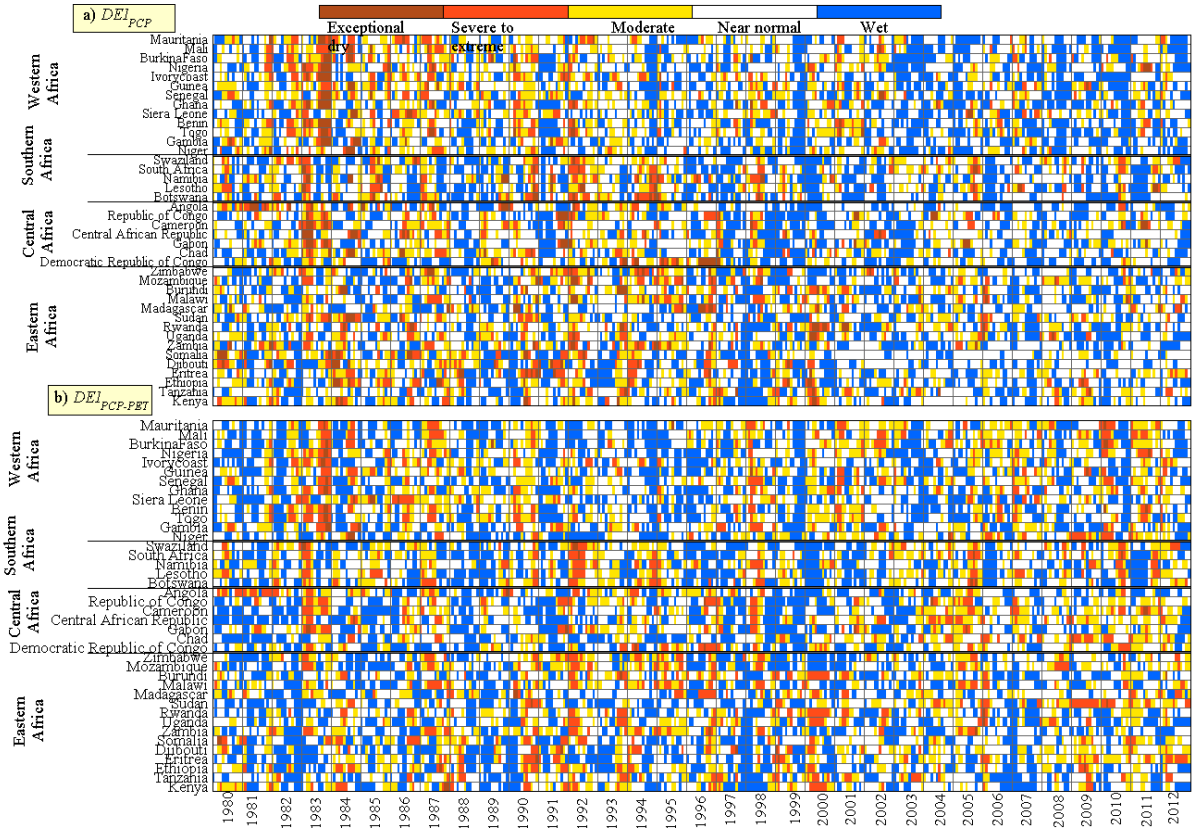

Figure S3.1. Country-level time series of monthly DEI_{PCP} (precipitation based Drought Exposure Index) and $DEI_{PCP\text{-}PET}$ (Drought Exposure Index based on the difference between precipitation and potential evapotranspiration) at three-months time scale during 1980–2012

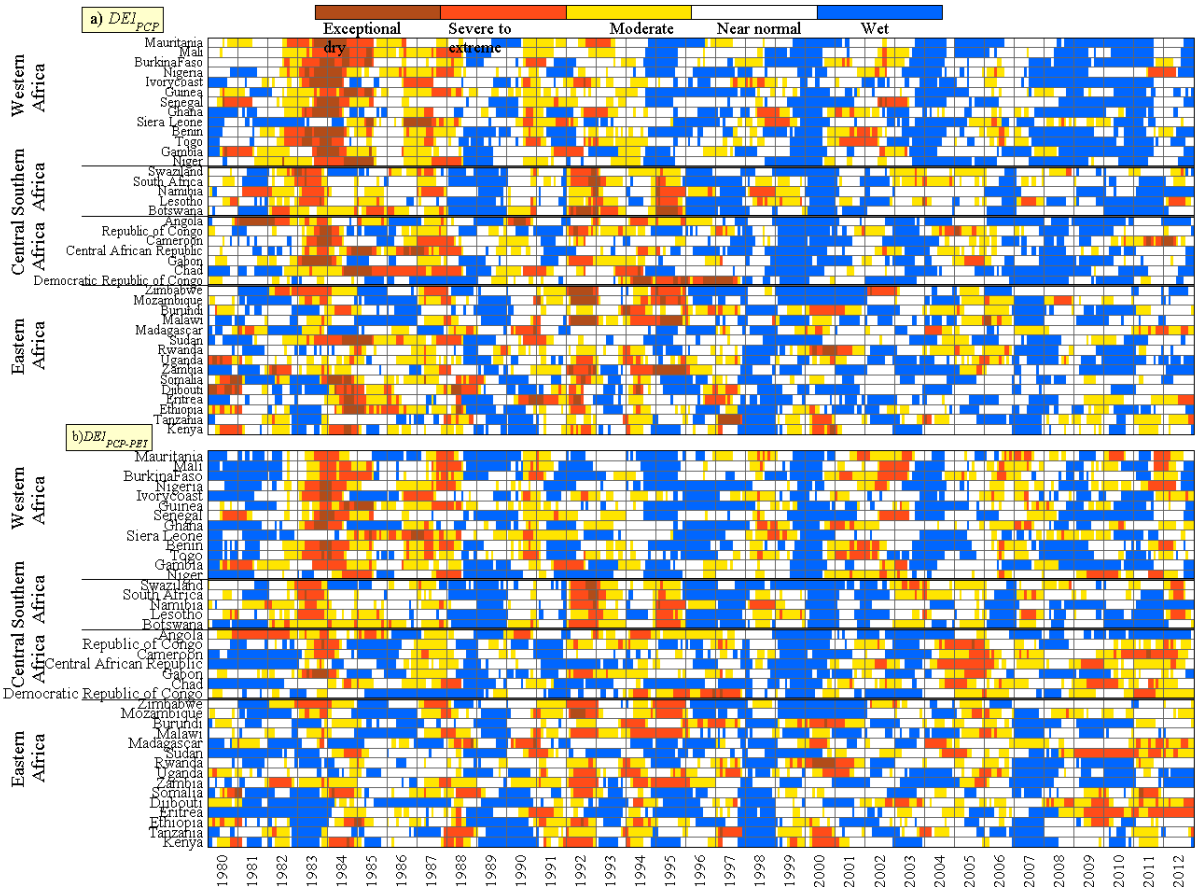

Figure S3.2. Country-level time series of monthly DEI_{PCP} (precipitation based Drought Exposure Index) and $DEI_{PCP\text{-}PET}$ (Drought Exposure Index based on the difference between precipitation and potential evapotranspiration) in 12-month time scale during 1980–2012

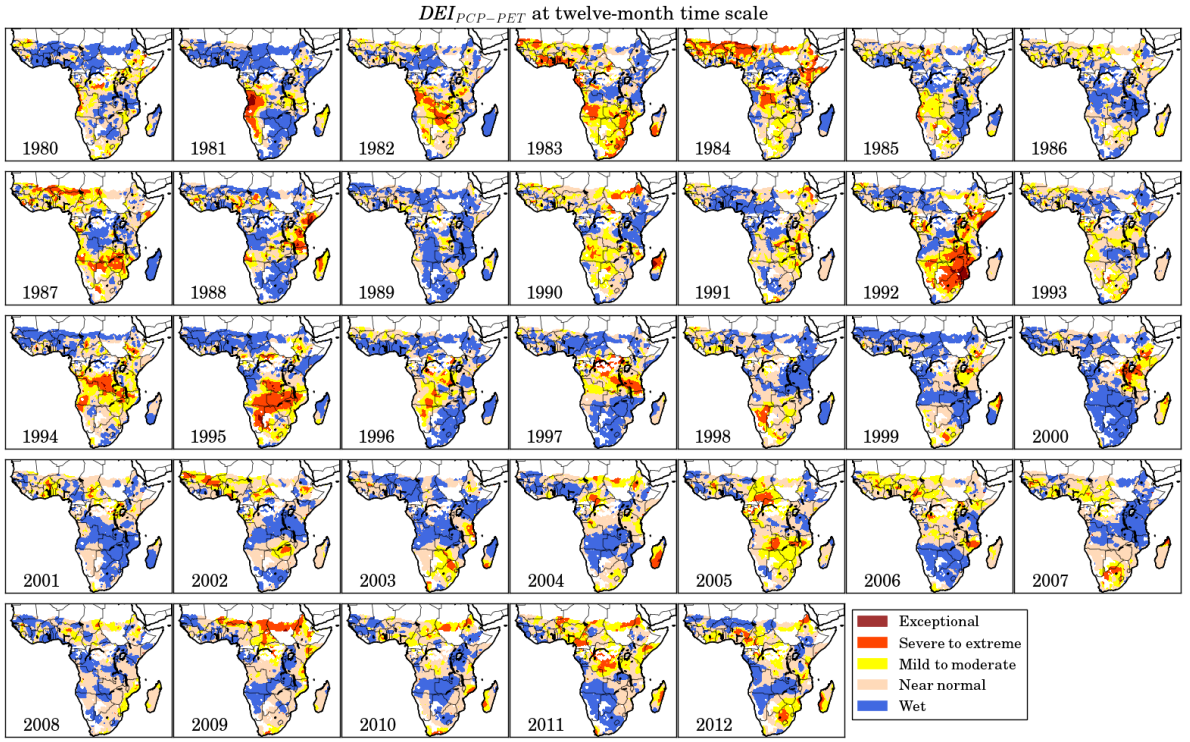

Figure S3.3. The grid-level annual spatial distribution of $DEI_{PCP-PET}$ at the twelve-month time scale (Drought Exposure Index based on the difference between precipitation and potential evapotranspiration) during 1981–2012

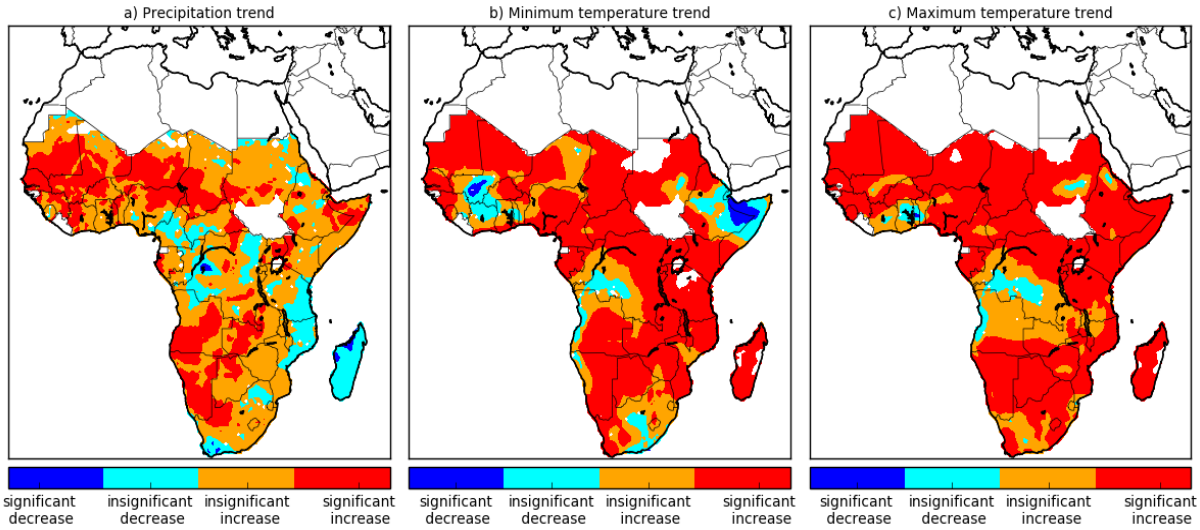

Figure S3.4. Drought trend based on Mann–Kendal trend analysis comparing: a) precipitation, b) minimum temperature, and c) maximum temperature during 1980–2012

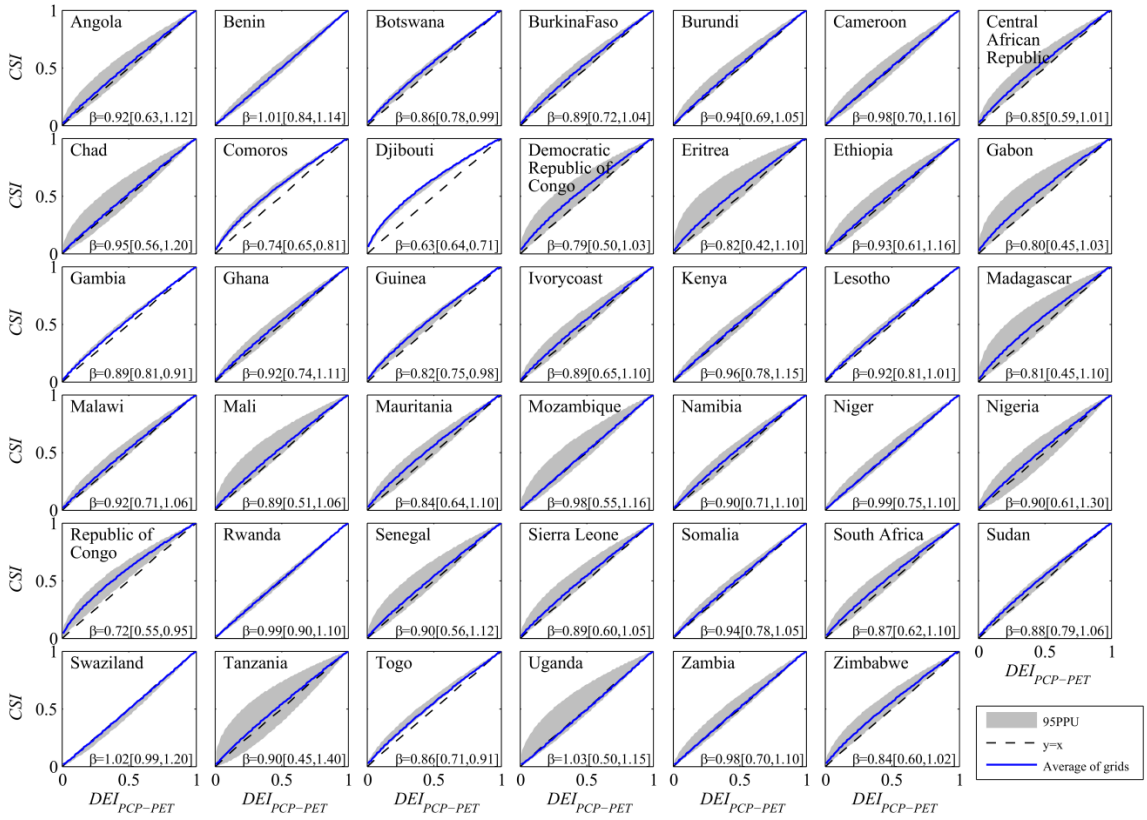

Figure S3.5. Country-level comparison of the interaction between precipitation based Drought Exposure Index ($DEI_{PCP\text{-}PET}$) and the Crop Sensitivity Index (CSI) using power curves fitted to each grid within a country. The grey band indicates 95PPU and the blue line is the average curve obtained from all fitted curves to grids of a country. The average, minimum, and maximum values of β are shown as: β= average β [minimum β, maximum β]

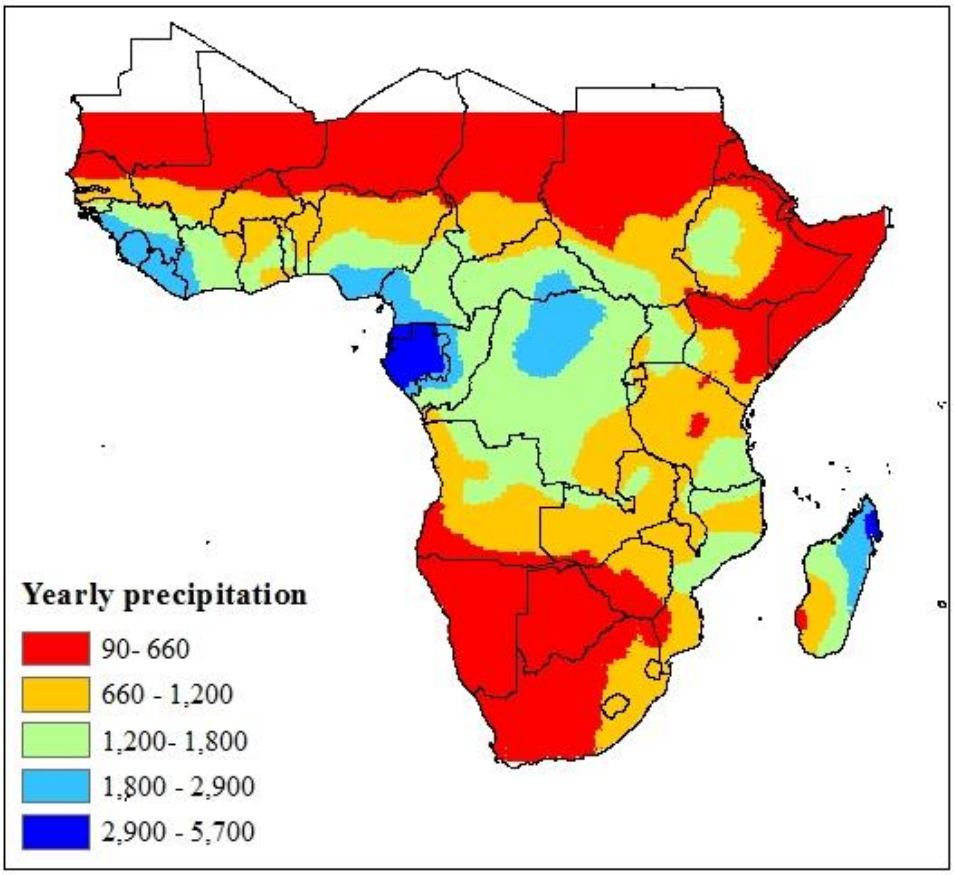

Figure S3.6. The spatial distribution of yearly precipitation (mm yr^{-1}) in SSA obtained from climate datasets used in this study is WFDEI-CRU (WATCH-Forcing-Data-ERA-Interim-Climate Response Unit)

Chapter 4

Drought vulnerability assessment of maize in Sub-Saharan Africa: insights from physical and social perspectives

Based on

Drought vulnerability assessment of maize in Sub-Saharan Africa: insights from physical and social perspectives,

Global and Planetary Change, 162: 266-274, (2018)

Bahareh Kamali[1,2], Karim C Abbaspour[1], Bernhard Wehrli[2], Hong Yang[1,3]

[1] *Eawag, Swiss Federal Institute of Aquatic Science and Technology, Duebendorf, Switzerland*

[2] *Institute of Biogeochemistry and Pollutant Dynamics, ETH Zurich, Switzerland*

[3] *Department of Environmental Sciences, University of Basel, Switzerland*

Abstract

Drought as a slow-onset phenomenon inflicts important losses to agriculture where the degree of vulnerability depends not only on physical variables such as precipitation and temperature, but also on societal preparedness. While the scopes of physical and social vulnerability are very different in nature, studies distinguishing these two aspects have been lacking. In this study, we address the physical and social aspects of drought vulnerability of maize ($CDVI_{phy}$ and $CDVI_{soc}$) in Sub-Saharan Africa (SSA). To quantify vulnerability, we applied a probabilistic framework combining a Drought Exposure Index (*DEI*) with a physical or social Crop Failure Index, CFI_{phy} or CFI_{soc}, respectively. *DEI* was derived from the exceedance probability of precipitation. Maize yields, simulated using the Environmental Policy Integrated Climate (EPIC) model, were used to build CFI_{phy}, whereas the residual of simulated and FAO recorded yields were used to construct CFI_{soc}. The results showed that Southern and partially Central Africa are more vulnerable to physical drought as compared to other regions. Central and Western Africa, however, are socially highly vulnerable. Comparison of $CDVI_{phy}$ and $CDVI_{soc}$ revealed that societal factors cause more vulnerability than physical variables in almost all SSA countries except Nigeria and South Africa. We conclude that quantification of both drought vulnerabilities help a better characterization of droughts and identify regions where more investments in drought preparedness are required.

4.1. Introduction

Crops exhibit known responses to climate variability (Challinor et al., 2009). Crop models can predict the vulnerability of food production to drought (Fraser et al., 2013). However, drought vulnerability is a complex, context-specific concept (Naumann et al., 2014) and its definition has evolved over time. According to the IPCC (Intergovernmental Panel on Climate Change) Forth Assessment Report (2011), vulnerability is defined as the degree to which an environmental or a social system is exposed to adverse effects of climate change and is a function of exposure, sensitivity, and adaptive capacity (IPCC, 2007; Nelson et al., 2007; Parry et al., 2007; Wilby and Wigley, 1997). The IPCC Fifth Assessment Report emphasizes on the social aspect of drought vulnerability (IPCC, 2013).

From the agricultural point of view, although the direct impact of precipitation shortfall is crop yield reduction, the underlying cause of this vulnerability to meteorological drought can be beyond the natural scope (Naumann et al., 2014). Generally speaking, "physical vulnerability" induces yield loss only due to water stress during crop growth, but reduced production in a drought event has multiple factors. Stressors making one region vulnerable may be different for another region and are highly dependent on the degree of development and socio-economic status of a particular community (Antwi-Agyei et al., 2012). Reasons like political, economic, and social conditions significantly exacerbate drought impacts especially in developing countries (Bashir and Schilizzi, 2013; O'Brien et al., 2004).

Turner and Dumas (2013) found that in many cases social factors dominate. These assessments indicate that climate change can affect crop production well beyond the physical drought stresses.

Given its complexity, many studies have conducted vulnerability quantification at different levels, from developing qualitative methods (Derbile, 2013; Fussel and Klein, 2006; Luers et al., 2003), to building and validating composite indicators (Carrão et al., 2016; Naumann et al., 2014; O'Brien et al., 2004), and to identifying factors influencing vulnerability (Antwi-Agyei et al., 2012; Bryan et al., 2009; Malcomb et al., 2014). The results show that some regions are at a higher risk of severe or even total crop production loss (Muller et al., 2011; Roudier et al., 2011) for a relatively mild drought. In countries of Sub-Saharan Africa (SSA), poverty limits installing adaptation measures to drought (Masih et al., 2014; Shi and Tao, 2014); therefore, the physical and social vulnerability to drought can be very different. However, few studies on drought vulnerability have measured the difference between physical and social drought vulnerability or highlighted their relative importance (Terence et al., 2017; Zarafshani et al., 2012). Therefore, there is a need to develop methods that quantify both aspects of drought vulnerability simultaneously. Such level of understanding is important to propose effective adaptation measures to drought and to enhance the resilience of agricultural production (Cooper et al., 2008).

This study bridges the existing gap in quantification of the two aspects of drought vulnerability for maize in SSA. A process-based EPIC crop model is used to simulate maize yields to derive information on crop's physical response to climate variability (Iglesias et al., 2012; Lobell and Burke, 2010). The reported yields by FAO reflect the impacts of both physical and social factors. We quantify maize drought vulnerability by incorporating drought exposure and crop failure indices in a probability framework. The regions that are physically and socially highly vulnerable are identified and implications of the two aspects of drought vulnerability are discussed.

SSA was chosen here because it is the home to 1 billion people (World Bank, 2016) frequently struck by droughts. Rainfall has large spatial and temporal variability in the region with significant impact on food production and livelihoods of the people (Hellmuth et al., 2007). The recurrence of droughts in the past decades has triggered many famines, resulting in the death of millions of people and food insecurity across the sub-continent. The expected adverse impacts of climate change on crop production in SSA add further risk to the future food security of the region (Liu et al., 2008; Muller, 2011; Roudier et al., 2011; Schlenker and Lobell, 2010).

4.2. Methodology

4.2.1. Simulation and calibration of maize yield using EPIC

Crop yield was simulated using EPIC^{+} which is an extended version of EPIC coupled with the Sequential Uncertainty Fitting (SUFI-2) algorithm for calibration (Kamali et al., 2018). EPIC is a bio-physical agronomic model developed in the mid-1980s (Williams et al., 1989). The crop growth

module of EPIC estimates crop yield by multiplying the above ground biomass at maturity with a water stress adjusted harvest index (Williams et al., 1989). The model operates on a daily basis and takes into account all relevant processes of soil–crop–atmosphere system, climate data, management data such as a leaf area index, a crop parameter for converting energy to biomass, and fertilizer deficiencies (Williams et al., 1989). Validation studies with EPIC applications on different scales have demonstrated satisfactory results in previous works (Causarano et al., 2008; Gaiser et al., 2010; Liu et al., 2013; Wang et al., 2012).

EPIC is originally a field-scale model. In EPIC^{+} as a spatially explicit model, the EPIC application is extended to larger scales using a Python framework following the work by Kamali et al. (2018). The framework divides the region of study into a numbers of grids based on a specified resolution (here 0.5°) and executes EPIC on each grid cell. The site-specific input data included longitude, latitude, slope, elevation (DEM), climate, soil, crop calendar, fertilizer, and soil (Table 4.1). All input data were converted into 0.5° resolution.

Table 4.1. Summary of the input data and the sources used for simulating maize in SSA. All data were transformed into a 0.5°x0.5° resolution.

Input data	Description	Resolution	Year	Source
DEM, Slope	Digital elevation model GTOPO30	1 km (5″x5″)	Edition 2004	U.S. Geological Survey (2004)
A_{RF}	Rainfed cultivated area	10 km (5′x5′)	2000	MIRCA2000[1] version 1.1 Portmann et al. (2010)
Climate	Daily maximum and minimum temperature, precipitation, solar radiation, relative humidity, wind speed, CO_2 concentration	50 km (0.5^{o}x0.5^{o})	1970-2012	WFDEI[2] meteorological forcing data Weedon et al. (2011)
Soil	Soil map and database	10 km (5′x5′)	2006	ISRIC-WISE[3] Batjes (2006)
Planting & harvesting dates	Based on temperature linked to crop calendar	50 km (0.5^{o}x0.5^{o})	1990s to early 2000s	SAGE[4] Sacks et al. (2010)
Fertilizer	Fertilizer use	National	2002	FertiStat (FAO, 2007)

[1] Monthly Irrigated and Rainfed Crop Areas
[2] WATCH-Forcing-Data-ERA-Interim
[3] International Soil Reference and Information Centre-World Inventory of Soil Emission Potentials
[4] Center for Sustainability and the Global Environment

In the developed framework, EPIC^{+} is equipped with the Sequential Uncertainty Fitting (SUFI-2) algorithm for automatic calibration (Abbaspour et al., 2004). The SUFI-2 algorithm maps all uncertainties in the output on the parameter ranges. The uncertainty is quantified by the 95% prediction uncertainty (95PPU) calculated at the 2.5% and 97.5% levels of cumulative distribution of

an output variable obtained through the Latin Hypercube Sampling in the parameters space. Two criteria, *r-factor* and *p-factor*, judge the goodness-of-fit and the level of uncertainty of the model. The *p-factor* criterion represents the fraction of measured data bracketed by the 95PPU uncertainty band and varies from 0 to 1, where 1 means 100% of the measured data are bracketed by the model simulation (expressed as the 95PPU). Values around 0.5 are usually acceptable for crop simulation (Abbaspour et al., 2015). The *r-factor* criterion is the average width of the 95PPU band divided by the standard deviation of the measured variable, which is a measure of the prediction uncertainty. The ideal value for *r-factor* is 0, with an acceptable practical value of around 2 for crop yield.

We simulated the maize for the years 1970-2012. Considering the first 10 years as equilibrating period for soil moisture and nitrogen initial conditions, we calibrated the model for the period 1980-2012. The *Standardized Root Mean Square Error* (*RSR*) criterion proposed by Singh et al. (2004) was selected as the objective function in the SUFI-2 algorithm to compare the performance of country level simulated yield (Y_{sim}) with national level FAO yield (Y_{obs}) (FAO, 2012) as:

$$RSR = \frac{RMSE}{STDEV_{obs}} = \frac{\sqrt{\sum_{t=1}^{33}(Y_{obs,t} - Y_{sim,t})^2}}{\sqrt{\sum_{t=1}^{33}(Y_{obs,t} - \bar{Y}_{obs})^2}} \quad (4\text{-}1)$$

Y_{sim} was obtained from simulating irrigated (Y_{IR}) and rainfed (Y_{RF}) yields in EPIC on *n* grids within a country and is then aggregated to country level using weighted areal averages as (Folberth et al., 2012):

$$Y_{sim} = \frac{\sum_{i=1}^{n} Y_{RF,i} \times A_{RF,i} + Y_{IR,i} \times A_{IR,i}}{\sum_{i=1}^{n} A_{RF,i} + A_{IR,i}} \quad (4\text{-}2)$$

where A_{IR} and A_{RF} are respectively irrigated and rainfed cultivated areas in each grid.

We simulated maize for the years 1970-2012. Considering the first 10 years as equilibrating period for soil moisture and nitrogen initial conditions, we calibrated the model for the period 1980-2012. Model calibration was implemented in three steps (Kamali et al., 2018). In the first step, planting dates at grid level were adjusted in 50 simulations and their values were fixed. In the next step, parameters related to agricultural operations including potential heat unit, planting density and different fertilization application rates (Nitrogen, Phosphorous, and Potassium) were calibrated. The best values were used as fixed values for the next step. Finally and in the last step, six Crop parameters (Biomass-energy ratio, Harvest index, Optimal temperature for plant growth, Minimum temperature for plant growth, Lower limit of harvest index, Fraction of water in crop yield) and two Model parameters (Water stress harvest index and SCS curve number index) highlighted as the most sensitive parameters

in literature were calibrated (Wang et al., 2012; Xiong et al., 2014). More details on the initial ranges of parameters are found in Kamali et al. (2018).

4.2.2. Conceptualizing crop drought vulnerability

Crop Drought Vulnerability Index (*CDVI*) was built with the Drought Exposure Index (*DEI*) as a measure of the degree of stresses on the system; and the Crop Failure Index (*CFI*) as the response of the system to the stress.

4.2.3. Definition of Drought Exposure Index (*DEI*)

DEI is derived from the Standardized Precipitation Index (*SPI*) (McKee et al., 1993). *SPI* is calculated first by fitting a two-parameters gamma distribution function to precipitation (*PCP*). Once the probability distribution function is determined, the Cumulative Distribution Function (CDF_{PCP}) is calculated and the inverse normal function is applied to obtain *SPI*. This means that *SPI* and its associated CDF_{PCP} can be converted to each other. We define *DEI* by using CDF_{PCP} , which was described by a two-parameters gamma distribution (Bordi et al., 2001b; Lloyd-Hughes and Saunders, 2002):

$$DEI = 1 - CDF_{PCP} \tag{4-3}$$

We tested the performance of normal, log-normal and two-parameter gamma distribution functions using the Kolmogorov-Smirnov (K-S) statistic test for the precipitation data. The results showed that all the three distributions show a good fit for all months and less than 5% of grid cells failed the test (Figure S4.1). The average *p-values* were slightly higher for the gamma distribution. A two-parameter gamma distribution was used. Other studies confirmed the suitability of gamma distribution function (Bordi et al., 2001a; Lloyd-Hughes and Saunders, 2002).

DEI varies between 0 and 1 with *DEI*>0.5 indicating drought situations and *DEI*<0.5 being equivalent to non-drought. Figure 4.1a presents the schematic representation of transforming *PCP* to CDF_{PCP}, and CDF_{PCP} to *DEI*. *DEI-X* is defined over different time scales (*X* = 1, 3, 6, 9, and 12-month(s)). *DEI-X* at each month is obtained from total precipitation over the last *X* months. For example, *DEI*-3 at the end of February compares the December–January–February precipitation totals in that particular year with the December–January–February precipitation totals of all other years. We also defined five categories within the ranges of CDF_{PCP} and *DEI* as: wet, near normal, mild to moderate drought, severe to extreme drought, and exceptional drought (Svoboda et al., 2002) (Table 4.2).

Table 4.2. Five categories of cumulative distribution functions (CDF_{PCP}, $CDF_{Y_{sim}}$, $CDF_{Y_{obs}-Y_{sim}}$) and their equivalent Drought Exposure (*DEI*) and Crop Failure Indices (*CFI*).

Category	CDF_{PCP}, $CDF_{Y_{sim}}$, $CDF_{Y_{obs}-Y_{sim}}$	*DEI*, *CFI*
Wet	0.692 to 1.00	0.00 to 0.308
Near normal	0.308 to 0.692	0.0308 to 0.692
Mild to moderate	0.115 to 0.308	0.692 to 0.885
Severe to extreme	0.023 to 0.115	0.885 to 0.115
Exceptional	0.00 or 0.0230	0.977 to 1.00

4.2.4. Definitions of the physical and social Crop Failure Indices (CFI_{phy} and CFI_{soc})

The physical Crop Failure Index (CFI_{phy}) considers only climatic influences and its computation is based on Y_{sim} obtained from the calibrated EPIC, which is not influenced by social factors as (Figure 4. 1b):

$$CFI_{phy} = 1 - CDF_{Y_{sim}} \tag{4-4}$$

According to this definition, crop failure occurs in years when *CFI* is larger than 0.5.

CFI_{soc} integrates the non-physical influence of drought on crop loss. It is important to point out that we do not aim to consider details of socio-economic factors influencing crop failure; but only imply that Y_{obs} is based on a combination of social and physical factors, while Y_{sim} merely considers the physical factors. Therefore, we use the residuals of Y_{obs} and Y_{sim} (Y_{obs}-Y_{sim}) to represent crop losses due to socio-economic factors and quantify it by CFI_{soc} as:

$$CFI_{soc} = 1 - CDF_{Y_{obs}-Y_{sim}} \tag{4-5}$$

According to the above definition, crop failure occurs when Y_{obs} is smaller than Y_{sim}. Positive residuals mean that the region is able to produce more crop than expected, considering the climate influence; whereas negative residuals indicate that the region did not adapt to climate stresses (Figure 4.1c). The five categories defined in Table 4.2 for *DEI* also remain valid for CFI_{phy} and CFI_{soc}.

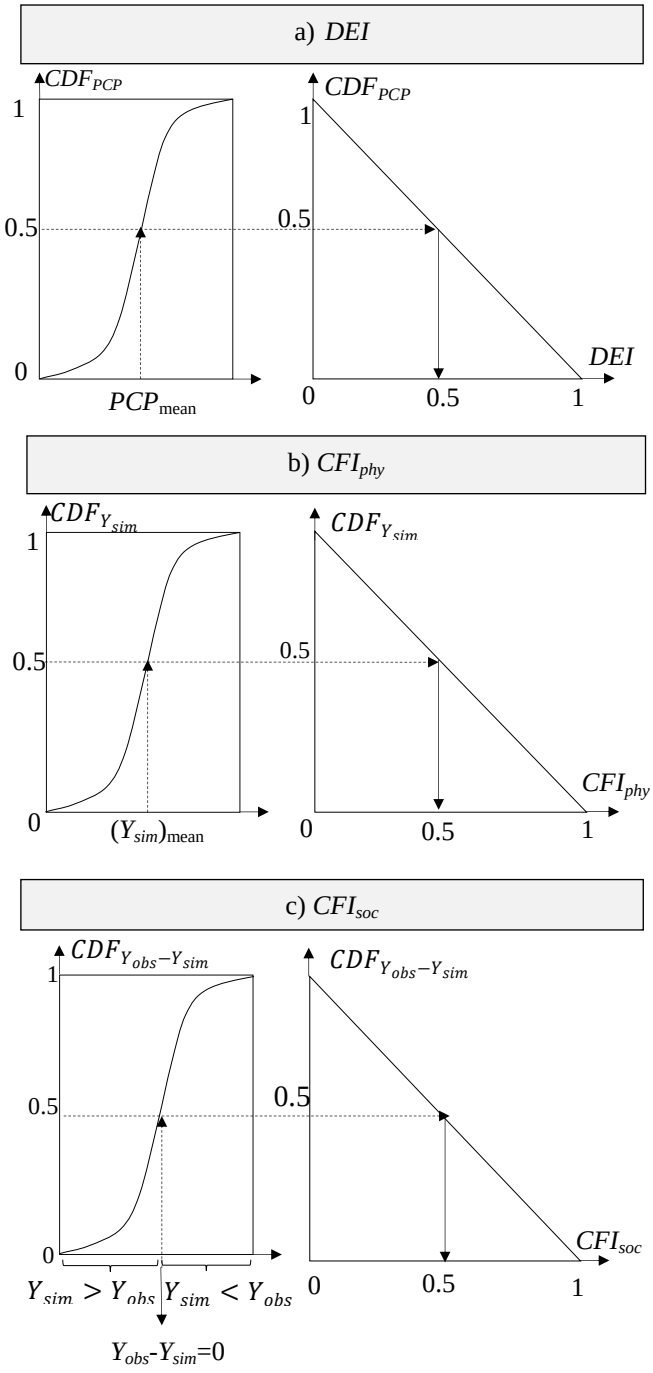

Figure 4.1. Schematic representation of transforming a) precipitation from its cumulative distribution function (CDF_{PCP}) to the Drought Exposure Index (*DEI)*; b) simulated maize yield (Y_{sim}) from its cumulative distribution function ($CDF_{Y_{sim}}$) to the physical Crop Failure Index (CFI_{phy}); and c) the residual of simulated and observed yields from its cumulative distribution function ($CDF_{Y_{obs}-Y_{sim}}$) to the socio-economic Crop Failure Index (CFI_{soc}).

4.2.5. Drought vulnerability definition based on incorporating *DEI* and *CFI*

The vulnerability of a system is defined as the ability to respond to variables of exposure. As the degree of exposure and the capacity to withstand them are uncertain, vulnerability is quantified

probabilistically (Foti et al., 2014). Physical ($CDVI_{phy}$) and social vulnerabilities ($CDVI_{soc}$) are defined as the probabilities that CFI_{phy} and CFI_{soc} , respectively, are larger than *DEI* (Foti et al., 2014); that is:

$$CDVI_{phy} = Pr\left[DEI < CFI_{phy}\right] = \Pr[DEI - CFI_{phy} < 0] \quad (4\text{-}6)$$
$$CDVI_{soc} = Pr[DEI < CFI_{soc}] = \Pr[DEI - CFI_{soc} < 0]$$

From probabilistic points of view, vulnerability depends on the mean, variance, and co-variance of *DEI*, CFI_{phy}, or CFI_{soc}. From probabilistic points of view, vulnerability depends on the mean, variance, and covariance of *DEI*, CFI_{phy}, or CFI_{soc}. Assuming $Z_{phy} = DEI - CFI_{phy}$ and $Z_{soc} = DEI - CFI_{soc}$ and in the case of non-Gaussian Z_{phy} and Z_{soc}, the above equations are written:

$$CDVI_{phy} = \frac{1}{2} + \frac{1}{2} erf\left[\frac{(-\mu_{DEI} + \mu_{CFI_{phy}})}{\sqrt{2\sigma^2_{Z_{phy}}}}\right]$$
$$CDVI_{soc} = \frac{1}{2} + \frac{1}{2} erf\left[\frac{(-\mu_{DEI} + \mu_{CFI_{soc}})}{\sqrt{2\sigma^2_{Z_{soc}}}}\right] \quad (4.7)$$

where *erf*() is the Gaussian error function, μ_{DEI} is the mean of *DEI*. More details on the derivation of above equations, their components and their influence on vulnerability are provided in Supplementary material (section 4.7).

4.3. Results

4.3.1. Calibration performance of EPIC

The results of simulated maize given in terms of *RSR* before and after calibration (Table 4.3) indicated significant improvement in model performance after calibration. The *RSR* values for all countries except Democratic Republic of the Congo, decreased to around 1 or less. The *RSR* value for Democratic Republic of the Congo decreased significantly from 45.9 to 6.27. The main reason for high *RSR* in this country is a reported constant yield of 0.8 t ha^{-1} for the whole 33-year period which does not seem to be realistic. Comparison of the average of simulated and observed yields during 1980-2012 shows that the differences are smaller than 0.1 t ha^{-1} in most countries suggesting satisfactory performance of the $EPIC^{+}$ in simulating crop yields.

Table 4.3. Country level results of the EPIC calibration with the SUFI-2 algorithm based on *RSR* before calibration, *RSR* after calibration, *p-factor* and *r-factor* criteria ($\bar{Y}_{obs}$ is the average observed maize yield and $\bar{Y}_{sim}$ is the average simulated yield) obtained from the work by Kamali et al. (2018).

	Country	$\bar{Y}_{obs}$	$\bar{Y}_{sim}$	*RSR*	*p-factor*	*r-factor*
Eastern Africa	Burundi	1.17	1.17	1.38	0.55	1.80
	Comoros	2.20	2.13	1.13	0.42	1.95
	Eritrea	0.63	0.39	1.45	0.58	1.98
	Ethiopia	1.78	1.80	0.91	0.52	1.81
	Kenya	1.67	1.69	0.86	0.61	1.74
	Madagascar	1.14	1.37	1.42	0.79	2.54
	Malawi	1.34	1.37	0.94	0.45	2.25
	Mozambique	0.68	0.64	1.12	0.61	1.56
	Rwanda	1.23	1.18	1.08	0.43	1.04
	Somalia	0.89	0.80	1.22	0.42	1.08
	Sudan	0.79	0.72	1.33	0.48	1.05
	Tanzania	1.48	1.10	1.20	0.58	0.94
	Uganda	1.59	1.62	0.85	0.58	2.48
	Zambia	1.85	1.86	0.89	0.45	1.31
	Zimbabwe	1.16	1.17	1.12	0.37	1.67
Central Africa	Angola	0.52	0.55	0.99	0.88	2.38
	Cameroon	1.81	1.79	1.00	0.48	1.38
	Central African Republic	0.94	1.05	1.16	0.49	0.74
	Chad	0.94	0.94	0.84	0.66	2.05
	Democratic Republic of the Congo	0.80	0.81	6.27	0.48	1.05
	Gabon	1.56	1.49	1.35	0.70	1.95
	Republic of Congo	0.76	0.75	2.16	0.88	2.39
Southern Africa	Botswana	0.29	0.30	1.39	0.52	2.33
	Lesotho	0.80	0.72	1.27	0.42	2.45
	Namibia	1.36	1.12	1.02	0.42	1.23
	South Africa	2.67	2.48	0.92	0.55	0.79
	Swaziland	1.35	1.39	1.06	0.42	1.49
Western Africa	Benin	1.03	1.08	0.99	0.70	1.83
	Burkina Faso	1.34	1.32	0.97	0.52	1.07
	Djibouti	1.80	1.84	1.20	0.70	2.73
	Gambia	1.30	1.29	0.93	0.82	2.97
	Ghana	1.37	1.46	1.07	0.52	1.14
	Guinea	1.23	1.27	1.96	0.45	2.02
	Ivory coast	1.51	1.73	1.08	0.48	1.44
	Mali	1.50	1.70	0.98	0.55	1.55
	Mauritania	0.70	0.67	1.18	0.61	2.25
	Niger	0.69	0.68	0.85	0.70	1.88
	Nigeria	1.44	1.39	0.98	0.70	1.84
	Sierra Leone	0.99	1.00	1.09	0.53	2.07
	Senegal	1.29	1.27	0.92	0.86	2.44
	Togo	1.08	1.19	1.26	0.52	1.18

4.3.2. Spatiotemporal pattern of *DEI* and CFI_{phy}

To identify the most relevant time scale of *DEI* for vulnerability analysis, the correlation coefficients between *DEI*-1, 3, 6, 9, and 12 during growing seasons and CFI_{phy} were calculated. The results showed higher correlation in Southern and Eastern Africa as well as Sahelian strip countries (mostly larger than 0.5) as compared to Central Africa and Southern regions of the Sahelian strip where the values ranged between 0.2 and 0.5 (Figure 4.2a-e). The lower correlation coefficient values in Central Africa and countries along the West coast of Western Africa are mostly related to high precipitation (larger than 1200 mm yr^{-1}), which indicates that crop losses are not correlated to water stress. *DEI*-12 was least correlated with CFI_{phy}, especially in most countries, indicating that longer exposure times are not adequate for agricultural loss assessment. *DEI*-3 and *DEI*-6 with the highest correlation coefficients in most cases were identified as the most representative time scales (Figure 4.2 c, b).

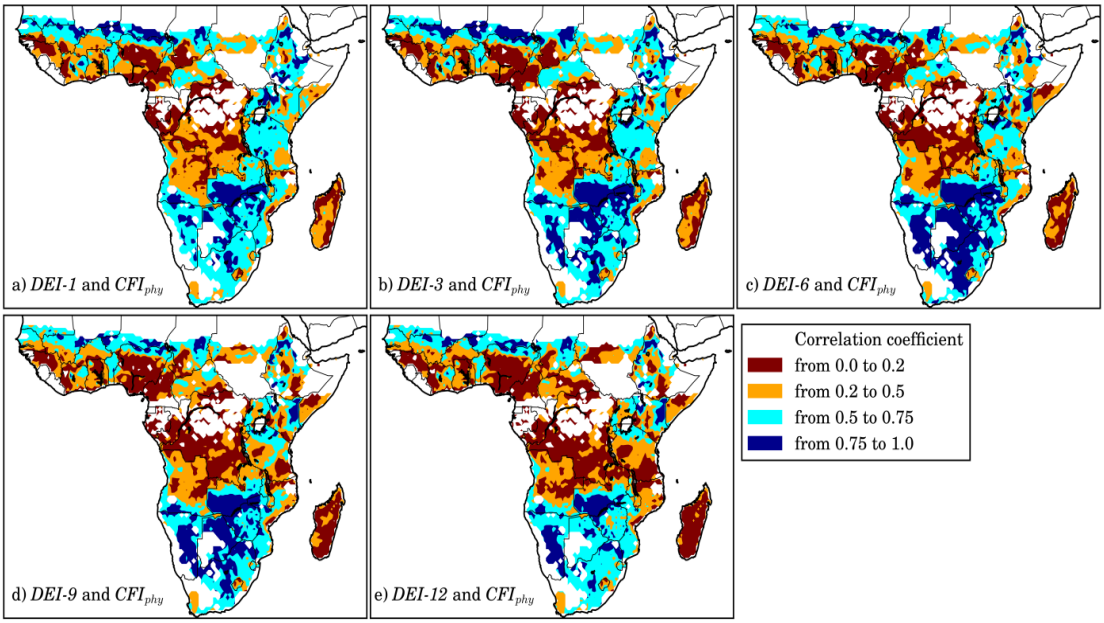

Figure 4.2. Correlation coefficients between different time scales of Drought Exposure Index (*DEI)* and physical Crop Failure Index (CFI_{phy}) for maize.

For each grid, we selected the time scale with the highest correlation for subsequent analysis of vulnerability. The grid level *DEI* between 1980 and 2012 indicates that SSA experienced many severe to extreme drought periods (Figure 4.3). Between 1982 and 1984, almost all countries experienced drought situations. The Southern and Western Africa experienced severe to extreme drought in 1987. Later, and between 1992 and 1995, Central and Southern African countries experienced severe and extreme drought situations. Between 1999 and 2012, less drought exposure was evident. However, Southern and Central Africa experienced the least wet period and rainfall were mostly in the near normal situation during the last decades. Yearly CFI_{phy} patterns (Figure 4.4) were approximately similar to the *DEI* patterns in Figure 4.3 for some regions whereas were different in others. The

drought period 1982-1984 significantly influenced Southern and Eastern Africa with severe to extreme intensity, whereas the Central African countries were least exposed to high CFI_{phy} and were mostly in the near normal situations (Figure 4.4). This clearly shows that drought periods identified by *DEI* did not reflect with the same intensity in CFI_{phy}.

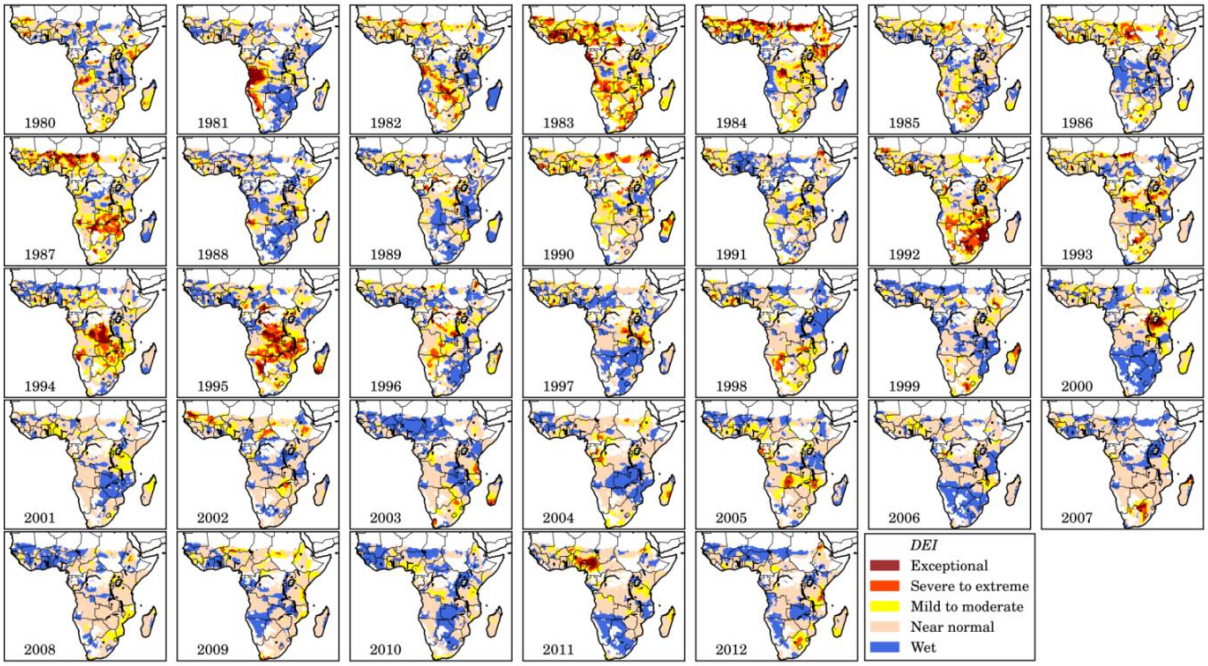

Figure 4.3. The grid level pattern of the annual Drought Exposure Index (*DEI*) during 1980 -2012.

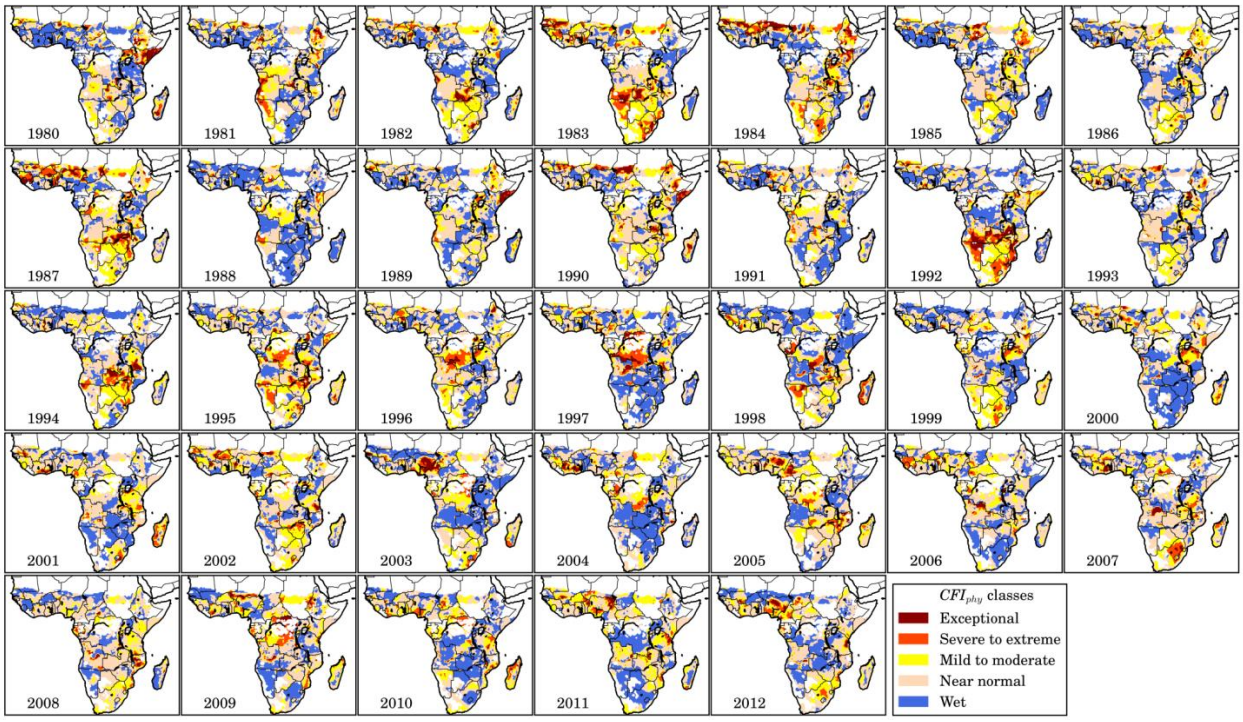

Figure 4.4. The grid level patterns of the annual physical Crop Failure Index (CFI_{phy}) during 1980-2012.

4.3.3. Physical and social crop drought vulnerability

The $CDVI_{phy}$ and $CDVI_{soc}$ calculated in this study (Eq. S4-4) quantifies vulnerability based on the interactions of *DEI*s and *CFI* for the 33 years of studied period and does not differentiate periods with high vulnerability from low ones. The $CDVI_{phy}$ distribution shows values larger than 0.46 in most SSA countries indicating that maize yield is vulnerable to climate variability (Figure 4.5a). Botswana, Zimbabwe, partially Mauritania, Western part of South Africa, and Central Tanzania with $CDVI_{phy}$ larger than 0.57 were identified as the most physically vulnerable regions. Namibia, Western Angola, north part of Central African Republic, and partially Democratic Republic of Congo with $CDVI_{phy}$ between 0.52 and 0.57 were placed in second vulnerable regions (Figure 4.5a).

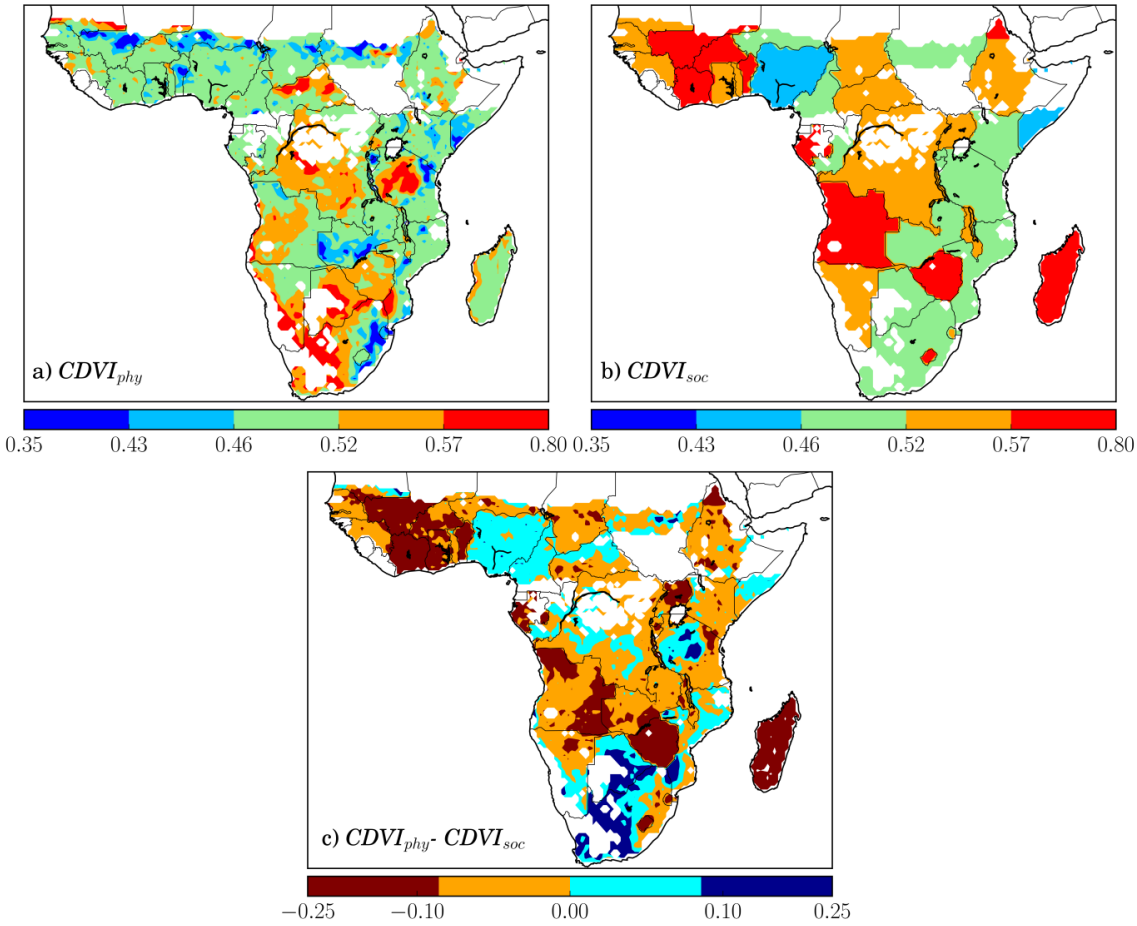

Figure 4.5. Spatial distribution of a) grid level physical maize drought vulnerability ($CDVI_{phy}$); b) country level social maize drought vulnerability ($CDVI_{soc}$); and c) the residual of $CDVI_{phy}$ and $CDVI_{soc}$. The results are based on the average vulnerability of 33-years.

The average $CDVI_{phy}$ calculated at the country level showed a very different picture from $CDVI_{phy}$. Overall, Western and Central African countries, Ethiopia, Zimbabwe, and Namibia were socially most vulnerable ($CDVI_{soc}$ >0.52) compared with Eastern Africa, South Africa, Sudan, and Chad. Nigeria and Somalia were least vulnerable as the $CDVI_{soc}$ was smaller than 0.46 (Figure 4.5b). Although,

Zimbabwe exhibited the highest degree of $CDVI_{phy}$ and $CDVI_{soc}$, the same was not true for countries like Madagascar, Mali, Benin, Burkina Faso, and Ivory Coast, where the degree of $CDVI_{phy}$ was not as high as $CDVI_{soc}$ (Figure 4.5a,b). The $CDVI_{phy}$ and $CDVI_{soc}$ values in Zimbabwe indicated that both climatic and social factors are the limiting factors for maize production in this country (Figure 4.5b). However, in other countries there was a large difference between $CDVI_{phy}$ and $CDVI_{soc}$, indicating a weak adaptive capacity of these countries to drought.

Due to lack of observed yields at grid level, we could calculate $CDVI_{soc}$ only at country level. To compare the two vulnerability types at grid level, we assigned the calculated country level values of $CDVI_{soc}$ to all grids within the country. The grid level residuals between two types of vulnerability i.e. $CDVI_{phy}$-$CDVI_{soc}$ was calculated at grid level (Figure 4.5c). In most countries, $CDVI_{soc}$ was larger than $CDVI_{phy}$ meaning that social vulnerability is more critical for the region than the physical one. The residuals exceeded 0.1 in countries like Ivory Coast, Benin, Mali, Zimbabwe, and Madagascar. In contrast, South Africa, Botswana, and Nigeria with a lower degree of $CDVI_{soc}$ were identified as drought-resilient countries.

We also compared the country level $CDVI_{soc}$ with median, 25th and 75th percentiles of $CDVI_{phy}$ calculated at grid level (Figure 4.6). The results showed that $CDVI_{soc}$ is larger than 75th percentiles of $CDVI_{phy}$ in most countries (Figure 4.6) indicating that in most parts of a country, $CDVI_{Isoc}$ is larger than $CDVI_{phy}$. Mauritania and Mali from Western Africa, Southern African countries, Gabon and Republic of Congo from Central Africa showed large variability in $CDVI_{phy}$, meaning that the degree of vulnerability is spatially different and therefore various adaptation strategies might be required depending on the residual between physical and social vulnerability. In Tanzania, for example, $CDVI_{soc}$ equals median of $CDVI_{phy}$, however over 50% of area are socially more vulnerable.

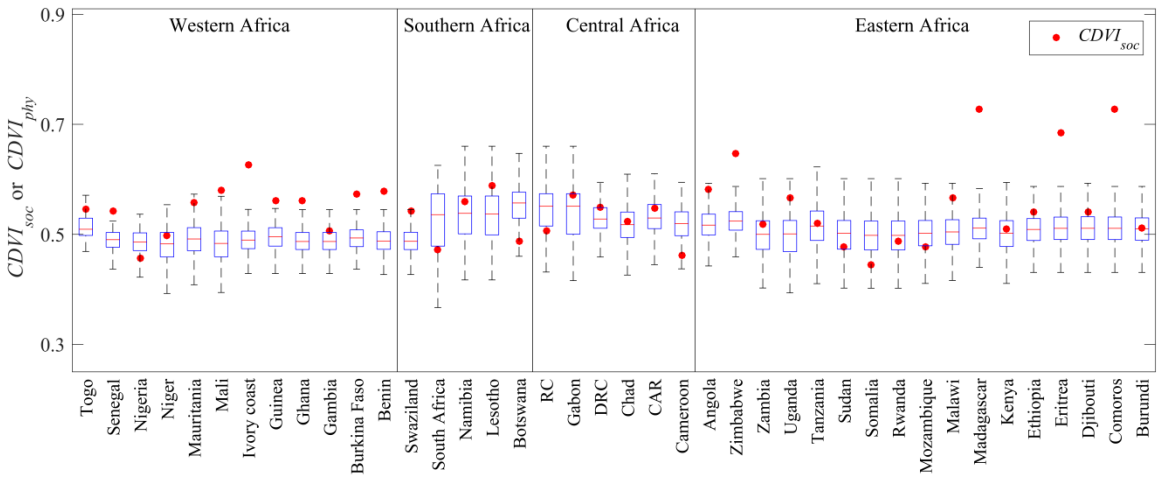

Figure 4.6. Country level comparison of the physical cumulative drought vulnerability indices $CDVI_{phy}$ (boxplot) and social indices $CDVI_{soc}$ (red points). The boxplots show the 25th and 75th percentiles of the spatial variability of $CDVI_{phy}$ from grids within a country.

4.4. Discussion

4.4.1. The effectiveness of proposed methodology for quantifying $CDVI_{soc}$ and $CDVI_{phy}$

This study demonstrated a method to distinguish and quantify physical and social crop drought vulnerability based on a quantitative assessment of *DEI* and *CFI*. Our analysis represents an important step forward in the current agricultural drought vulnerability assessment. Such level of understanding is particularly significant in SSA due to intrinsic climatic variability, reliance on rainfed agriculture as well as lack of coping infrastructure and resources of the society.

We applied a probabilistic methodology to define vulnerability and its components (*DEI*, *CFI*, *CDVI*). Integrating the probabilistic concept supports a more reliable inference of the likelihood and relevance of each index. Besides, it allows for explicit inclusion of thresholds, as all indices are transformed to the same range from 0 to 1 with five classes (Table 4.2). Using standardized definitions of *DEI* and *CFI*, one can normalize the degrees of severity for each single value, which facilitates the comparison on different spatial resolutions or with other available standardized indices in literature.

We inferred that the residual of the simulated and observed yields reflects the socio-economic indicator of vulnerability because the application of EPIC did not consider man-made effects such as developments in the agricultural machinery and technology. However, a certain degree of uncertainties associated with model simulation which might slightly influence our analysis. We accounted for model uncertainty by linking SUFI-2 to EPIC (details previously mentioned in Kamali et al. (2018)). The uncertainty in the observed yield, however, was more difficult to address and requires more details at smaller spatial scales. To partially account for it, we only took those observed yields, which were outside the 95% prediction uncertainty (95PPU) band of the simulated yields. The residual between Y_{obs} and Y_{sim} was also used in previous works as a criteria to distinguish regions that are resilient and sensitive to drought (Bryan et al., 2015).

Moreover, the magnitude of socioeconomic factors is substantially larger in most of countries. Comparing Y_{obs} with Y_{sim} in countries such as Burkina Faso, Ghana, Ivory coast, and Nigeria (Figure S4.2), one can see significant agreement between the average of simulated and observed yields (Table 4.3). However, the existing trend in observed yields cannot be related to modeling uncertainty, but stems from socioeconomic factors. It is clear that model uncertainty does not follow a trend (Figure S4.2). Therefore, not surprisingly, social vulnerability maps revealed clear differences between countries with a relatively strong economy such as Nigeria and South Africa, and Tanzania with other countries like Zambia and Ivory Coast where rather poor social adaptive capacity exacerbated vulnerability.

4.4.2. Implications of $CDVI_{phy}$ and $CDVI_{soc}$ for SSA countries

We found that $CDVI_{soc}$ was higher than $CDVI_{phy}$ for most countries revealing that there is a significant potential to increase maize yield by designing adaptation strategies and farmer-managed agricultural interventions. Using our vulnerability maps, one can identify promising hotspots for drought adaptation investment. Despite different initial assumptions, our results show some consistency with the findings of HarvestChoice (2013), where normalized potential maize yields were compared against actual yield. Their analysis also highlighted South Africa, Lesotho, and Tanzania as countries with high-level productivity despite low level of inherent potential yields. By contrast, Madagascar, Mali, and Senegal were marked as countries with a relatively large gap between actual and potential yields. The major difference between the outcomes of HarvestChoice (2013) and our results is that their actual yields, which encompassing the influence of both social and physical measures, were compared with potential yields, which was defined as the yield without any climate and nutrition stress; while we measured the gap according to the degree of exposure to climate stresses.

In this study, we do not discuss on the socio-economic factors which might influence vulnerability, as it is beyond the scope of this study and will be investigated in the follow-up study. However, the influence of these factors is reflected in the $CVDI_{soc}$. In Tanzania, for example, lower $CVDI_{soc}$ may be related to research and extension efforts applied in the fields as well as the use of improved maize seeds (Stephen et al., 2014). While in Nigeria strategies such as using hybrid varieties of seeds, availability of subsidized fertilizer, as well as improved infrastructure and extension services may have helped to adapt to climate variability. The maize revolution in Nigeria advanced the country to the tenth largest producer of maize in the world, and the largest maize producer in Africa. Democratic Republic of Congo suffered from years of war and political upheaval, and continues to face significant humanitarian challenges. No significant improvement in maize yield is reported over the last three decades. In Kenya, maize yield increased after liberation, however, it showed a slight decline between 1980 and 2013 presumably due to a lack of access to credit and finance to enable adoption of improved seeds (Abate et al., 2015).

Finally, the degree of vulnerability might vary over time, but we here quantified it for the whole studied period. Therefore, the social vulnerability of Nigeria with high maize yield in the last decade is of the same magnitude in Somalia where highest maize yield was seen in the first decade. In Nigeria, the most significant changes occurred after 2000. On the other hand, Somalia had its peak in maize production in the 1980's and the country experience an average of about 57% decrease over the last two decades in maize production in 1990's and 2000's due to famine, damages from pest, ethnic wars, and regime change. All these changes resulted in poor nutritional status of farmers, and fields being abandoned due to insecurity (Rashid and Zejjari, 1997). Similar situation occurred in Madagascar where yield increased after 2000 and therefore the country were placed as socially vulnerable regions.

4.5. Conclusion and limitation

Our proposed methodology quantified the physical and social crop drought vulnerabilities and highlights countries where adaptation capacities are weak. The results show that Southern and Eastern African countries are physically more vulnerable to drought as compared to other regions. Central and Western Africa, however, are socially highly vulnerable. Our analysis of social vulnerability was limited to the country scale due to the lack of spatially well-resolved crop yields which was the main limitation of this study. However, it is evident that the proposed methodology is valid and can be adapted to any spatial scale depending on the available data for the region. Smaller resolution of data will help to increase the reliability of the calibrated models and to better understand the effectiveness of adaptation strategies can be applied to each regions. Here, we assumed that social vulnerability is the same in all grids within the country and equals the average of the country. This study does not provide a detailed investigation of factors that influence the difference between physical and social vulnerability. However, our preliminary discussion of the social drought vulnerabilities in SSA countries shows that such a systematic analysis would provide a more reliable basis for analysis of crop production risks and failure in various regions.

4.6. Reference

Abate, T., Mugo, S., De Groote, H., and Regassa, M. W. (2015). A quarterly bulletin of the drought tolerant maize for Africa project. *In* "Tolerant Maize for Africa", Vol. 4, pp. 1-4.

Abbaspour, K. C., Johnson, C. A., and van Genuchten, M. T. (2004). Estimating uncertain flow and transport parameters using a sequential uncertainty fitting procedure. *Vadose Zone Journal* **3**, 1340-1352.

Abbaspour, K. C., Rouholahnejad, E., Vaghefi, S., Srinivasan, R., Yang, H., and Klove, B. (2015). A continental-scale hydrology and water quality model for Europe: Calibration and uncertainty of a high-resolution large-scale SWAT model. *Journal of Hydrology* **524**, 733-752.

Antwi-Agyei, P., Fraser, E. D. G., Dougill, A. J., Stringer, L. C., and Simelton, E. (2012). Mapping the vulnerability of crop production to drought in Ghana using rainfall, yield and socioeconomic data. *Applied Geography* **32**, 324-334.

Bashir, M. K., and Schilizzi, S. (2013). Determinants of rural household food security: a comparative analysis of African and Asian studies. *Journal of the Science of Food and Agriculture* **93**, 1251-1258.

Batjes, N. H. (2006). ISRIC-WISE derived soil properties on a 5 by 5 arc-minutes global grid. ISRIC - World Soil Information, Wageningen, Netherlands.

Bordi, I., Frigio, S., Parenti, P., Speranza, A., and Sutera, A. (2001a). The analysis of the Standardized Precipitation Index in the Mediterranean area: large-scale patterns. *Annali Di Geofisica* **44**, 965-978.

Bordi, I., Frigio, S., Parenti, P., Speranza, A., and Sutera, A. (2001b). The analysis of the standardized precipitation index in the mediterranean area: large-scale patterns. *Annali Di Geofisics* **44**, 965-978.

Bryan, B. A., Huai, J., Connor, J., Gao, L., King, D., Kandulu, J., and Zhao, G. (2015). What actually confers adaptive capacity? Insights from agro-climatic vulnerability of Australian wheat. *Plos One* **10**.

Bryan, E., Deressa, T. T., Gbetibouo, G. A., and Ringler, C. (2009). Adaptation to climate change in Ethiopia and South Africa: options and constraints. *Environmental Science & Policy* **12**, 413-426.

Carrão, H., Naumann, G., and Barbosa, P. (2016). Mapping global patterns of drought risk: An empirical framework based on sub-national estimates of hazard, exposure and vulnerability. *Global environmental Change* **39**, 108-124.

Causarano, H. J., Doraiswarny, P. C., McCarty, G. W., Hatfield, J. L., Milak, S., and Stern, A. J. (2008). EPIC modeling of soil organic carbon sequestration in croplands of Iowa. *Journal of Environmental Quality* **37**, 1345-1353.

Challinor, A. J., Ewert, F., Arnold, S., Simelton, E., and Fraser, E. (2009). Crops and climate change: progress, trends, and challenges in simulating impacts and informing adaptation. *Journal of Experimental Botany* **60**, 2775-2789.

Cooper, P. J. M., Dimes, J., Rao, K. P. C., Shapiro, B., Shiferaw, B., and Twomlow, S. (2008). Coping better with current climatic variability in the rain-fed farming systems of Sub-Saharan Africa: An essential first step in adapting to future climate change? *Agriculture Ecosystems & Environment* **126**, 24-35.

Derbile, E. K. (2013). Reducing vulnerability of rain-fed agriculture to drought through indigenous knowledge systems in north-eastern Ghana. *International Journal of Climate Change Strategies and Management* **5**, 71-94.

FAO (2007). FertiSTAT - Fertilizer Use Statistics. Food and Agricultural Organization of the UN, Rome, http://www.fao.org/ag/agl/fertistat/index_en.htm.

FAO (2012). FAOSTAT Statistical Database. Rome: Food and Agricultural Organization of the UN.

Folberth, C., Yang, H., Wang, X. Y., and Abbaspour, K. C. (2012). Impact of input data resolution and extent of harvested areas on crop yield estimates in large-scale agricultural modeling for maize in the USA. *Ecological Modelling* **235**, 8-18.

Foti, R., Ramirez, J. A., and Brown, T. C. (2014). A probabilistic framework for assessing vulnerability to climate variability and change: the case of the US water supply system. *Climatic Change* **125**, 413-427.

Fraser, E. D. G., Simelton, E., Termansen, M., Gosling, S. N., and South, A. (2013). "Vulnerability hotspots": Integrating socio-economic and hydrological models to identify where cereal production may decline in the future due to climate change induced drought. *Agricultural and Forest Meteorology* **170**, 195-205.

Fussel, H. M., and Klein, R. J. T. (2006). Climate change vulnerability assessments: An evolution of conceptual thinking. *Climatic Change* **75**, 301-329.

Gaiser, T., de Barros, I., Sereke, F., and Lange, F. M. (2010). Validation and reliability of the EPIC model to simulate maize production in small-holder farming systems in tropical sub-humid West Africa and semi-arid Brazil. *Agriculture Ecosystems & Environment* **135**, 318-327.

HarvestChoice (2013). Minding the yield gap in Africa: a country-level analysis.

Hellmuth, M. E., Moorhead, A., Thomson, M. C., and Williams, J. (2007). Climate risk management in Africa: learning from practice. International Research Institute for Climate and Society (IRI), , Columbia University, NewYork, USA.

Iglesias, A., Garrote, L., Quiroga, S., and Moneo, M. (2012). A regional comparison of the effects of climate change on agricultural crops in Europe. *Climatic Change* **112**, 29-46.

IPCC (2007). Climate change 2007: impact adaptation and vulnerability, contribution of working Group II to the third assessment report of the introgovernmental panel on climate change In: Parry M.. et al, . intergovernmental Panel on Climate Change

IPCC (2013). Climate Change 2013: The Physical Science Basis. Contribution of Working Group I to the Fifth Assessment Report of the Intergovernmental Panel on Climate Change, United Kingdom and New York, 1535 pp.

Kamali, B., Abbaspour, K. C., Lehmann, A., Wehrli, B., and Yang, H. (2018). Uncertainty-based auto-calibration for crop yield – the EPIC^{+} procedure for a case study in Sub-Saharan Africa. *European Journal of Agronomy* **19**, 57–72.

Liu, J. G., Folberth, C., Yang, H., Rockstrom, J., Abbaspour, K., and Zehnder, A. J. B. (2013). A global and spatially explicit assessment of climate change impacts on crop production and consumptive water use. *Plos One* **8**.

Liu, J. G., Fritz, S., van Wesenbeeck, C. F. A., Fuchs, M., You, L. Z., Obersteiner, M., and Yang, H. (2008). A spatially explicit assessment of current and future hotspots of hunger in Sub-Saharan Africa in the context of global change. *Global and Planetary Change* **64**, 222-235.

Lloyd-Hughes, B., and Saunders, M. A. (2002). A drought climatology for Europe. *International Journal of Climatology* **22**, 1571-1592.

Lobell, D. B., and Burke, M. B. (2010). On the use of statistical models to predict crop yield responses to climate change. *Agricultural and Forest Meteorology* **150**, 1443-1452.

Luers, A. L., Lobell, D. B., Sklar, L. S., Addams, C. L., and Matson, P. A. (2003). A method for quantifying vulnerability, applied to the agricultural system of the Yaqui Valley, Mexico. *Global Environmental Change-Human and Policy Dimensions* **13**, 255-267.

Malcomb, D. W., Weaver, E. A., and Krakowka, A. R. (2014). Vulnerability modeling for Sub-Saharan Africa: An operationalized approach in Malawi. *Applied Geography* **48**, 17-30.

Masih, I., Maskey, S., Mussa. F. E. F., and P., T. (2014). A review of droughts in the African Continent: a geospatial and long-term perspective. *Hydrology and Earth System Sciences* **18**, 2679-2718.

McKee, T. B., Doesken, N. J., and kleist, J. (1993). The relationship of drought frequency and duration to time scales. *In* "In proceedings of the 8th Conference on Applied Climatology", pp. 179- 184.

Muller, C. (2011). Agriculture: Harvesting from uncertainties. *Nature Climate Change* **1**, 253-254.

Muller, C., Cramer, W., Hare, W. L., and Lotze-Campen, H. (2011). Climate change risks for African agriculture. *Proceedings of the National Academy of Sciences of the United States of America* **108**, 4313-4315.

Naumann, G., Barbosa, P., Garrote, L., Iglesias, A., and Vogt, J. (2014). Exploring drought vulnerability in Africa: An indicator based analysis to be used in early warning systems. *Hydrology and Earth System Sciences* **18**, 1591-1604.

Nelson, D. R., Adger, W. N., and Brown, K. (2007). Adaptation to environmental change: Contributions of a resilience framework. *Annual Review of Environment and Resources* **32**, 395-419.

O'Brien, K., Leichenko, R., Kelkar, U., Venema, H., Aandahl, G., Tompkins, H., Javed, A., Bhadwal, S., Barg, S., Nygaard, L., and West, J. (2004). Mapping vulnerability to multiple stressors: climate change and globalization in India. *Global Environmental Change-Human and Policy Dimensions* **14**, 303-313.

Parry, M., Canziani, O., Palutikof, J., van der Linden, P., and Hanson, C. (2007). Climate change 2007: impacts, adaptation and vulnerability, Cambridge University Press, Cambridge, UK,, 273–313.

Portmann, F. T., Siebert, S., and Doll, P. (2010). MIRCA2000-Global monthly irrigated and rainfed crop areas around the year 2000: A new high-resolution data set for agricultural and hydrological modeling. *Global Biogeochemical Cycles* **24**, 1-24.

Rashid, A., and Zejjari, M. (1997). FAO/WFP crop and food supply assessment mission to somali. *FAO special report*.

Roudier, P., Sultan, B., Quirion, P., and Berg, A. (2011). The impact of future climate change on West African crop yields: What does the recent literature say? *Global Environmental Change-Human and Policy Dimensions* **21**, 1073-1083.

Sacks, W. J., Deryng, D., Foley, J. A., and Ramankutty, N. (2010). Crop planting dates: An analysis of global patterns. *Global Ecology and Biogeography* **19**, 607-620.

Schlenker, W., and Lobell, D. B. (2010). Robust negative impacts of climate change on African agriculture. *Environmental Research Letters* **5**.

Shi, W. J., and Tao, F. L. (2014). Vulnerability of African maize yield to climate change and variability during 1961-2010. *Food Security* **6**, 471-481.

Singh, J., Knapp, H. V., and Demissie, M. (2004). Hydrologic modeling of the Iroquois river watershed using HSPF and SWAT. Illionois State Water Survey, Champaign, IL, USA.

Stephen, L., Zubeda, M., and Hugo, D. G. (2014). The use of improved maize varieties in Tanzania. *African Journal of Agricultural Research* **9**, 643-657.

Svoboda, M., LeComte, D., Hayes, M., Heim, R., Gleason, K., Angel, J., Rippey, B., Tinker, R., Palecki, M., Stooksbury, D., Miskus, D., and Stephens, S. (2002). The drought monitor. *Bulletin of the American Meteorological Society* **83**, 1181-1190.

Terence, E. E., James, D. F., and Shuaib, L. (2017). Projections of maize yield vulnerability to droughts and adaptation options in Uganda. *Land Use Policy* **65**, 154–163.

Turner, B. S., and Dumas, A. (2013). Vulnerability, diversity and scarcity: on universal rights. *Medicine Health Care and Philosophy* **16**, 663-670.
U.S. Geological Survey (2004). Global Digital Elevation Model (GTOPO30). (ESRI, ed.), Redlands, California, USA.
Wang, X., Williams, J. R., Gassman, P. W., Baffaut, C., Izaurralde, R. C., Jeong, J., and Kiniry, J. R. (2012). EPIC and APEX: model use, calibration, and validation. *Transaction of the ASABE* **55**, 1447-1462.
Weedon, G. P., Gomes, S., Viterbo, P., Shuttleworth, W. J., Blyth, E., Osterle, H., Adam, J. C., Bellouin, N., Boucher, O., and Best, M. (2011). Creation of the WATCH forcing data and its use to assess global and regional reference crop evaporation over land during the twentieth century. *Journal of Hydrometeorology* **12**, 823-848.
Wilby, R. L., and Wigley, T. M. L. (1997). Downscaling general circulation model output: a review of methods and limitations. *Progress in Physical Geography* **21**, 530-548.
Williams, J. R., Jones, C. A., Kiniry, J. R., and D.A., S. (1989). The EPIC crop growth model. *Transaction of the ASAE*, 497-454.
World Bank (2016). World Bank Open Data;http: //data.worldbank.org/indicator/SP.POP.TOTL. Washington, DC.
Xiong, W., Balkovic, J., van der Velde, M., Zhang, X. S., Izaurralde, R. C., Skalsky, R., Lin, E., Mueller, N., and Obersteiner, M. (2014). A calibration procedure to improve global rice yield simulations with EPIC. *Ecological Modelling* **273**, 128-139.
Zarafshani, K., Sharafi, L., Azadi, H., Hosseininia, G., De Maeyer, P., and Witlox, F. (2012). Drought vulnerability assessment: The case of wheat farmers in Western Iran. *Global and Planetary Change* **98-99**, 122-130.

4.7. Supplementary material

Defining *Z* as the difference between *DEI* and *CFI*, i.e. *Z=DEI-CFI*, Eq. 4.6 is written as:

$$CDVI = Pr[DEI - CFI < 0] = Pr[\frac{Z - \mu_Z}{\sigma_Z} < \frac{\mu_Z}{\sigma_Z}] \quad \text{(S4.1)}$$

where $\mu_Z = \mu_{DEI} - \mu_{CFI}$ and $\sigma_z = {\sigma_{DEI}}^2 + {\sigma_{CFI}}^2 - 2cov(DEI, CFI)$. Depending on whether CFI_{phy} or CFI_{soc} is used, the term *CDVI* is defined as $CDVI_{phy}$ or $CDVI_{soc}$. μ_{DEI}, μ_{CFI}, σ_{DEI}, σ_{CFI}, and $cov(DEI, CFI)$ are mean, standard deviation and covariance of *DEI* and *CFI* respectively. The total change in vulnerability (*dCDVI*) are then expressed as a function of the individual contributions of changes in μ_{DEI}, μ_{CFI}, σ_{DEI}, σ_{CFI}, and $cov(DEI, CFI)$ as follows:

$$dCDVI = \frac{\partial CDVI}{\partial \mu_{DEI}} d\mu_{DEI} + \frac{\partial CDVI}{\partial \mu_{CFI}} d\mu_{CFI} + \frac{\partial CDVI}{\partial \sigma_{DEI}} d\sigma_{DEI} + \frac{\partial CDVI}{\partial \sigma_{CFI}} d\sigma_{CFI} + \frac{\partial CDVI}{\partial cov(DEI, CFI)} dcov(DEI, CFI) \quad \text{(S4.2)}$$

In Eq. S4.2, each of the partial derivatives represents the sensitivity of the vulnerability to unit changes in each of the independent variables μ_{DEI}, μ_{CFI}, σ_{DEI}, σ_{CFI}, and $cov(DEI, CFI)$. Considering normal distribution for *Z*, we can rewritten Eq. S4.2 as:

$$CDVI = [2\pi{\sigma_Z}^2]^{-0.5} \int_{-\infty}^{0} e^{-\frac{(Z-\mu_Z)^2}{2\sigma_Z^2}} dz \quad \text{(S4.3)}$$

In the case of non-Gaussian Z, Eq. S4.3 corresponds to a First Order Second Moment approximation. Carrying out the integral of Eq. S4.3 yields:

$$CDVI = \frac{1}{2} + \frac{1}{2}\text{erf}[\frac{(-\mu_{DEI} + \mu_{CFI})}{\sqrt{2\sigma_Z^2}}] \quad \text{(S4.4)}$$

where erf() is the Gauss error function (also known as the probability integral).

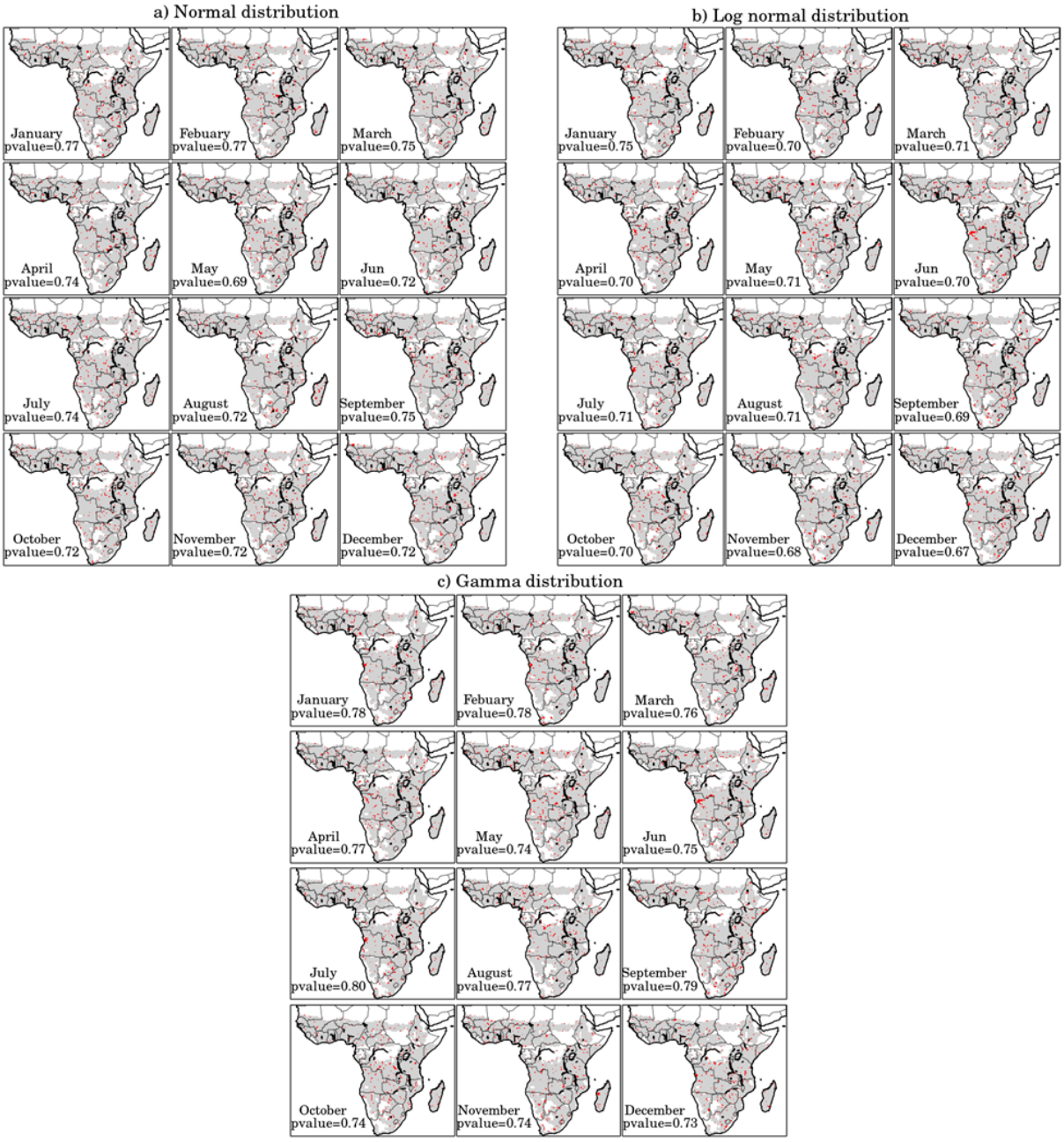

Figure S4.1. K-S test results for precipitation on monthly data using (a) normal, (b) Log normal, and (c) gamma distributions. Red shading indicates rejection of probability distribution function at the 5% significance level

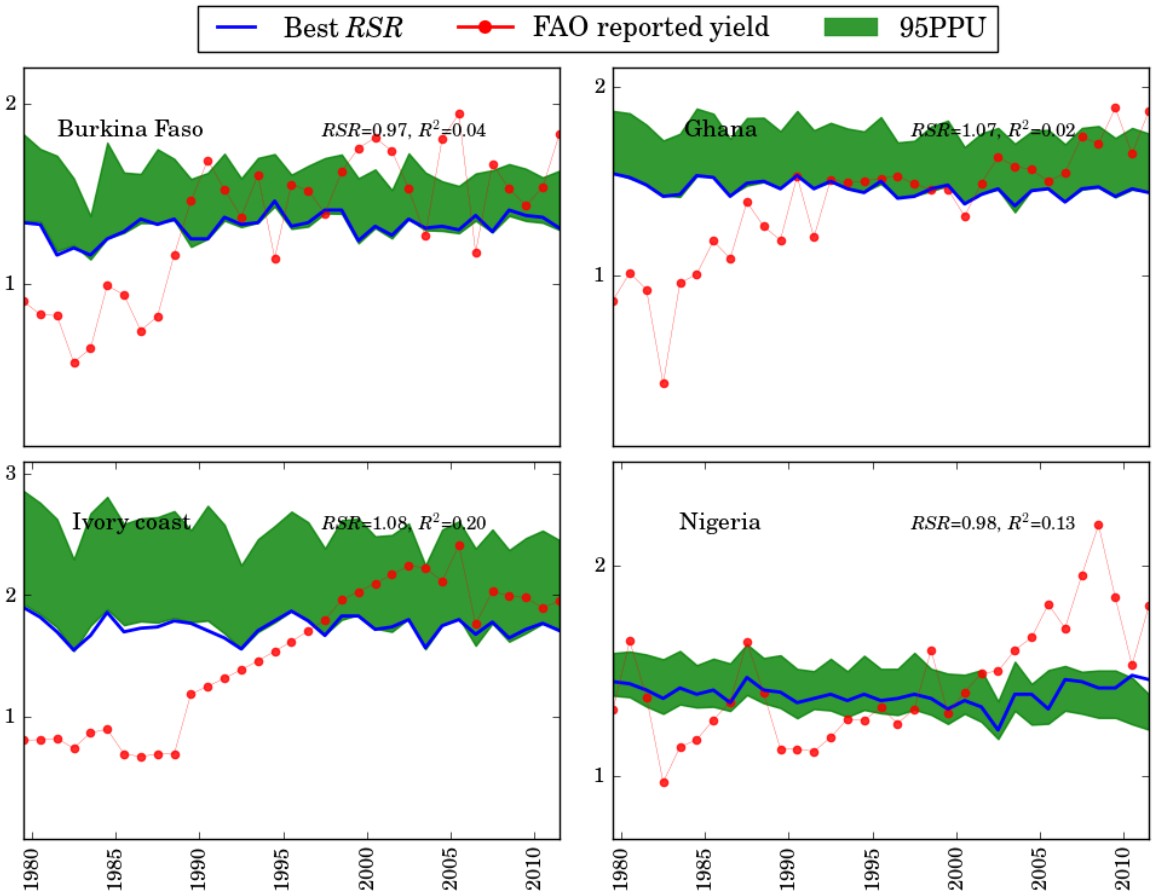

Figure S4.2. Comparison of the FAO reported (red line) and simulated maize yields expressed as 95PPU prediction uncertainty band (green bound) and the best simulation (blue line) in Burkina Faso, Ghana, Ivory coast, and Nigeria obtained from work by Kamali et al. (2018)

Chapter 5

A quantitative analysis of socio-economic determinants conferring crop drought vulnerability in Sub-Saharan Africa

Based on

A quantitative analysis of socio-economic determinants conferring crop drought vulnerability in Sub-Saharan Africa

Environmental Science and Policy, submitted

Authors

Bahareh Kamali[1,2 *], Karim C. Abbaspour[1], Bernhard Wehrli[2], Hong Yang[1,3]

[1] Eawag, Swiss Federal Institute of Aquatic Science and Technology, *Dübendorf*, Switzerland

[2] Institute of Biogeochemistry and Pollutant Dynamics, ETH Zurich, Switzerland

[3] Department of Environmental Sciences, University of Basel, Switzerland

Abstract

Drought events around the world have had significant impacts on agricultural production. Sub-Saharan Africa (SSA) is at the core of this threat, as agricultural production in most countries is rainfed and relies on precipitation. Socio-economic factors have tremendous influence on whether a farmer or a nation can adapt to these climate stressors. This study aims to examine the extents to which these factors affecting vulnerability to drought in SSA, using maize as a case study. In order to distinguish sensitive regions from resilient ones, we defined a crop drought vulnerability index (*CDVI*) calculated by comparing the actual recorded yield with the expected yield simulated by the Environmental Policy Integrated Climate (EPIC) model during 1990-2012. We then assessed the relationship between *CDVI* and potential socio-economic variables using the regression techniques. Key variables, which have significantly influence on *CDVI*. The results show that the level of fertilizer use is highly influential on vulnerability. In addition, countries with higher fertilizer application, human development index, and better infrastructure are more resilient to drought, thus have lower vulnerability. The role of government effectiveness was less apparent due to the generally low level and static status of the this variable across the SSA countries. We concluded that investing into infrastructure, improving fertilizer distribution and fostering economic development would all contribute to drought resilience amid the expected intensification of drought in terms of frequency and severity in the future.

5.1. Introduction

Current world population already reached seven billion and by 2050 is estimated to increase to nine billion with the largest increase concentrated in South Asia and Sub-Saharan Africa (SSA) (Lipper et al., 2014; United Nations, 2015). Meeting world's food demand requires doubling food production, which will dramatically increase the pressure on global agriculture resources (Foley et al., 2011). On the other hand, climate change and increased temperature have exacerbated the situation due to occurrence of many drought events around the globe with major impacts on agricultural production. As agriculture in most countries of SSA is mostly rainfed, the region is at the core of this thread. Achieving food security in SSA is an enormous challenge give the currently weak institutions, poor infrastructure and high social dependence on degraded natural resources (Webber et al., 2014). Therefore, it is essential to incorporate socio-economic aspects in mitigating drought vulnerability in SSA.

Drought is a natural disaster and the degree of its impacts is well recognized in terms of the magnitude of vulnerability. Various definitions have been proposed for vulnerability. The Intergovernmental Panel on Climate Change (IPCC) defined vulnerability as a function of exposure, sensitivity, and adaptive capacity (IPCC, 2014). The fifth IPCC assessment report focused on socio-economic aspects and prioritizing adaptation interventions. The adaptive capacity is the ability of a system to cope with the consequence of drought and represents the potential to implement measures that help reducing potential impacts (Adger, 2006). The quantification of adaptation capacity is a

challenge for two reasons. First, it is the latent property of a system and manifests only when the system is exposed to the shock (Williges et al., 2017). Second, it is space and time specific and therefore it is difficult to generalize a set of universal factors that enhance adaptive capacity in different regions over time.

Several studies attempted to incorporate adaptive capacity in the vulnerability assessment using different approaches such as aggregated quantitative indicators (Fraser et al., 2013; Simelton et al., 2012; Yeni and Alpas, 2017) or semi-structured interviews (Bahadur Kc et al., 2017; Blauhut et al., 2016; Bryan et al., 2015). Indicators of adaptive capacity have been also grounded in sustainable livelihood theory as proposed by Ellis (2000) which is based on different forms of assets to which people have access i.e. financial, human, resource, or physical assets. This approach calculates a composite index for each constituent asset. During the last two decades, many studies applied the sustainable livelihood concept in their analysis of vulnerability (Bryan et al., 2015; Huai, 2016; Keshavarz et al., 2017).

The use of indicators is one of the most common ways to define factors influencing vulnerability. Despite extensive research on these factors, improvement is required for identifying driving forces and choosing appropriate indicators to accurately determine the relationship between socio-economic factors and vulnerability (Vincent, 2007). A key question to answer is whether an improvement in a specific indicator can significantly reduce drought vulnerability. Detailed studies along these lines have been recently conducted at the European scale (Blauhut et al., 2015; Blauhut et al., 2016; Williges et al., 2017), Australia (Bryan et al., 2015; Huai, 2016, 2017), and in very limited cases at the global scale (Ericksen et al., 2011; Yeni and Alpas, 2017), but the issue has not been thoroughly addressed in SSA. Naumann et al. (2014) calculated composite indicators that reflect different aspects of vulnerability and adaptive capacity at Pan-African level. Their study, however, lacks an empirical and analytical framework that can clearly explain the direction and magnitude of effectiveness (or influence) of individual factors on vulnerability. This limitation impedes policy development to mitigate vulnerability. Several studies have used regression models to analyze the relationship between the socio-economic variables and crop drought vulnerability in some individual countries in SSA (Epule et al., 2017; Gbetibouo et al., 2010). However, these studies are case specific, and it is difficult to upscale their findings to the whole of SSA.

In assessing the factors influencing vulnerability to drought, most studies have conducted the investigation without considering the time series variations in different countries. Multivariable regression models used for these analyses often take the average situation of individual countries over a certain period. In reality, the level of vulnerability may be influenced by time and the severity of drought in different years. It is of importance to consider changes in vulnerability and factors influence it on temporal dimension. Nowadays, with increasing data availability even in developing countries, panel data analysis, referring to time series observations of a number of individual factors, provides

the larger basis for modeling the complexity of socio-economic factors influencing vulnerability than a single cross section or time series analysis (Hsiao, 2007). Such an analysis has not been conducted in the context of crop drought-vulnerability assessment in SSA.

In the literature, most studies quantifying the drought vulnerability are based on some kind of arithmetic aggregation of a number of representative components. Very few have quantified the drought vulnerability by comparing the expected crop yield under certain climate conditions with the actual recorded yield. The magnitude of the difference between modeled expectation and actual yield is an indicator for a country or region being 'sensitive' or 'resilient' to drought occurrence. Process-based crop models are effective tools to measure how yield changes in response to climate variability or drought. Linking the drought vulnerability defined as distance between the expected and actually recorded yield with socio-economic variables may therefore inform the choice of management options.

The aim of this study is to identify socio-economic variables contributing to drought-vulnerability of maize production in SSA. In order to develop a quantitative framework we will proceed by:

1) structuring a definition of Crop Drought Vulnerability Index (*CDVI*) obtained from linking simulated yield from a crop model to the country level recorded yield data;
2) cross-country comparison of adaptive capacity variables from economical, human, resource, infrastructure, and governmental categories in SSA;
3) applying multivariable panel data regression analyses to identify socio-economic variables influencing *CDVI* for maize;
4) discussing the implications of the results for mitigation of maize vulnerability to drought in SSA.

The study builds on previous methodological work (Chapter 2) and its application to identify and discuss the physical and climatic factors affecting drought vulnerability in SSA (Chapter 3 and 4).

5.2. Methodology

5.2.1. Site description

SSA is home to over one billion people with average annual precipitation of 795 mm yr^{-1} diversely distributing in different regions (Ward et al., 2016). Small landholders depend on rainfed agriculture as their primary livelihood source. Population increases and climate change have exacerbated the risk of hunger (Iglesias et al., 2011). Therefore, reducing crop vulnerability is essential for this region. Maize is the most widely grown crop and staple food in SSA (Folberth et al., 2014) and therefore represents a relevant case for this study. Since the last two decades, average maize yields in SSA have increased from around 1.4 to 1.8 t ha^{-1} with over 40% increase in South Africa, but are still at the very bottom of globally reported maize yields (FAO, 2012).

5.2.2. Quantifying drought exposure index

Drought exposure index, used in this study to separate drought from non-drought years, was obtained from the Standardized Precipitation Index (*SPI*). To obtain *SPI*, first a suitable cumulative probability distribution function (here Gamma distribution) (Bordi et al., 2001; Lloyd-Hughes and Saunders, 2002) is fitted to the precipitation. *SPI* is then obtained from applying the inverse normal function with mean 0 and standard deviation of 1 to the cumulative distribution function. Precipitation is obtained from grid level WFDEI (WATCH-Forcing-Data-ERA-Interim) meteorological forcing data (Weedon et al., 2011) aggregated to the national level using weighted areal average of maize cultivated lands (Portmann et al., 2010). The analysis was carried out for years 1990-2012. After transformation, 99.7% of data vary between -3 and 3. Negative values are representative of drought situations, whereas the positive values show non-drought cases (Table 5.1). The five classifications within this range i.e. [-3, 3] is defined as: wet, near normal, mild drought, moderate drought, and severe drought (Lloyd-Hughes and Saunders, 2002) (Table 5.1). We also tested the suitability of 1, 3, 6, 9, and 12 months' time scales. For each country, we selected the time scale with highest correlation with maize yield during growing season (see Chapter 2.3).

Table 5.1. Five categories of the Standardized Precipitation Index (*SPI*) selected to separate drought and non-drought(Lloyd-Hughes and Saunders, 2002)

category	*SPI* or *CDVI*
Wet	1.0 and more
Near normal	0.0 to 1.0
Mild	-1.0 to 0.0
Moderate	-1.5 to -1.0
Severe	-1.50 or less

5.2.3. Definition of Crop Drought Vulnerability Index (*CDVI*)

The vulnerability of a system is a function of its ability to respond to inherent stress variables. In this study, we specifically focus on maize vulnerability in response to the drought occurrences (drought exposure). The definition of maize *CDVI* followed the study by Bryan et al. (2015) in which *CDVI* was presented as the difference between the actual harvested yield and the expected yield. In our study, drought exposure is linked to vulnerability using a crop model, which simulates the impact of drought on maize yield. The yield simulated by a crop model reflects the influence of climate variability on crop production and therefore is representative of the expected yield (Y^{Exp}). The actual yield (Y^{Act}) is obtained from the reported yield at national level (FAO, 2010). Both, climate factors and socio-economic factors determine the recorded yield.

According to the above definition, if Y^{Act} is larger than Y^{Exp} (positive Y), then the region harvests a higher yield than expected meaning that it is resilient to the occurred climate condition and so the

vulnerability is low. However, in cases where Y^{Exp} is larger than Y^{Act} (negative *Y*), the maize production is sensitive to climate variability and consequently the vulnerability is high. The zero value of *Y* shows effective adaptation. For better spatial and temporal comparisons of *Y* across SSA, we normalized it using *Z-score* transformation (Potopová et al., 2015) calculated as:

$$CDVI_t = \frac{Y_t - Mean(Y)}{STD(Y)} \quad (5.1)$$

where Y_t is the yield residuals for year *t* i.e. $Y_t = Y_t^{Act} - Y_t^{Exp}$, $Mean(Y)$ and $STD(Y)$ are the mean and standard deviation of the yield residuals. Similarly and using this transformation, *CDVI* can be classified into five classes as shown in Table 5.1.

We obtained Y^{Exp} from yields simulated in the EPIC (Environmental Policy Integrated Climate) model (Williams et al., 1989). EPIC is a field-scale crop model designed to simulate the different processes of farming systems as well as their interactions using data such as weather, soil, land use, crop management parameters (Williams et al., 1989). EPIC operates on a daily time step and is capable of simulating crop growth under various climate and environment conditions, as well as complex management schemes. Further information on EPIC crop-related processes is given in Williams et al. (1989). In order to extend the EPIC application to larger scales, we developed a spatially explicit EPIC interface (hereafter EPIC^{+}) programmed in Python, which executes EPIC on each grid cell at the spatial resolution of 0.5° and aggregates the results to any desired scale (Liu et al., 2016) (See Chapter 2).

5.2.4. Selecting socio-economic variables relating to *CDVI*

To select the variables influencing *CDVI*, we used the following step-wise approach:

1) Candidate socio-economic variables were collected as recommended by Brooks et al. (2005) and Naumann et al. (2014). The two studies together introduced over 50 socio-economic variables that might be important for climate vulnerability assessments at the national scale. We selected 17 variables that were specifically relevant for drought vulnerability and had data available for more than 50% of the studied period (1990-2012). The list of variables, their definition, and the sources of data are provided in Table 5.2. The year 1990 was selected as the starting point. After that date, the relevant socio-economic data were available in most SSA countries. To fill the missing values of the remaining variables, we used the spline interpolation procedure applied also by Simelton et al. (2012). For some variables such as fertilizer use temporal variability was missing for several consecutive years. In these cases we used the average of years with available data. For convenience, we classified these variables into five categories as: economic, human, resource, infrastructure, and governance (Table 5.2).

2) The variables were expressed in a variety of statistical units, ranges or scales. They were transformed into a uniform dimension to avoid problems in mixing measurement units. We use the *Z-score* transformation as the normalization technique calculated as the ratio of the residual of the variable and its mean divided by the standard deviation as (Damm, 2009):

$$Nvariable_{t,i} = \frac{variable_{t,i} - Mean(variable_i)}{STD(variable_i)} \quad (5.2)$$

Where $Mean(variable_i)$ and $STD(variable_i)$ are the mean and standard deviation of variable *i* (*i*=1,2,…17) in year *t*. Eq. 5.2 converts all variables to a common scale with an average of 0 and standard deviation of 1. It is also consistent with the standardized scale of *CDVI*. For those variables such as *Interest payment* (Table 5.2), which are negatively correlated to *CDVI*, the inverse of values were used (i.e. 1/variable) in normalization. We did not transform variables of the governance category as they were already normalized during their development procedure (Kaufmann et al., 2010).

3) The influence of 'multicollinearity' is an important issue in regression models which can seriously distort the interpretation of a model (Tu et al., 2005). This is related to situations when predictors are correlated not just to the response variable, but also to each other. Therefore, some factors will be redundant. To avoid the redundancy of variables, a bivariate correlation matrix was constructed between *Nvariable*s of each category. This helped us to evaluate the strength and direction of the linear relationships between the variables (Damm, 2009). The statistically most significant variables were selected and the rest was removed from further assessment.

4) The selected variables of each country were averaged to obtain an aggregated value for the economic, human, resource, infrastructure, and governance categories. This facilitated the spatial comparison of selected aspects and provided insights into the adaptive capacity of different countries.

5) Statistical regression models were constructed to analyze the role of selected variables in Step 3 for characterizing *CDVI* (see next section for details).

Table 5.2. Potential socio-economic variables influencing drought vulnerability and their definitions

Category	Variable	Definition	Unit
Economic	*GDP/capita*	Gross domestic product	US$/capita per year
	Interest payment	Interest payments on external debt	% GNI
	GNI	Gross national income	US$/capita per year
	Agriculture GDP	Agriculture GDP	% GDP in total GDP
Human	*HDI*	Human development index	ratio ranging from 0 to 1
	Health expenditure	Health expenditure per capita	US$/capita
	Maternal mortality	Maternal mortality ratio	per 100,000 live births
	Calorie intake	Calorie intake per capita per day	Calorie per capita per day
	Food production index	food crops that are edible and contain nutrients excluding coffee and tea. (average of 2004-2006 equals 100)	ratio of each year to the base period (2004-2006)
Resource	*Agricultural area*	per capita land area that is either arable, under permanent crops, or under permanent pastures	ha/capita
	Fertilizer use	Nitrogen fertilizer use tons per hectare	tons/ha per year
Infrastructure	*Water access*	% of population with access to improved drinking water source	percentage
	Electricity access	% of rural population with access to electricity	percentage
Governance	*Control of corruption*	The extent to which public power is exercised for private gain, including both petty and grand forms of corruption, as well as "capture" of the state by elites and private interests	normalized values ranging from -2.5 to 2.5
	Government effectiveness	The quality of public and civil service, policy formulation and implementation, the degree of its independence to political pressures, the credibility of the government's commitment to policies	normalized values ranging from -2.5 to 2.5
	Political stability	The likelihood that the government will be destabilized or overthrown by unconstitutional or violent means	normalized values ranging from -2.5 to 2.5
	Voice & accountability	The extent to which a country's citizens are able to participate in selecting their government, freedom of expression, freedom of association, and a free media	normalized values ranging from -2.5 to 2.5

Sources: The variables in the first four categories were obtained from the World bank (http://www.worldbank.org/). The variables for the governance category were obtained from Kaufmann et al. (2010) and can be downloaded from www.govindicators.org

5.2.5. Linking *CDVI* and socio-economic variables using regression models

Two model formulations were constructed and their results were compared to get some insights into the influence of temporal dimension on explanatory models. In both models, the socio-economic variables selected in Step 3 were considered as explanatory variables and *CDVI* as dependent variable. The first model (Model I) does not take into account temporal variability of explanatory and dependent variables. Only the average of explanatory and dependent variables were included. The aim of this model is to check if the temporally aggregated (variables during drought years) can explain the relation between socio-economic conditions and maize vulnerability. Model I is expressed as

$$\text{Model I: } \overline{CDVI_i} = \alpha_0 + \beta \bar{x}_i + \varepsilon_i \tag{5.3}$$

Where $\overline{CDVI_i}$ and $\bar{x}$ stand for the average of *CDVI* and selected socio-economic variables for country i during drought years, α_0 is a constant intercept term, and β is a vector of coefficient for each explanatory variable and ε_i is the error term.

Model II takes into account the temporal dimension of socio-economic factors using the panel data statistical regression method. We compared the widely used fixed-effect and random-effect techniques to analyze panel data. The formulation for Model II is expressed as:

$$\text{Model II: } CDVI_{i,t} = \begin{cases} \alpha_0 + \beta x_{i,t} + \varepsilon_{i,t} & if\ fixed-effect\ model\ is\ applied \\ \alpha_0 + \beta x_{i,t} + \varepsilon_{i,t} + u_i & if\ random-effect\ model\ is\ applied \end{cases} \tag{5.4}$$

where $CDVI_{i,t}$ is the dependent variable at time t for entity (country) i, x stands for socio-economic variables selected, u_i is the random term. In this study, *country* was added as random factor in the random-effect model. Models were fitted with all socio-economic variables. The model was simplified by comparing versions with and without a certain explanatory term using Likelihood Ratio Tests. In each step, we removed insignificant terms until all remaining factors are significant at 1%, 5% or 10% levels. MATLAB was used as the software for implementing the statistical regression models.

5.3. Results

5.3.1. Temporal and spatial patterns of *CDVI*

The spatial and temporal distribution of yearly drought exposure during 1990 and 2012 based on *SPI* showed many drought events in all SSA countries with higher severity from 1990 to 1996 compared to the period 2000-2012 (Figure 5.1). Between 1990 to 1995, almost all countries experienced drought events. The most severe intensity occurred in 1992 in Southern Africa, in Central Africa during 1994-1995, and in Western Africa in 1990. From 1996 to 2012, less severe drought

events were recorded. The severe droughts were only observed in Western African countries in 2002 and in Eastern African countries in 2004. Other countries mostly experienced mild to moderate droughts (Figure 5.1).

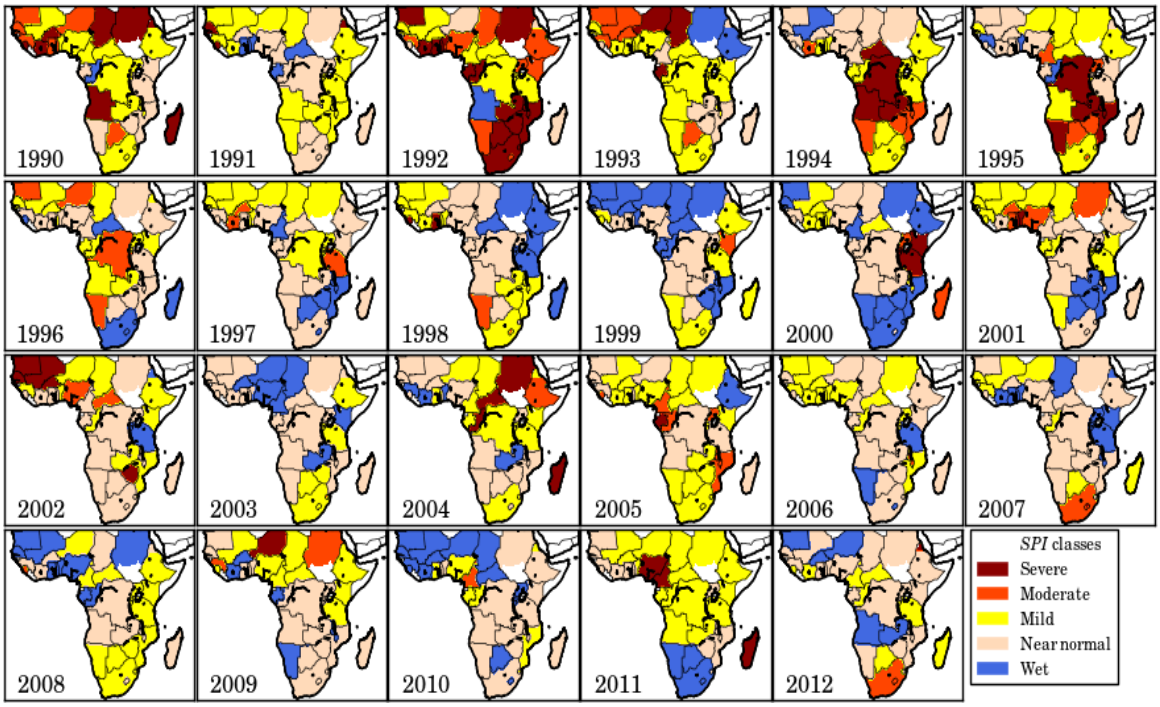

Figure 5.1. Country level spatial distribution of yearly *SPI* (Standardized Precipitation Index) during 1990-2012; the classifications are in accordance to Table 5.1.

CDVI calculated based on the difference between actual and expected yield identified sensitive and resilient countries during 1990 and 2012 (Figure 5.2). The expected yield was obtained from the crop model, which was only reflecting climate-induced production. By contrast, the recorded harvest yields was influenced by many socio-economic variables. Sensitive cases or high vulnerability had negative *CDVI*, whereas resilient cases with low vulnerability exhibited positive values. The yearly national level *CDVIs* showed many severe to moderate intensity of vulnerability during 1990-2012.

During 1990-2012, *CDVI* showed similar temporal trends as *SPI*. Both indices showed higher vulnerability and drought exposure during 1990-1999 as compared to 2000-2012. However, the two indices displayed different pictures in terms of severity revealing that different countries had varying resiliency during drought. The Sothern African countries were less affected by extreme *CDVI* especially after 2000, indicating higher resiliency of these regions. For example, the moderate drought in 2012 in South Africa (Figure 5.1) did not cause the same level of vulnerability (Figure 5.2). The 2011 drought occurred in most SSA countries (Figure 5.1) had different vulnerabilities across countries affected by the drought (Figure 5.2). An opposite situation occurred in 1999 where a wet condition resulted in moderate vulnerabilities in Western Africa.

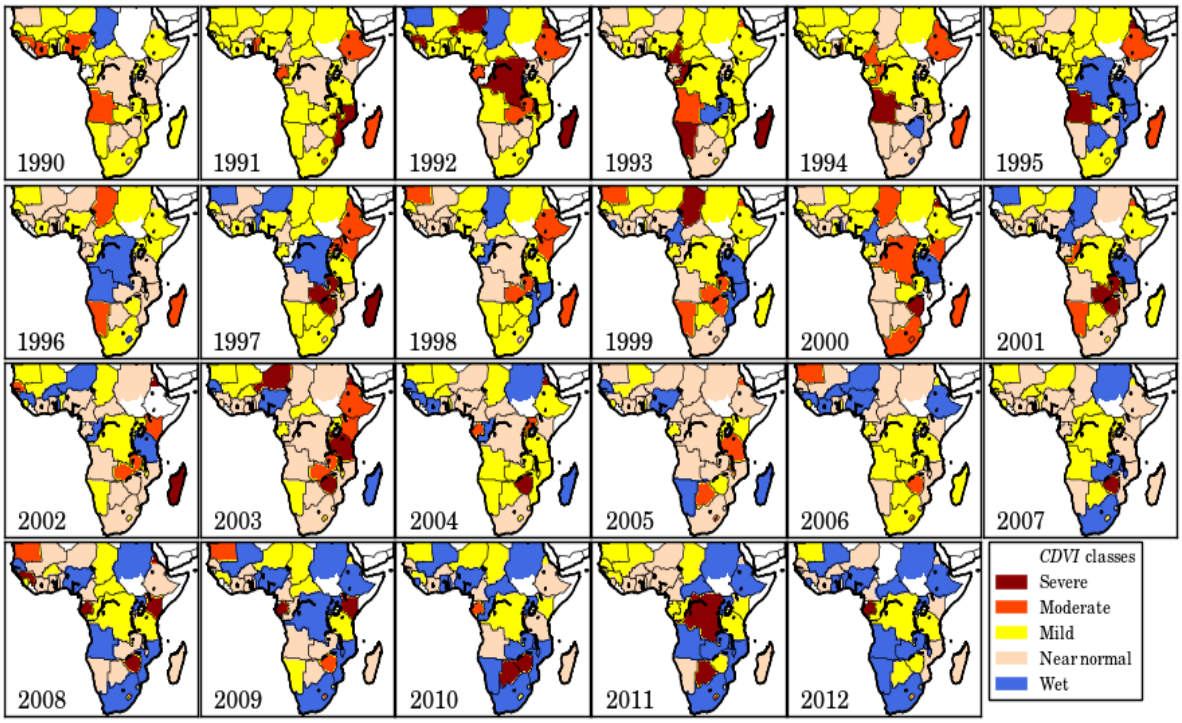

Figure 5.2. Country level spatial distribution of yearly *CDVI* (Crop Drought Vulnerability Index) calculated based on the difference between the actual and expected yields. The classifications are defined in Table 5.1.

Overall, Southern African countries, Kenya, Tanzania, and Ethiopia from Eastern Africa, and Mali, Niger, Nigeria, Botswana, Chad and Central African Republic were more exposed to severe droughts whereas Central African countries, Madagascar experienced less severe droughts due to occurrence of higher rainfall (Figure 5.3a). On the other hand, *CDVI* showed a different picture as South Africa, Botswana, Mozambique, Nigeria, and Cameroon were less vulnerable (Figure 5.3b). The severity of vulnerability was lower than the severity of drought in countries such as Kenya, Tanzania, and Mali.

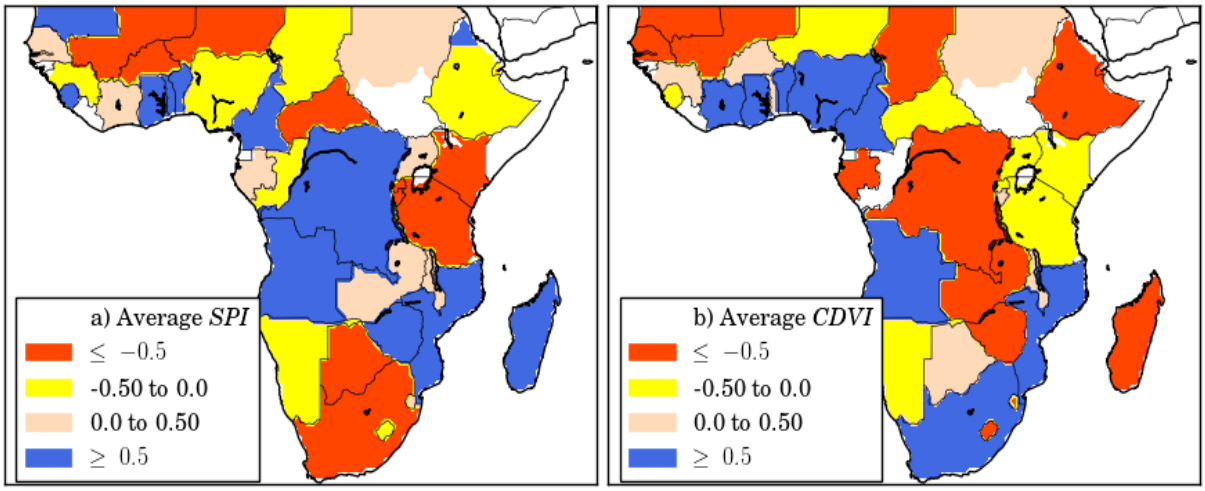

Figure 5.3. Country level comparison of a) average *SPI* and b) average *CDVI* during 1990 to 2012.

5.3.2. Socio-economic factors influencing *CDVI*

The bivariate correlation coefficient values between normalized variables were calculated to identify variables that are significantly correlated to each other (Step 3). In the economic category, the highest correlation coefficient was found between *GDP/capita* and *Interest payment* with a value of 0.64, between *GDP/capita* and *GNI* with 0.83, and between *Interest payment* and *GNI* with 0.59 (Figure S5.1). This shows that the three variables have similar effect. Therefore, we selected *GDP/capita* and *Agricultural GDP* as the final variables from the economic category.

In the human category, the correlation coefficient between the pairwise variables showed high correlation values between variables (Figure S5.2). For example, the correlation coefficient between *HDI* and *Health expenditure* is 0.84 and between *Calorie intake* and *Food production index* is 0.73 (Figure S5.2). *HDI* was selected as the most representative variable, since it is a composite statistic of life expectancy, education, and per capita income and encompasses a more general aspect of human development. Besides, *Food production index* was selected due to the significant correlation with other variables. It was also an indicator for of human nutrition status and representative of health aspects (definition in Table 5.2). While *HDI* and *Food production index* were also correlated, we select both at this step and check the suitability of one or both for the regression model. We retained all variables in the resource and infrastructure categories due to their importance. Similarly, the correlation coefficient between pairwise four variables of the governance category showed values larger than 0.75 (Figure S5.3). As explained by Kaufmann et al. (2010) (Table 5.2), *Government effectiveness* is a more general indicator and encompasses political, rules, and regulatory aspects. Therefore, it was selected as the representative variable of this category.

Table 5.3. The 9 socio-economic variables in the five categories (economic, human, resource, infrastructure, and governance) selected after the pairwise correlation analysis (Step 3)

Category	Variable	5^{th}, 50^{th}, 95^{th} percentiles			
		Eastern SSA	Southern SSA	Central SSA	Western SSA
Economic	GDP/capita	177, 330, 700	696, 3025, 4455	224, 911, 6060	253, 551, 924
	Agriculture GDP	16, 36, 50	3.4, 8, 11.6	7.2, 23.2, 52.3	6.7, 34, 48.5
Human	HDI	0.3, 0.39, 0.48	0.46, 0.6, 0.9	0.3, 0.4, 0.6	0.26, 0.39, 0.49
	Food production index	82, 93, 101	89,95,103	87, 90, 108	82, 88, 97
resource	Agricultural area	0.23,0.99,3.4	0.53, 3.2,5.8	1.1, 2.2, 21	0.43, 0.88, 12.3
	Fertilizer use	1.7, 5.7, 34	3.1, 7.8, 58	0.35, 3.5, 8.9	0.62, 7.8, 31
Infrastructure	Water resource access	32, 55, 78	54, 79, 95	45, 63, 84.6	44,63, 83
	Electricity access	0.9, 2.6, 16	2.0, 17, 47	1,13, 31	1, 8.2, 25
Governance	Government effectiveness	-1.4, -0.7, -0.4	-0.7, 0.2, 0.6	-1.8, -1.2, -0.6	-1.3,-0.8, -0.1

Overall, from the 17 initially selected variables, only 9 variables remained. As shown in Table 5.3, the absolute values of these variables vary significantly from one region to the other. For example, variables such *GDP/capita, HDI, Fertilizer use* are significantly larger in Southern SSA in terms of 5^{th}, 50^{th}, 95^{th} percentiles. *Agricultural GDP* is significantly larger in Central Africa, while variables such as *Food production index* show approximately similar percentiles in the four SSA regions (Table 5.3).

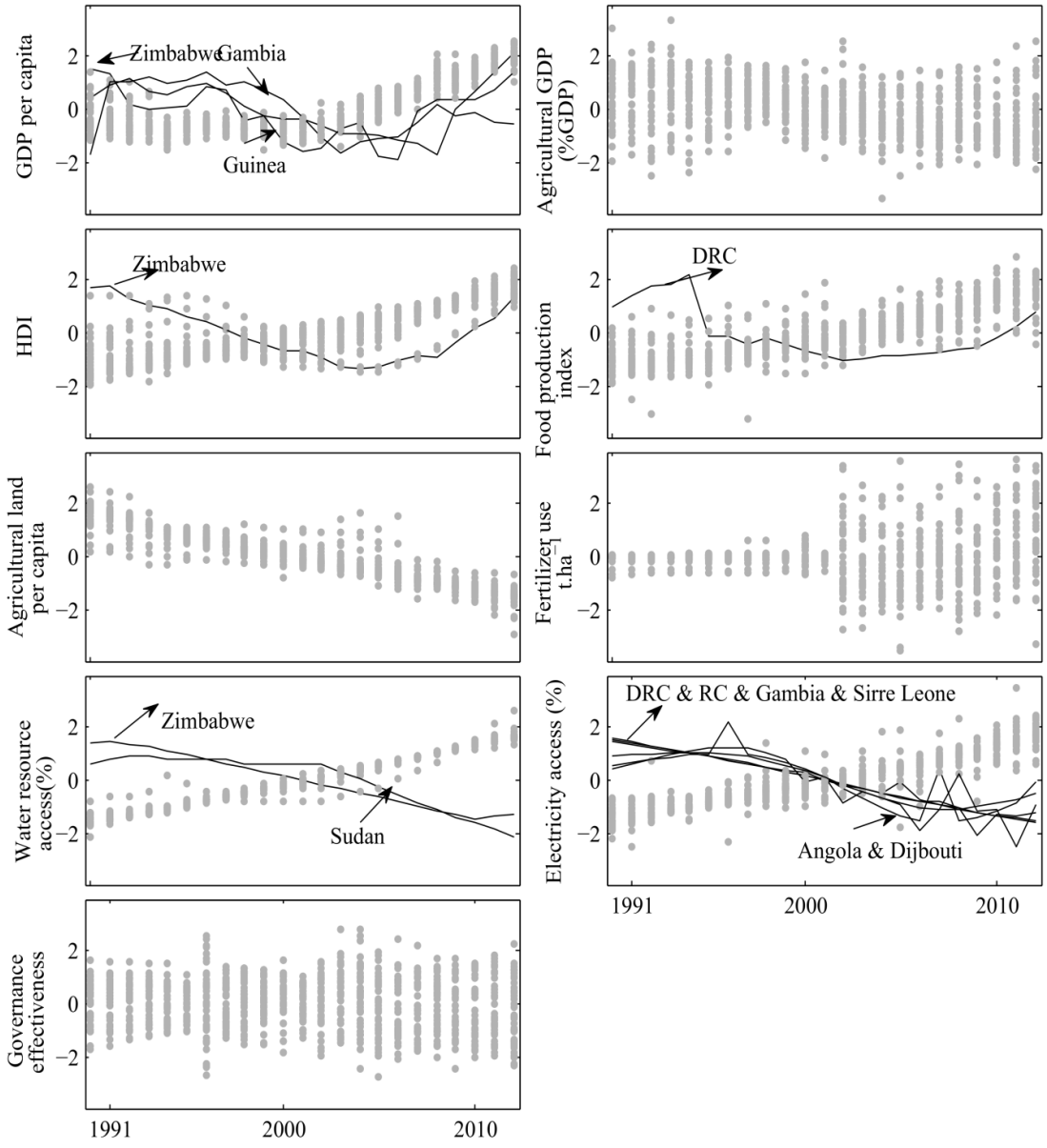

Figure 5.4. Temporal variability of 9 selected socio-economic variables during 1990 and 2012; the variables are normalized using *Z-score* in SSA (DRC: Democratic Republic of Congo)

The temporal variability of 9 selected normalized variables showed various patterns for different variables and countries. Regarding *GDP/capita*, almost all SSA countries, except Zimbabwe, Gambia, and Guinea showed an increasing trend with a rather steep slope after 2000 (Figure 5.4). *Agricultural*

GDP exhibited different temporal variability across different countries. Both *HDI* and *Food production index* show increasing trends all over SSA with the exception of Zimbabwe (see *HDI*) and Democratic Republic of Congo (see *Food production index*). As the temporal variability of *Fertilizer use* for years 1990-2000 was not available, we used the average of the period 2001-2012. In the case of the two infrastructure variables, *Water resource access* showed similar trends and values in all countries except Zimbabwe and Sudan, but *Electricity access* was more variable across countries. Concerning *Government effectiveness*, the large variability between countries masked any temporal trends (Figure 5.4).

To see the spatial variability of selected socio-economic variables across countries in each category, we aggregated variables of each category into one indicator by calculating the average of their normalized values (Step 4). In all five categories, Southern African countries had higher values (higher adaptive capacity) in terms of the respective variables. In the economic category (Figure 5.5a), Western and Eastern SSA showed approximately similar low values. Other countries like Zimbabwe, Zambia, and Angola were placed between the highest and lowest with aggregated values between -0.35 and 0. The human aspect showed lowest values in Ethiopia, Angola, Niger, and Mali followed by most Western African countries such as Angola and Namibia (Figure 5.5b). In the resource category, mostly Central Africa showed lowest values (between -0.85 and -0.35) (Figure 5.5c). The infrastructure exhibited a different picture with mostly low values for most Central and Eastern African countries (Figure 5.5d). All SSA countries showed very poor capacity in terms of Governance with the exception of Botswana and South Africa (Figure 5.5e).

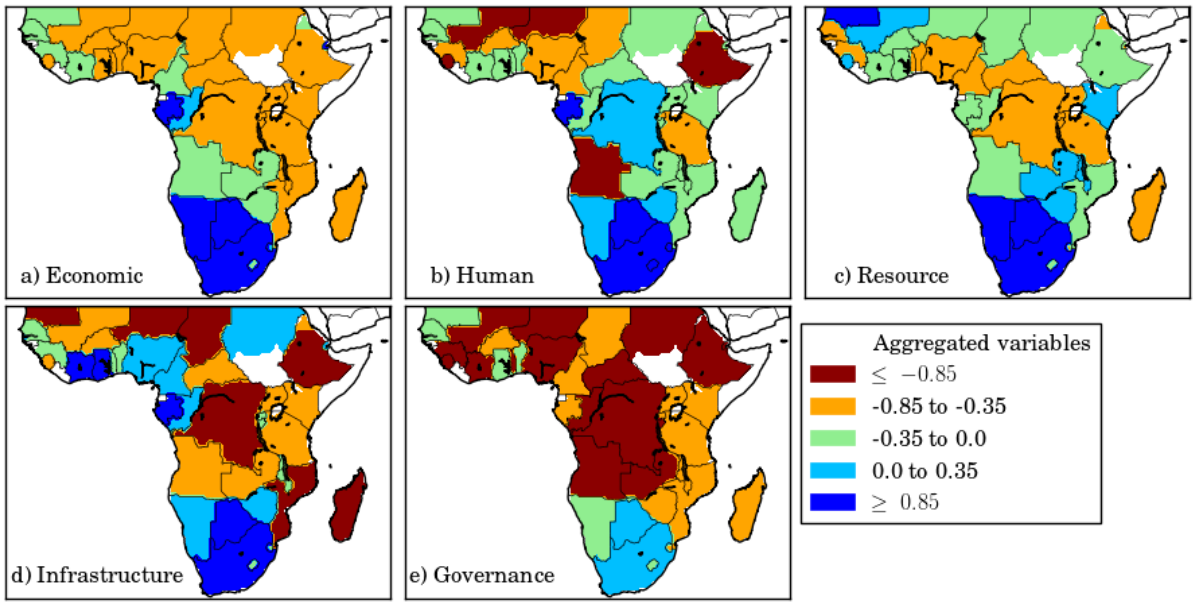

Figure 5.5. The spatial variability of aggregated indicators in five categories: a) economic, b) human, c) resource, d) infrastructure, e) governance obtained from the average of selected normalized socio-economic variables in each category.

5.3.3. Relations between time-invariant socio-economic variables and *CDVI*

We calculated the average of 9 selected socio-economic variables (as explanatory variables) and *CDVI* (as dependent variables) during drought years (*SPI*<0) (Step 5). All variables were fixed at this step and a multiple regression model was constructed (Model I) to check the suitability of mean independent and dependent variables for model explanation, and then to determine which of the 9 selected socio-economic variables can explain vulnerability of maize to drought. All variables were initially included in Model I. The model was then simplified by excluding those variables that were not significant at the 1%, 5%, or 10% levels and had no influence on the R^2 values. We continued this procedure until all remaining variables were significant at the 1%, 5%, or 10% levels. The relatively low R^2 value of 0.30 (Table 5.4) indicates that the time-invariant model is probably not sufficient. Of the 9 variables, only three including *Agricultural GDP, Food production index* , and *Electricity access* were identified as statistically significant variables, for reducing the vulnerability to drought. The highest β value for *Agricultural GDP* with value of -0.72 indicated that the factor was the most influential for reducing vulnerability followed by *Electricity access* (β=0.34) and *Food production index* (β=0.32).

Table 5.4. The time-invariant socio-economic factors influencing maize drought vulnerability obtained from Model I. The average of socio-economic variables and *CDVI* were used in the analysis. Only variables that were significant at 1%, 5%, or 10% levels were included in the model. The empty rows (-) pertain to those that were not significant (*SE*: standard error).

Model I: Fixed effect model using mean of 11 selected variables: R^2=0.30

Variable	*β*	*SE*	*t-stat*	*P-values*
Intercept	-0.01	0.1	0.01	0.9
GDP/capita	-	-	-	-
Agriculture GDP	-0.72	0.25	-2.87	**0.007**
HDI	-	-	-	-
Food production index	0.32	0.16	1.99	**0.050**
Agricultural land	-	-	-	-
Fertilizer use (t/ha)	-	-	-	-
Water resource access	-	-	-	-
Electricity access	0.34	0.18	1.90	**0.055**
Government effectiveness	-	-	-	-

5.3.4. Assessing relations between time-variant socio-economic variables and *CDVI*

The temporal variability of socio-economic variables (as explanatory variables) and *CDVI* (as dependent variables) were considered during 1980-2012. Since variables have both time and

individual (country) dimensions, panel data regression models were carried out. We tested and compared two different models. In the first model (Model IIa), variables during drought and non-drought years (1980-2012) were included, while in the second model (Model IIb), only drought years were included. The main reason for comparing these two models was to check whether influential factors differ depending on climate stress. Besides, drought has long term effect and the influence of some factors might be revealed in non-drought years. We also performed a preliminary analysis to test the suitability of the fixed-effect and random-effect models in the panel-data regression analysis and noticed significant outperformance when *country* was added as a random effect in the model, emphasizing the importance of considering probable random differences between countries on the intercept of the model (Table 5.5).

We started with variables in the economic category i.e. *GDP/capita* and *Agricultural GDP* and then added variables of other categories one by one to first check if their inclusion will improve the performance of the model and to test whether the added variable is a significant explanatory factor. The comparison was based on the Likelihood Ratio Test. The results show significant improvement as the R^2 values are 0.63 in Model IIa and 0.60 in Model IIb (Table 5.5) over that from Model I. Model IIa slightly outperformed Model IIb. The *SE* values of the socio-economic variables were slightly lower compared to Model I in Table 5.4. This indicates that Model II is promising to identify factors that are important to reduce maize vulnerability to drought. Including temporal variability of indicators is critical to better characterize the effects of socio-economic factors on vulnerability mitigation.

Comparison of influential variables of Model I with Model II shows that more factors were significant for vulnerability in Model II. Apart from the three significant variables of Model I, *HDI*, *Agricultural land* , and *Fertilizer use* were significant in Model IIa and Model IIb at 1%, 5%, or 10% levels. *Government effectiveness* was only significant in Model IIa. Besides, the influential factors of Model I, *Agriculture GDP*, *Food production index*, and *Electricity access*, were significant at 1% level (higher confidence), indicating their importance for vulnerability mitigation. All other variables were significant at 5% level. In both Model IIa and Model IIb, *Food production index* and *Electricity access* showed higher β values.

Comparison of Model IIa with Model IIb showed that *Government effectiveness* was only statistically significant in Model IIa when all years were included. The β value for *Fertilizer use* was slightly higher in Model IIb compared with Model IIa, indicating that as drought was occurring, the influence of fertilizer application was becoming more important as an adaptation strategy. Besides, the β values of the human category i.e. *HDI* and *Food production index* were slightly higher, suggesting that their influence might be more important during drought (Table 5.3). The two variables of *GDP/capita*, and *Water resource access* were not significant in the three models.

Table 5.5. The time-variant socio-economic factors influencing maize drought vulnerability obtained from the random-effect panel data regression model (Model II). The time series of socio-economic variables were used in the analysis. Only variables that were significant at 1%, 5%, or 10% levels were included in the model. The empty rows (-) pertain to those that were not significant (*SE*: standard error).

Model IIa: Random-effect regression model based on including drought and non-drought years: R^2=0.63				
Variable	*β*	*SE*	*t-stat*	*P-values*
Intercept	-2.007	0.385	-5.2	<**0.001**
GDP/capita	-	-	-	-
Agriculture GDP	-0.31	0.052	6.13	<**0.001**
HDI	0.15	0.058	2.69	**0.007**
Food production index	1.75	0.194	9.29	<**0.001**
Agricultural land	0.099	0.047	2.08	**0.037**
Fertilizer use	0.055	0.03	1.71	**0.067**
Water resource access	-	-	-	-
Electricity access	1.962	0.329	5.94	<**0.001**
Government effectiveness	0.176	0.067	2.90	**0.0038**
Model IIb: Random-effect regression model based on only including drought years: R^2=0.60				
Variable	*β*	*SE*	*t-stat*	*P-values*
Intercept	-2.02	0.408	-4.96	<**0.001**
GDP/capita	-	-	-	-
Agriculture GDP	-0.23	0.072	3.05	**0.02**
HDI	0.14	0.059	-2.02	**0.04**
Food production index	1.82	0.273	6.604	<**0.001**
Agricultural land	0.14	0.064	2.14	**0.03**
Fertilizer use	0.10	0.045	1.95	**0.050**
Water resource access	-	-	-	-
Electricity access	1.89	0.49	3.77	<**0.001**
Government effectiveness	-	-	-	-

5.4. Discussion

5.4.1. Changes in crop drought vulnerability

This study assessed the relationship between maize drought vulnerability and socio-economic variables influencing vulnerability at the national level of SSA during 1990-2012. We identified those socio-economic factors that predispose an area's maize harvest to be resilient or sensitive to drought. The residuals of simulated yield in the EPIC crop model and observed yield were identified as a

prominent indicator to resilient and sensitive with regard to drought vulnerability as the simulated yield can better reflect the dynamic of climate on rainfed maize production in SSA. This is advantageous over many other studies where the expected yields were calculated by implementing de-trending methods such as third or fourth order auto-regression modeling (Potopová et al., 2015; Simelton et al., 2012), as such de-tending procedure does not reflect the accurate influence of climate variability on yield.

The overall patterns resemble the insights that different countries exposed to different levels of drought are coping differently with the occurring drought. An interesting finding of our study is that maize vulnerability to drought has become less serious recent years. For example, while the drought exposure is higher in Eastern and Southern African countries due to lower amounts of rainfall occurring in these regions after 2000, the vulnerability of maize production is declining. This corroborates the results of Naumann et al. (2014) where these regions were less vulnerable. It suggests that there might be generic socio-economic factors that help mitigating vulnerability in different regions. We should emphasize that our analysis excluded extreme drought events occurred in late 1980s over whole SSA. Including this period might significantly improve the assessment of changes in *CDVI* and factors influencing the trend. However, since most socio-economic variables were not available prior to the 1990s, this period was not included, which is a limitation of this study.

5.4.2. Major factors influencing drought vulnerability

We constructed 17 potential socio-economic variables influencing maize drought vulnerability and classified them into five categories as economic, human, resource, infrastructure, governance. This classification helps disclosing different aspects of adaptive capacities and the relevant potential for reducing vulnerability. While this classification is not ideal and some indicators may fall in more than one category, it gives more details on adaptive capacity of different aspects. We also mapped the spatial and temporal dynamic of selected variables. Out of 17 variables, 9 remained after the collinearity analysis from which between 3-7 variables were significant in the regression models. The following conclusion can be drawn for the variables in each of the five categories:

Economic category: *GDP/capita* was not a statistically significant factor. This is probably because the definition of *HDI* already encompass the economic status of a country. *Agricultural GDP*, as a more specific variable for agriculture, was associated with high vulnerability of maize in all models (Model I, Model IIa, and Model IIb) at 1% or 5% levels. The negative sign of β coefficient indicates that the large share of the. *Agricultural GDP* in total GDP can have significant effect for reducing the ability to cope with drought effect. A strong economy secures the system by facilitating implementation of coping strategies against environmental risk and drought exposure. It also provides possibility to higher investment in weather forecasting, which may help farmers to be prepared for

drought. A weak economy, often represented by the large share of agricultural sector in GDP, has the opposite effect (Patt and Gwata, 2002; Simelton et al., 2012; Vincent, 2007).

Human category: *Food production index* was identified as a statistically significant factor in both time-variant and time-invariant models with relatively high positive β coefficient. The index is a measure of food nutritional status which is consistent with the situation in SSA where maize is one of the staple crops and its vulnerability can significantly influence human health status in Africa. It is also representative of economic conditions of a country. The effect of *HDI* in reducing vulnerability is apparent when time-variant factors were included. This suggest that more investment on increasing life expectancy and education (as components of *HDI*) will be helpful to reduce vulnerability. Bahadur Kc et al. (2017) also showed that increasing *HDI* can result in an additional 6.8 million tons of maize production at global level and the increase is more remarkable for developing countries such as Africa.

Resource category: Three variables were representative of system's natural resources from which only *Agricultural land* and *Fertilizer use* had significant roles. Both variables displayed more influential roles during drought periods (higher β coefficients in Model IIa and Model IIb). This suggests that fertilizer is increasingly used to mitigate the impact of drought on maize. The lower β coefficient of *Fertilizer use* compared to variables in other category might be related to missing values for the period 1990-2000 when most significant droughts occurred. The models used the average of 2001-2012 to substitute the missing data. Obtaining more accurate values for fertilizer application in SSA will help to better understand the potential benefits. The statistical significance of *Agricultural land* warns that population growth together with limited land resources will be a significant threat for maize-based food security in the future.

Infrastructure category: *Water resource access* showed no statistical significance in all models. This might be due to the temporal variation of this variable in Figure 5.4 which shows only a linear increasing trend with no significant variability across countries and inter-annually. By contrast, *Electricity access* with more regional variability (Figure 5.4) and with high β coefficients in all models is a better candidate.

Governance category: *Governance effectiveness* was also identified as key factor for reducing vulnerability in Model IIa. As mentioned by Keshavarz and Karami (2013), adaptation at government level can help creating a set of effective, long-term plans and policies which may enhance the capacity to develop, revise, and execute drought policies. The variable was less significant in Model IIb because of using constant values for the period 1990-1995 (due to missing data) when extreme drought occurred. No significant variability was noticed in the variable *Governance effectiveness* during drought years.

5.4.3. Comparison of models explaining the relationship between *CDVI* and socio-economic variables

We tested the suitability of time-variant and time-invariant variables and concluded that including the temporal dimension of variables was necessary for the determination of socio-economic factors influencing drought. Drought is a time dependent phenomenon and is characterized by climate conditions for a certain period. Panel data regression was a method of choice to evaluate socio-economic variables. As socio-economic variables differ significantly from one year to another, aggregating the severity of multiple drought years by calculating their average disguises the influence that a specific socio-economic variable might have in a certain year. Implementing panel data results in a more accurate inference of model parameters as these models usually have more degrees of freedom and more sample variability.

We also compared the performance of the fixed-effect and random-effect models in panel data analysis using time-variant explanatory and independent variables. The results showed significant improvement in model performance when the *country* was added as a random effect. The major reason is that the fixed-effect model assesses only the net effect of the predictors (explanatory variable) on the outcome (dependent variable). Random effect takes into account the variation across country and is more suitable when the difference across countries have some influence on our dependent variable. The spatial maps of socio-economic factors in the five categories (Figure 5.5) indicate the *country* should be included as random effect to take into account the difference between countries on overall intercept.

5.4.4. Limitation and conclusion of the study

Overall, our results underline the suitability of regression models for identifying how socio-economic factors influence the way that drought affected maize production between 1990- 2012 in SSA. Despite the usefulness, some limitations to the data used in this study call for caution in the interpretation and further empirical efforts to improve data quality. Our spatial scale lacks detail at the sub-national level, as socio-economic data and maize yield were reported at national level. As also mentioned by Conway and Schipper (2011); Simelton et al. (2009), regional or gridded data could identify which regions contribute most to national food insecurity. The World Bank databases reporting country level data were the only available sources with time series of socio-economic variables.

There are also some other factors such as pest or disease that might have resulted in harvest loss and therefore increasing crop drought vulnerability. However, we did not have access to these types of crop failure data. Such levels of information will depend on farm-level surveys. Another limitation is that the selected explanatory variables are not crop specific or even agriculture specific. Other factors

such as heat or cold spells might have influenced crop vulnerability. However, such specifications demand more work at the farm scale, which takes into account other drivers of vulnerability.

In conclusion, the current study was a preliminary but novel effort in identifying influential socio-economic factors on drought vulnerability across SSA. The results and the approaches developed can be used as a baseline study for further attempts to analyze crop drought vulnerability and its mitigation. As the quality and resolution of the data improves, a better understanding of the interaction of variables and their effects on drought vulnerability will be achieved.

5.5. Reference

Adger, W. N. (2006). Vulnerability. *Global Environmental Change-Human and Policy Dimensions* **16**, 268-281.

Bahadur Kc, K., Legwegoh, A. F., Therien, A., Fraser, E. D. G., and Antwi-Agyei, P. (2017). Food price, food security and dietary diversity: A comparative study of urban Cameroon and Ghana. *Journal of International Development*.

Blauhut, V., Gudmundsson, L., and Stahl, K. (2015). Towards pan-European drought risk maps: quantifying the link between drought indices and reported drought impacts. *Environmental Research Letters* **10**, 1-9.

Blauhut, V., Stahl, K., Stagge, J. H., Tallaksen, L. M., De Stefano, L., and Vogt, J. (2016). Estimating drought risk across Europe from reported drought impacts, drought indices, and vulnerability factors. *Hydrology and Earth System Sciences* **20**, 2779-2800.

Bordi, I., Frigio, S., Parenti, P., Speranza, A., and Sutera, A. (2001). The analysis of the Standardized Precipitation Index in the Mediterranean area: large-scale patterns. *Annali Di Geofisica* **44**, 965-978.

Brooks, N., Adger, W. N., and Kelly, P. M. (2005). The determinants of vulnerability and adaptive capacity at the national level and the implications for adaptation. *Global Environmental Change-Human and Policy Dimensions* **15**, 151-163.

Bryan, B. A., Huai, J., Connor, J., Gao, L., King, D., Kandulu, J., and Zhao, G. (2015). What actually confers adaptive capacity? Insights from agro-climatic vulnerability of Australian wheat. *Plos One* **10**.

Conway, D., and Schipper, E. L. F. (2011). Adaptation to climate change in Africa: Challenges and opportunities identified from Ethiopia. *Global Environmental Change-Human and Policy Dimensions* **21**, 227-237.

Damm, M. (2009). Mapping Social-Ecological Vulnerability to Flooding-A sub-national approach for Germany, Bonn, Rheinischen Friedrich-Wilhelms-Universität.

Ellis, F. (2000). The determinants of rural livelihood diversification in developing countries. *Journal of Agricultural Economics* **51**, 289-302.

Epule, T. E., Ford, J. D., and Lwasa, S. (2017). Projections of maize yield vulnerability to droughts and adaptation options in Uganda. *Land Use Policy* **65**, 154-163.

Ericksen, P., Thornton, P., Notenbaert, A., Cramer, L., Jones, P., and Herrero, M. (2011). Mapping hotspots of climate change and food insecurity in the global tropics.

FAO (2010). FAOSTAT statistical database. Food and Agricultural Organization of the UN, Rome.

FAO (2012). FAOSTAT Statistical Database. Rome: Food and Agricultural Organization of the UN.

Folberth, C., Yang, H., Gaiser, T., Liu, J. G., Wang, X. Y., Williams, J., and Schulin, R. (2014). Effects of ecological and conventional agricultural intensification practices on maize yields in Sub-Saharan Africa under potential climate change. *Environmental Research Letters* **9**, 1-12.

Foley, J. A., Ramankutty, N., Brauman, K. A., Cassidy, E. S., Gerber, J. S., Johnston, M., Mueller, N. D., O'Connell, C., Ray, D. K., West, P. C., Balzer, C., Bennett, E. M., Carpenter, S. R., Hill, J., Monfreda, C., Polasky, S., Rockstrom, J., Sheehan, J., Siebert, S., Tilman, D., and Zaks, D. P. M. (2011). Solutions for a cultivated planet. *Nature* **478**, 337-342.

Fraser, E. D. G., Simelton, E., Termansen, M., Gosling, S. N., and South, A. (2013). "Vulnerability hotspots": Integrating socio-economic and hydrological models to identify where cereal production may decline in the future due to climate change induced drought. *Agricultural and Forest Meteorology* **170**, 195-205.

Gbetibouo, G. A., Ringler, C., and Hassan, R. (2010). Vulnerability of the South African farming sector to climate change and variability: An indicator approach. *Natural Resources Forum* **34**, 175-187.

Hsiao, C. (2007). Panel data analysis - advantages and challenges. *Test* **16**, 1-22.

Huai, J. J. (2016). Integration and typologies of vulnerability to climate change: A case study from Australian wheat sheep zones. *Scientific Reports* **6**.

Huai, J. J. (2017). Dynamics of resilience of wheat to drought in Australia from 1991-2010. *Scientific Reports* **7**.

Iglesias, A., Quiroga, S., and Diz, A. (2011). Looking into the future of agriculture in a changing climate. *European Review of Agricultural Economics* **38**, 427-447.

IPCC (2014). Climate Change 2014: Impacts, Adaptation, and Vulnerability.

Kaufmann, D., Kraay, A., and Mastruzzi, M. (2010). The Worldwide Governance Indicators: Methodology and Analytical Issues.

Keshavarz, M., and Karami, E. (2013). Institutional adaptation to drought: The case of Fars Agricultural Organization. *Journal of Environmental Management* **127**, 61-68.

Keshavarz, M., Maleksaeidi, H., and Karami, E. (2017). Livelihood vulnerability to drought: A case of rural Iran. *International Journal of Disaster Risk Reduction* **21**, 223-230.

Lipper, L., Thornton, P., Campbell, B. M., Baedeker, T., Braimoh, A., Bwalya, M., Caron, P., Cattaneo, A., Garrity, D., Henry, K., Hottle, R., Jackson, L., Jarvis, A., Kossam, F., Mann, W., McCarthy, N., Meybeck, A., Neufeldt, H., Remington, T., Sen, P. T., Sessa, R., Shula, R., Tibu, A., and Torquebiau, E. F. (2014). Climate-smart agriculture for food security. *Nature Climate Change* **4**, 1068-1072.

Liu, W., Yang, H., Folberth, C., Wang, X., Luo, Q., and Schulin, R. (2016). Global investigation of impacts of PET methods on simulating crop-water relations for maize. *Agricultural and Forest Meteorology* **221**, 164–175.

Lloyd-Hughes, B., and Saunders, M. A. (2002). A drought climatology for Europe. *International Journal of Climatology* **22**, 1571-1592.

Naumann, G., Barbosa, P., Garrote, L., Iglesias, A., and Vogt, J. (2014). Exploring drought vulnerability in Africa: An indicator based analysis to be used in early warning systems. *Hydrology and Earth System Sciences* **18**, 1591-1604.

Patt, A., and Gwata, C. (2002). Effective seasonal climate forecast applications: examining constraints for subsistence farmers in Zimbabwe. *Global Environmental Change-Human and Policy Dimensions* **12**, 185-195.

Portmann, F. T., Siebert, S., and Doll, P. (2010). MIRCA2000-Global monthly irrigated and rainfed crop areas around the year 2000: A new high-resolution data set for agricultural and hydrological modeling. *Global Biogeochemical Cycles* **24**, 1-24.

Potopová, V., Boroneanț, C., Boincean, B., and Soukup, J. (2015). Impact of agricultural drought on main crop yields in the Republic of Moldova. *International Journal of Climatology*.

Simelton, E., Fraser, E. D. G., Termansen, M., Benton, T. G., Gosling, S. N., South, A., Arnell, N. W., Challinor, A. J., Dougill, A. J., and Forster, P. M. (2012). The socioeconomics of food crop production and climate change vulnerability: A global scale quantitative analysis of how grain crops are sensitive to drought. *Food Security* **4**, 163-179.

Simelton, E., Fraser, E. D. G., Termansen, M., Forster, P. M., and Dougill, A. J. (2009). Typologies of crop-drought vulnerability: an empirical analysis of the socio-economic factors that influence the sensitivity and resilience to drought of three major food crops in China (1961-2001). *Environmental Science & Policy* **12**, 438-452.

Tu, Y. K., Kellett, M., Clerehugh, V., and Gilthorpe, M. S. (2005). Problems of correlations between explanatory variables in multiple regression analyses in the dental literature. *British Dental Journal* **199**, 457-461.

United Nations (2015). World Population Prospects: The 2015 Revision, Key Findings and Advance Tables. Department of Economic and Social Affairs, Population Division.

Vincent, K. (2007). Uncertainty in adaptive capacity and the importance of scale. *Global Environmental Change-Human and Policy Dimensions* **17**, 12-24.

Ward, C. S., Torquebiau, R., and Xie, H. (2016). improved agricultural water management for Africa's Washington, D.C. .

Webber, H., Gaiser, T., and Ewert, F. (2014). What role can crop models play in supporting climate change adaptation decisions to enhance food security in Sub-Saharan Africa? *Agricultural Systems* **127**, 161-177.

Weedon, G. P., Gomes, S., Viterbo, P., Shuttleworth, W. J., Blyth, E., Osterle, H., Adam, J. C., Bellouin, N., Boucher, O., and Best, M. (2011). Creation of the WATCH forcing data and its use to assess global and regional reference crop evaporation over land during the twentieth century. *Journal of Hydrometeorology* **12**, 823-848.

Williams, J. R., Jones, C. A., Kiniry, J. R., and D.A., S. (1989). The EPIC crop growth model. *Transaction of the ASAE*, 497-454.

Williges, K., Mechler, R., Bowyer, P., and Balkovic, J. (2017). Towards an assessment of adaptive capacity of the European agricultural sector to droughts. *Climate Services* **7**, 47–63.

Yeni, F., and Alpas, H. (2017). Vulnerability of global food production to extreme climatic events. *Food Research International* **96**, 27-39.

5.6. Supplementary material

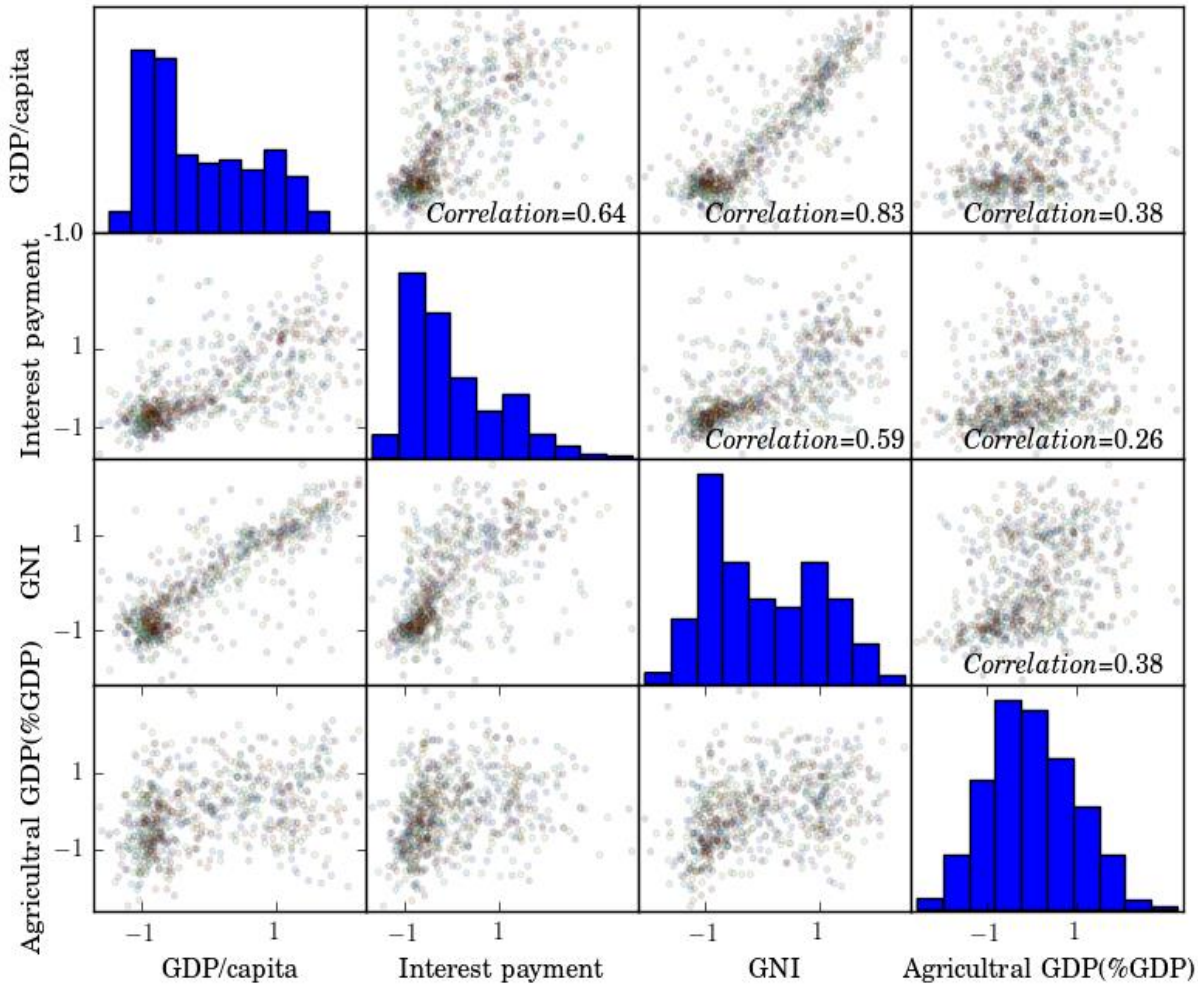

Figure S5.1. The visual representation of scatter plots generating correlation coefficient between normalized variabls of the economic category

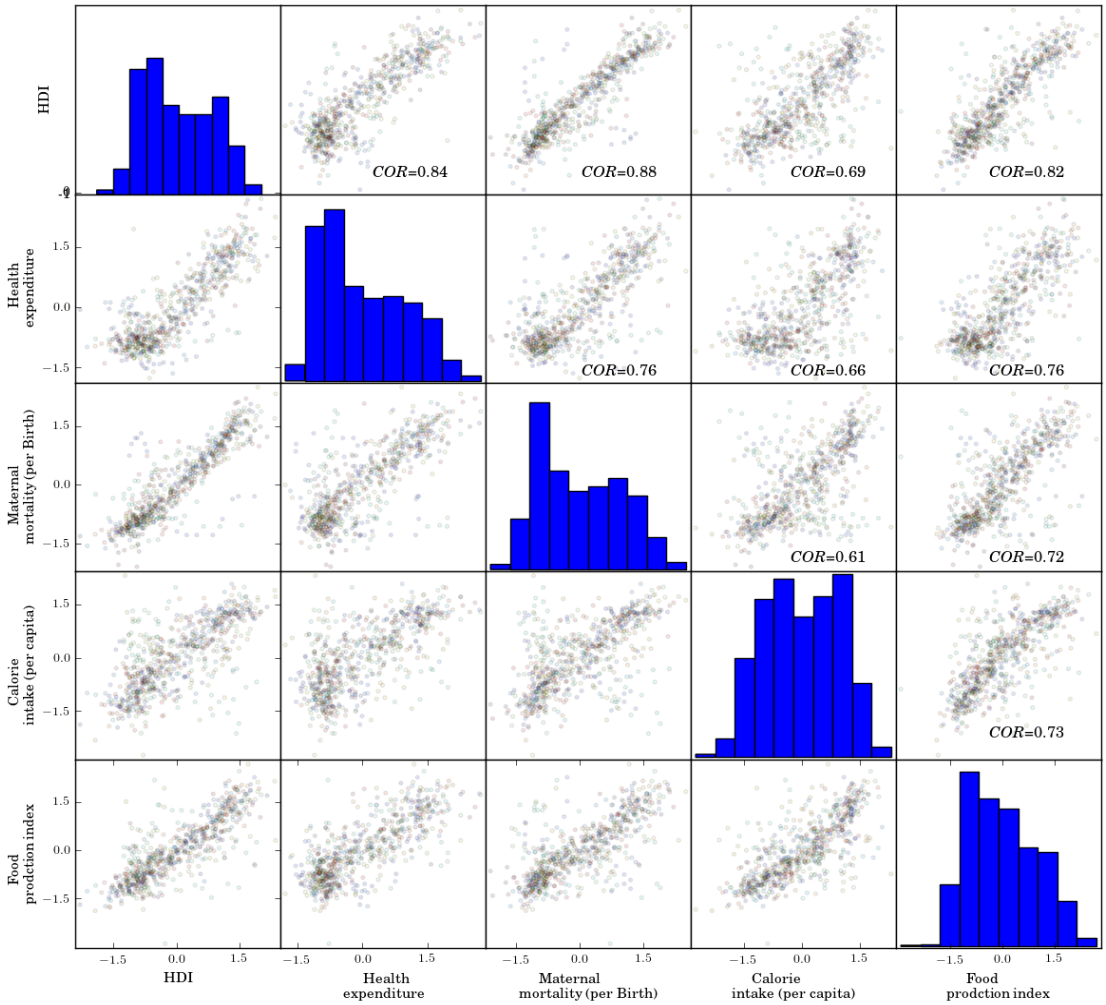

Figure S5.2. The visual representation of scatter plots generating correlation coefficient between normalized variables of the human category

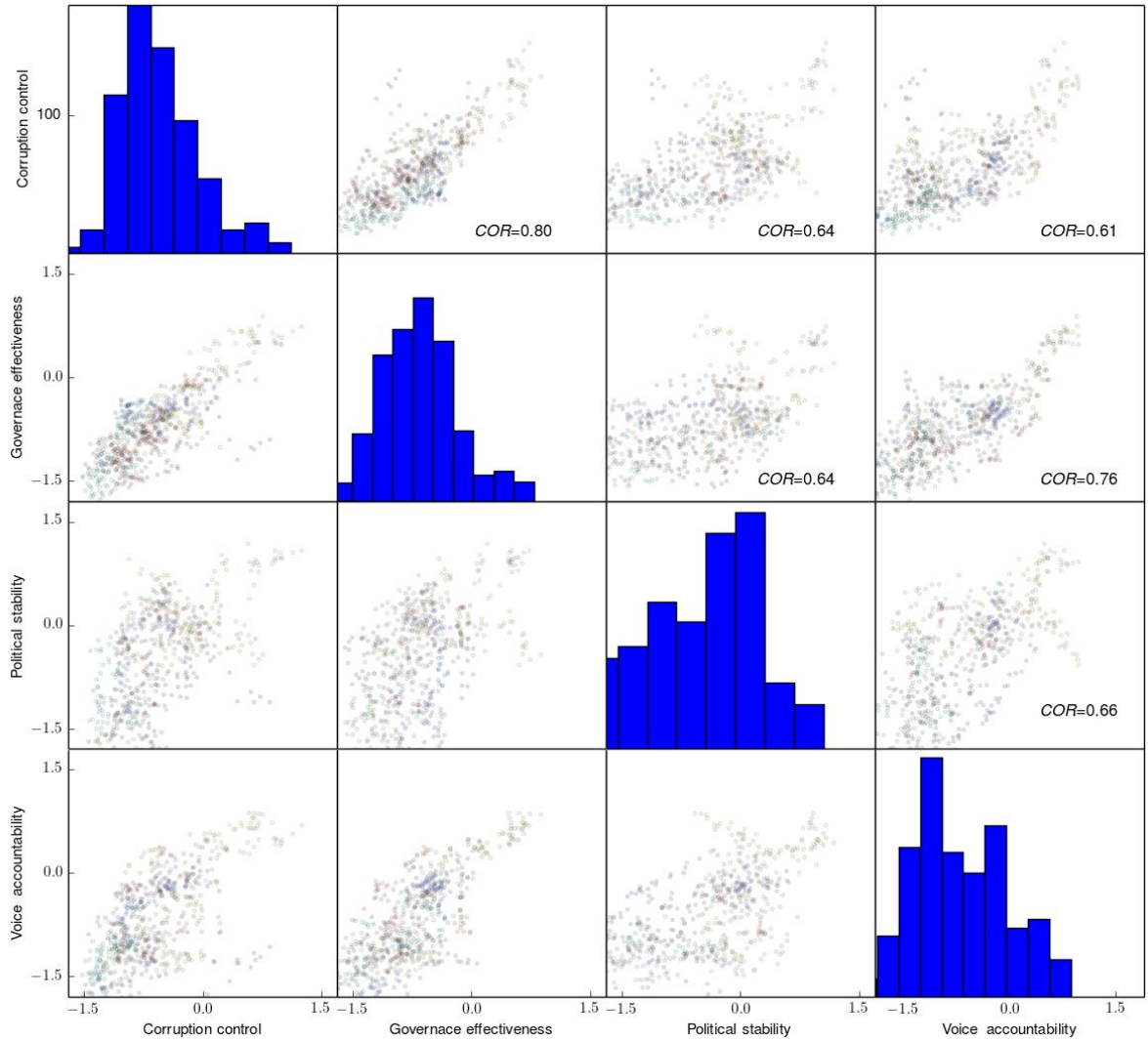

Figure S5.3. The visual representation of scatter plots generating correlation coefficient between normalized proxies of the governance category

Chapter 6

General conclusion and outlook

6.1. General conclusion

The goal of this study was to apply a specially explicit crop model to assess the impact of historic drought on crop yield in SSA and to quantify the physical and socio-economic crop drought vulnerability. With this aim, we developed a grid-based EPIC^{+} model programmed in Python to simulate crop yield under given climate and agronomic conditions with rigorous procedures for calibration and uncertainty analysis. Besides, we identified model parameters at the country level, instead of the continental level as commonly seen in previous studies. The output of the model provided a basis to quantify the biophysical and socio-economic crop drought-vulnerability indices. Finally, the regression techniques were applied to determine the key socio-economic factors, which make one region resilient or sensitive against drought occurrence.

EPIC^{+} was tested to assure that it replicates maize yield during historic periods and captures the inter-annual maize yield variability in relation to climate anomaly. For the first time, we calibrated the EPIC crop model against observed maize yield over entire SSA for a time-span longer than 3 decades (33 years from 1980 to 2012) and estimated a separate parameter set for each individual country. Such detailed calibration is particularly important for drought-vulnerability assessment, since drought is a time-dependent phenomenon and it is necessary to capture temporal variability over long periods. Apart from the model performance, which was satisfactory compared to literature, for the first time we enhanced the reliability of grid-based maps of planting date by adjusting their grid values between the earliest and latest planting dates. The produced maps depicted more spatial heterogeneity within each country. We also obtained a better estimation of parameters related to agricultural operations such as fertilizer application rate or PHU, so that, their values become more representative for entire studied years. We finally measured the uncertainty associated with the Crop and Model parameters through achieving the best compromise between *P-factor* and *R-factor* as the two key criteria of the SUFI-2 technique. Overall, the estimated values of parameters are particularly important for projecting future impacts of drought on crop yield and their values can be used as a base for many studies, Additionally, the developed EPIC^{+} model can be utilized on any application at any scale.

Having simulated maize yield at grid level, we quantified maize biophysical drought vulnerability for each grid through the relative change of crop failure in relation to change in drought exposure. Our proposed methodology for measuring vulnerability and its two components i.e. *DEI* and *CFI* had two specific and unique features, which made the study novel compared to the literature. First, both *DEI* and *CFI* were defined according to the same probability framework, therefore, their values varied within the same ranges i.e. [0, 1] and a certain value of *DEI* or *CFI* showed the same severity of crop failure or drought exposure. This facilitated not only the inter-comparison of two components, but also the spatial comparison of different grids regarding *DEI* or *CFI*. Second, after relating *DEI* to *CFI* in a power function, we classified vulnerability into five levels based on the shape of a power function. This was a significant new achievement in measuring the degree of the crop drought vulnerability. Overall, we found that Southern African countries and some regions of Sahelian strip are highly vulnerable to drought due to experiencing more water stress, whereas vulnerability in Central African countries pertains to temperature stresses.

An important feature of drought is that its impacts are not the same in all regions and times. Sometimes a small drought has a major effect on agricultural production whereas a large drought might not trigger a serious crop failure. Therefore, in reality factors beyond physical variables (stemming from climate anomaly) influence the severity of vulnerability (called socio-economic vulnerability). Measuring the difference between biophysical and socio-economic vulnerability ($CDVI_{phy}$ and $CDVI_{soc}$ respectively) was the core of the analysis. We defined *DEI* with the same procedure previously explained. Two different *CFI*s were used for defining $CDVI_{phy}$ and $CDVI_{soc}$. The comparison of the two vulnerability maps showed that socio-economic vulnerability was larger than physical vulnerability in all SSA countries revealing that SSA experienced more vulnerability than what is physically expected. The distance between $CDVI_{phy}$ and $CDVI_{soc}$ was large in countries like Ivory Coast, Benin, Mali, Zimbabwe, and Madagascar. In contrast, South Africa, Botswana, and Nigeria with a lower degree of $CDVI_{soc}$ were identified as drought-resilient countries, with smaller distance. Overall, Southern and partially Central Africa are more vulnerable to physical drought as compared to other regions. Central and Western Africa, however, are socially highly vulnerable.

Having quantified the distance between physical and socio-economic vulnerability, in the last part of this study, we identified the socio-economic factors making countries in SSA resilient or sensitive to droughts. For the first time, we implemented the panel data regression analysis to take into account "temporal" together with *country* dimensions in the regression model. The finding of the analysis led us to propose a series of socio-economic factors being important for mitigating maize vulnerability to drought. We found that human development index and infrastructure play key roles in adaptation to occurring droughts. In addition, we also identified *agricultural GDP*, *Fertilizer rate* and G*overnment effectiveness* as factors explaining the differences in *CDVI* across regions and over time.

6.2. Limitations

Based on the available data, the constructed EPIC$^+$ model was calibrated as thoroughly as possible. However, the calibration procedure was restricted by the lack of some input data and also spatially observed maize yield data required for reducing the uncertainty in crop modeling. For example, we did not have records on temporal values of fertilizer application (or more specifically nitrogen) or rainfed cultivated area. As the fertilizer application values were only available at country level the same value was defined for all grids within a country in a given year. Moreover, as FAO yield data was at the country level, we calibrated the model and estimated parameters only at national level. Therefore, the spatial variability within a country could not be resolved. All of these limitations show that further improvement in model performance largely depends on the quality and resolution of data available for calibration.

Besides, due to the lack of observed maize yield at sub-country level, socio-economic crop drought vulnerability was mapped at a national scale. Therefore, it was not possible to determine areas with higher socio-economic vulnerability within a country. We face similar data limitations to relate vulnerability to socio-economic factors. While the selected factors considered in the regression model are relevant for agricultural vulnerability, they are not exclusively related to agricultural practice. More specific information on factors like "farmers' insurance after crop failure" or "government subsides during drought" are critical and important to identify strategies for reducing vulnerability, but was not available at the scale of SSA.

The structure of EPIC$^+$ has some limitations. This study is the first application and validation of EPIC$^+$. While the proposed calibration scheme used for SSA can in principle be adapted to any region, scale and crop, detailed evaluation of model performance is necessary, which was not feasible in this study due to time constraint. We encountered another limitation of EPIC itself for assessing the impacts of drought during different stages of crop growth. The EPIC structure does not consider crop phenology explicitly. Therefore, we only implicitly considered the influence of drought on crop yield during growing season by applying different time scales of drought exposure and did not measure crop failure at each separate growth stage. We could overcome this limitation by adjusting the subroutine equations of EPIC, but this was beyond the scope of this study.

Last but not least, due to time constraint and lack of detailed information on crop varieties and despite the importance of other staple crops such as sorghum, millet and wheat, only maize was included for the analysis in this study. Modeling crops such as cassava, which contributes with a similar amount to the human diets in tropical regions of SSA is also difficult with the current modeling approach because cassava is a perennial crop and its cultivation may take from 12 to 36 months. Such detailed information is not available at the scale of SSA for crop modeling. Future research should consider the vulnerability and resilience of other crops in order to obtain a more complete picture of vulnerability of food system to drought in SSA.

6.3. Outlook

There is a wide range of possible ways that could strengthen our study of crop drought vulnerability assessment for which EPIC$^+$ was designed. Among them, I highlight the three most important projects to improve the model capabilities and to address key scientific issues of draught vulnerability (Figure 6.1):

- Project-1: Extending the EPIC$^+$ features by embedding more windows for calibrating soil parameters and applying different calibration techniques.
- Project-2: Upgrading EPIC capability for modeling crop phenology and defining biophysical vulnerability at different stages of crop growth.
- Project-3: Assessing the impact of applying a combination of management scenarios and future climate-change scenarios to identify pathways for reducing crop drought vulnerability.

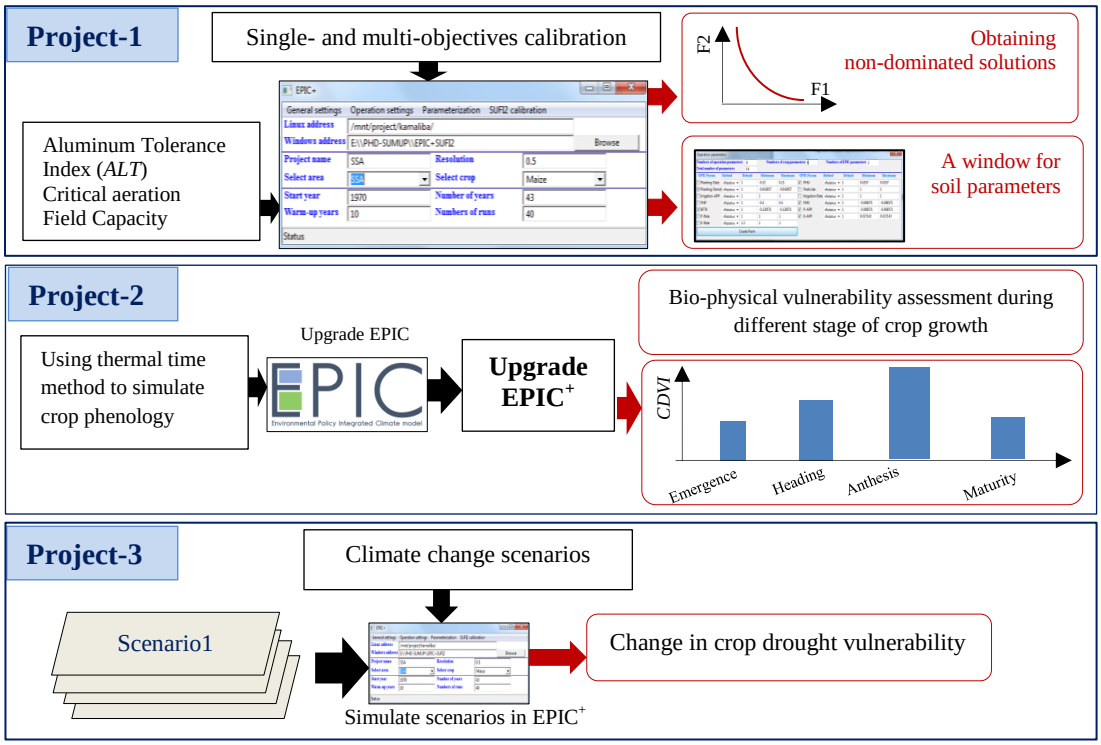

Figure 6.1. Schematic representation of the three outlooks suggested for future development of this study

The initial test of EPIC$^+$ shows promising results at country scale. However, further improvement of EPIC$^+$ in terms of incorporating other calibration tools such as Particle Swarm Optimization or Generalized Likelihood Uncertainty Estimation can be thoroughly tested. Besides, we only looked at the single objective calibration. As mentioned by Vrugt et al. (2003), multi-objective optimization can better capture all characteristics of the observed data that are deemed important. Embedding these techniques, we can further evaluate model performance. If spatially well resolved data become

available, future studies could look at the effectiveness of EPIC^{+} at smaller scales and against more observed variables such as evapotranspiration and soil moisture.

Another important issue is to extend the discussion of drought stress and food security for climate studies in a more comprehensive manner with explicit consideration of crop phenology with evolution of different growth stages. This is important as for example, maize water requirement is low at early growth stages then reaches on peak at reproductive growth stages and during terminal growth stages requirement of water again lowers down. Therefore, droughts during maize reproductive stages caused the highest maize yield loss. A more detailed description of plant physiology could be implemented by adding some subroutines in the EPIC model for each growing stage.

Finally, this study mainly focused on measuring vulnerability during historic period. It also lacks analysis on the effectiveness of management strategies such as irrigation application, changing planting date, or fertilization application rate for vulnerability mitigation. Such strategies should be evaluated based on trade-offs between available resources for food demand and environmental conservation. For example, increasing irrigation should be evaluated with requirements for environmental flows in river systems and fertilizer application should be assessed with a perspective of potential coastal eutrophication and greenhouse gas emissions. Aligning such a comprehensive understanding with future scenarios of climate change can help to identify strategies for a drought resilient crop production system.

6.4. Reference

Vrugt, J. A., Gupta, H. V., Bastidas, L. A., Bouten, W., and Sorooshian, S. (2003). Effective and efficient algorithm for multiobjective optimization of hydrologic models. *Water Resources Research* **39**.

Acknowledgement

Firstly, I would like to express my sincere gratitude to Prof. Hong Yang and Prof. Karim Abbaspour for their continuous support of my PhD study and the related research, for their patience, motivation, and immense knowledge given on designing project and writing scientific papers. Their guidance helped me during all the time of this research. I would also thank Prof. Bernhard Wehrli for his continues support and great motivation during my study. I am also thankful to Prof. Stefan Siebert for serving as external examiner despite his busy work schedule. I am also thankful to Swiss National Science Foundation for the financial support.

Next, I thank my fellow officemates Dr. Wenfeng Liu, Dr. Delaram Houshmand Kouchi, Dr. Diana Dogaru, Dr. Jose Monteiro, and Dr. Saeed Ashref Vaghefi, and also Suxia Li, Julia Stefanovic, and Farshid Jahanbakhshi who provided great working experiences during these four years. Thank goes to all colleagues at Siam department of Eawag with special thanks to Karin Ghilardi for managing administrative issues. Also I thank all my friends in Switzerland which made my life full of joy. There are a lot of precious memories.

Many thanks for other scientists provided generous support of my work Dr. Jimmy Williams, Dr. Christian Folberth, Dr. Susan Wang, Prof. Jaehak Joeng, and Prof. JungioLiu who answered all questions regarding EPIC. The IT support of Eawag: Canan Aglamaz, Franz Werder, Gerard Mohler, and Roul Schaffner are acknowledged for solving all my computer related problems. I would also like to thank the team of clustered server Hypatia at Empa: Danieller passeroni and Patrik Burkhalter for extensive support with my simulations. Much of this work would have been impossible without their efforts to maintain the server. Last but not the least, I would like to thank my parents, my partner, my sister and her family, and my brother for supporting me spiritually throughout writing this thesis and in my life in general.

Curriculum Vita

Current positions

Bahareh Kamali

Postdoctoral researcher since 2018
Leibniz Centre for Agricultural Landscape Research (ZALF)
Eberswalder Straße 84
15374 Müncheberg

T +49 (0)33432 82-411
F +49 (0)33432 82-334
E-mail bahareh.kamali@zalf.de
kamali.civil@gmail.com

Education

2013-2017	PhD candidate in Environmental Systems Sciences ETHZ Zurich, and at the Swiss Federal Institute of Aquatic Science and Technology, Eawag (Switzerland) **Dissertation title:** Application of a spatially explicit bio-physical crop model to assess drought impact on crop yield and crop drought vulnerability in Sub-Saharan Africa. In progress
2007-2010	Master of Science in Water Resource Planning and Management, Department of Environmental and Civil Engineering, Amirkabir University of Technology, Tehran (Iran) **Dissertation title:** Automatic calibration of hydrologic model; simulation-optimization approach
2003-2006	Bachelor of Science in Civil Engineering**,** Faculty of Engineering, Urmia University (Iran)

Research Interest Areas

- Physically based hydrological, and crop and grassland modeling
- Calibration and uncertainty analysis in environmental systems and model prediction
- Interdisciplinary concepts in hydrology, landscape, and climatology
- Vulnerability of environmental systems to drought, climate variability and climate change

Academic Experiences

March 2016	Conducting a workshop on "SWAT calibration, validation and uncertainty analysis using SWAT-CUP" organized by University of Geneva (Switzerland)
2012-2013	Visiting scholar at Swiss Federal Institute of Aquatic Science and Technology (Switzerland)

Research topic: Application of SWAT for modeling vulnerability of drought at the watershed and country levels in the context of climate change

2011-2012 University lecturer for three courses (namely): "Hydraulic" (2 credit point BSc program), "Fluid Mechanic" (3 credit points BSc program), and "Hydraulic and Hydro Structures" (3 credit Points BSc program) at Qazvin Islamic Azad University, Qazvin (Iran)

2010-2012 Teaching assistant at Amirkabir University of Technology for two courses (namely): "Hydrology" (2 credit points BSc program); "Advanced hydrology" (3 credit points MSc program), and "Urban storm water management" (3 credit points MSc program), Tehran (Iran)

Professional Experiences

- Data collection to evaluate farmer's perception on climate change, 2015, Laikipia and Nairobi (Kenya)
- Co-supervision of MSc thesis, 2011, Simin Etesami, "Application of hydrologic condition on water quality using Qual2k model – Case Study, Garmsar River, Saveh, Iran" (Iran)
- Co-principal investigator of a project (with Prof. Morteza Kolahdoozan), 2011, entitled "Application of flushing operation on large dam, simulation– optimization approach, Case study, Ekbatan Dam", Water Research Institute, Tehran (Iran)
- Caspian consulting engineer, Tehran, Iran, 2010-2012 as Urban storm water collection designer and urban drainage designer

Awards, Honours, and Fellowship

- Aug-Nov 2013: Scholarship from Eawag Partnership Program (EPP) for developing countries for four months visiting of Eawag
  Research topic: "Modeling vulnerability of drought at the watershed and country levels in the context of climate change: Application of SWAT model"
- 2009 and 2010: High honor and outstanding student with GPA 18.68/20
- 2007: high honor student: Ranking 2nd place out of 40.

Publications: Peer-reviewed Journal

15. **Kamali B,** Yang H, Abbaspour KC, (in preparation), "Comparison of methods for mapping maize drought vulnerability in Sub-Saharan Africa".
14. **Kamali B,** Abbaspour KC, Lehmann A, Wehrli B, Yang H, (in review), "A quantitative analysis for determining socio-economic factors conferring crop drought vulnerability".
13. **Kamali B,** Abbaspour KC, Lehmann A, Wehrli B, Yang H, (in revision), "Spatial assessment of maize physical drought vulnerability in Sub-Saharan Africa: Linking drought exposure with crop failure".
12. **Kamali B.,** Abbaspour KC, Lehmann A, Wehrli B, Yang H, 2018, "Drought vulnerability assessment of maize in Sub-Saharan Africa: insights from physical and social perspectives". *Global and Planetary Change*, 162, 266-274 https://doi.org/10.1016/j.gloplacha.2018.01.011
11. **Kamali B**, Abbaspour KC, Lehmann A, Wehrli B, Yang H, 2018, "Uncertainty-based auto-calibration for crop yield – the EPIC+ procedure for a case study in Sub-Saharan Africa", *European Journal of Agronomy, 93, 57-72*.

10. **Kamali B,** Yang H, Abbaspour KC, 2017, "Assessing the uncertainties of different input datasets in simulation of water resources components", *Water, 9*(9), 709; doi:10.3390/w9090709

9. **Kamali B**, Houshmand Kouchi D, Yang H, Abbaspour KC, 2017, "Multilevel drought hazard assessment under climate change scenarios in semi-arid regions - A case study of the Karkheh River Basin in Iran", *Water, 9(4),* doi:10.3390/w9040241

8. Vaghefi S, Abbaspour N, **Kamali B**, Abbaspour KC, 2017, "A toolkit for climate change analysis and pattern recognition for extreme weather conditions–Case study: California-Baja California Peninsula", *Environmental Modeling and software*, 97, 181-198, https://doi.org/10.1016/j.envsoft.2017.06.033

7. Stefanovic J, Yang H, Zhou Y, **Kamali B**, Sarah A Ogalleh SA, 2017, "Adaption to climate change: A case study of two agricultural systems from Kenya", *climate and development*, https://doi.org/10.1080/17565529.2017.1411241

6. **Kamali B**, Abbaspour KC, Lehmann A, Wehrli B, Yang H, 2015, "Identification of spatiotemporal patterns of biophysical droughts in semi-arid region – A case study of the Karkheh river basin in Iran", HESS, 12 (6): 5187-5217

5. Monteiro JAF, **Kamali B**, Srinivasan R, Abbaspour KC, Gücker B, 2015, "Modelling the effect of riparian vegetation restoration on sediment transport in a human-impacted Brazilian catchment", Ecohydrology Journal, 9 (7): 1289-1303

4. **Kamali B**, Mousavi SJ, 2014, "Automatic calibration of conceptual HEC-HMS using multi objective fuzzy optimal models", Civil Engineering Infrastructures Journal, 47(1): 1 – 12, 4

3. **Kamali B**, Mousavi SJ, Abbaspour KC, 2012, "Automatic calibration of HEC-HMS using single-objective and multi-objective PSO algorithm". Hydrological Processes Journal. 27 (26): 4028-4042

2. **Kamali B**, Mousavi SJ, 2012, "Automatic calibration of hydrologic event-based model using PSO meta-heuristic Algorithm", Journal of Amirkabir University (in Persian)

1. Mousavi SJ, Abbaspour KC, **Kamali B**, Amini M, Yang H, 2011, "Uncertainty-based automatic calibration of HEC-HMS model using sequential uncertainty fitting approach". Journal of Hydroinformatics 14: 286-309

Conference Proceedings

14. Nendel C, Griffiths P, Frantz D, Schwieder M, **Kamali B**, Stella T. Berg M, Hostert P, " Crop and crop management identification from space for national-scale modeling", AgMIP's 7th Global Workshop, April 24-26, 2018 San Jose, Costa Rica

13. Yang H, **Kamali B,** Abbaspour KC, "Drought Vulnerability Assessment of Maize in Sub-Saharan Africa: Insights From Physical and Social Perspectives" Asia Oceania Geosciences Society (AOGS), 15th Annual Meeting 3-8 JUN, 2018, Honolulu, Hawai

12**. Kamali B**, Abbaspour KC, Yang H., 2016, "An introduction to EPIC+SUFI2 for calibrating EPIC crop model at different scales", International SWAT Conference & Workshops 2016, Beijin, China

11. **Kamali B**, Houshmand Kouchi D, Abbaspour KC, Yang H., 2016. "Assessment of bio-physical drought hazards. A case study of Karkheh River basin in Iran", EGU General Assembly 2016

10. Griensven A, Vetter T, Piontek F, Gosling SN, **Kamali B**, Reinhardt J, Dinkneh A, Yang H, Alemayehu T, 2016, "Inter-sectoral comparison of model uncertainty of climate change impacts in Africa", EGU General Assembly 2016

9. **Kamali B**, Abbaspour KC, Yang H, 2016,"Drought vulnerability assessment of wheat and barley production under climate change-A case study of Karkheh River Basin in Iran", Association of American Geographers (AAG) 2016

8. **Kamali B**, Abbaspour KC, Yang H, 2015, "Assessing drought vulnerability of agricultural production systems in the context of agro-hydrological modeling-A case study of Karkheh River Basin", International SWAT Conference & Workshops 2015, Sardinia, Italy

7. **Kamali B**, Mousavi SJ, Abbaspour KC, Yang H, 2013, The Impact of climate data uncertainty on calibration of the SWAT model, International SWAT Conference & Workshops 2013 - Toulouse, France

6. **Kamali B**, Mousavi SJ, Abbaspour KC, Yang H, 2013, Impact of Input Data on Distributed Hydrologic Modeling under Future Climate Change Scenarios:, Symposium The Water Cycle in a Changing Climate 2013

5. **Kamali B**, Mousavi SJ, Shiry S, "Meta-modeling for calibration of HEC-HMS rainfall-runoff model', 9th International Congress on Civil Engineering, May 8-10, 2012, Isfahan University of Technology, Isfahan, Iran

4. **Kamali B**, Mousavi SJ, "Automatic calibration of HEC-HMS model, simulation-optimization approach", Proceedings of 5th conference of Civil Engineering, 2010, Mashhad, Iran, pp 93-109 (in Persian)

3. **Kamali B**, Mousavi SJ, Ardeshir A, Maknoon R, 2011, "Application of best management practice on urban storm water management, 4th water Resource Conference, Tehran, IRAN (in Persian)

2. Parekar A, Mousavi SJ, **Kamali B**, 2011, "Comparing Green-Ampt and SCS Loss model on automatic calibration of HEC-HMS, 4th water resource conference, Tehran, IRAN (in Persian)

1. Fallah F, **Kamali B**, Mirzaeie M, 2011, "Application of rainfall temporal distribution on HEC-HMS and SWMM model", 6th Conference of Civil Engineering, Semnan, Iran, (in Persian)

Scientific and Educational Software Qualifications

1. Environmental Policy Integrated Climate (EPIC)
2. Soil and Water Assessment Tools (SWAT) and SWAT-CUP calibration tool for calibrating SWAT
3. ArsGIS –Esri
4. Hydrologic Engineering Center- Hydrologic Modeling System (HEC-HMS)
5. Hydrologic Engineering Center-River Analysis System (HEC-RAS)
6. Storm Water Management Model (SWMM)
7. Development of EPIC^{+} by Bahareh Kamali, A software for extending application of EPIC on large scale and uncertainty based model calibration

Programming Skills

1. MATLAB – Professional
2. Python- Professional
3. R- statistical programming

Professional services: reviewer for Journals

1. Environmental Modeling and Software,
2. Hydrology
3. Water
4. Natural Hazards
5. Arabian Journal of Geosciences

Language Experiences

- Persian (Native)
- Kurdish (Native)
- English (proficient)
- German (Level B1)
- Turkish (Native)

Interests

- Volleyball
- Swimming